

Antimicrobial surfaces based on self-assembled nanoreactors : from block copolymer synthesis to bacterial adhesion studies

Nicolas Cottenye

▶ **To cite this version:**

Nicolas Cottenye. Antimicrobial surfaces based on self-assembled nanoreactors : from block copolymer synthesis to bacterial adhesion studies. Other. Université de Haute Alsace - Mulhouse; Universität Basel. Philosophisch-naturwissenschaftliche Fakultät, 2010. English. NNT : 2010MULH5351 . tel-00598560

HAL Id: tel-00598560

https://theses.hal.science/tel-00598560

Submitted on 6 Jun 2011

HAL is a multi-disciplinary open access archive for the deposit and dissemination of scientific research documents, whether they are published or not. The documents may come from teaching and research institutions in France or abroad, or from public or private research centers.

L'archive ouverte pluridisciplinaire **HAL**, est destinée au dépôt et à la diffusion de documents scientifiques de niveau recherche, publiés ou non, émanant des établissements d'enseignement et de recherche français ou étrangers, des laboratoires publics ou privés.

Antimicrobial surfaces based on self-assembled nanoreactors: from block copolymer synthesis to bacterial adhesion study.

Inauguraldissertation / Manuscrit de These

Zur Erlangung der Würde eines / en vue d'obtenir le

Doktorat der Philosophie vorgelegt der Philosophisch- Naturwissenschaftlichen Fakultät der Universität Basel	Doctorat en Chimie de L'Université de Haute Alsace

Auf der Basis eines Cotutelle-vertrags/ dans le cadre d'un accord de cotutelle.

Von/ par

Nicolas Cottenye

Aus/né à Roubaix (Frankreich/France)

Basel, 2010

Original document stored on the publication server of the University of Basel: **edoc.unibas.ch**

This work is licenced under the agreement „Attribution Non-Commercial No Derivatives – 2.5 Switzerland". The complete text may be viewed here: **creativecommons.org/licenses/by-nc-nd/2.5/ch/deed.en**

creative commons

Attribution-Noncommercial-No Derivative Works 2.5 Switzerland

You are free:

to Share — to copy, distribute and transmit the work

Under the following conditions:

Attribution. You must attribute the work in the manner specified by the author or licensor (but not in any way that suggests that they endorse you or your use of the work).

Noncommercial. You may not use this work for commercial purposes.

No Derivative Works. You may not alter, transform, or build upon this work.

- For any reuse or distribution, you must make clear to others the license terms of this work. The best way to do this is with a link to this web page.
- Any of the above conditions can be waived if you get permission from the copyright holder.
- Nothing in this license impairs or restricts the author's moral rights.

Your fair dealing and other rights are in no way affected by the above.

This is a human-readable summary of the Legal Code (the full license) available in German: http://creativecommons.org/licenses/by-nc-nd/2.5/ch/legalcode.de

Disclaimer:
The Commons Deed is not a license. It is simply a handy reference for understanding the Legal Code (the full license) — it is a human-readable expression of some of its key terms. Think of it as the user-friendly interface to the Legal Code beneath. This Deed itself has no legal value, and its contents do not appear in the actual license. Creative Commons is not a law firm and does not provide legal services. Distributing of, displaying of, or linking to this Commons Deed does not create an attorney-client relationship.

Quelle: http://creativecommons.org/licenses/by-nc-nd/2.5/ch/deed.en Datum: 3.4.2009

Genehmigt von der Philosophisch-Naturwissenschaftlichen Fakultät auf Antrag von

Prof. Dr. Wolfgang Meier, supervisor
Dr. K. Anselme, supervisor
Dr. L.Ploux, supervisor
Prof. Dr. Marcus Textor, referee
Dr. Helmut Schlaad, referee

Basel, den 14 Dezember 2010

Dekan
Prof. Dr. Martin Spiess

PhD titles.

English.

Antimicrobial surfaces based on self-assembled nanoreactors: from block copolymer synthesis to bacterial adhesion studies

Français.

Surfaces antimicrobiennes basées sur l'auto-assemblage de nanoréacteurs: de la synthèse du copolymère à l'étude de l'adhésion bactérienne.

Keywords.

English.

Polymer, amphiphile, vesicle, bacteria, biofilm, antimicrobial, surfaces

Français.

Polymère, amphiphile, vésicule, bactérie, biofilm, antimicrobien, surfaces

Laboratories.

Department of Chemistry
University of Basel
Klingelbergstrasse 80
CH-4056 Basel, Switzerland
Tel: +41 (0)61 267 38 00
Fax: +41 (0)61 267 38 55

IS2M (CNRS LRC7228)
Institut de Science des Matériaux de Mulhouse
15, rue Jean Starcky - BP 2488
68057 Mulhouse cedex, France
Tel: +33 (0)3 89 60 87 00
Fax: +33 (0)3 89 60 87 99

Abstracts.

English.

The aim of this work is to develop a new strategy for the prevention of biofilm growth. For this purpose, we prepared bioactive surfaces resulting from the surface-immobilization of nanoreactors self-assembled from amphiphilic poly(isobutylene)-block-oligonucleotide copolymers. The block copolymer was synthesized and characterized via appropriate complementary techniques. Self-assembly into vesicles allowed the functional encapsulation of enzymes, as assayed through enzyme activity monitoring, leading to a prodrug-drug system. The self-assembled structures were specifically immobilized on surfaces via base pairing between the oligonucleotide block of the copolymer and the surface tethered complementary nucleotide sequence.

Using *E.coli* strains, we first observed an influence of the two density of oligonucleotides immobilized on the surface on the number of adherent bacteria. This influence may be due to an effect of surface charge density. We then confirmed the well-known role of curli in biofilm cohesion, and we showed gene over-expression associated with curli production on oligonucleotide-modified surfaces. We demonstrated that gene over-expression does not depend on the topographical features of the surface or on the composition of the nucleotide sequences used in this study. Finally, we demonstrated that the presence of the vesicular structure is able to produce strong anti-adhesive properties of the surface. We assume, from observations of bacterial response in dynamic conditions, that this effect is due to increased bacterial motility on the surface, leading to a high detachment rate. Which is further confirms by a comparable bacterial response observed on agar hydrogel of different hardnesses. This result provides a preliminary outcome, paving the way to new approaches to antimicrobial strategies.

Français.

Ce travail a pour but le développement d'une nouvelle classe de surfaces destinée à la lutte contre la formation de biofilms. Ces surfaces se basent sur l'immobilisation de nanoréacteurs, résultant de l'auto-assemblage d'un copolymère amphiphile poly(isobutylène)-bloc-oligonucléotide sous forme de vésicules encapsulant une enzyme. Le rôle de cette enzyme est de produire des agents antimicrobiens à partir de précurseurs inactifs. Le copolymère a été synthétisé et caractérisé par des techniques complémentaires et le maintien de l'activité enzymatique a été démontré. Les surfaces bioactives sont finalement obtenues par l'immobilisation des nanoréacteurs grâce aux capacités d'hybridation des séquences nucléiques complémentaires.

Nous avons d'abord montré l'influence des deux densités d'oligonucléotides utilisées sur le nombre *d'E.coli* adhérentes, due probablement aux variations de charges surfaciques associées. Nous avons ensuite confirmé l'influence des curli sur la cohésion des biofilms et mis en évidence une surexpression de la production de curli en présence d'oligonucléotides sur les surfaces, et ce, indépendamment de la séquence et de la topographie considérées. Finalement, nous avons observé un effet antiadhésif lié aux structures vésiculaires indépendant de la topographie de la surface. L'étude complémentaire, menée en mode de culture dynamique, a conduit à envisager que les propriétés mécaniques de la surface affectent la rétention des bactéries en modifiant leur mobilité sur la surface. L'analogie avec des résultats obtenus sur des hydrogels d'agar de différentes duretés conforte cette hypothèse. Ces résultats posent les fondements permettant d'envisager de nouvelles stratégies dans la lutte contre la formation des biofilms.

Acknowledgment.

A number of people helped and were involved in this work more or less directly. I wish to thank them all. I wish in particular to cite some of them for their invaluable help and contribution.

The committee: Prof. Dr. M. Textor, Prof. Dr. H. Schlaad and Prof. Dr. T. Pfohl are acknowledged for having agreed to consider and report on this thesis.

My supervisors: Prof. Dr. W. Meier, Dr. K. Anselme, Dr. L. Ploux and Dr. C. Vebert-Nardin are acknowledged for their help, discussions, sympathy and, moreover, their patience and compliance with my dramatic writing skills.

Collaborators are thanked for having shared their unique skills, discussions and sympathy: Dr A. Ponche and P. Fioux (XPS), Dr. S. Rigolet (solid state NMR), Dr. O. Onaca (molecular biology), Dr. K. Mougin (ellipsometry and contact angle measurements), G. Persy (TEM), Dr. A. Ziegler (CD spectroscopy) and M.Inglins for critical review of this thesis.

Trainee students are acknowledged for their contribution as the small hands of some parts of this work: J. Sonnet, L. Costato and M. I. Syga.

My close colleagues: J. Böhmler and K. Langowska are thanked for their everyday contribution, discussion and happiness (or not…), my Basler "Menschen" office roommate for a cool work atmosphere and the Mulhouse office girls for more girly but still cool ambiance.

All people from the labs in Basel and Mulhouse: colleagues, administrative staff, technicians, etc... I enjoyed my work in those labs, thanks to you.

Finally I would like to provide more personal thanks to my wife, Sandra, who always supports me in all my choices; thanks my love.

To close this acknowledgment section, since nothing is possible without a little bit of money, I would like to thank the financial supports of this work:

The SNSF (200020-121822), the NCCR-*NANO* and the "CRUS stipend fur cotutelle de thèse, Programme 2010".

Content.

PHD TITLES. **4**
ENGLISH. 4
FRANÇAIS. 4
KEYWORDS. **4**
ENGLISH. 4
FRANÇAIS. 4
LABORATORIES. **4**
ABSTRACTS. **5**
ENGLISH. 5
FRANÇAIS. 6
ACKNOWLEDGMENT. **7**
CONTENT. **8**
GENERAL INTRODUCTION. **12**
BIOFILMS AND THEIR CONTROL. 12
AMPHIPHILES, VESICLES, AND THEIR APPLICATIONS. 15
SCOPE OF THE THESIS. 17
REFERENCES. 19
PART I: POLYMERS, NANOREACTORS, AND HYBRIDIZATION FOR CONTROLLED SURFACE PREPARATION. **22**
A. *Introduction.* *23*
B. *State of the art.* *25*
B.1 Amphiphilic block copolymers, amphiphilic "chimeras" their properties and synthesis. 25
B.2 Nanoreactors: Definition, description and limitations. 28
B.3 Prodrug-drug system. 31
B.4 Immobilization of vesicles to surfaces: possible strategies. 33
B.5 Oligonucleotide hybridization. 35
B.6 Vesicles mechanical properties. 36
C. *Materials and methods.* *37*
C.1 Oligonucleotide-based amphiphilic block copolymer synthesis. 37
C.1.a Materials. 37
C.1.b Solid phase synthesis. 38
C.2 Chemical analysis of the diblock copolymer. 38
C.2.a Nuclear magnetic resonance (NMR). 38
C.2.b Fourier Transform Infrared Spectroscopy (FTIR). 39
C.2.c Elementary analysis. 39
C.3 UV-Vis spectroscopy for polymer concentration quantification. 39
C.4 Self-assembly of the diblock copolymer. 39
C.5 Self-assembly characterisation and chain configuration. 39

C.5.a Circular Dichroism Spectrocscopy (CD). 39
C.5.b Transmission Electron Microscopy (TEM). 40
C.5.c Scanning Electron Microscopy (SEM). 40
C.5.d Dynamic Light Scattering (DLS). 40
C.6 Nanoreactor preparation and characterization. 40
C.6.a Materials. 40
C.6.b Nanoreactor preparation. 41
C.6.c Nanoreactor purification. 41
C.6.d Other samples and sample names. 42
C.6.e Polymer and enzyme concentration determination. 43
C.6.f Enzyme activity monitoring and concentration determination from Michaelis-Menten kinetics measurement by fluorescence spectroscopy. 44
C.7 Vesicle Labeling. 45
C.8 Oligonucleotide modified surfaces. 45
C.8.a Materials. 45
C.8.b Oligonucleotide self-assembled monolayer (SAM) modified surfaces. 45
(i) Protocol for “low density” oligonucleotide modified surfaces. 45
(ii) Protocol for“high density”oligonucleotide modified surfaces. 46
C.8.c Type of oligonucleotide modified surfaces. 46
C.9 Vesicle modified surfaces. 47
C.9.a Surfaces on the immobilization of vesicles through nonspecific base pairing. 47
C.9.b Surfaces resulting from the immobilization of vesicles though hybridization. 47
C.9.c Reference surfaces. 47
C.10 Surface characterization. 48
C.10.a Fluorescence microscopy. 48
C.10.b X-ray Photoelectron Spectroscopy (XPS). 48
C.10.c Contact angle measurements. 48
C.10.d Ellipsometry. 49
C.10.e Atomic force microscopy (AFM). 49
C.10.f Quartz crystal microbalance with dissipation monitoring QCM-D. 49
CHAPTER 1. BLOC COPOLYMER SYNTHESIS AND CHARACTERIZATION 51
1.1. Results and discussion 51
1.1.a. Chemical analysis. 51
1.1.b. Self-assembly and chain configuration. 56
1.2. Conclusion 60
CHAPTER 2. NANOREACTOR PREPARATION AND CHARACTERIZATION 62
2.1. Results and discussion 63
2.1.a. Nanoreactor preparation and purification: step by step characterization. 63
2.1.b. Nanoreactor activity, Michaelis-Menten kinetics and encapsulation efficiency. 67
2.1.c. Proteinase K experiment. 69
2.2. Conclusion 70

CHAPTER 3. SURFACES BASED ON VESICLES DEPOSITION 71
3.1. Results and discussion 72
3.1.a. Oligonucleotide self-assembled monolayers (SAM) modified surfaces. 72
3.1.a.i. "Low density" oligonucleotide modified surfaces. 72
3.1.a.ii. "High density" oligonucleotide modified surfaces. 77
3.1.b. Surface based on immobilization of vesicles through nonspecific interaction. 79
3.1.c. Surface resulting from hybridization of vesicles on oligonucleotide modified surfaces. 81
3.2. Conclusion 85
CONCLUSION TO PART I 86
References 87
PART II: BACTERIAL ADHESION TO NANOREACTOR-BASED SURFACES: INFLUENCE OF CHEMISTRY, TOPOGRAPHY AND MECHANICAL PROPERTIES ON BACTERIA-SURFACE INTERACTIONS. 93
A. *Introduction.* *94*
B. *State of the art.* *95*
B.1 Biofilm formation. 95
B.2 Influence of surface chemical and biochemical function. 96
B.3 Influence of surface topographical properties. 97
B.4 Influence of surface mechanical properties on bacterial adhesion. 99
B.5 Oligonucleotides as a support for bacterial adhesion. 100
B.6 Curli: description and biological function. 101
B.7 Bacterial motility at interfaces. 102
C. *Materials and methods.* *104*
C.1 Surfaces and their sterilization. 104
C.2 Bacterial strains, culture condition and observation under static culture condition. 106
C.2.a Bacterial strains. 106
C.2.b Culture medium and inoculum. 106
C.2.c Static culture condition. 107
C.2.d Cytotoxicity of the surface. 107
C.2.e Biofilm observation and fluorescence staining. 107
(i) Differed observation. 108
(ii) Time series differed observation. 108
C.3 Setup, culture and observation under flow culture condition. 108
C.3.a Flow cell design and setup configuration. 108
C.3.b Bacterial culture and real-time observation under flow condition. 109
C.4 Analysis of biofilm micrographs. 110
C.5 Quality control. 111
D. *Results.* *111*
D.1 Surface supernatant toxicity test. 111
D.2 Bacterial adhesion study. 112
D.2.a Bacterial adhesion, proliferation and biofilm formation on oligonucleotide modified surfaces. 112
D.2.b Influence of oligonucleotide strand type and density. 113

D.2.c Influence of topography. 116
D.2.d Influence of vesicles mechanical properties. 117
D.3 Adhesion and detachment experiment under flow. 119
D.4 Complementary experiment with an agar coating: link between mechanical properties, bacterial adhesion and bacterial motility. 125
D.5 Curli expression study 130
E. *Discussion*. *132*
E.1 Surface toxicity. 132
E.2 Influence of surface chemistry and surface charge. 133
E.2.a Chemistry and charge effect on bacterial adhesion. 133
E.2.b Chemistry and charge effect on curli expression. 134
E.3 Influence of surface topography. 136
E.4 Influence of surface mechanical properties on bacterial adhesion and motility. 138
F. *Conclusion*. *141*
G. *References*. *143*
GENERAL CONCLUSION. **148**
OUTLOOK. **150**
LIST OF ABBREVIATIONS. **151**
IMPACT OF THE WORK. **152**
PUBLISHED WORK: 152
PUBLICATION UNDER PREPARATION: 152
ORAL CONTRIBUTIONS IN CONFERENCE: 152
POSTER IN CONFERENCE: 152
SEMINARS AND WORKSHOPS: 153
AWARDS: 153
INDEPENDENT GRANT AND FINANCIAL SUPPORT: 153
CURRICULUM VITAE **154**

General introduction.

Biofilms and their control.

Over recent decades, the concept of "biofilm" has made breakthroughs in microbiology especially in healthcare, leading to new concepts in the field of surface bacteria interactions and the development of novel strategies to fight pathogens.

Thirty years ago, Costerton introduced the notion of a "biofilm" and defined it as matrix-enclosed bacterial population adherent to surfaces or at interfaces [1]. This definition included microbial aggregates, floccules and also adherent populations within the spaces of porous media. More than just a bacterial response to specific stresses induced by the environment, as was first believed, it is now accepted that a biofilm is the most common bacterial mode of life [2]. Thus, more than 99% of bacteria living on Earth are thought to compose biofilms [3]. This communal mode of life includes specific metabolic and developmental growth of bacteria [4-6]. In particular, it has been demonstrated that the intensity of gene expression of bacteria living in biofilms varies by many tens of percents compared to planktonic bacteria [7]. Furthermore, far from being a mere accumulation of bacteria, biofilms develop by the proliferation of pioneer-bacteria, i.e. newly adhered, following typical processes that are schematized in Figure 1 (details will be given in the State of the Art of Part II). Briefly, after primary adhesion to the surface, pioneer bacteria proliferate and synthesize exobiopolymers, mainly exopolysaccharides, which constitute the matrix of the biofilm. Biofilms are dynamic systems, evolving in respect with the 3D structure and metabolism of constituent bacteria, with some parts of the biofilm even detaching, for further colonization of new surfaces [8].

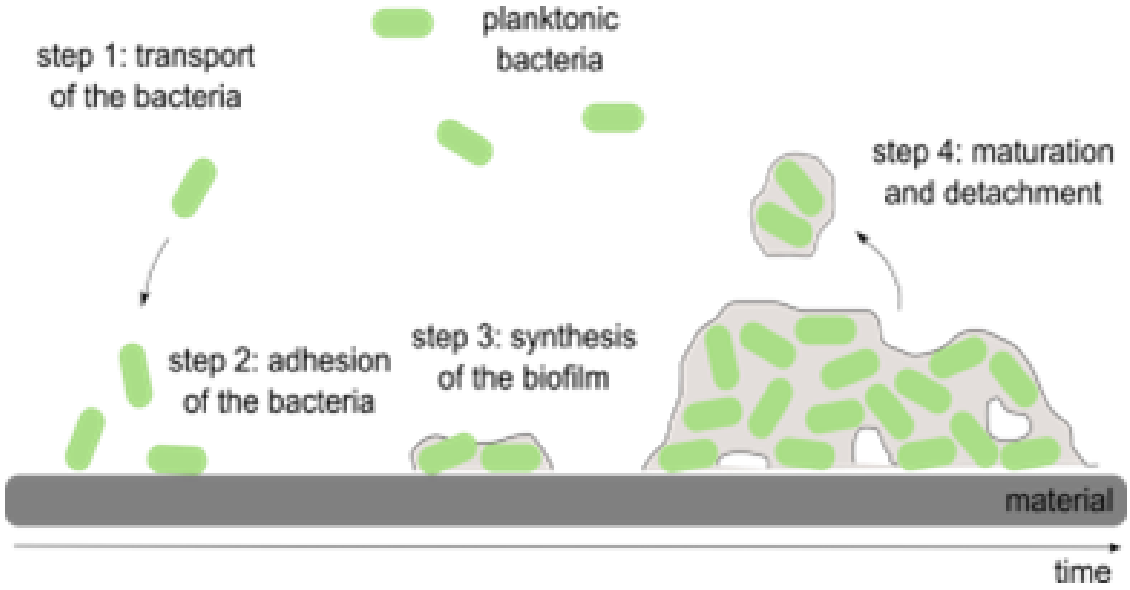


Figure 1: Scheme of a classical biofilm formation process (Illustration from L. Ploux et al. [9])

When living in a biofilm, bacteria are protected from stresses induced by the environment such as extreme temperatures, dry conditions, antiseptic or antimicrobial chemicals agents, or antibodies and phagocytes [1-3,10]. Therefore, since classical efforts to fight pathogens focus on systemic treatments targeting planktonic bacteria, they are usually inefficient against bacteria-associated biofilm growth. Typical examples of surface-related infections are listed in Figure 2(a), whereas examples of biofilm-related infections in human disease are listed in Figure 2(b). Unfortunately, an increase in invasive surgery that makes use of biomaterial implantation within the last 50 years has led to an increase in the prevalence of such biofilm-associated infections [10]. Therefore, new antimicrobial strategies specifically focusing on surface-related infections have become essential. Research in this field has thus advanced rapidly in the last twenty years [11-15].

a/

Infection or disease	Common biofilm bacterial species
Dental caries	Acidogenic Gram-positive cocci (e.g., *Streptococcus*)
Periodontitis	Gram-negative anaerobic oral bacteria
Otitis media	Nontypable strains of *Haemophilus influenzae*
Musculoskeletal infections	Gram-positive cocci (e.g., staphylococci)
Necrotizing fasciitis	Group A streptococci
Biliary tract infection	Enteric bacteria (e.g., *Escherichia coli*)
Osteomyelitis	Various bacterial and fungal species—often mixed
Bacterial prostatitis	*E. coli* and other Gram-negative bacteria
Native valve endocarditis	Viridans group streptococci
Cystic fibrosis pneumonia	*P. aeruginosa* and *Burkholderia cepacia*
Meloidosis	*Pseudomonas pseudomallei*
Nosocomial infections	
ICU pneumonia	Gram-negative rods
Sutures	*Staphylococcus epidermidis* and *S. aureus*
Exit sites	*S. epidermidis* and *S. aureus*
Arteriovenous shunts	*S. epidermidis* and *S. aureus*
Schleral buckles	Gram-positive cocci
Contact lens	*P. aeruginosa* and Gram-positive cocci
Urinary catheter cystitis	*E. coli* and other Gram-negative rods
Peritoneal dialysis (CAPD) peritonitis	A variety of bacteria and fungi
IUDs	*Actinomyces israelii* and many others
Endotracheal tubes	A variety of bacteria and fungi
Hickman catheters	*S. epidermidis* and *C. albicans*
Central venous catheters	*S. epidermidis* and others
Mechanical heart valves	*S. aureus* and *S. epidermidis*
Vascular grafts	Gram-positive cocci
Biliary stent blockage	A variety of enteric bacteria and fungi
Orthopedic devices	*S. aureus* and *S. epidermidis*
Penile prostheses	*S. aureus* and *S. epidermidis*

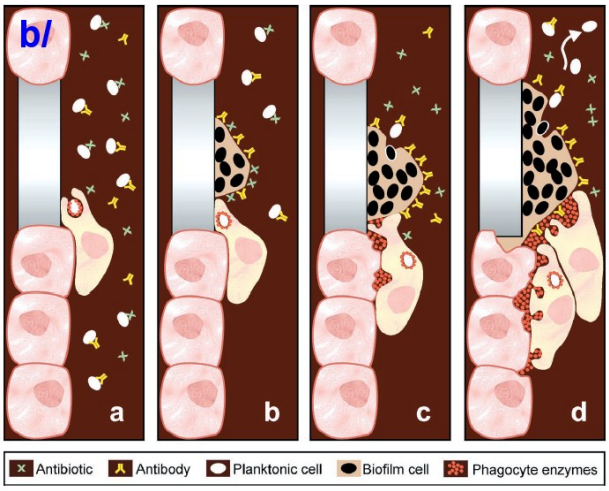


Figure 2: (a) Typical examples of human infections involving biofilms. (b) Scheme of a medical biofilm. Planktonic bacteria can be cleared by antibodies and phagocytes, and are susceptible to antibiotics. Adherent bacterial cells form biofilms preferentially on inert surfaces, and these sessile communities are resistant to antibodies, phagocytes, and antibiotics. Phagocytes are attracted by the biofilms. Phagocytosis is frustrated but phagocytic enzymes are released. Phagocytic enzymes damage tissues around the biofilm, and planktonic bacteria are released from the biofilm. Release may cause dissemination and acute infection in neighboring tissues. Both illustrations were extracted from Costerton et al. [10]

Two main approaches have been considered to fight biofilms. A first approach is to neglect the surface and concentrate on the mature biofilm through the optimization of the diffusion of antibacterial molecules into the biofilm matrix [16-18]. The second approach consists in modifying the surface in order to prevent or treat biofilm formation, which is the approach that drives our interest. In this context, the opportunity to act at various stages of development has been taken into consideration [19,20]. In general, the various strategies can be divided in two main categories, the passive and the active.

In the passive strategy, the surface is modified to avoid bacterial adhesion by altering the inherent properties of the surface. Several possibilities have been reported: first, several physico-chemical properties of the surface have been demonstrated as efficient in reducing bacterial adhesion. These include, for example, high hydrophobicity of a surface Teflon coating [21], charge modification of the surface [15], and surface energy or entropic shielding by grafting of polymer brushes [22]. A second strategy consists in grafting molecules that can

repel or kill bacteria as soon as they adhere to the surface. This strategy was widely applied by grafting antibiotics [23], enzymes [24] and antimicrobial polymers (chitosan, methacryloylethyl trialkyl phosphonium chlorides/*N*-isopropylacrylamide copolymer, for examples) [25,26]. However, most of those techniques show considerable limitations. The first difficulty is in associating preventive or antibacterial effects with biocompatibility for mammalian cells, which is an issue rarely considered in the biofilm context. The second important limitation arises from the large variety of bacterial physico-chemical properties [27-29] (different negative charge of membrane surface, various shapes and various hydrophobicity to cite few), which limits the spectrum of action of the considered strategy. Finally the major disadvantage of such an approach is lifetime, since scratches or conditioning may offer anchoring points for bacteria, sufficient to locally counter any anti-adhesive surface property [30,31].

The active strategy has recently become the most widely studied and was shown to be more reliable than the passive approach to avoid contamination of biofilm formation, for example on catheters [32]. This strategy consists in incorporating antimicrobial agents in materials or material coatings and controlling their release to the surroundings. This control constitutes the major challenge of this approach, since release of doses too high may induce toxicity and immune response [33], while release of too low doses may be ineffective and may induce a bacterial resistance mechanism [34]. Both active doses and treatment time must therefore be well controlled. For this purpose, two approaches are mainly proposed: continuous release and responsive release. Due to its relative simplicity, continuous release has been developed the most. Antimicrobial agents such as antibiotics or silver nanoparticles are embedded in a polymeric matrix (immobilized in a hydrogel [14] or polymer coating [12] for example) and release is obtained by diffusion of the molecules through the matrix. This diffusion process is then the critical aspect to control the release [35] and is driven by the physicochemical properties of the matrix, such as hydrogel cross-link density and its interactions with the antimicrobial agent. Products based on continuous release are already commercially available for several medical applications [36,37]. Nevertheless, this approach is disputable, because release continues even if not needed, potentially leading to bacterial resistance induced by continuous antimicrobial use. Responsive release should therefore be preferred. This approach consists on releasing the bioactive agent in response to external stimuli, which limits the quantity of released agent. Limiting the quantity of released agent decreases the subsequent potential secondary effects, such as enhancement of bacterial resistance and short lifetime of the antibacterial coatings, for example. Several stimuli have been considered, including response to pH or ionic strength [37], response to light [38] or mechanical stimulus [39] and response to temperature [38] or electric stimulus [39]. Responsive approaches have already demonstrated their relevance in antimicrobial coating application, but some questions remain, such as biocompatibility for *in vivo* application, which is an important issue for some coatings [40]. Moreover, despite improvement compared to non-responsive bioactive coatings, the current responsive approaches do not solve the limited lifetime issue due to the limited content of active agent (i.e. when all active agent is released, the coating becomes inactive). In addition, a sufficient release rate should be ensured during the lifetime of the coating.

Finally, despite diverse attempts to overcome these limitations by combining, for example, passive and active strategies [14] in the same coating [13,14], some limitations and problems remain [11], essentially due to limited lifetime resulting from a limited amount of active component. Thus new approaches need to be developed to overcome the issue of release limitation.

Amphiphiles, vesicles, and their applications.

Amphiphilic molecules contain polar and non-polar moieties, respectively hydrophilic and hydrophobic moieties. Due to this chemical incompatibility, amphiphilic molecules self-assemble in aqueous solution and organize at aqueous interfaces. Self-assembly leads to a wide variety of structures depending on several factors such as temperature, solvent composition, concentration, molecular weight or hydrophilic to hydrophobic volume fraction, charge, etc. Examples of those structures are displayed in Figure 3 for linear amphiphilic block copolymers, consisting of a hydrophilic block covalently linked to a hydrophobic polymer segment. All of those structures result from a self-assembly process, which is either thermodynamically or kinetically driven [41]. The morphology of the self-assembled structure is defined to minimize the free energy of the system by lowering the surface tension [42]. Taking into account potential interactions such as electrostatic repulsion or hydrogen bonding, as well as molecular weight and hydrophobic to hydrophilic volume fraction, specific amphiphilic macromolecules can be tailored to control the resulting characteristics of the self-assembled structure [41,43].

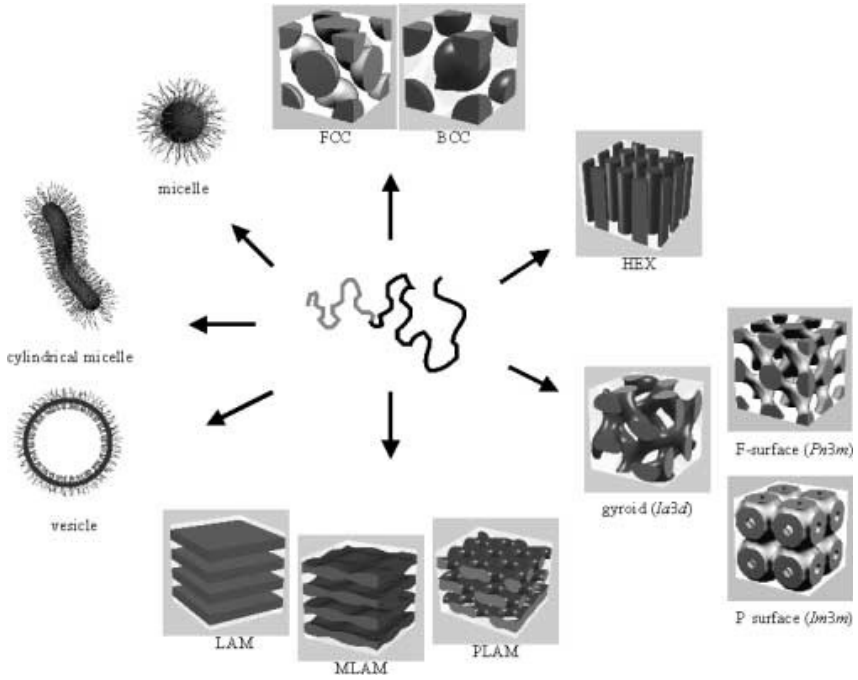


Figure 3: Self-organized structures of amphiphilic block copolymers: spherical micelles, cylindrical micelles, vesicles, face center cubic (fcc) and body centered cubic (bcc) packed spheres, hexagonally packed cylinders (HEX), various minimal surfaces (area minimizing surfaces such as gyroid, F surface, P surface), simple lamellae (LAM), as well as modulated and perforated lamellae (MLAM, PLAM) can be self-assembled (from Förster et al. [44]).

For biomedical application, concepts using self-assembled structures from amphiphiles have been largely developed in the field of targeted drug delivery [45,46]. For such applications, amphiphiles present the advantages of being soluble in dilute aqueous media, in which the predominant morphologies are spherical or cylindrical core shell micelles and vesicles [47]. Amphiphilic block copolymers are therefore selected for their ability to assemble into micelles or vesicles in order to carry drugs, genes [48] or silencing RNA [49], for example. An illustration of the formation of the vesicular structure subsequent to bilayer formation and closure is given in Figure 4. In addition, chemical modifications of the vesicle outer shell can be performed to tune vesicular properties and to enhance targeting and transport, as illustrated in Figure 5. Lipids, which are the low molecular weight analogues of amphiphilic linear block copolymers, are also considered for such an approach [49-51]. However, due to their low molecular weight compared to block copolymers, to their low stability and to their short-shelf-life, lipid formulations remain problematic [45]. In this context, amphiphilic polymers are of interest due to the higher stability of the resulting self-assembly. Moreover, macromolecular chemistry enables infinite combinations in the design of functional copolymers. Despite these advantages of block copolymers, they remain rarely used [52] due to a lack of FDA (Food and Drug Administration) approval [53], in comparison to the wide use of lipids [54].

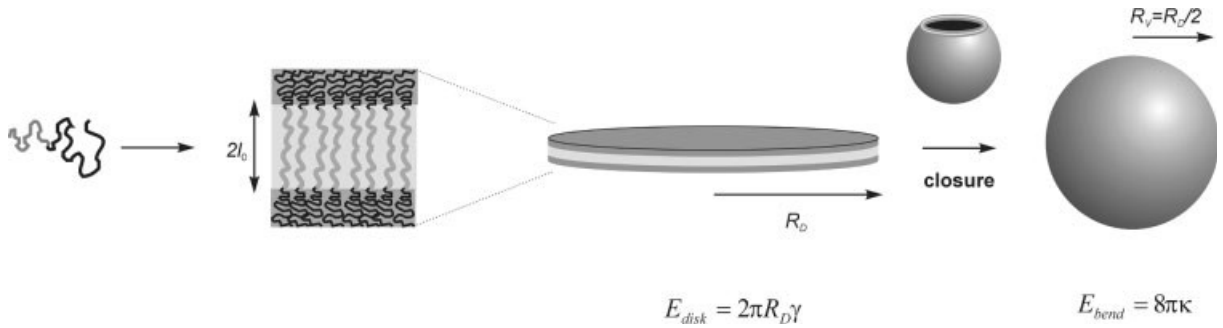


Figure 4: Schematic representation of bilayer formation and closure into self-assemble vesicles, minimizing the free energy of the system. (Antonietti et al. [41])

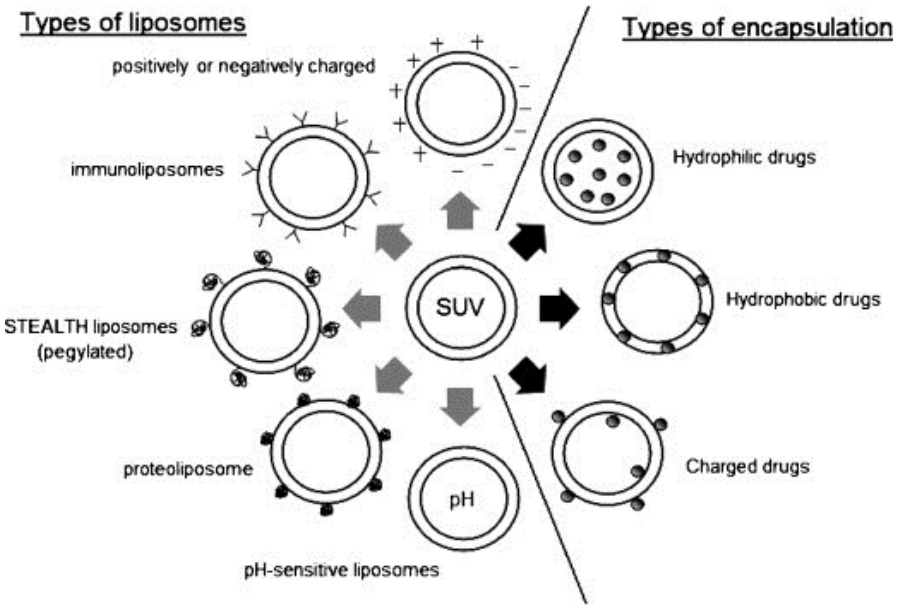


Figure 5: Liposomal drug delivery system: typical strategies (Drulis-kawa et al. [45])

The virtual infinite number of possibilities to synthesize self-assembling and functional polymers for a specific application is the key to their potential uses for biomedical applications. A need for the design of such suitable amphiphilic copolymers has already driven research interests in the field of macromolecular chemistry, synthesis and design of amphiphilic copolymer-based nanocontainers [55] or nanoreactors [56] for drug and gene delivery [57,58] or enzymatic cascade reactions [59].

Scope of the thesis.

There is an evident need to define new strategies for the design of antimicrobial coatings that combat biofilm formation and growth. Basic and applied research therefore remains necessary to develop such suitable surfaces, especially those capable of avoiding initial bacterial colonization. In addition, complementary criteria must be addressed to ensure the design of efficient antimicrobial surfaces: Surfaces must be biocompatible and overcome the issue of coating lifetime. In order to address these requirements, we aimed at producing bioactive surfaces based on the immobilization of polymeric vesicles on surfaces, allowing a combination of passive and active antimicrobial strategies. For this purpose we proposed designing, synthesizing, and using amphiphilic block copolymers capable of inducing both bacterial and cellular responses to create biocompatible and anti-adhesive surfaces. The polymer should self-assemble into structures that can be immobilized on surfaces to produce coatings that can release a controlled amount of drug over time.

Aside from the development and characterization of coatings suitable for antibacterial applications, this work provided the opportunity to investigate several fundamental aspects. Initially, polymer synthesis and characterization of nucleotide-based block copolymers was investigated to elucidate polymer self-assembly in

solution. The nanoreactors were then prepared and their activity studied. Finally, surface immobilization of vesicular structures was carried-out and studied to demonstrate the conservation of vesicular structure upon immobilization. Moreover, we investigated the influence of the chemical, topographical, and mechanical properties of the surface on the number of adherent bacteria as well as on the expression of bacterial adhesion proteins, such as curli.

The manuscript that presents this research is divided into two parts. The first part considers surface preparation and is divided into three chapters. The first chapter presents polymer synthesis and characterization to investigate the self-assembly process of the block copolymer. The second chapter deals with nanoreactor preparation and demonstrates their efficiency. Finally the third chapter presents the characteristic of the different surfaces produced in this study in order to finally graft the polymeric nanoreactors to surfaces while vesicular structure remains unaffected. The second part of this manuscript is dedicated to the study of bacterial adhesion on the surfaces thus prepared and especially to the consideration of the influence of surface properties on bacterial adhesion and curli expression. To this end, the second part of this work is organized around a consideration of the influence of chemistry, the influence of topography and of the surface mechanical properties induced by vesicle structure and shape on bacterial adhesion, both in term of quantity of adherent bacteria and of bacterial curli expression.

References.

[1] J.W. Costerton, G.G. Geesey, K. Cheng, How Bacteria Stick, Sci Am. 238 (1978) 86-95.

[2] J.W. Costerton, Z. Lewandowski, D.E. Caldwell, D.R. Korber, H.M. Lappin-Scott, Microbial Biofilms, Annu. Rev. Microbiol. 49 (1995) 711-745.

[3] J.W. Costerton, K.J. Cheng, G.G. Geesey, T.I. Ladd, J.C. Nickel, M. Dasgupta, Bacterial Biofilms in Nature and Disease, Annu. Rev. Microbiol. 41 (1987) 435-464.

[4] K. Sauer, A.K. Camper, G.D. Ehrlich, J.W. Costerton, D.G. Davies, Pseudomonas aeruginosa Displays Multiple Phenotypes during Development as a Biofilm, J. Bacteriol. 184 (2002) 1140-1154.

[5] M.E. Davey, G.A. O'toole, Microbial Biofilms: from Ecology to Molecular Genetics, Microbiol. Mol. Biol. Rev. 64 (2000) 847-867.

[6] G. Dykes, Planktonic or biofilm growth affects survival, hydrophobicity and protein expression patterns of a pathogenic Campylobacter jejuni strain, International Journal of Food Microbiology. 89 (2003) 1-10.

[7] C. Beloin, J. Ghigo, Finding gene-expression patterns in bacterial biofilms, Trends in Microbiology. 13 (2005) 16-19.

[8] J.B. Kaplan, M.F. Meyenhofer, D.H. Fine, Biofilm Growth and Detachment of Actinobacillus actinomycetemcomitans, J. Bacteriol. 185 (2003) 1399-1404.

[9] L. Ploux, K. Anselme, A. Ponche, Bacteria/material interfaces: role of the material and cell wall properties, J Adhes Sci Technol. in press (2010).

[10] J.W. Costerton, Bacterial Biofilms: A Common Cause of Persistent Infections, Science. 284 (1999) 1318-1322.

[11] I. Ofek, D.L. Hasty, N. Sharon, Anti-adhesion therapy of bacterial diseases: prospects and problems, FEMS Immunology & Medical Microbiology. 38 (2003) 181-191.

[12] K. Vasilev, V. Sah, K. Anselme, C. Ndi, M. Mateescu, B. Dollmann, Tunable Antibacterial Coatings That Support Mammalian Cell Growth, Nano Lett. 10 (2010) 202-207.

[13] X. Xu, Q. Yang, Y. Wang, H. Yu, X. Chen, X. Jing, Biodegradable electrospun poly(l-lactide) fibers containing antibacterial silver nanoparticles, European Polymer Journal. 42 (2006) 2081-2087.

[14] H. Yu, X. Xu, X. Chen, T. Lu, P. Zhang, X. Jing, Preparation and antibacterial effects of PVA-PVP hydrogels containing silver nanoparticles, Journal of Applied Polymer Science. 103 (2007) 125-133.

[15] M. Dathe, Optimization of the antimicrobial activity of magainin peptides by modification of charge, FEBS Letters. 501 (2001) 146-150.

[16] L. Marcotte, H. Therien-Aubin, C. Sandt, J. Barbeau, M. Lafleur, Solute Size Effects on the Diffusion in Biofilms of Streptococcus mutans, Biofouling: The Journal of Bioadhesion and Biofilm Research. 20 (2004) 189 - 201.

[17] L. Marcotte, J. Barbeau, M. Lafleur, Permeability and thermodynamics study of quaternary ammonium surfactants--phosphocholine vesicle system, Journal of Colloid and Interface Science. 292 (2005) 219-227.

[18] L. Marcotte, J. Barbeau, M. Lafleur, Characterization of the Diffusion of Polyethylene Glycol in Streptococcus mutans Biofilms by Raman Microspectroscopy, Applied Spectroscopy. 58 (2004) 1295-1301.

[19] W. Costerton, The application of biofilm science to the study and control of chronic bacterial infections, Journal of Clinical Investigation. 112 (2003) 1466-1477.

[20] A. Smith, Biofilms and antibiotic therapy: Is there a role for combating bacterial resistance by the use of novel drug delivery systems?, Advanced Drug Delivery Reviews. 57 (2005) 1539-1550.

[21] B.A. Jucker, H. Harms, A.J. Zehnder, Adhesion of the positively charged bacterium Stenotrophomonas (Xanthomonas) maltophilia 70401 to glass and Teflon, J. Bacteriol. 178 (1996) 5472-5479.

[22] W. Senaratne, L. Andruzzi, C.K. Ober, Self-Assembled Monolayers and Polymer Brushes in Biotechnology: Current Applications and Future Perspectives, Biomacromolecules. 6 (2005) 2427-2448.

[23] J. Huang, R.R. Koepsel, H. Murata, W. Wu, S.B. Lee, T. Kowalewski, Nonleaching Antibacterial Glass Surfaces via "Grafting Onto": The Effect of the Number of Quaternary Ammonium Groups on Biocidal Activity, Langmuir. 24 (2008) 6785-6795.

[24] J. Vartiainen, M. Rättö, S. Paulussen, Antimicrobial activity of glucose oxidase-immobilized plasma-activated polypropylene films, Packaging Technology and Science. 18 (2005) 243-251.

[25] E. Kenawy, S.D. Worley, R. Broughton, The Chemistry and Applications of Antimicrobial Polymers: A State-of-the-Art Review,

Biomacromolecules. 8 (2007) 1359-1384.

[26] C.H. Kim, J.W. Choi, H.J. Chun, K.S. Choi, Synthesis of chitosan derivatives with quaternary ammonium salt and their antibacterial activity, Polymer Bulletin. 38 (1997) 387-393.

[27] B. Bendinger, H.H.M. Rijnaarts, K. Altendorf, A.J.B. Zehnder, Physicochemical Cell Surface and Adhesive Properties of Coryneform Bacteria Related to the Presence and Chain Length of Mycolic Acids, Appl. Environ. Microbiol. 59 (1993) 3973-3977.

[28] C. Matz, K. Jurgens, Effects of Hydrophobic and Electrostatic Cell Surface Properties of Bacteria on Feeding Rates of Heterotrophic Nanoflagellates, Appl. Environ. Microbiol. 67 (2001) 814-820.

[29] M.C. van Loosdrecht, J. Lyklema, W. Norde, G. Schraa, A.J. Zehnder, Electrophoretic mobility and hydrophobicity as a measured to predict the initial steps of bacterial adhesion., Appl. Environ. Microbiol. 53 (1987) 1898-1901.

[30] T.J. Marrie, J.W. Costerton, Scanning and transmission electron microscopy of in situ bacterial colonization of intravenous and intraarterial catheters., J. Clin. Microbiol. 19 (1984) 687-693.

[31] M. Gyo, T. Nikaido, K. Okada, J. Yamauchi, J. Tagami, K. Matin, Surface Response of Fluorine Polymer-Incorporated Resin Composites to Cariogenic Biofilm Adherence, Appl. Environ. Microbiol. 74 (2008) 1428-1435.

[32] A. Casey, L. Mermel, P. Nightingale, T. Elliott, Antimicrobial central venous catheters in adults: a systematic review and meta-analysis, The Lancet Infectious Diseases. 8 (2008) 763-776.

[33] M.A. El-Harouny, A.A. Zalata, M.E. Naser, H.M. Abo El-Atta, I.M. El-Shawaf, T. Mostafa, Long-term ofloxacin testicular toxicity: an experimental study, Andrologia. 42 (2010) 92-96.

[34] J. Altenburg, C.S. de Graaff, T.S. van der Werf, W.G. Boersma, Immunomodulatory Effects of Macrolide Antibiotics - Part 2: Advantages and Disadvantages of Long-Term, Low-Dose Macrolide Therapy, Respiration. (2010).

[35] G.F. Mehyar, Z. Liu, J.H. Han, Dynamics of antimicrobial hydrogels in physiological saline, Carbohydrate Polymers. 74 (2008) 92-98.

[36] K. Kulthong, S. Srisung, K. Boonpavanitchakul, W. Kangwansupamonkon, R. Maniratanachote, Determination of silver nanoparticle release from antibacterial fabrics into artificial sweat, Part Fibre Toxicol. 7 (2010) 8.

[37] Y. Murali Mohan, K. Vimala, V. Thomas, K. Varaprasad, B. Sreedhar, S. Bajpai, Controlling of silver nanoparticles structure by hydrogel networks, Journal of Colloid and Interface Science. 342 (2010) 73-82.

[38] B. Dizman, M.O. Elasri, L.J. Mathias, Synthesis and Characterization of Antibacterial and Temperature Responsive Methacrylamide Polymers, Macromolecules. 39 (2006) 5738-5746.

[39] J.W. Costerton, B. Ellis, K. Lam, F. Johnson, A.E. Khoury, Mechanism of electrical enhancement of efficacy of antibiotics in killing biofilm bacteria., Antimicrob. Agents Chemother. 38 (1994) 2803-2809.

[40] J.D. Denstedt, T.A. Wollin, G. Reid, Biomaterials Used in Urology: Current Issues of Biocompatibility, Infection, and Encrustation, Journal of Endourology. 12 (1998) 493-500.

[41] M. Antonietti, S. Förster, Vesicles and Liposomes: A Self-Assembly Principle Beyond Lipids, Advanced Materials. 15 (2003) 1323-1333.

[42] J.N. Israelachvili, D.J. Mitchell, B.W. Ninham, Theory of self-assembly of hydrocarbon amphiphiles into micelles and bilayers, J. Chem. Soc., Faraday Trans. 2. 72 (1976) 1525.

[43] P.L. Soo, A. Eisenberg, Preparation of block copolymer vesicles in solution, Journal of Polymer Science Part B: Polymer Physics. 42 (2004) 923-938.

[44] S. Förster, T. Plantenberg, From Self-Organizing Polymers to Nanohybrid and Biomaterials, Angewandte Chemie International Edition. 41 (2002) 688-714.

[45] Z. Drulis-Kawa, A. Dorotkiewicz-Jach, Liposomes as delivery systems for antibiotics, International Journal of Pharmaceutics. 387 (2010) 187-198.

[46] A.S. Ulrich, Biophysical aspects of using liposomes as delivery vehicles, Biosci. Rep. 22 (2002) 129-150.

[47] D.E. Discher, A. Eisenberg, Polymer Vesicles, Science. 297 (2002) 967-973.

[48] D.W. Pack, A.S. Hoffman, S. Pun, P.S. Stayton, Design and development of polymers for gene delivery, Nat Rev Drug Discov. 4 (2005) 581-593.

[49] S. Oliveira, G. Storm, R.M. Schiffelers, Targeted Delivery of siRNA, J. Biomed. Biotech. 2006 (2006) 1-10.

[50] X. Guo, F.C. Szoka, Chemical Approaches to Triggerable Lipid Vesicles for Drug and Gene Delivery, Accounts of Chemical Research. 36 (2003) 335-341.

[51] J.N. Israelachvili, D. Mitchell, B.W. Ninham, Theory of self-assembly of lipid bilayers and vesicles, Biochimica Et Biophysica Acta (BBA) - Biomembranes. 470 (1977) 185-201.

[52] G. Gaucher, M. Dufresne, V.P. Sant, N. Kang, D. Maysinger, J. Leroux, Block copolymer micelles: preparation, characterization and application in drug delivery, Journal of Controlled Release. 109 (2005) 169-188.

[53] M.L. Adams, A. Lavasanifar, G.S. Kwon, Amphiphilic block copolymers for drug delivery, J. Pharm. Sci. 92 (2003) 1343-1355.

[54] T. Lian, R.J.Y. Ho, Trends and developments in liposome drug delivery systems, J. Pharm. Sci. 90 (2001) 667-680.

[55] K. Kataoka, A. Harada, Y. Nagasaki, Block copolymer micelles for drug delivery: design, characterization and biological significance, Advanced Drug Delivery Reviews. 47 (2001) 113-131.

[56] C. Nardin, J. Widmer, M. Winterhalter, W. Meier, Amphiphilic block copolymer nanocontainers as bioreactors, The European Physical Journal E. 4 (2001) 403-410.

[57] V. Balasubramanian, O. Onaca, R. Enea, D.W. Hughes, C.G. Palivan, Protein delivery: from conventional drug delivery carriers to polymeric nanoreactors, Expert Opin. Drug Deliv. 7 (2010) 63-78.

[58] A. Blanazs, S.P. Armes, A.J. Ryan, Self-Assembled Block Copolymer Aggregates: From Micelles to Vesicles and their Biological Applications, Macromolecular Rapid Communications. 30 (2009) 267-277.

[59] D. Vriezema, P. Garcia, N. Sancho Oltra, N. Hatzakis, S. Kuiper, R. Nolte, Positional Assembly of Enzymes in Polymersome Nanoreactors for Cascade Reactions, Angew. Chem. Int. Ed. 46 (2007) 7378-7382.

Part I: Polymers, nanoreactors, and hybridization for controlled surface preparation.

A. *Introduction.*

The antimicrobial surfaces we aim to produce are based on vesicle immobilization on a surface. The choice of vesicle immobilization has been driven by the ability to provide antimicrobial properties in diverse way, as schematized in Figure 6. Designing a polymer that self-assembles in vesicles that possess bacteria-repellent characteristics inherent to the polymer chain properties is an initial way to produce an antimicrobial surface based on vesicular structures. The second strategy consists in designing active antimicrobial systems that result from the self-assembly of a polymer, which does not necessarily possess anti-adhesive properties, into nanocontainers containing an antimicrobial drug that can be released in a controlled way. The third possibility consists in preparing nanoreactors that result from the self-assembly of a copolymer that does not necessarily reveal anti-adhesive properties but drives the production of an antimicrobial substance from an inactive prodrug.

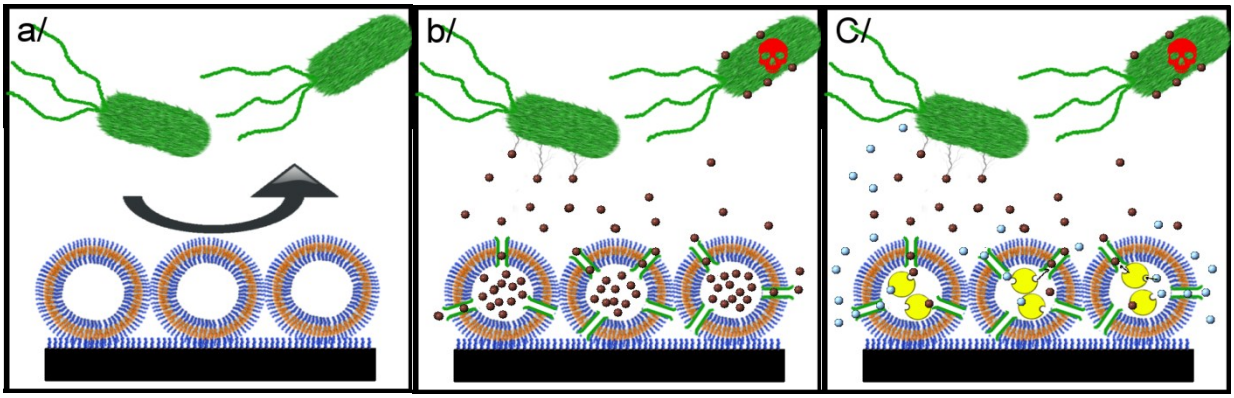


Figure 6: Three possible strategies leading to antimicrobial properties of surfaces based on vesicles immobilization: (a) Vesicles inherent anti-adhesive properties, (b) antimicrobial nanocontainers, (c) antimicrobial nanoreactors.

These three possibilities are not comparable in their efficiencies and limitations. The first possibility, consisting of selecting amphiphilic molecules capable of forming repellent vesicular structures is limited. As in all passive strategies and as discussed in the General Introduction, the spectrum of action (bacterial diversity prevents finding a polymer that acts against all strains) and possible defects and scratches of the surface are large limitation (which may offer anchoring points for bacterial adhesion). In the second strategy, vesicles are used as nanocontainers, encapsulating an antimicrobial drug. Release of the bioactive molecule requires controlled permeability of the vesicle wall. Achieving controlled release is difficult and this strategy leads to a limitation in the size of active molecules to be released. Finally, the third possibility consists in using nanoreactors resulting from the encapsulation of an enzyme in the vesicles (The nanocontainers also display the disadvantage of limited release lifetime). The enzymes enables conversion of an inactive prodrug (Figure 6(c) ─ light blue sphere) into an active antimicrobial substance (Figure 6(c) ─ dark red sphere). The main advantage of this last possibility is avoiding issues concerning both the small and limited capacity of the active agent reservoir and the limited release of active agents through the vesicles shell (for this purpose, the proper selection of the pore molecular weight cut-off enabling nanoreactor permeability for the selected prodrug). Nevertheless, this strategy also has limitations,

since the antimicrobial action will be limited by the rate of diffusion and conversion of the prodrug by an enzyme, which can be too slow to fight primary colonizing bacteria.

To overcome the limitations of the diverse strategies and to combine their advantages, we have chosen to design surfaces compiling active and passive properties. This should allow us to take advantage of polymer repellent properties, while forming antimicrobial nanoreactors as schematized in Figure 7. A surface that combines the inherent anti-adhesive properties of the vesicles with antimicrobial activity of the nanoreactors, should overcome these limitations. Anti-adhesive properties should counter act early bacterial adhesion, leaving time for prodrug diffusion and allowing nanoreactors to then be fully efficient. Possibly adhering bacteria should then be killed by the nanoreactor-produced antimicrobial molecules. With the use of nanoreactors, the system will achieve "smart" behavior by activation as a function of the concentration of the prodrug in the medium, which could result merely by adding a prodrug to the medium.

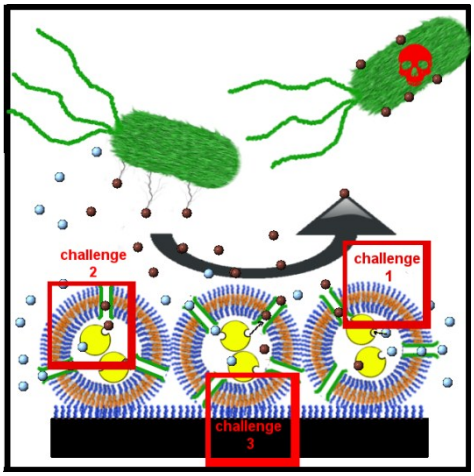


Figure 7: Strategy developed in this study, combining a passive (polymer repellent properties) and an active strategy (nanoreactors) to prevent bacterial adhesion and biofilm formation. Three challenges are highlighted: Amphiphile design (challenge 1), nanoreactor activity (challenge 2) and vesicle immobilization on the surface (challenge 3).

To develop this antimicrobial strategy, three achievements are foreseen. First, the polymer used to self-assemble the nanoreactors is designed according to three criteria: Amphiphile has to be able to self-assemble into vesicular structures, the polymer should bear chemical functions allowing grafting onto the surface, and finally the polymer should allow the formation of bacteria-repellent structures while being biocompatible. To meet this first challenge, we synthesized and characterized the block copolymer poly(butadiene)-block-oligonucleotide, according to the three criteria. This first challenge will be the topic of the first chapter: polymer synthesis and characterization (Chapter 1).

Secondly, nanoreactors assembled from vesicular structures must enable the controlled release of an antimicrobial substance from an inactive prodrug. This release has to be sufficient, stable over time, and of sufficient life time. For this purpose we will assemble nanoreactors from the poly(butadiene)-block-

oligonucleotide block copolymer, encapsulating the lactoperoxidase enzyme, with a channel protein (OmpF) inserted in the vesicular shell providing permeability to the vesicular structure. The preparation and demonstration of nanoreactor function and stability is the topic of the second chapter: Nanoreactor preparation and characterization (Chapter 2).

Finally, the self-assembled nanoreactors need to be immobilized on surfaces. The grafting must be controlled, should allow the retention of the vesicular shape and ensure nanoreactor activity as well as long-term stability to avoid vesicle detachment. For this purpose different surfaces will be prepared on the basis of oligonucleotide grafting approaches, followed by vesicle immobilization through either non-specific interaction or specific oligonucleotide hybridization. The preparation and characterization of the different types of surfaces obtained by these specific or non-specific immobilizations of vesicles will be the subject of the third chapter: Surface preparation and characterization (Chapter 3)

B. *State of the art.*

In this part we will start by looking at current knowledge and definitions related to amphiphilic block copolymers, their properties and routes of synthesis. We will then focus on amphiphilic "chimeras" and especially oligonucleotide-based amphiphilic block copolymers and their applications. Then, as needed for our application, we will focus on nanoreactors, their definition, preparation and limitations. Following this, we will define and describe prodrug-drug systems. Finally, we will describe the different ways to immobilize vesicles and we will focus on the immobilization through oligonucleotide hybridization, which is the technique of interest for the purpose of these investigations.

B.1 Amphiphilic block copolymers, amphiphilic "chimeras" their properties and synthesis.

In contrast to homopolymers resulting from the covalent binding of a single type of monomer, copolymers result from the covalent binding of at least two types of monomers along the same polymer chain. As presented in Figure 8, various chain configurations can be achieved, from alternate to random through linear block copolymers. The macromolecular configuration of interest herein is that of block-copolymers, which consist of at least two homopolymer [1] segments or blocks which are covalently linked. As shown in Figure 9, several architectures might be synthesized, such as linear or star copolymers. The use of block copolymer allows providing different properties to spatially defined parts of the polymer, providing unique properties to the macromolecule such as amphiphilicity [2] or zwitterionic [3] properties.

In this work we consider linear amphiphilic block copolymers. Amphiphilicity is provided when at least two blocks of a copolymer display differing phobicities. The most common approach uses a hydrophilic block that is associated with a hydrophobic block along the same macromolecule [4]. The chemical incompatibility between the monomers drives the self-organization of the copolymers into larger units by the formation of micro-

domains at the nanoscale [5], due to phase separation between the incompatible monomers. This micro-phase separation leads, as explained in the General Introduction, to various self-assembled structures depending on the specific architecture and modes of interaction of the underlying macromolecule. A wide variety of morphologies can be assembled either in bulk or in solution, depending on several parameters and, in particular, on the relative volume fractions of the blocks, leading to structures such as cylindrical or body-centered cubic micellar structures [6].

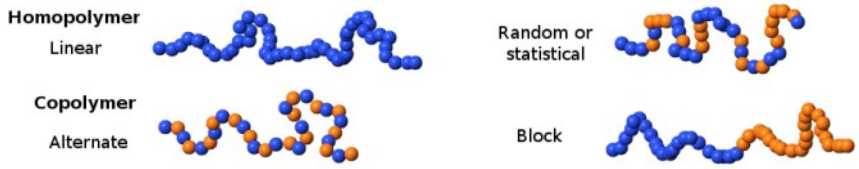


Figure 8: Scheme of the different chain configurations achievable by copolymer synthesis.

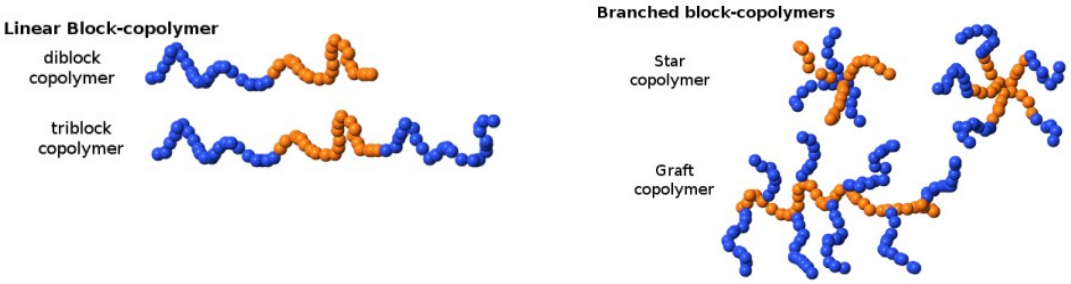


Figure 9: Possible macromolecular architectures of block copolymers.

In the present study we consider the coupling of an oligonucleotide as the hydrophilic block and poly(isobutylene) as the hydrophobic block to obtain an amphiphilic diblock copolymer. When one of the building blocks of the copolymer is based on biological macromolecules, the block copolymer is qualified as a "molecular chimera". The concept of "molecular chimeras," also called "hybrids," was introduced by H. Schlaad et al. [7] to define block copolymers composed of both synthetic and amino acid segments. This "molecular chimeras" were the first type of macromolecules combining the advantages of synthetic polymer (protein repellent properties as due to steric hindrance induced by non-charged macromolecules or hydrophobic properties, such as for poly(butadiene)), with the properties of biomolecules [8] (molecular specific recognition or biological function, for example). This term was extended to polymers combining synthetic and biological blocks [9], the latter including e.g. proteins [10] or DNA/ RNA [11].

Control over the synthesis is required to produce amphiphilic block copolymers with specific self-assembling properties. The covalent linkage between two blocks of opposite polarity is the major problem in the synthesis of amphiphilic block copolymers. Two main routes [2] of block copolymer synthesis can be distinguished.

The first possibility consists in synthesizing the block copolymer in a good solvent (solvent medium able to fully solubilize the macromolecule), growing each block sequentially from a precursor, which is also called an initiator. Several synthesis routes have been published, including macroinitiator polymerization [12] (polymerization initiated from a macromolecule), coupled polymerization ROP/ATRP [13] (ring opening polymerization/atom transferred radical polymerization) or homopolymer coupling [14]. These synthesis routes allow the control of block length, control of polydispersity and a wide variety of polymer compositions by using various monomers (methylmethacrylate, butadiene, as examples). In this approach, the major difficulty is the solubilization of monomers or homopolymers, since, due to copolymer amphiphilicity, both blocks display opposite polarity and are not always soluble in a common solvent. To overcome this, techniques such as micro and mini-emulsion can be considered [15]. They consist of stabilizing an emulsion of two non-miscible solvents, each solvent containing a monomer or homopolymer, while the reaction, or coupling, occurs at the solvent-solvent interface.

The second route is solid phase synthesis. Block copolymer solid phase synthesis consists in synthesizing the first block on a solid support or a porous resin, and then synthesizing or grafting the second block to the surface-synthesized homopolymer [16]. This technique has several advantages over coupling in solution, such as eliminating solvent incompatibility issues [17]. However, this synthesis can be limited by the diffusion of the reactants, limiting the use of porous solid beads, for example, to low molecular weight block copolymers (10 000 g/mol) [18].

Amphiphiles based on DNA fragments or nucleotide sequences were first reported by Mirkin [19], Jeong and Park [20]. Thoseamphiphiles, based on lipids coupled to single stranded DNA, were first synthesized to improve hybridization processes in applications such as biosensing [21,22]. Subsequent to these, investigations on block copolymers composed of at least a synthetic block and a DNA strand emerged. Such block copolymers can self-assemble into core-shell particles. For this purpose Kataoka et al. focused on coupling a hydrophilic synthetic block to single stranded DNA, using DNA hybridization to form the core [23]. On the other hand, some other groups, e.g. Hermann et al., focused on the synthesis of DNA-based and oligonucleotide-based amphiphiles by coupling a hydrophobic block to the biological moieties [24-28]. For this purpose, different synthesis strategies were developed using the formation of an amide [29] or disulfide bond [30] and Michaelis addition [30] to coule synthetic block and the oligonucleotide.

In the present work we used the formation of an amide bond to couple a hydroxyl terminated oligonucleotide to an amino-terminated hydrophobic polymer synthesized on a solid support, as reported by Teixeira et al. [29]. The incompatibility between both blocks does not allow solubilization in a common solvent. Since solid phase synthesis can be adapted to the synthesis of amphiphilic “chimera” [31,32], the coupling of nucleotide sequences with synthetic poly(isobutylene) was performed by solid phase synthesis on porous phosphoramidite. We are therefore limited to synthesis of small nucleotide-based amphiphiles (10 000 g/mol maximum).

Amphiphilic "chimeras" based on oligonucleotides or DNA form a wide variety of structures – mainly micelles [33] but also micellar tubes [11] and vesicles [29] – driven by either the hydrophobic to hydrophilic balance or oligonucleotide hybridization properties. Those block copolymers were developed for various applications, for example to template inorganic compound synthesis [25], to produce biosensor and gene microarrays [21,22] and pootential drug delivery systems [33-40]. For the latter purpose, the use of block copolymers in general has been widely investigated [40-42] and recent developments in the preparation of nanoreactors have driven interests in using amphiphilic "chimera" to provide biocompatibility, cellular response and targeting properties to the nanoreactors [43] assuming that the biological function of biological sequences is retained upon chemical modification and subsequent self-assembly.

B.2 Nanoreactors: Definition, description and limitations.

Nanoreactors are defined as nanoscale devices that permit a chemical reaction to take place *in situ*. This concept is widely used for the synthesis of nanoparticles [44] by providing a nanoscale reactor to template the chemical reaction (and then template nanoparticle size and shape). Another use of the concept of nanoreactors is the mimicking of biological functions by filling the aqueous pools of vesicular structures with active biological substances such as enzymes [45]. Since they remain stable over weeks, polymeric vesicles are particularly suited for this purpose [46]. Moreover, the versatility of polymer chemistry enables specific modification to mimics biomembranes. Enzyme encapsulation in polymeric vesicles to produce nanoreactors was mainly developed by the groups of W. Meier [47-50] and J. Van Hest [51-55] within the last decade [56]. All of those studies established the proof of concept [52], but also demonstrated the efficient activity of nanoreactors along with protection of the encapsulated enzyme [46]. They also demonstrated the possibility of replacing deficient biological systems [57] and performing multi-enzymatic cascade reactions by co-encapsulation of several enzymes [51]. Moreover these studies allowed the determination of the critical factors leading to efficient encapsulation [46,48], and enzyme activity retention [55] as well as the definition of the limitations of polymer self-assembly to design such devices, such as the permeability issues [54-58].

To facilitate efficient encapsulation, the ratio between the size vesicle and enzyme is the critical factor. For this purpose, the block copolymer length, which will affect the size of the vesicle, is critical. It is assumed that increasing vesicles diameter to encapsulate an enzyme [45] of given molecular weight will allow improving the encapsulation efficiency. For this purpose, the synthesis of rather large block copolymers that can self-assemble in large vesicles is a good strategy. In this work, we did not optimize our system based on this assumption, because the chemical route does not allow the synthesis of large macromolecules (larger than 10 000 g/mol). Nevertheless, selection of the right-sized enzyme to be encapsulated enabled achieving the encapsulation efficiency.

Considering nanoreactor activity [59], the enzyme activity is the critical factor. For this purpose, the selection of an enzyme with a high substrate-to-product conversion is important. Moreover the interaction of the

enzyme with the polymeric shell can be dramatically detrimental in terms of reducing enzyme activity. Unfortunately, no global rules exist for optimization and experimental assay are the only way to ensure enzyme activity upon encapsulation.

Finally the permeability of the polymeric shell is the critical limitation in the design of polymeric nanoreactors encapsulating biologically active material. The permeability has to be sufficient to avoid any diffusion-limited activity of the enzymatic process, whereas the nanoreactors have to retain the encapsulated enzyme. For this purpose the two groups previously mentioned developed different approaches. J. Van Hest et al. developed block-copolymers that self-assemble into vesicles for which the permeability is inherent to the composition of the macromolecule [54] (steric hindrance due to lateral cycle of poly(styrene) is at the origin of the permeability). This nanoreactor design is illustrated in Figure 10. The second approach was developed by the group of W. Meier. Due to the low glass transition temperature (T_g) of the hydrophobic polymer segment composing the self-assembling copolymer, naturally occurring bacterial channel proteins can be functionally incorporated in the polymer shell to ensure diffusion of solute through the pores [46]. Such functional nanoreactors are illustrated in Figure 11. In this study we will follow the approach of the group of W. Meier. This approach is suitable for our purpose, since it allows higher flexibility in the selection of the block copolymer hydrophobic block [45], whereas the approach of J. Van Hest is limited to a few hydrophobic blocks such as a poly(styrene) based copolymer [53], which provide sufficient steric hindrance to induce vesicular shell permeability.

The possibility of selecting a hydrophobic polymer with a low glass transition temperature is a key step to pore integration and also for the selected synthesis route on a solid support, for which a hydrophobic block with a high glass transition temperature and/or high steric hindrance, such as poly(styrene), will not diffuse through the pores of the resin and will decrease the reaction yield.

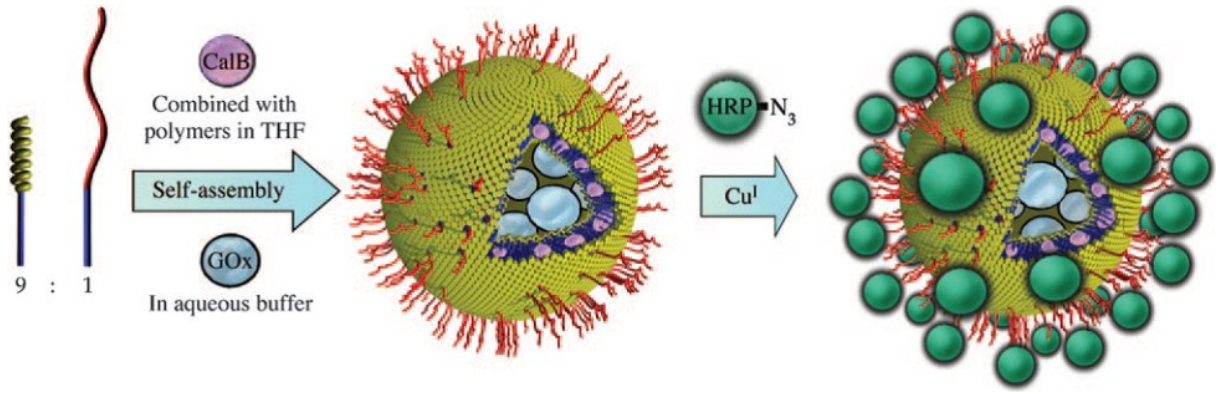


Figure 10: Nanoreactor made of polystyrene$_{40}$-b-poly(lisocyanoalanine(2-thiophen-3-yl-ethyl)amide)$_{50}$. The activity is achieved by encapsulating two enzymes in the polymersome and a third is grafted to the polymeric external shell. Permeability is ensured by the inherent permeability of the polymer self-assembly (from Vriezema et al. [53])

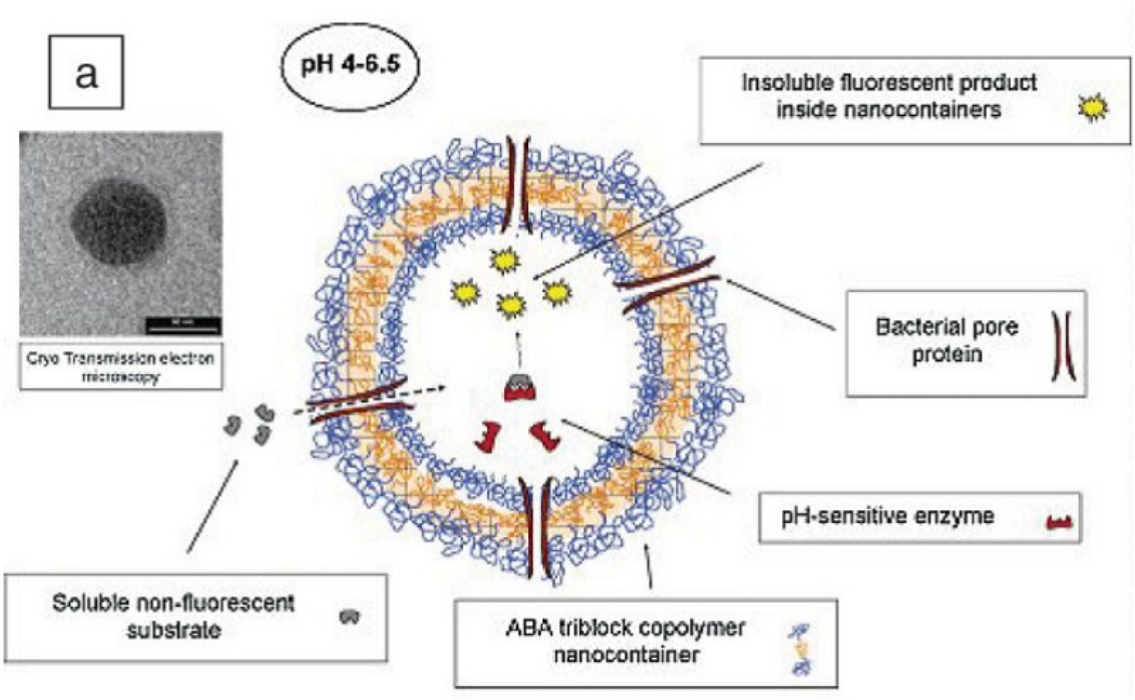


Figure 11: Schematic illustration of enzymatic nanoreactors based on the incorporation of pores in the polymeric shell. The activity of the nanoreactor is demonstrated by the enzymatic reaction of the non-fluorescent substrate yielding an internalized fluorescent product. The process is allowed due to substrate permeability, ensured by bacterial pore protein integration in the polymeric membrane. (From Broz et al. [59])

The functional embedding of bacterial pores in the vesicular shell is not yet fully understood. It has been observed experimentally that the size of the hydrophobic block composing the self-assembling copolymer should match the size of the hydrophobic domain of the pore protein. Furthermore, the glass transition temperature of the polymer segment must be low, allowing flexibility of the membrane so as not to disturb the functional structure and dynamics of the protein (as illustrated in Figure 12). The insertion efficiency depends on the combination of flexibility and length of the hydrophobic block [45].

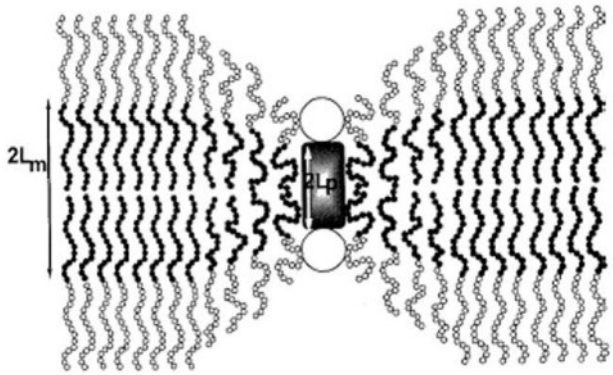


Figure 12: Conformation of AB diblock copolymer chains in the vicinity of a protein inserted in a polymeric bilayer. A match of protein height, in this case half the thickness of the membrane, is easily achieved through polymer chain stretching (From Kitatokarczyk et al [45])

The most widely used membrane protein to induce permeability of self-assembled vesicular structures is the bacterial pore OmpF. OmpF is an *Escherichia coli* membrane channel composed of a trimer of proteins. This trimer forms a fully opened channel with a M_w cut-off of 600 Da for globular molecules, i. e. the minimal pore size is 7−11 Å. The channel has a hydrophobic domain of 23.7 ± 0.9 Å, as illustrated in Figure 13.

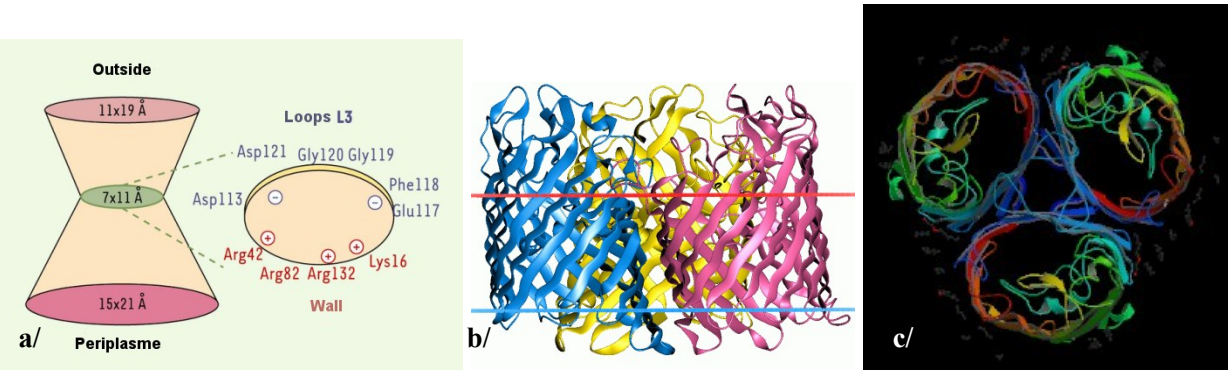


Figure 13: (a) OmpF typical shapes and sizes.The restrictive area in the center of the channel and the charged amino acids present in this domain are labeled. (b) Side view of OmpF trimer. The blue line shows the position of bacterial membrane inside, whereas the red line shows the position of the external side of the membrane. (c) Front view of the OmpF trimer. Pictures adapted from http://opm.phar.umich.edu/protein.php?pdbid=1hxx (September 2010)

Therefore, we designed nanoreactors incorporating OmpF pores in the shells of self-assembled vesicular structures. Encapsulation of active enzymes has been described in the literature for chemical reactions [49], cascade chemical reactions [52] and antioxidant functions [58]. To reach our specific goal we will adapt this approach to produce an antimicrobial compound that is released subsequent to the enzymatic reaction with a prodrug. For this purpose we will integrate a prodrug-drug enzymatic system into a nanoreactor. As a first step, a description of such a system is needed.

B.3 Prodrug-drug system.

The concept of prodrug therapy emerged in the 80s with the improvement of cancer therapy [60]. Drugs used in chemotherapy are highly toxic, and therefore they are not administered directly but as inactive precursors (prodrugs). In this therapeutic strategy, the conversion of the prodrug into the drug [60-62] is ensured by an enzyme which is part of the targeted cell metabolism [63]. For example, enalapril is converted by esterase to the active enalaprilate, which is an angiotensin converting enzyme (ACE) inhibitor, used in the treatment of hypertension and some types of chronic heart failure [64]. Recent improvements have been obtained with respect to prodrug design in targeting a specific enzyme as a converter [65].

During the last ten years, the concept of prodrug systems was used to fight resistant bacteria [66]. In these new developments, the idea was to exploit the activity of β-lactamase, an enzyme produced by bacteria such as

the multi-resistant *Staphylococcus aureus*. An inactive prodrug was synthesized by organic chemistry to be a substrate of β-lactamase that will degrade into antibiotics [66] such as a cephalsporin-taxol [67] combination. β-lactamase is not the only enzyme used in antimicrobial strategy. Other natural enzymatic systems have also been used as prodrug-drug systems and have been demonstrated as efficient in antimicrobial applications [68]. For example a wide range of peroxidases, such as salivary peroxidase [69], have been shown to possess antimicrobial activity. Among those, the milk-associated protein, lactoperoxidase, has been widely studied and is currently recommended as a preservative of milk [70-73].

Lactoperoxidase, which is naturally present in bovine milk, has antimicrobial activity when associated with the prodrug, thiocyanate. This system has been intensely studied [72,74-76]. The inactive thiocyanate is oxidized to the antimicrobial hypothiocyanate by lactoperoxidase in the presence of hydrogen peroxide as a cosubstrate. The process is schematized in Figure 14. Finally the lactoperoxidase system is known to be non-species selective. All bacteria, gram negative and gram positive, are sensitive [77]. It was further demonstrated that the lactoperoxidase-thiocyanate system does not induce resistance in the treated strains [78]. Due to its close similarity to the peroxidase-thiocyanate system naturally present in saliva and lungs [69], lactoperoxidase is not toxic to mammalian cells [79].

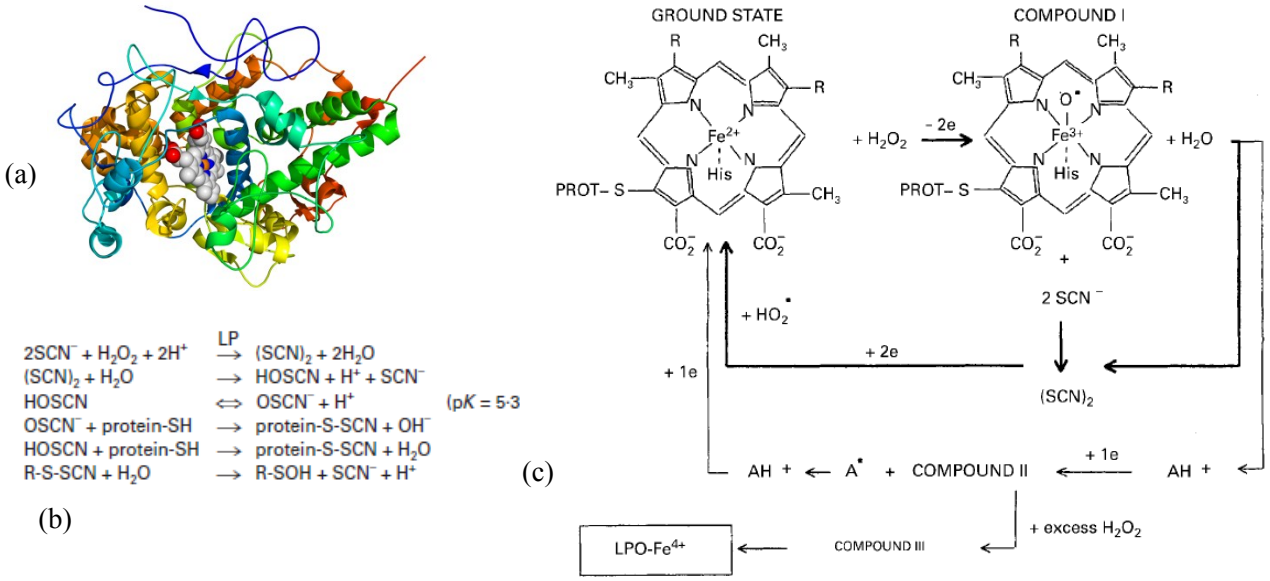


Figure 14: Lactoperoxidase structure and the prodrug-drug system mechanism. (a) Structure, (b) Details on the antimicrobial action of the lactoperoxidase (LPO) system due to the oxidation of the sulphydryl group of the enzyme, catalysed by LPO and mediated by oxidation products of SCN_2. (c) Pathways of the lactoperoxidase-catalysed reaction mechanism, mediated by the ferrous complex core of the lactoperoxidase (a from Singh et al. [80], b and c from Kussendrager et al. [81])

Such a system is therefore of great interest for our application. Lactoperoxidase can be encapsulated in vesicular nanoreactors, while the prodrug (thiocyanate) and the cosubstrate (hydrogen peroxide) should be delivered in the aqueous surroundings as inactive compounds. The nanoreactor would then convert thiocyanate into the active hypothiocyanate, which is antimicrobial or bacteriostatic, depending on the concentration [72].

Considering the use of nanoreactors grafted to surfaces, we will thus have a relatively high concentration of active molecules close to the surface, while the rest of the environment would mainly contain only inactive prodrug. This should allow tighten control of the treated location, limited immune response and limited bacterial flora elimination or resistance mechanisms activation for *in vivo* applications. Since *in vivo* application is beyond the scope of this thesis, we will only demonstrate the encapsulation process and the efficiency of the nanoreactors by enzymatic reaction monitoring, and demonstrate the possibility to tightly graft a layer of vesicles to surfaces.

B.4 Immobilization of vesicles to surfaces: possible strategies.

Vesicle deposition on surfaces is a significant challenge due to the delicate thermodynamic equilibrium that gives rise to the vesicular shape. Indeed, for most polymeric vesicles, vesicular shape corresponds to a kinetically frozen thermodynamic state, meaning that molecular rearrangement due to equilibrium displacement by grafting vesicles onto surfaces should be slow enough to ensure the retention of the vesicular shape in order to provide extended life to the so-produced surfaces. For this purpose, different strategies have been reported in the literature [49,82-85]. One strategy is to use physico-chemical interactions to bind vesicles to the surface [86-88]. Electrostatic interactions are mainly exploited to ensure vesicle adsorption [88]. However, variations in the surrounding medium are likely to affect vesicle/surface interactions, leading to massive release of vesicles [89]. Moreover, precise control of deposition is not straight forward by this approach [90].

The second strategy consists on binding vesicles to the surface by stronger interactions such as covalent binding, protein-substrate binding, antibody binding, or oligonucleotide hybridization [82-84,91]. We have chosen to immobilize vesicle on surfaces by using vesicle/surface interactions strong enough to prevent uncontrolled vesicle release.

Various strategies have been explored to bind vesicles tightly to surfaces and most have concerned liposomes. The first strategy is to create covalent chemical bonding via a chemical reaction between compatible moieties such as benzotriazole carbonate- (BTC) modified lipids that react with primary amines [82]. The liposomes can be grafted to an amino-modified polymer layer previously deposited on the surface [82]. The major issue with this strategy is the difficulty of maintaining vesicular shape throughout the grafting procedure due to the high disturbing effect of the chemical bonding on vesicle thermodynamic stability [92]. Another issue is the difficulty of achieving coupling in aqueous, solvent-free medium, which is necessary to retain the vesicular shape. This constraint further limits possible routes through chemistal bond formation.

Biologically-inspired approaches have also been proposed to achieve strong vesicle/surface binding. Binding properties of antibodies [83], proteins [91] and DNA [84] have been considered in particular. Antibodies were mainly used to prepare immunoliposomes for biosensing applications in which the antigen of interest is targeted by the immunoliposome carrying the suitable antibody [83]. Immunoliposomes were produced for the cell receptor targeting properties [93]. Protein binding properties have already been investigated to graft vesicles,

liposomes, and nanoreactors for various applications such as biosensing [94] and drug delivery [91]. Biotin–avidin binding has mainly been used for this purpose. This approach is illustrated in Figure 15, from Grzelakowski et al. [49]. This technique was widely applied in conceptual studies, but the stability of the binding system is an issue that limits its use to *in vitro* applications.

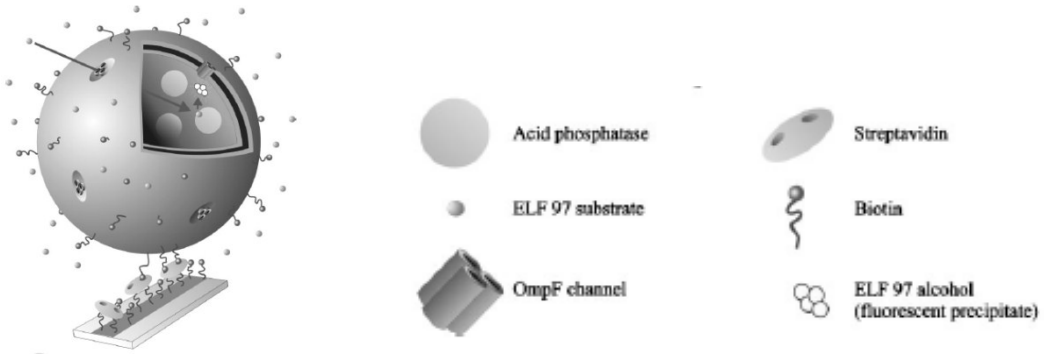


Figure 15: Schematic representation of the immobilization of a nanoreactor system on a glass surface. The biotinylated vesicles were immobilized on a glass surface previously coated with streptavidin patterns through biotin-streptavidin interaction. [49].

Single stranded oligonucleotides and DNA have also been used for vesicles immobilization. The technique consists on grafting vesicles through oligonucleotide hybridization and has been investigated in recent years to develop liposome-based nanosensors [95]. The main advantage of this technique is the specificity of oligonucleotide hybridization, allowing tight control of vesicle deposition. The control is obtained by modulating the position and density of the grafting of the complementary strand. This strategy is illustrated in Figure 16, which is taken from Yoshina-Ishii et al. [84]. This possible control of the grafting, combined with the obvious relevance of such a technique when working with polymer-oligonucleotide copolymer based vesicles, is influential in our choice of this strategy.

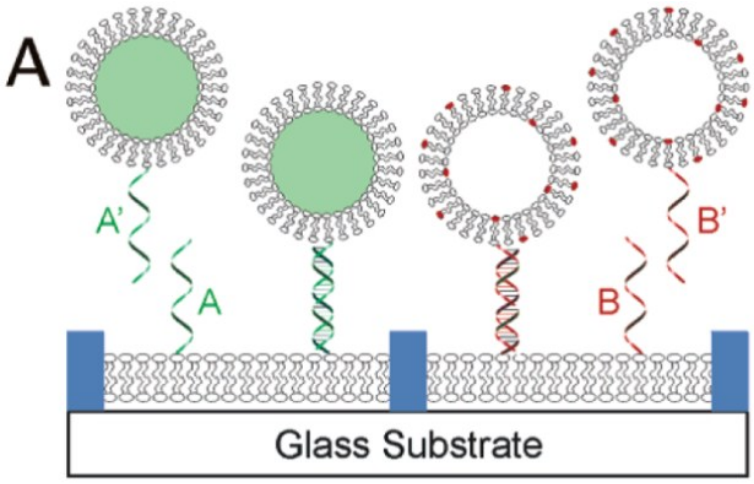


Figure 16: (A) Schematic diagram of liposomes that display differing oligonucleotides (denoted A', green content labeled, and B', red lipid labeled) on their lipid headgroups and tethered to complementary sequences (denoted A and B, respectively) displayed on a fluid-supported lipid bilayer formed on a patterned surface [84].

B.5 Oligonucleotide hybridization.

Oligonucleotide hybridization is a natural process that plays a key role in living cells by guaranteeing genome conservation. Hybridization of oligonucleotides is involved in the formation of a doubled stranded helix by non-covalent Crick-Watson base pairing (i.e. hydrogen bound formation between cytosine and guanine and between thymine and adenine as illustrated in Figure 17). This process provides strong binding similar to reversible covalent bonding [96]. This strong binding is assured by base pairing in water-based medium. Crick Watson base pairing is the most energetically favorable pairing process compared to non-Crick-Watson base pairing (i.e. involving paring different from Crick-Watson base pairing, such as guanine-guanine pairing in guanine quadruplex [97]). Crick-Watson pairing is involved in DNA, RNA and oligonucleotides. This binding involves oligobases specifically interacting through hydrogen bonding. This specificity allows the design of oligonucleotides that display a low probability of mismatch pairing [95]. It is therefore of interest to induce, in our case, a tight control of vesicle immobilization on surfaces.

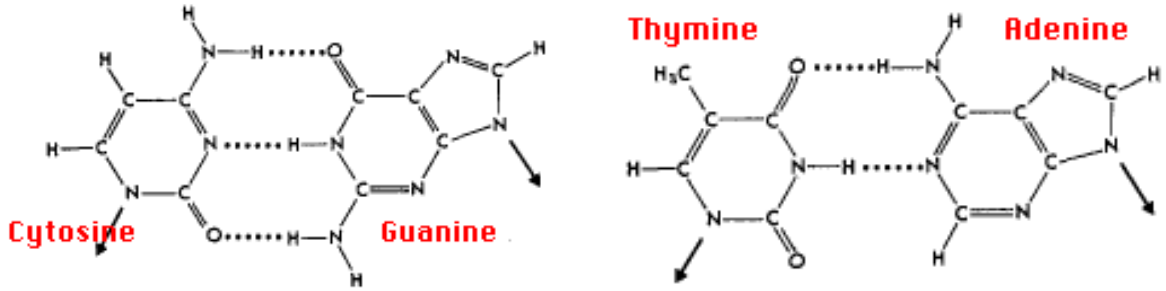


Figure 17: Oligobases and their specific base pairing. (From http://www.bio.miami.edu/~cmallery/150/gene/BasePairing.gif, September 2010)

Additional unspecific modes of interactions such as guanine quadruplex formation or Hoogsteen pairing [98] are involved in DNA recognition properties. Depending on the sequence composition, DNA fragments can therefore adopt various chain conformations such as linear or hairpin-like structures driven by self-hybridization [99]. These unique molecular recognition properties of DNA currently focus research efforts toward potential applications such as DNA templated synthesis [100,101], biosensor technology [102], recognition systems and nanodevices [103,104] as well as human therapy [105,106]. Mismatch pairing such as Hoogsteen pairing [107], G-quartet formation [97], etc. can also be of interest to graft vesicles onto surfaces and are studied in general for their lower energy barrier.

Hybridization between oligonucleotides of the vesicular shell and oligonucleotide- modified surfaces is a promising strategy to perform strong, specific and controlled immobilization of oligonucleotide based vesicles on surfaces through specific hybridization between the complementary strands. Moreover, mismatch pairing can be

used to study the influence of surface properties and topography for a fundamental understanding of bacterial adhesion on these surfaces, as discussed in Part II.

B.6 Vesicles mechanical properties.

Visco-elastic properties of polymer vesicles have been discussed in the literature [108-112] on the basis of experimentation [110], simulation [108] and in analogy with liposomes [113]. These properties depend on the polymer constituting the vesicular shell but some general rules could be highlighted. In the case of a block copolymer made from a hydrophobic block with a low glass transition (below 0 °C), the vesicular shell displays intermediate properties between a solid shell and a fluid membrane [114], being the elasticity close to that observable in a fluid-lipid membrane. Elasticity of polymersomes has been investigated by several authors [109,115], in particular B.M. Discher [110], who investigated poly(ethylene)-block poly(ethylene oxide) vesicle shell elasticity. Due to this elasticity, interaction of vesicles with either a surface or a bacterium should induce a deformation of the self-assembled membrane. The pseudo-fluidic response of vesicles upon interaction with planar surfaces has been discussed by Lipowsky [108] who proposed, on the basis of simulations, different scenarios of shape transformation assessed by a change in area at constant volume (Figure 18) observable through micropipette aspiration experiment as described below. Moreover, polymeric vesicles are structures self-assembled in solution and, due to this mechanism of formation, a high softness and shape fluctuation of the vesicular membrane should be expected [108,116]. Such softness and shape fluctuation is classically observable in vesicular solution by the formation of ellipsoid and tube-like vesicles [41]. The nanoreactors of the present study are based on a block copolymer of low glass transition hydrophobic block. Unique mechanical properties are therefore expected, providing a soft, viscous, hydrated and pseudo-fluidic shell at the surface/liquid interface.

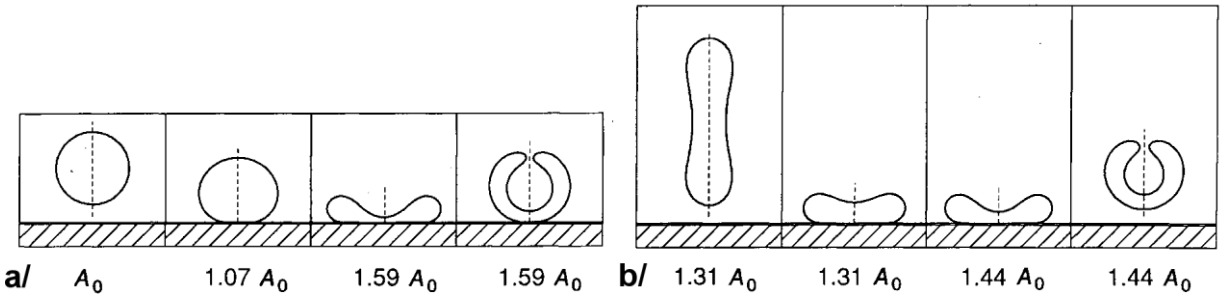


Figure 18: Possible shape transformations of a vesicle interacting with a planar surface. These transformations are induced by a change in area at constant volume. The initial state is a sphere with an area of A_0. (a) and (b) sequences corresponding to two different contact potentials resulting from differing interaction strengths between vesicles and the surface. (From Lipowsky [108])

Those vesicular properties can be assessed by different techniques. For micrometer scale vesicles, micromanipulations consist on aspiration of vesicles into micropipettes and measurement of the vesicular shell area variation. This assay leads to the determination of the bending and expansion modulus [110]. In the case of nanometer scale vesicles, visco-elastic properties are rather determined by indirect methods such as dissipative

quartz microbalance (QCM-D). Using a model to describe visco-elastic properties of a polymer layer at a fluid-solid interface, the dissipative properties of a layer of vesicles deposited on a surface can be estimated. Voigt-Voinova model [117] provides the determination of the layer surface viscosity [118] and shear modulus [117]. The determination of those parameters with the QCM-D was discussed by Reviakine et al. [119,120] who demonstrated the impact of these visco-elastic properties on QCM-D response, leading to the determination of layer viscosity, elastic modulus, thickness and density. We have used this approach in the present study.

C. *Materials and methods.*

C.1 Oligonucleotide-based amphiphilic block copolymer synthesis.

C.1.a Materials.

The various nucleotide strands (desalted purity grade) used in the present study are listed in Table 1. They were purchased from Microsynth Laboratory (Balgash, Switzerland).

shortcut	Strand	Modification
(G_7A_5)-resin	5'-GGGAGAGAGAGA-3'	**5': Carboxy-C9-** **3': linked to phosphoramidite resin**
(A_5G_7)-resin	5'-AGAGAGAGAGGG-3'	**5': Carboxy-C9-** **3': linked to phosphoramidite resin**
(T_5C_7)-resin	5'-CCCTCTCTCTCT-3'	**5': Carboxy-C9-** **3': linked to phosphoramidite resin**
(C_7T_5)-resin	5'-TCTCTCTCTCCC-3'	**5': Carboxy-C9-** **3': linked to phosphoramidite resin**

Table 1: Modified oligonucleotides used in this study.

The chemicals used for synthesis, dichloromethane (DCM) (IR spectroscopy grade) and N,N′-diisopropylcarbodiimide (DIC) (≥98.0% pure) were purchased from Fluka (Buchs, Switzerland). Ammonium hydroxide (28% NH_3 in H_2O) was purchased from Sigma-Aldrich (Schnelldorf, Germany).

The synthetic block, amino terminated poly(isobutylene) was provided by BASF (Ludwigshafen, Germany) with molecular weight, Mw = 1742 g/mol and polydispersity index, PDI < 1.17. Amino-terminated poly(butadiene) was produced according to the one-pot synthesis route reported by S. Nosov et al. [121] was kindly provided by A. Müller. This synthesis route yields quantitative amounts of amino-terminated 1,4-poly(butadiene), with a narrow molecular weight distribution (molecular weight, Mw = 3554 g/mol. Polydispersity index, PDI < 1.10).

C.1.b Solid phase synthesis.

The grafting of the polymer to the nucleotide sequence follows the route previously published by F. Teixera et al. [29]. Briefly, the nucleotide sequences terminated by a carboxylic group at their 5'-ends are linked to a phospharamidite resin through their 3'-ends. The solid-supported nucleotide sequences are mixed in a dichloromethane (DCM) organic solution of the amino modified hydrophobic polymers. The reaction is performed in the presence of N,N′-diisopropylcarbodiimide (DIC), an activating agent for the formation of the peptide bond between both blocks. Subsequent removal of the non-reacted amino-modified polymers is easily performed by washing the resin with DCM. Finally, a cleavage step performed in an alkaline medium releases the oligonucleotide-modified polymers and non-reacted DNA fragments. Separation from non-reacted oligonucleotides is thus carried-out by size exclusion chromatography (Sephadex G50, GE Healthcare, Glattbrugg, Switzerland) or by dialysis (Slide-A-Lyzer 10K MWCO Dialysis Cassette, Piercenet, Lausanne, Switzerland).

We synthesized the following four diblock copolymers through this chemical route:
Poly(isobutylene)-block-5'-GGGAGAGAGAGA-3' (PIB_{31}-G_7A_5),
Poly(butadiene)-block-5'-AGAGAGAGAGGG-3' (PB_{65}-A_5G_7),
Poly(butadiene)-block-5'-CCCTCTCTCTCT-3' (PB_{65}-T_5C_7) and
Poly(isobutylene)-block-5'-TCTCTCTCTCCC-3' (PIB_{31}-C_7T_5).

The four copolymers have the same 58% C-G ratio (i.e: guanosine and cytosine content to total composition ratio) and are composed of hydrophobic polymer segments of low glass transition temperature (245 K for PB and 208 K for PIB).

C.2 Chemical analysis of the diblock copolymer.

C.2.a Nuclear magnetic resonance (NMR).

Liquid and solid state NMR measurements were recorded at room temperature in all cases. For liquid NMR, samples were shaken in deuterated chloroform ($CDCl_3$ 99.8% D, 0.1% TMS, Aldrich, Schnelldorf, Germany) and then filtered through Millipore filter membranes (PTFE 0.45 μm). ^{1}H NMR spectra were recorded with a Bruker DPX-400 spectrometer. The signals were referenced to that of TMS at $\delta = 0.00$ ppm.

Solid-state ^{13}C-NMR was performed on the lyophilized product obtained after dialysis. Cross polarization magic angle spinning (CP-MAS) experiments were performed on a Bruker Avance II 400 spectrometer with a Bruker double channel 4 mm probe. Zirconium rotors were employed at 100.6 MHz using a pulse angle of $\pi/4$, a recycling delay of 60 s, a spin frequency of 4 kHz and high-power proton decoupling during the acquisition.

C.2.b Fourier Transform Infrared Spectroscopy (FTIR).

FTIR measurements were carried out using a single reflection diamond ATR on a FTIR-8400S spectrophotometer (Shimadzu). Spectra were recorded after 96 scans of 2 cm^{-1} resolution.

C.2.c Elementary analysis.

N, H and C content were measured by a combustion method using a LECO CHN-900 apparatus with detection limits of 0.001% (mass) for C, and 0.01% (mass) for N and H.

C.3 UV-Vis spectroscopy for polymer concentration quantification.

Measurements were performed on a Perkin-Elmer Lambda 35 UV-Vis spectrometer. Spectra were recorded between 200 and 400 nm with a slit width of 0.5 nm and a scan rate of 120 nm sec^{-1}. At low concentration, scattering effects were negligible compared to absorption. Absorbance follows the Beer-Lambert law:

$$A = \varepsilon.l.c \quad \text{(Equation 1)}$$

where A is the measured absorbance, ε the extinction coefficient at a given wavelength, l the path length through the solution, and c the concentration of the polymer.

Absorbance was then directly correlated to the concentration of oligonucleotide-modified polymer through a linear regression. Measurements were compared with spectra from the "spectrum prediction tools" developed by A. V. Tataurov et al. [122].

C.4 Self-assembly of the diblock copolymer.

Self-assembly was induced by bulk swelling [45] of 1 mg of the block-copolymer in 1 mL of doubly-distilled water. After shaking for over 24 hours at room temperature, the solutions were clarified to eliminate non-dissolved polymer through filtration with Millipore filters (HN 0.45 µm).

C.5 Self-assembly characterisation and chain configuration.

C.5.a Circular Dichroism Spectrocscopy (CD).

Circular dichroism (CD) spectra (200 − 350 nm) were recorded to determine the impact of polymer coupling on dichroic properties of the polymer-modified nucleotide sequences. Measurements were performed with an Applied Photophysics Chirascan CD spectrometer. Spectra were recorded in doubly-distilled water or NaCl solutions at various concentrations.

C.5.b Transmission Electron Microscopy (TEM).

The samples were examined with a transmission electron microscope (Philips Morgagni 268D) at 293 K. Dispersions of oligonucleotide modified polymers were negatively stained with a 2% uranyl acetate solution and deposited on a carbon-coated copper grid. Analysis without staining was also performed.

C.5.c Scanning Electron Microscopy (SEM).

Solutions of oligonucleotide-modified polymer were deposited on a clean silicon wafer by drop drying. The wafer was then rinsed three times with doubly-distilled water. The surface was coated with 3 nm of sputtered platinum before being examined by SEM (Hitachi S-4800 FEG, Japan) operated at 5 kV accelerating voltage.

C.5.d Dynamic Light Scattering (DLS).

The dynamic light scattering experiments were performed using a commercial goniometer (ALV-Langen, Germany) equipped with a He−Ne laser (λ = 633 nm) at scattering angles between 30° and 150°. An ALV-5000/E correlator calculated the photon intensity autocorrelation function $g^2(t)$ [39]. The samples were prepared by clarifying the solutions through Millipore filters (HN 0.45 μm) into 10 mm quartz cells. These cells were mounted in a thermostated optical matching vat with a temperature accuracy of T = 0.02 K. The experiments were performed at T = 293 K.

Over the course of a DLS experiment, a time decay correlation function is measured, allowing the determination of the cooperative translatory diffusion coefficient D_m at a concentration c:

$$D_m = D_0(1 + k_d c) \quad \text{(Equation 2)}$$

where D_m is a z-averaged cooperative translational diffusion coefficient and k_d the diffusion virial coefficient. The extrapolation to zero concentration yields a diffusion coefficient D_0, which allows the calculation of the hydrodynamic radius R_h via the Stokes−Einstein equation [6].

C.6 Nanoreactor preparation and characterization.

C.6.a Materials.

For the design of polymeric nanoreactors we used the amphiphile PIB_{31}-G_7A_5, which self-assembles into vesicles. We induced porosity in these vesicles by the insertion of bacterial OmpF into the polymeric vesicular shell. The OmpF were produced by the BL21(DE3)omp8 *Escherichia coli* (*E.*coli) strain [123] and purified as described by A. Graff [124]. Briefly, the BL21 (DE3)omp8 *E.coli* strain containing the pGompF plasmid were grown in Luria-Bertani Lysogenic Broth at 37 °C under 250 rpm shaking. After 4 hours, OmpF overexpression was induced by adding IPTG 1mM (isopropyl β-D-1-thiogalactopyranoside). After 6 hours of growth, cell pellets

were collected, cells were lysed and OmpF proteins were collected with 3% octyl-POE (ALEXIS company), yielding a solution of OmpF in 3% octyl-POE, 20 mM NaH_2PO_4 pH 7.3. The concentration was adjusted with 20 mM NaH_2PO_4 pH 7.3 buffer to 1 mg/mL for the stock solution.

Lactoperoxidase (LPO) from bovine milk (lyophilized powder, salt-free, ≥80 units/mg protein, Sigma-Aldrich) was freshly dissolved in sterile NaCl buffer (150 mM) to prepare a stock solution of 10 µM. Tyrosine (reagent grade, ≥ 98%, Sigma-Aldrich) was freshly dissolved to obtain a stock solution of 0.14 mg/mL in sterile NaCl buffer (150 mM). Hydrogen peroxide was diluted as a 16 µM stock solution (stabilized, 30 wt. % in H_2O, Sigma-Aldrich) in sterile NaCl buffer (150 mM). Proteinase K (BioUltra, for molecular biology, ≥ 30 units/mg protein, lyophilized powder, Sigma-Aldrich) was freshly dissolved in sterile NaCl buffer (150 mM) for a stock solution of 20 mg/mL.

C.6.b Nanoreactor preparation.

During nanoreactor preparation, protein insertion, enzyme encapsulation and vesicle formation must be achieved simultaneously. To induce self-assembly of PIB_{31}-G_7A_5, the most efficient technique, which was used in this study, is bulk swelling. Briefly, a 0.3 mg/mL block copolymer solution was obtained by adding 0.3vmg polymer powder to 1 mL of 150 mM NaCl solution containing the 10µM LPO stock solution and 20µL of the OmpF stock solution while shaking for 6 hours at room temperature.

The solution was then filtered three times on a Millex-HV Filter, 0.45 µm (PVDF, 33 mm, sterilized, Milipore). This filtration allowed improvement in the size distribution of the nanoreactors by breaking the existing aggregates, due to bulk swelling, apart.

C.6.c Nanoreactor purification.

At this stage, the suspension of nanoreactors contains non-encapsulated enzymes and non-inserted OmpF. Nanoreactors were separated from non-encapsulated enzymes and non-inserted OmpF by centrifugal filtration. Nanoreactor purification was performed by filtration through centrifugal filtration units (Amicon Ultra-0.5, Ultracel-100 Membrane, 100 kDa, Milipore) with a Mw cut-off of 100 kDa and a spin speed of 4000 rpm. The process is illustrated in Figure 19. Briefly, the solution was placed in the upper part of the centrifugal device. Then, through the centrifugation process, buffer and solute particles of Mw smaller than 100 kDa, i.e. free enzyme, OmpF and surfactant passed through the filter membrane, while bigger objects, such as vesicles and aggregates thereof, stayed in the upper part and were concentrated.

After separation, the content of the upper part (containing the nanoreactors) was adjusted to 500 µl. The whole separation procedure was repeated five times, according to Vriezema et al. [53]. At each separation steps,

the polymer concentration and enzyme activity were determined for both the suspended nanoreactors and the fraction collected at the bottom part of the centrifugal device.

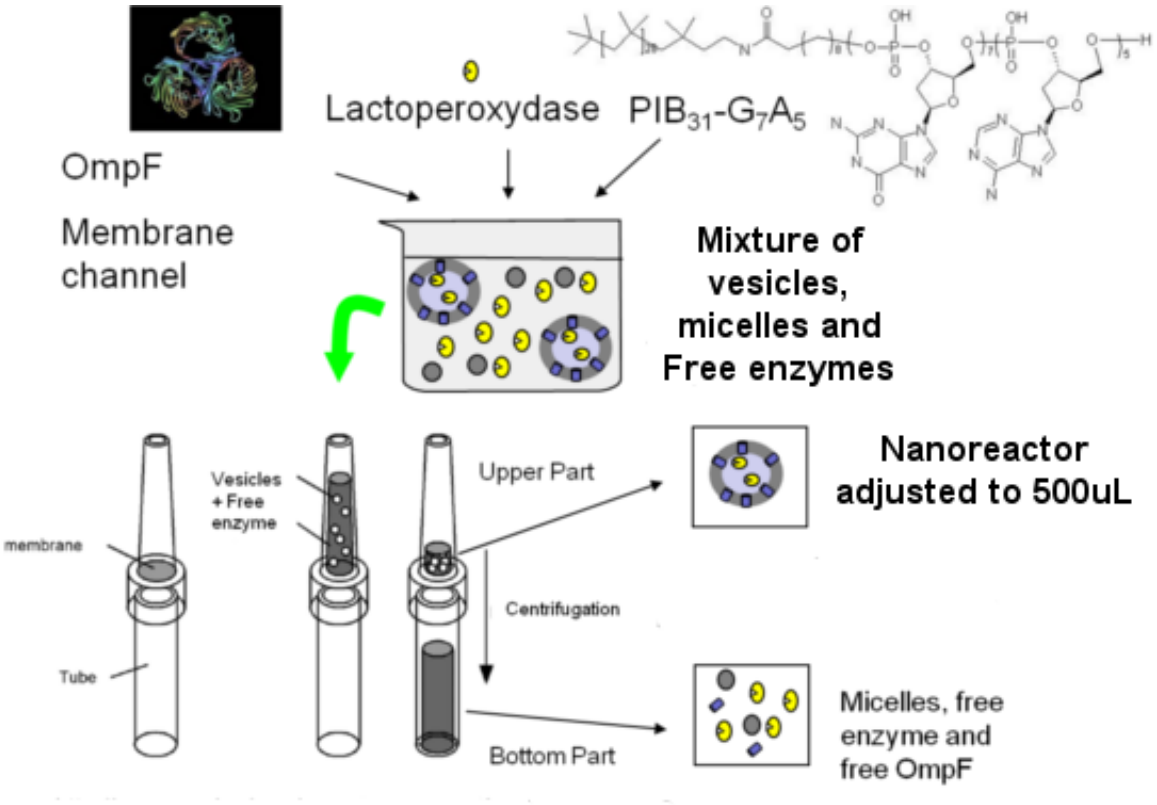


Figure 19: Descriptive scheme of nanoreactor purification using centrifugal devices. (Image modified from: http://pages.usherbrooke.ca/bcm-514-bl/centricon.gif. Of the 5 September 2010)

With this technique, two fractions were collected at each step of the purification: the fraction in the upper part of the centrifugal device, which will be called the nanoreactor fraction and the fraction in the bottom part of the filtration device, which will be called the "other compound" fraction.

C.6.d Other samples and sample names.

In order to evaluate and discuss the quality of purification and the efficient activity of the nanoreactors, two additional samples were prepared. First, the same procedure (shaking + purification) was used to prepare only a pure solution of the free enzyme at 10µM. The second sample consisted of a polymer solution (final concentration of 0.3 mg/mL) that was shaken along with 1 mL of the 10µM stock solution of LPO, 20 µL of a 3% octyl-POE and 20 mM NaH_2PO_4 pH 7.3, leading to the formation of non-porous nanoreactors. Non-porous nanoreactors are not expected to be enzymatically active, since both the substrate and the product cannot diffuse across the vesicular membrane. For clarity in the discussion, the samples used in chapter 2 are described in the Table 2. As described above, the separation is repeated five times. The completely purified nanoreactor solution is then called FPAG1YC5U.

A set of experiments was performed to determine the protective effect of the polymeric shell for the encapsulated enzyme. These assays, including incubation with proteinase K, were performed by mixing 200 µL of solution obtained after purification (FPAG1YC5U, FPAG2YC5U and FREFYC5U) with 50 µL of a 20 mg/mL Proteinase K for 4 h at 37 °C.

Purification step		Sample name		
		Functional nanoreactors	Non porous nanoreactors	Free enzyme solutions
After preparation		OPAG1	OPAG2	OREF
After Millex-HV filtration		FPAG1	FPAG2	FREF
After first separation through centrifugal filtration device	Fraction in upper part (nanoreactor)	FPAG1YC1U	FPAG2YC1U	FREFYC1U
	Fraction in bottom part of device	FPAG1YC1B	FPAG2YC1B	FREFYC1B
After X separation through centrifugal filtration device	Fraction in upper part (nanoreactor)	FPAG1YCXU	FPAG2YCXU	FREFYCXU
	Fraction in the bottom part of the device	FPAG1YCXB	FPAG2YCXB	FREFYCXB
Incubation with proteinase K	From fraction in upper part (nanoreactors) after successive separation steps	FPAG1YCPK	FPAG2YCPK	FREFYCPK

Table 2: Sample labeling at each successive preparation and purification step

C.6.e Polymer and enzyme concentration determination.

Polymer and enzyme concentrations were determined by UV-Vis spectroscopy. Measurements were performed on a Perkin-Elmer Lambda 35 UV-Vis spectrometer. Spectra were recorded between 200 and 400 nm with a slit width of 0.5 nm and a scan rate of 120 nm sec^{-1} in 10 mm quartz cuvettes. As described above, the oligonucleotide concentration linearly follows absorption at 253 nm, which allows an accurate determination of the polymer concentration for dilute solutions. In concentrated solutions, however, scattering effects prevent any linear correlation between the concentration and the absorption. Since LPO absorbs at 280 nm, the presence of the enzyme yields a small contribution to the absorption, easily observable in the free enzyme solution. Nevertheless, the signal associated to LPO is weak compared to that of the nucleotide-based copolymer, which allows the determination of the nanoreactor concentration without significant error.

In order to quantify the enzyme concentrations, absorption spectra at 280 nm were recorded for solutions of free enzyme. However, as evoked above for polymer containing solutions, enzyme absorption was hidden by the high intensity of polymer absorption signals. Therefore, the encapsulated enzyme can be detected by enzyme activity monitoring, and concentration is determined from the Michaelis-Menten kinetics measurement.

C.6.f Enzyme activity monitoring and concentration determination from Michaelis-Menten kinetics measurement by fluorescence spectroscopy.

Two assays were performed: In the first experiment the activity of the LPO was followed by the conversion of tyrosine in dityrosine when H_2O_2 is present as a cosubstrate. Enzyme activity was monitored by mixing 50 µL of nanoreactors or non-porous nanoreactors or free enzyme with 150 µL of H_2O_2 stock solution, 50 µL of the tyrosine stock solution and 200 µL of NaCl buffer (150 mM pH 6.5). The time course of emitted fluorescence signal at 415 nm was recorded with a Jasco F-P-773 spectrofluorimeter (excitation at 316 nm [125]). The assay was conducted for different enzyme concentrations to qualitatively estimate the equivalent concentration based on the activity of the free enzyme and nanoreactors.

The second enzymatic assay aimed to determine the Michaelis-Menten kinetics [126] parameters. In this assay, the reaction speed is determined as a function of the tyrosine concentration varying from 0.014 to 0.049 $mg.mL^{-1}$. This kinetics enables the determination of the enzyme parameter: the affinity constant for the substrate and the enzyme Km, and the turnover constant of the enzyme (i.e. the processing speed of the enzyme) Kcat. Those values are characteristic of the enzyme-substrate system.

The reaction involving one substrate, one enzyme and one product, is is a first order reaction. From this kinetics (Equation 3) we can extract the Michaelis-Menten equation [126] (Equation 4). Knowing the reaction speed (V), using different initial substrate concentration ($[S]_{ini}$), we can determine K_{cat}, K_M and [E] (enzyme concentration) by fitting the obtained hyperbolae, or graphically with the Lineweaver-Burk representation [127].

$$E+S \underset{K_{-1}}{\overset{K_1}{\rightleftharpoons}} ES \xrightarrow{K_2} E+P \qquad \text{(Equation 3)}$$

$$V = \frac{k_{cat}[S]_{ini}}{K_M + [S]_{ini}}[E] \qquad \text{(Equation 4)}$$

The reaction was performed with a fixed value of H_2O_2 (1.6 µM) and the reaction between tyrosine and LPO was considered a pseudo first order reaction due to the fixed value of H_2O_2, allowing the determination of Km, Kcat and concentration. Kinetics parameters were recorded for the free lactoperoxidase at 0.5 µM in NaCl (150 mM, pH 6,5) and for the nanoreactor solution (FPAG1YC5U).

C.7 Vesicle Labeling.

Labeled vesicles were prepared by mixing 0.3 mg PIB_{31}-G_7A_5 bulk polymer with 1 µL of 50 µg/mL Nile Red (Sigma-Aldrich) in DMSO into 1 mL of NaCl buffer (150 mM, pH 6.5). Solution was mixed in a dark flask for 4 hours at room temperature and stored overnight at 4 °C. Vesicle purification was performed through size exclusion chromatography on Sephadex G100 (GE-Healthcare) size exclusion chromatography gel.

C.8 Oligonucleotide modified surfaces.

C.8.a Materials.

3-aminopropyltriethoxysilane 99% (APTES), anhydrous toluene 99%, glutaraldehyde 25% solution grade II, propylamine 98%, formamide were purchased from Sigma-Aldrich, Switzerland. Chloroform 99% was purchased from J. T. Baker, Switzerland. Sodium cyanoborohydrate was purchased from Fluka, Switzerland. Amino-modified oligonucleotides strands (desalted purity grade) used are listed in Table 3. They were purchased from Microsynth Laboratory (Balgash, Switzerland).

Silicon wafers, single-side polished, orientation N/Phos <100>, 525 ± 25 µm thickness, 1-30 Ohm.cm^{-1} resistivity were purchased from Si-Mat Silicon Materials, Landsberg am Lech, Germany. Doubly-distilled water was used for the preparation of all samples.

shortcut	Strand	Modification
(C_7T_5)-NH_2	5'-TCTCTCTCTCCC-3'	**5': NH_2-C_3H_6-** **3': None**
(A_5G_7)-NH_2	5'-AGAGAGAGAGGG-3'	**5': NH_2-C_3H_6-** **3': None**

Table 3: Amino-modified oligonucleotides used in this study.

C.8.b Oligonucleotide self-assembled monolayer (SAM) modified surfaces.

(i) Protocol for "low density" oligonucleotide modified surfaces.

A non-degradative procedure previously described by P. Müller-Buschbaum [128] was chosen to clean the silicon wafers. Polished silicon wafers were cut into pieces of approximately 1 cm by 1 cm. The wafers were ultrasonically cleaned three times in chloroform for 5 minutes and rinsed with chloroform three times. To expose hydroxyl surface groups, samples were activated in an UV/ozone chamber (UV0-cleaner, model 42-220, Jelight Company Inc. USA) for 15 min (step 0).

The grafting followed a procedure modified from that previously published by Y. Jiang et al. [129]: The cleaned wafers were immediately transferred to a 3-aminopropyltriethoxysilane (APTES) 1.0 v/v% toluene solution and incubated for 2 h in a sealed vessel protected from moisture. The samples were then rinsed two times

ultrasonically for 5 minutes in toluene in a waterproofed ware to remove non-covalently bound silane from the surface and rinsed three times with toluene (step 1). According to the procedure described by L. Longo et *al.* [130], the silanized wafers were activated by incubation in a 10 v/v% glutaraldehyde solution prepared in doubly-distilled water (pH 5-6) for 2 h at room temperature and then rinsed three times with water (step 2). The wafers were immersed in a 10^{-8} M solution of the hybridized oligonucleotide (150 mM NaCl, 10^{-4} M ethylenediaminetetraacetic acid (EDTA), pH 5) for 17 h at 4 °C. The oligonucleotide duplex solution was used to ensure that only the NH_2 group at the 5′–end of the oligonucleotide sequence was reacting and linked to the glutaraldehyde modified surface (step 3). The wafers were then immersed in a 0.01 M propylamine solution for 1 h to react with the terminal aldehyde groups which did not react (step 4). Finally, they were immersed under sterile condition in 50% formamide for 1 h to obtain surface functionalization with single-stranded oligonucleotides (step 5). Stepwise characterization was performed in triplicate after each step of the grafting procedure. Samples were stored in sterile buffer (150 mM NaCl, 20 mM phosphate, pH 7.4) at 4 °C until use.

(ii) Protocol for "high density" oligonucleotide modified surfaces.

Surfaces of high grafting density were prepared with the protocol used for preparing surfaces of "low oligonucleotide density", with a modification of the quenching step. To obtain surfaces at high grafting density, sodium cyanoborohydrate was used to reduce the Schiff-base formed between the amino-termination of the oligonucleotide and the aldehyde moiety of the surface [131]. With this reduction, the linkage became irreversible and the grafted oligonucleotides are protected from detachment during dehybridization. Indeed, this release of nucleotide sequences from the surface is probably higher without the use of sodium cyanoborohydrate, due to linkage hydrolysis during the dehybridization step.

Differences between both protocols thus allow obtaining high and low oligonucleotide surface densities, respectively, by using or not sodium cyanoborohydrate.

C.8.c Type of oligonucleotide modified surfaces.

For the preparation of the oligonucleotide self-assembled monolayer (SAMs), A_5G_7 (5'-AGAGAGAGAGGG-3') or the complementary oligonucleotide sequence, i.e. the C_7T_5 (5'-CCCTCTCTCTCT-3') was used. Nucleotide compositions were different, but size, charge and C/G ratio (this ratio defines the quantity of available hydrogen bonds potentially provided by oligonucleotides) were conserved. These two types of oligonucleotide modified surfaces with complementary strands minimize risks of modifying surface properties other than chemistry. In addition, both sequences were grafted at the 5' end, as described above.

This strategy was used to produce the various vesicle-based surfaces for hybridization or mismatch driven immobilization.

C.9 Vesicle modified surfaces.

C.9.a Surfaces on the immobilization of vesicles through nonspecific base pairing.

The preparation procedure for this type of surface is based on non-specific base mismatch pairing, ensuring surface stability. Vesicle-coated surfaces were prepared by deposition of poly(butadiene)-block-5'-AGAGAGAGAGGG-3' (PB_{65}-A_5G_7) amphiphilic block copolymer vesicles [29] onto A_5G_7 (5'-AGAGAGAGAGGG-3') oligonucleotide SAMs.

Deposition was performed by drop evaporation performed twice prior to rinsing with sterile phosphate buffer saline (PBS). The self-assembly was stabilized by UV-induced cross-linking polymerization of the poly(butadiene) polymer segment of the copolymer (30 min, 254 nm). The cross-linking step ensures the mechanical "stiffness" of the immobilized vesicles. This preparation ultimately produces a surface with controlled topographical features while ensuring the chemical homogeneity of the surface.

C.9.b Surfaces resulting from the immobilization of vesicles though hybridization.

The second type of vesicle-coated surfaces was prepared by incubating a solution containing vesicular structures of poly(isobutylene)-block-5'-GGGAGAGAGAGA-3' (PIB_{31}-G_7A_5) in a well containing a surface coated with the complementary, single-stranded oligonucleotide C_7T_5 (5'-CCCTCTCTCTCT-3'). After 12 h incubation at room temperature, the vesicle-coated surface, obtained by spontaneous hybridization was rinsed three times with NaCl buffer (NaCl 150mM) and was sterilized 30 min under UV (180nm) in NaCl buffer.

With this procedure two types of vesicle-coated surfaces were obtained, depending on the vesicle solution preparation. To obtain a "smooth" vesicle surface, the vesicles solution, obtained by bulk swelling, was filtered three times at 0.45µm and then three times at 0.2 µm to break apart all aggregates of vesicles. To obtain the "rough" surface, filtration was limited to 0.45µm.

C.9.c Reference surfaces.

Reference surfaces consisted of Silicon wafers and glass cover slips.

Silicon wafers were prepared as follow: They were cleaned three times in chloroform under sonication for 15 min. Wafers were then activated by 15 min UV treatment (UV/ozone cleaner, λ=180nm). Finally, wafers were sterilized by a dried heat procedure (1 h, 180 °C).

Glass control surfaces consisting of 12 mm diameter glass cover slips were prepared by washing with a chlorydric acid/ethanol solution (1:9 v/v ratio) for 20 minutes. They were then rinsed with distilled water, first for 20 min and twice for 10 min. Finally they were dried under nitrogen. Samples were sterilized by dry heat at 180 °C for 1 h.

C.10 Surface characterization.

C.10.a Fluorescence microscopy.

An upright CLSM (LSM700 – Zeiss, Germany) was used to follow vesicle deposition over time. A laser at 405 nm was used for excitation in the reflection imaging mode. To observe Nile Red [132] fluorescence, laser at 532 nm was used for excitation, and emission was collected at 550 nm - 630 nm, and images were taken every 2 minutes.

Fluorescence microscopy under flow was performed with the help of the Upright CLSM (LSM700 – Zeiss, Germany) and the flow cell as described in Materials and methods of Part II. Briefly, the flow cell was mounted using the protocol described in the Materials and methods of Part II, with a surface coated with an oligonucleotide SAM (C_7T_5). The flow of NaCl buffer (150 mM, pH: 6.8) continued for two hours and the surface was imaged over time (every 2 minutes). Flow was then stopped and 5 mL of a fluorescently labeled vesicles solution (Nile Red) was injected in the flow cell without flow. Labeled vesicles and surfaces were incubated without flow for 12 h. Images were still taken every 2min in reflection and fluorescence modes. Then medium flow was turned on for 2 h with imaging procedures as described above.

C.10.b X-ray Photoelectron Spectroscopy (XPS).

X-ray photoelectron spectroscopy was performed with the LEYBOLD LHS11 spectrometer. It was equipped with a non-monochromatized Mg $K\alpha_{1,2}$ X-ray source (1253.6 eV) and a concentric hemispherical analyser. Photo-emitted electrons were collected at take-off angles of 90° and 45° with the substrate, with electron detection in the constant analyser energy mode. Survey spectrum signals were recorded with a pass energy of 50 eV and for high resolution areas (C1s, O1s and N1s) the pass energy was set to 20 eV. Peak fitting was done with mixed Gaussian-Lorentzian (30 %) components with equal full-width-at-half-maximum (FWHM) using the CASAXPS software. The surface composition expressed in atom percent was determined using integrated peak areas of each component, taking into account the transmission factor of the spectrometer, the mean free path, and Scofield sensitivity factors for each atom (C1s: 1.00, O1s: 2.85 and N1s: 1.77).

C.10.c Contact angle measurements.

Contact angle measurements were carried out using the sessile drop technique [134]. Briefly, a droplet of pure water (pH = 5.5, 1- 2 µL) was deposited onto the surface and the contact angle was measured with a KRUSS G1 contact angle meter. The contact angle measurements were carried out on dry samples (1 cm ×1 cm) after each step of the grafting procedure. Reported values are the averages of the contact angles (right and left) of three droplets repeated three times (on three different samples, i.e. average of nine measurements). No change in the measured contact angle was observed during a 1 min measurement.

C.10.d Ellipsometry.

Ellipsometric analyses were performed with an Optrel GdBR Multiskop in order to determine the thickness of the thin films. Measurements were conducted using a laser beam at 532 nm, 0.6 mm, and 20 mW wavelength, diameter and intensity characteristics, respectively. Data evaluation was performed with the Elli program developed by Optrel GdBR.

This analysis was done after each step of the grafting procedure, in air and in liquid (doubly-distilled water). In aqueous solution, according to A. G. Markelz et al. [135], who reported the change in the refractive index with the degree of hydration of the oligonucleotide layers, we can assess a refractive index of n = 1.35. In air, the refractive index of an oligonucleotide layer is assumed to be n = 1.46 [136], and all other refractive indices (including silicon, APTES, glutaraldehyde) were assumed to be around 1.5 and were refined by software iterative calculations.

C.10.e Atomic force microscopy (AFM).

Tapping mode AFM analysis of samples was performed using a PycoLE system, Molecular Imaging, with silicon nitride cantilevers, k = 42 N/m, scan rate 0.5 lines/s. Different locations of the samples were monitored. All experiments were done in air at room temperature.

C.10.f Quartz crystal microbalance with dissipation monitoring QCM-D.

QCM-D experiments were performed with Qsense (Göteborg, Sweden) Quartz Cristal Microbalance (QCM-D). Sensors were QSX 303 silicon dioxide coated sensors. Experiments were performed at 25°C and data were extracted with the QTools software [119].

To follow oligonucleotide grafting and vesicle deposition, the protocol for “surfaces resulting from the immobilization of vesicles though hybridization” (Part I - C.9.b) was first followed and adapted to the QCM. Briefly, the silicon dioxide coated crystal was cleaned in chloroform under sonication (3 times, 15 min) before being activated by UV-ozone treatment (UV0-cleaner, model 42-220, Jelight Company Inc. USA) for 15 min. Then the wafer was silanised with APTES and rinsed as described in the protocol for “high density” oligonucleotide modified surfaces. The silanized crystal is mounted in the QCM-D chamber and buffer (NaCl 9 g/l, pH 6.8) is injected. Frequency and dissipation shifts were recorded. The injection of glutaraldehyde, double stranded oligonucleotide, glycine (with sodium cyanoborohydride), urea and vesicles were performed in real time. Prior to each injection, the solution is thermally equilibrated (injection in the thermal equilibration loops) and then the chamber is flushed with 1 mL of the solution of interest (chamber volume 40µl). After stabilization of the signals, the chamber is flush three times with thermally equilibrated buffer (NaCl 9 g/l, pH 6.8, 1mL each time) to remove non grafted molecules/vesicles.

The collected data were analysed with the Qtools software to extract frequency and dissipation shifts of the crystal. The extracted data were processed with either the Saeurbrey, Maxwell or Voigt-Voivona models, depending on the dissipative properties of the deposited layer [133].

Chapter 1. Bloc copolymer synthesis and characterization

We describe herein the self-assembly of four DNA-based amphiphilic block copolymers, differing in the composition of either the hydrophobic block and/or the nucleotide sequence.

Synthesis was realized on a large scale with a reasonable yield, compared to the expected yield for such a solid phase synthesis route, enabling the use of a broad variety of characterization techniques in order to propose a mechanism of structure formation and interaction of the resulting DNA-based amphiphilic block copolymer.

1.1. Results and discussion

1.1.a. Chemical analysis.

Since the chemistry route previously reported [29] has been slightly adapted to scale-up the synthesis process, we performed an initial chemical analysis to demonstrate that steric hindrance due to greater amounts of material does not affect reaction efficiency and actually leads to larger yields. In the characterization reported here, identification with the characteristic fingerprints of the nucleotide sequence has been highlighted. To keep the discussion clear, we always refer to PIB_{31}-G_7A_5 if not stated otherwise (noticeable effects of the nucleotide or polymer chemical composition on the investigated properties of the self-assembly are analyzed by comparative investigations with PIB_{31}-G_7A_5).

Due to the grafting of a highly polar hydrophilic block, namely the nucleotide sequence, to a hydrophobic synthetic polymer, there are no good solvents for the nucleotide-based amphiphilic block copolymer. Partial solubility was achieved in chloroform, whereas spontaneous self-assembly took place in aqueous solution. ^{1}H-NMR was thus performed in $CDCl_3$.

Considering the partial solubility of the hydrophilic polymer segment, it becomes meaningless to discuss peak integer and molar mass from such an experiment. The qualitative analysis of this result leads to assigning the following peaks to the chemical groups along the poly(isobutylene) backbone, in agreement with the expected chemical shift 0.94 ppm, 0.99 ppm are allocated to methyl groups; 1.13, 1.17, 1.51 and 1.65 ppm are allocated to methylene groups (Figure 20).

The characteristic peaks arising from the presence of the sugar backbone of the oligonucleotide were clearly identified as well. The peaks assigned to the hydrogen of the deoxyribose ring were respectively found at 2.22, 2.53, 4.36 and 6.14 ppm. The signal due to the presence of the amino group hydrogen, which is expected between 8.50 ppm and 14.00 ppm, is completely hidden, which is certainly due to embedding of the nucleotide sequences within the PIB shell of the self-assembled structure. In the case of poly(butadiene)-based amphiphiles, the signal expected from the oligonucleotide sugar backbone is too close to the noise background and cannot be properly resolved. This is likely due do the higher glass transition temperature of PB in comparison to PIB, which

induces slower mobility of the PB chain in the solvent [134] and further decreases the already low mobility of the nucleotide-based amphiphilic copolymer in chloroform.

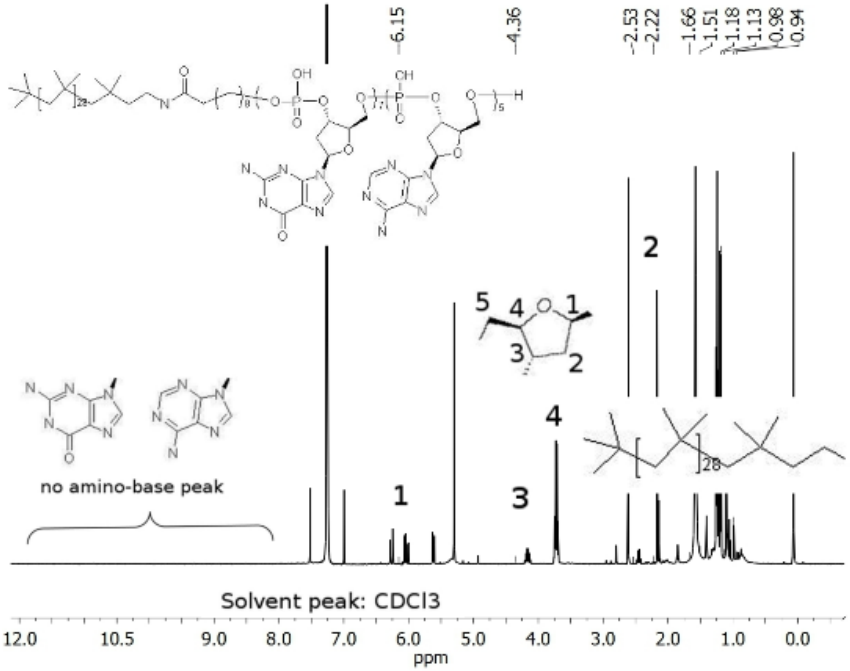


Figure 20: H^1-NMR spectrum of PIB_{31}-G_7A_5 obtained in deuterated chloroform. Peaks were assigned to the poly(isobutylene) block and the oligonucleotide sugar backbone. No peak could be assigned to the nucleotide sequence, probably due to the self-assembly of structures in which the nucleotide sequences are embedded in a poly(isobutylene) shell.

^{13}C CP-MAS NMR spectrometry was performed to assess the efficiency of coupling between the nucleotide sequence and the hydrophobic synthetic polymer.

All significant resonance peaks were addressed (Figure 21). Poly(isobutylene) was identified by signals at 22, 31 and 39 ppm, corresponding to the carbon elements from the methyl groups and resonances at 33 - 34 ppm which have been assigned to the carbon elements of the PIB chain. The oligonucleotide sugar backbone is represented by the signal at 60 ppm, which corresponds to the carbon linked to the oxygen/phosphate along the oligonucleotide backbone, whereas at 66, 78 and 85 ppm the carbons from the sugar backbone are revealed. The resonances at 119, 138, 149, 159 and 167 ppm correspond to the carbon of the guanosine bases whereas those at 127, 138, 149, 154 and 159 ppm are related to the carbon of the adenosine bases. Finally, the linker was identified at 25 - 30 ppm for the carbon of the linear linker while the carbons from the amide linker have been identified at 175 ppm. Additional signals were detected at 10 ppm corresponding to the methyl end of a linear carbon chain, this peak arise from impurities of the poly(isobutylene) used (low quantity of synthesis side product from starting material). Resonances at 114 and 131 ppm were assigned to nucleotide bases. They likely arise from intermolecular interactions between the nucleotide sequences, which shift some of the characteristic peaks. It was possible to clearly identify the resonances corresponding to the PIB and nucleotide sequences as well as the

peptide-bond linker, demonstrating the efficient grafting of the synthetic polymer segment to the oligonucleotide fragment through the amide bond.

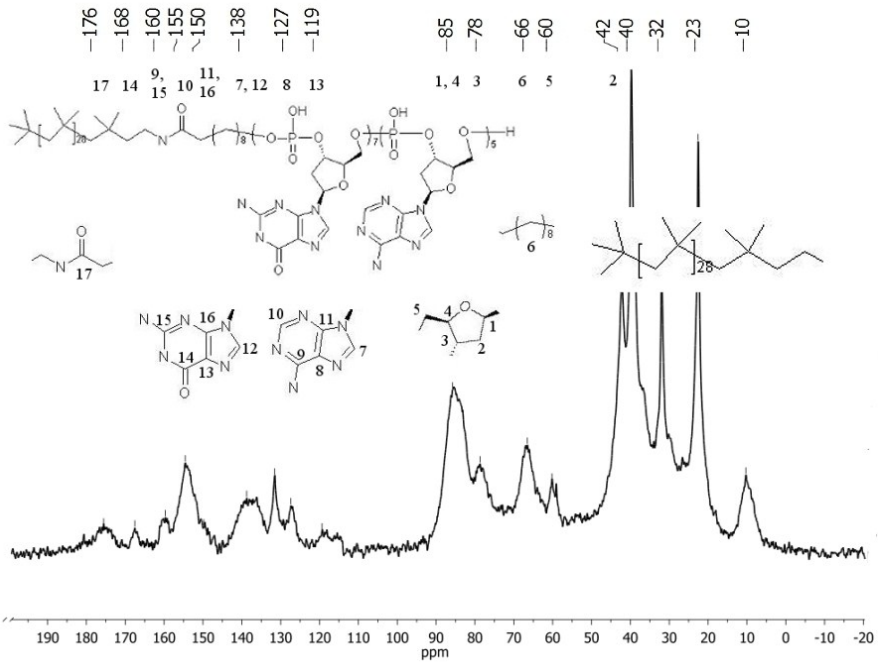


Figure 21: ^{13}C-CPMAS NMR of PIB_{31}-G_7A_5: Each peak can be assigned to a carbon-based group of the polymer. Each chemical environment is addressed on the spectrum. The global structure of the block copolymer is shown on the graph as a reminder.

To control the chemical environment and the integrity of chemical groups of the polymer-modified nucleotide sequences, FTIR spectroscopy was further performed.

Comparative analysis of non-modified PIB (Figure 22a) and PIB_{31}-G_7A_5 (Figure 22b) provides clear evidence of the presence of a nucleotide sequence coupled to the polymer segment. As expected, the signal arising from PIB is characterized by the methyl stretching at 2954 and 2897 cm^{-1}, the methyl/methylene deformation at 1473 cm^{-1}, the gem-dimethyl deformation at 1390 and 1367 cm^{-1} and the strong methyl rock vibration at 1230 cm^{-1}, as well as the weaker methyl rock vibration at 924 and 951 cm^{-1} [135]. These peaks are detected on both PIB and PIB_{31}-G_7A_5 spectra. Concerning the nucleotide sequence, the peaks depend on the number and nature of the bases composing the sequence. However, typical peaks are all expected to range between 1400 and 1700 cm^{-1}, which is the "fingerprint region" of nucleic bases as displayed on the FTIR spectra in Figure 22(b). The signal observed on the same spectra between 1000 and 1200 cm^{-1} is characteristic of the sugar-phosphate backbone [136,137], confirming the presence of the oligonucleotide sequence.

For PB-based copolymers (data not shown), the FTIR spectra show the typical peaks for PB. Methylene stretching peaks are located at 2918 and 2846 cm^{-1} for the *trans* configuration and at 2945 and 2854 for the *cis* configuration, whereas *cis* C-H bending is observed at 741 cm^{-1}. In addition, the vinyl component of the *trans* configuration leads to peaks of large intensity at 912, 966 and 993 cm^{-1} and methylene bending leads to a signal at 1436 and 1450 cm^{-1}. However, the oligonucleotide sequence cannot be completely described, since these peak

locations overlap with the oligonucleotide fingerprint region (1500 cm^{-1}). Similarly, the proximity of the vibration signal of the strong vinyl peak and the vibration of moieties along the sugar-phosphate backbone prevent a clearer interpretation of the spectra. Assessment of the presence of the oligonucleotide was achieved by measuring spectra against a poly(butadiene) background (data not shown), thus allowing peak assignment corresponding to the oligonucleotide.

Finally, FTIR spectra of both poly(isobutylene) and poly(butadiene) based block copolymer clearly confirm the presence and show the integrity of the synthetic polymer and the oligonucleotide sequence.

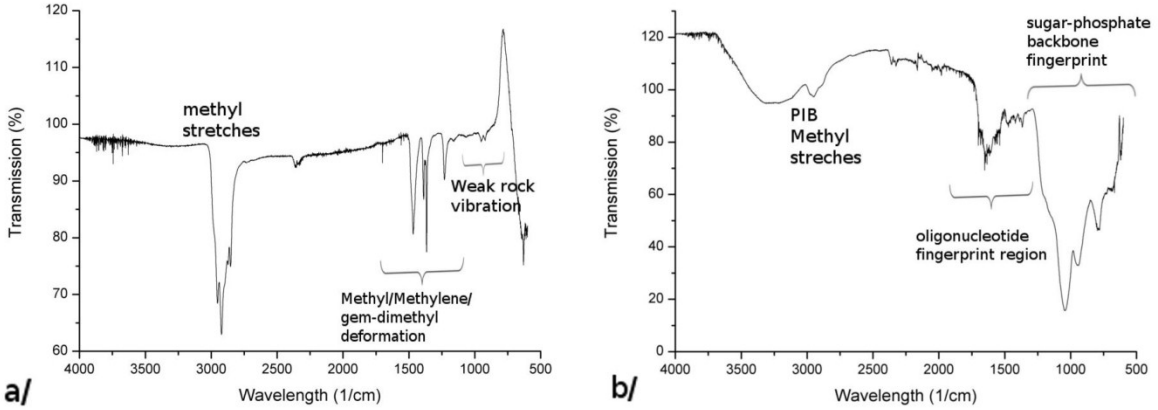


Figure 22: FTIR spectra of (a) Amino-modified PIB and (b) PIB_{31}-G_7A_5. Both spectra were recorded on air background. Most significant regions are highlighted to provide the fingerprint of the polymer-modified oligonucleotide.

Chemical characterization of the oligonucleotide-based copolymer was reinforced by the determination of the polymer purity and the synthesis yield. The purity of the oligonucleotide-modified polymer has been assessed by elementary analysis. Knowing that the theoretical formula of PIB_{31}-G_7A_5 is $C_{252}H_{397}O_{69}N_{61}P_{12}$ for a molar mass of 5757 Da, the nitrogen to carbon ratio was used to verify that SEC and dialysis separated the non-reacted nucleotide sequences from the synthesized block copolymer.

As reported in Table 4, the major part of the solid content is not organic and is due to the presence of the sodium and counter-ion salts used for SEC purification. The concentration of sodium chloride is estimated by elementary analysis at 36 mM for one gram of the solid dissolved in doubly-distilled water, which is in good agreement with the expected amount of residual salt subsequent to SEC (performed in a 150 mM sodium chloride solution) followed by dialysis (efficiency of dialysis estimated at 76% of salt removal). The comparison between the theoretical and experimental ratio of the mass of each element reveals an excess of hydrogen, which should be attributed to water contamination of the hygroscopic polymer. Nevertheless, the good agreement between the theoretical and the experimental nitrogen to carbon ratio (24.8%) allows to assume a high purity of the oligonucleotide-modified polymer, since no traces of non-reacted oligonucleotide or poly(isobutylene) were detected. The small difference between the theoretical and experimental carbon to nitrogen ratio is in agreement with polydispersity inherent to block copolymer synthesis. The elementary analysis finally showed that around

30% of the bulk material by mass corresponds to pure polymer, which is confirmed by UV-is spectroscopy at 260 nm, as detailed below.

	Experimental %	Theoretical ratio in %	Experimental ratio in %
C	18.00 ± 1.00	N/C 28.22	**24.80**
H	3.64 ± 0.09	H/N 46.83	**83.00**
N	**4.50 ± 0.30**	/	/

Table 4: Elementary analysis of carbon, hydrogen and nitrogen performed on PIB_{31}-G_7A_5. This analysis provided the mass proportion of each studied element starting from an NaCl aqueous solution of 5 mg of polymer (2.1 mg of salt per gram of polymer).

First, we ensured the linear relationship between absorbance at 260 nm and concentration for molarities below 11 µM (0.125 mg mL^{-1}). For concentrations above 11 µM, the scattering effect due to self-assembly induces a shift in the absorbance peak, which prevents the use of the Beer-Lambert law. However, we were able to quantify the concentration of the nucleotide-modified polymer by UV-Vis spectroscopy. Since we demonstrated by elementary analysis that the copolymer did not contain any free oligonucleotide, the comparison between the mass of polymer-modified nucleotide sequences dissolved and the polymer quantity evaluated according to the extrapolated Beer-Lambert law (see Part I – Materials and methods) leads the determination of a polymer content of 30% of the mass initially dissolved. This result is in agreement with elementary analysis. We can thus precisely calculate the synthesis yield. The yield value varies between 15 to 30% from batch to batch and was allowed by optimization of the reactant size and coupling. This yield is high in comparison to values previously reported by Z. Li et al. ranging from 2 to 4% [138] for a similar solid phase synthesis. The low efficiency of such solid phase synthesis, compared to classical polymer synthesis in solution is due to hindrances to diffusion of the reactants through the pores of the solid support.

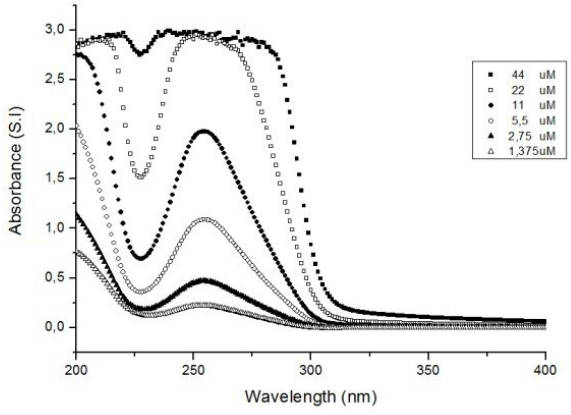


Figure 23: UV-Vis spectroscopy of PIB_{31}-G_7A_5 self-assembled in water for several dilution factors, from 1 to 32 folds. For concentrations below 11µM, the absorbance follows the Beer-Lambert law; when above, scattering effects hinder the linear relation between absorbance and concentration.

1.1.b. Self-assembly and chain configuration.

The self-assembly properties of amphiphilic copolymer in dilute aqueous solution are driven by the hydrophilic to total mass ratio. According to D. E. Discher and A. Eisenberg [139], self-assembly in vesicular structures should be expected for a ratio of 35 ± 10 %, whereas inverted structures or micelles should self-assemble for characteristic ratios below 25% or above 45 %. Since the hydrophilic to total mass ratio of the four copolymers investigated in this study are 48 and 51% for PB_{65}-T_5C_7 and PB_{65}-A_5G_7 respectively, and increases to 67 and 70 % for PIB_{31}-C_7T_5 and PIB_{31}-G_7A_5 respectively, micelles should be expected. However, the properties of the structures resulting from the self-assembly of nucleotide based amphiphilic copolymers should be affected by the twelve negative charges of these copolymers in a pH range between 5 and 9, due to the presence of the phosphate group along the nucleotide backbone (pKa values are 1 for the phosphate group, 3.8 for the nitrogen 1 of adenine, 4.5 for the nitrogen 1 of thymine, 9.4 and 9.5 for the nitrogen 1 of guanosine and cytosine respectively, and finally 2.4 for nitrogen 7 of guanosine [140]). Inter- and intra-molecular interactions arising from electrostatic interactions, hydrogen bonding, and formation of secondary structures should occur. In this context, M. Antionetti & S. Förster [141] reported that the vesicular structure formation of amphiphilic block copolymers with a characteristic hydrophilic to total mass ratio outside of the classical range is favored by peculiar properties such as the rigidity of the hydrophilic bloc, which can drive the self-assembly. A specific example is described in a publication of Kukula et al. [142], who synthesized poly(butadiene)-block-poly(L-glutamate), with a characteristic hydrophilic to total mass ratio around or above 50%, which results in self-assembly in stable "dread-lock vesicles" driven by the packing of the hydrophilic α-helix.

To determine if a similar force driving self-assembly in vesicular structures exists for the structure formation of the copolymers investigated in this study, we used circular dichroism (CD). The response of the hydrophilic block, namely the oligonucleotide sequence (Figure 24), provides clear evidence that the grafting of the nucleotide sequence to the polymer and the self-assembly process do not disturb the configuration of the nucleotide sequence. The CD spectrum of the pristine oligonucleotide is exactly the same than that of the nucleotide sequence modified with the hydrophobic polymer. Moreover, the chemical composition of the hydrophobic block, either PIB or PB, does not interfere with the configuration of the nucleotide sequence: PB and PIB nucleotide-based copolymers induce a similar CD response for a given nucleotide sequence, which only depends on the composition of the nucleotide sequence (data not shown). The wavelengths of the typical ellipticity maxima are slightly shifted, depending on the oligonucleotide composition: 275 nm for C_7T_5, and 260 nm for G_7A_5. The typical minimum at about 245 nm corresponds to a B-form conformation of the DNA fragment as reported by Kypr et al. [143]. In addition, D. M. Hatters et al. [144] reported a compact and cylindrical secondary structure of single stranded oligonucleotides. Based on the CD response of the self-assembled nucleotide-based amphiphilic copolymers, we can assume that the twelve-oligonucleotide bases adopt a B-form helical configuration. This should confer a cylindrical shape to the molecule, which is retained by polymer

modification and subsequent self-assembly. This secondary structure of the hydrophilic bloc, combined with the low glass transition temperature of the hydrophobic block, ensures flexibility of the self-assembling macromolecule. The rigidity and packing of the hydrophilic block allows overcoming the effect of the hydrophilic to hydrophobic ratio on the formation of vesicles, as demonstrated by Kukula et al. in the case of poly(butadiene)-block-poly(L-glutamate) [142].

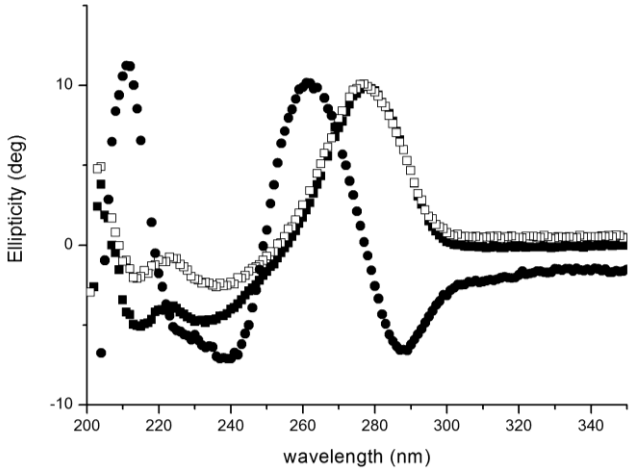


Figure 24: CD spectra of PIB_{31}-G_7A_5 (black circle), PIB_{31}-C_7T_5 (black square) and free C_7T_5 (white square). Spectra of the free oligonucleotide and corresponding polymer-modified oligonucleotide are comparable. The spectra from amphiphiles differing in the composition of the oligonucleotide sequences change according to the expected spectra of the non-modified oligonucleotide. CD spectra demonstrate the retention of the chain conformation of the oligonucleotide subsequent to polymer modification by solid phase synthesis and subsequent self-assembly.

The identification of the nucleotide chain conformation is not only crucial to establishing the mechanism of structure formation of the self-assembling nucleotide-based amphiphilic copolymers, but it further helps to ascertain the fundamentals for further hybridization studies of the polymer modified nucleotide sequences: the secondary structure of the oligonucleotide in the self-assembly is similar to that of the non-modified oligonucleotide. The B-type helix ensures that the configuration requirements for efficient hybridization are preserved by polymer coupling and subsequent self-assembly.

Knowing the chain conformation of the polymer-modified nucleotide sequence, the self-assembling amphiphilic diblock copolymer can be modeled as a macromolecule consisting of a B-form hydrophilic helix, which matches a cylindrical shape of 4.08 nm in length (0.34 nm between two base planes) and 2 nm in diameter. The hydrophobic polymer segment is a soft, flexible polymer that can be described by the freely jointed model [145]. Using a fixed valence angle (109° for a carbon backbone), the radius of gyration is 0.7 nm for PIB and 1.05 nm for PB. Thus, the full length of the self-assembling polymer-modified nucleotide sequences is 5.48 nm for the PIB-block-oligonucleotide and 6.18 nm for the PB-block-oligonucleotide. Consequently, the average diameter of micelles should be 12 nm (twice the polymer length) and at least 24 nm for vesicles (four time polymer length due to bilayer formation). The different self-assembly processes involved in both micelle and

vesicle formations are represented in Figure 25. On the basis of polymer secondary structures, the vesicle formation is expected as the major self-assembled structures but the bulk swelling technics is known [45] to induce dispersity in the obtained structures leading to the formation of micelles.

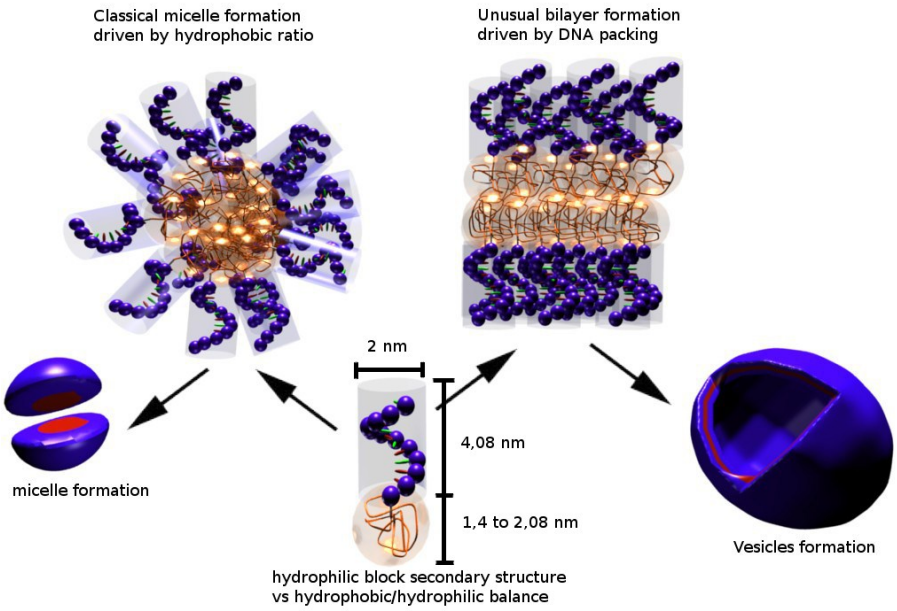


Figure 25: Scheme of possible structures achievable by different self-assembly processes of polymer-b-DNA in aqueous solution. Two main processes are hypothesized: a classical micelle formation driven by hydrophilic to hydrophobic volume fraction and a vesicular self-assembly driven by DNA packing.

TEM was used to observe the morphology of the self-assembled structures from the polymer-modified nucleotide sequences. Spherical shapes with sizes ranging between 15 and 120 nm were observed as shown in Figure 26, showing that spontaneous self-assembly certainly induces the formation of a mixture of micelles and vesicles.

Owing to the electron dense phosphorous groups along the oligonucleotide backbone, sufficient contrast for imaging with TEM without staining enables measurement of the wall thickness of a vesicle to identify the mechanism of self-assembly. From analysis of 20 images, we estimated a membrane thickness of 11 ± 3 nm, as illustrated in Figure 26(b), which agrees particularly well with the theoretical length of the macromolecule self-assembling into spherically closed bilayers, as discussed above. Moreover, the TEM images obtained with the self-assembled structures from PIB_{31}-G_7A_5 (Figure 26(a)), PIB_{31}-C_7T_5 and PB_{65}-T_5C_7 (data not shown) reveal self-assembled structures of comparable size. The PB-block-oligonucleotide diblock copolymers seem to self-assemble into slightly larger structures with sizes between 20 and 150 nm. This is in agreement with the different size and rigidity for the PB, which is longer and of higher glass transition temperature than PIB. These observations are in agreement with the hypothesis developed above: The hydrophobic block induces self-assembly by soft molecular arrangement, whereas the hydrophilic block determines the shape and size due to its

rigid secondary helical structure and existing unspecific intermolecular interactions, leading to a mixture of classically induced micelles and less usual vesicular structures.

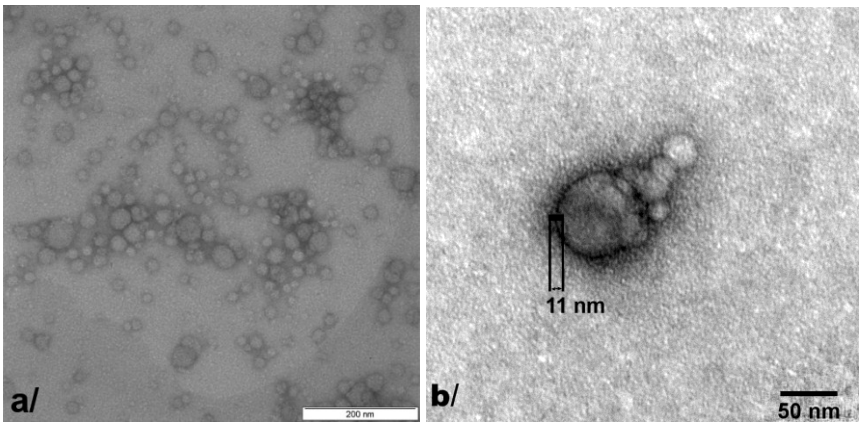


Figure 26: TEM micrographs of (a) PIB_{31}-G_7A_5 stained (b) PIB_{31}-G_7A_5 not stained, allowing to measure membrane thickness

SEM pictures further confirmed the presence of vesicles of sizes above 60 nm, as shown in Figure 27. Spherical structures with sizes between 30 and 100 nm are observed, which is compatible with the typical size of vesicles. These structures are aggregated (Figure 27a) or isolated (Figure 27b). Some of these structures collapsed in the high vacuum of the experimental SEM set-up, as shown in Figure 27c, which confirm the hollow structure of those particles as expected for vesicles.

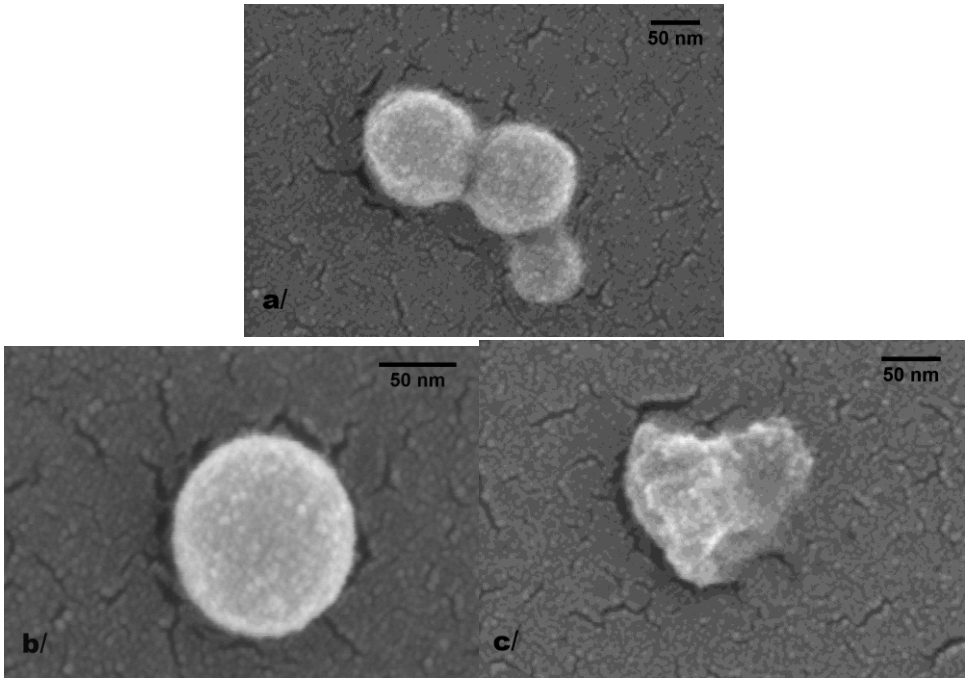


Figure 27: SEM micrographs of PIB_{31}-G_7A_5 self-assembled structures: (a, b) vesicle aggregates and a single vesicle respectively, (c) a collapsed vesicle.

To confirm the results obtained by TEM and SEM and to accurately quantify the size of the self-assembled structures, DLS was performed to determine the average hydrodynamic radius of the self-assembled structures.

As classically done with conventional, self-assembling copolymers, the size and size distribution of the self-assembled structures were reduced by sequential extrusions through membrane filters. The concentration reduction due to retention of some of the material in the filter membrane was controlled by UV spectroscopy before any subsequent measurement. As expected, because of the breakage of the larger aggregates, the hydrodynamic size measured by DLS decreased with the size of the membrane pore size. As presented in Table 5, after sequential filtration through 0.45 µm and 0.2 µm pore-size filters, C_7T_5 based block copolymers have a characteristic hydrodynamic radius of 84 ± 12 nm and 46 ± 16 nm respectively. The size distributions (around 20%) are typical of self-assembled vesicular structures [146]. DLS also reveals that A_5G_7-based block copolymers form compound structures with sizes larger than expected. In that specific case, two diffusion times were monitored through analysis of the correlation function (data not shown). The results are in agreement with the hypothesis of the formation of a mixture composed of vesicular and micellar structures. Intermolecular interactions between guanines in addition to electrostatic interactions between the negatively charged self-assembled structures in the presence of a low amount of counter ions probably favor the formation of aggregates made of vesicles and micelles clustering together, leading to a larger apparent hydrodynamic size. A thorough study to differentiate the effect of electrostatic interactions from the other modes of binding is an interesting perspective of this work.

	PB_{65}-A_5G_7	**PIB_{31}-G_7A_5**	**PIB_{31}-C_7T_5**	**PB_{65}-T_5C_7**
Filtration 0.45 µm	/	248 ± 68 nm	80 ± 18 nm	78 ± 29 nm
Filtration 0.2 µm	236 ± 9 nm	160 ± 14 nm	84 ± 12nm	46 ± 16 nm

Table 5 : Hydrodynamic radius obtained with DLS. The residual salt and counter-ion concentration was estimated at 36 mM by combined elementary analysis and UV-spectroscopy.

1.2. Conclusion

In this study we achieved the solid-phase coupling of either poly(isobutylene) or poly(butadiene) to nucleotide sequences differing in their composition by means of solid-phase synthesis. We demonstrated that the scale-up of the synthesis route reported previously led to oligonucleotide-block-copolymer amphiphiles of high purity with yields up to 30%. We further demonstrated that the block copolymers form spontaneous self-assembled structures. A combination of theoretical and experimental considerations provided tracks that the self-assembly driven by the oligonucleotide configuration and inter-molecular interaction upon grafting a hydrophobic polymer segment to the nucleotide sequence leads to vesicular structures and micelles.

The formation of these vesicles allows the production of nanoreactors, as studied in Chapter 2.

Coming back to the main topic, i.e. preparation of antimicrobial surface, we can foresee the various advantages of using this DNA based copolymer: an oligonucleotide shell should ensure biocompatibility and may even allow directed cell response. In the same way, specific response from bacteria may be expected, which will be addressed in Part 2. Furthermore, since single stranded oligonucleotides undergo specific binding properties with their complementary strands, they can be exploited for surface immobilization.

Chapter 2. Nanoreactor preparation and characterization

Subsequent to the synthesis of oligonucleotide based amphiphilic copolymer, which self-assembles in vesicular structures, we prepared nanoreactors by encapsuling an enzyme as the reactive part of the reactor and inserting channel protein to provide vesicular membrane permeability.

The specific role of the polymer, of encapsulated enzyme of inserted channel protein in the design of the nanoreactors was reported in the state of the art sections of this Part I. Concerning the polymer, we demonstrated in the previous chapter that the PIB_{31}-G_7A_5 able to form vesicles, which is essential for efficient encapsulation of a water soluble active enzyme. Furthermore, since this polymer has a low glass transition temperature and an adequate membrane thickness (11 ± 3 nm), it should allow the use of OmpF as a channel protein to provide permeability to the vesicle polymeric shell. Concerning the enzyme, we also previously discussed, based on the literature, the ability of LPO to produce antimicrobial compounds, which raises interest in using this enzyme as the active part of the nanoreactors.

In this chapter we will describe the preparation of the nanoreactors resulting from the self-assembly of PIB_{31}-G_7A_5, encapsulating lactoperoxidase with OmpF embeded in the polymeric shell as schematized in Figure 28. We will also demonstrate the possibility to obtain a solution of pure nanoreactors, assessing the purity throughout the entire process by UV-Vis spectroscopy and enzymatic activity. Then, we will determine the efficiency of the encapsulation process and discuss the enzyme activity and kinetics of the nanoreactor system in comparison to the free enzyme in terms of Michelis-Menten kinetics. As a final assay, we will measure nanoreactor activity in a solution containing proteinase K, demonstrating the protective effect of encapsulation.

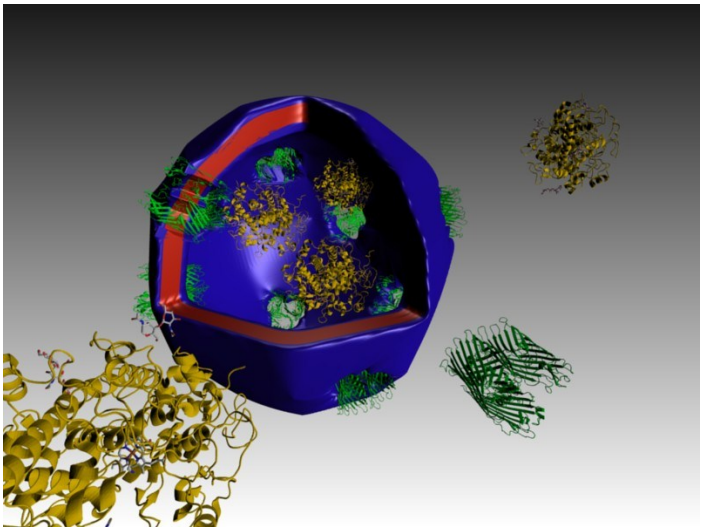


Figure 28: Illustration of a self-assembled nanoreactor encapsulating lactoperoxidase (yellow), with OmpF embedded in the membrane (green). Free OmpF and lactoperoxidase are also present in the surrounding. In the schematized vesicle, the red color corresponds to the hydrophobic membrane whereas the hydrophilic shell is represented in blue.

2.1. Results and discussion

2.1.a. Nanoreactor preparation and purification: step by step characterization.

To assess the preparation and purification of nanoreactors, we based our work on a comparative study among functional nanoreactors, non-porous nanoreactors and a reference solution of free enzymes. In this comparative study, we aimed at demonstrating that the nanoreactor activity measured at the end of the purification process cannot be attributed to residual free enzyme (comparison with solution of free enzyme subsequent to purification process), or to non-encapsulated enzyme adsorbed on the vesicular external shell (comparison with solution of non-porous nanoreactors subsequent to purification process). Since activity cannot be observed with non-porous vesicles, the OmpF insertion and the retention of vesicular structures throughout the preparation and purification process are needed. To perform this comparative study, samples were collected at each preparation and purification step and named as described in Materials and methods.

The first step in the characterization is to determine the polymer concentration in solution immediately after preparation. Subsequent to preparation, the solution contains, in addition to the mixture of nanoreactors, free enzyme and non-inserted OmpF, and a non-negligible quantity of non-dissolved polymer. This non dissolved polymer is eliminated through the filtration of the solution with a Millex-HV filter as described in Materials and methods. To follow this elimination, UV-Vis spectroscopy was performed immediately after the preparation of the solution and subsequent to Millex-HV filtration. The spectra are displayed in Figure 29. Considering the samples containing the block copolymer, OPAG1 and OPAG2, we can observe intense scattering effects before Millex-HV filtration corresponding to aggregates and non-dissolve particles of the copolymer, which is further corroborated by the milky appearance of the solution, which slowly disappears over time upon decantation. After Millex-HV filtration, both solutions labeled FPAG1 and FPAG2 appeared clear and their UV-spectra revealed a decrease in scattering effects, which shows the elimination of highly scattering particles. Nevertheless, these spectra are still saturated at 253 nm, revealing a high concentration of self-assembled nucleotide-based copolymers (close to 1 mg/mL) in the solution. Besides the comparison of OREF and FREF, samples demonstrate also that the filtration process (Millex-HV filter) did not affect the free enzyme concentration.

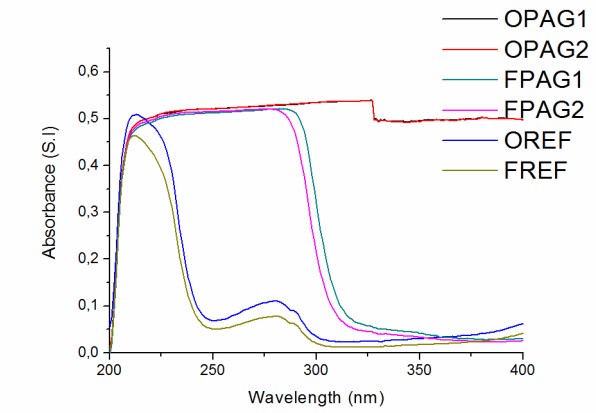


Figure 29: UV-Vis spectra of the different solutions before and subsequent to Millex-HV filtration, for the three solutions of nanoreactor, non-porous nanoreactor, and free enzyme reference.

The second step of characterization concerns the centrifugal purification and its efficiency. In this purification, we aimed to separate nanoreactors from other compounds in the solution (free enzyme, non-inserted OmpF, micelles, surfactant). For this purpose we used, as described in Materials and methods, centrifugal separation devices. After each centrifugal separation step, we collected 2 fractions: One "nanoreactor" fraction and one "other compound" fraction. To demonstrate the possibility of obtaining a solution of highly pure nanoreactors, we need to determine the polymer content, with UV-Vis spectroscopy of both the "nanoreactor" fraction and the "other compound" fraction. This characterization was performed at each step of purification (the purification contains five identical steps) allowing us to follow the quantity of polymer eliminated in the "other compound" fraction and to quantify the nanoreactor concentration in the "nanoreactor" fraction. The results are displayed in Figure 30.

First, we observed a decrease in the absorption maximum in the "other compound fraction" for both nanoreactors and non-porous nanoreactors over the successive filtration steps. This absorption at 253 nm, highlights the elimination of small polymer based elements (like micelles or free polymer). The decrease of the absorption in this fraction means that the amount of removed copolymer material going through the filter is decreased upon successive separations. This is confirmed by spectroscopy of the corresponding solution collected in the upper part of the centrifugal device, in which the polymer concentration rapidly reaches a steady state.

Through this UV-Vis monitoring, we can assess that, after 5 centrifugation steps, the polymer remains in the upper fraction and is self-assembled into vesicles or larger aggregates (of the copolymer) that cannot go through the filter, due to their size.

For the sample containing only free enzyme, the purification process is fast, since after only three filtrations all enzymes have crossed the filter membrane. This experiment demonstrates the efficiency of the technique in eliminating free enzymes.

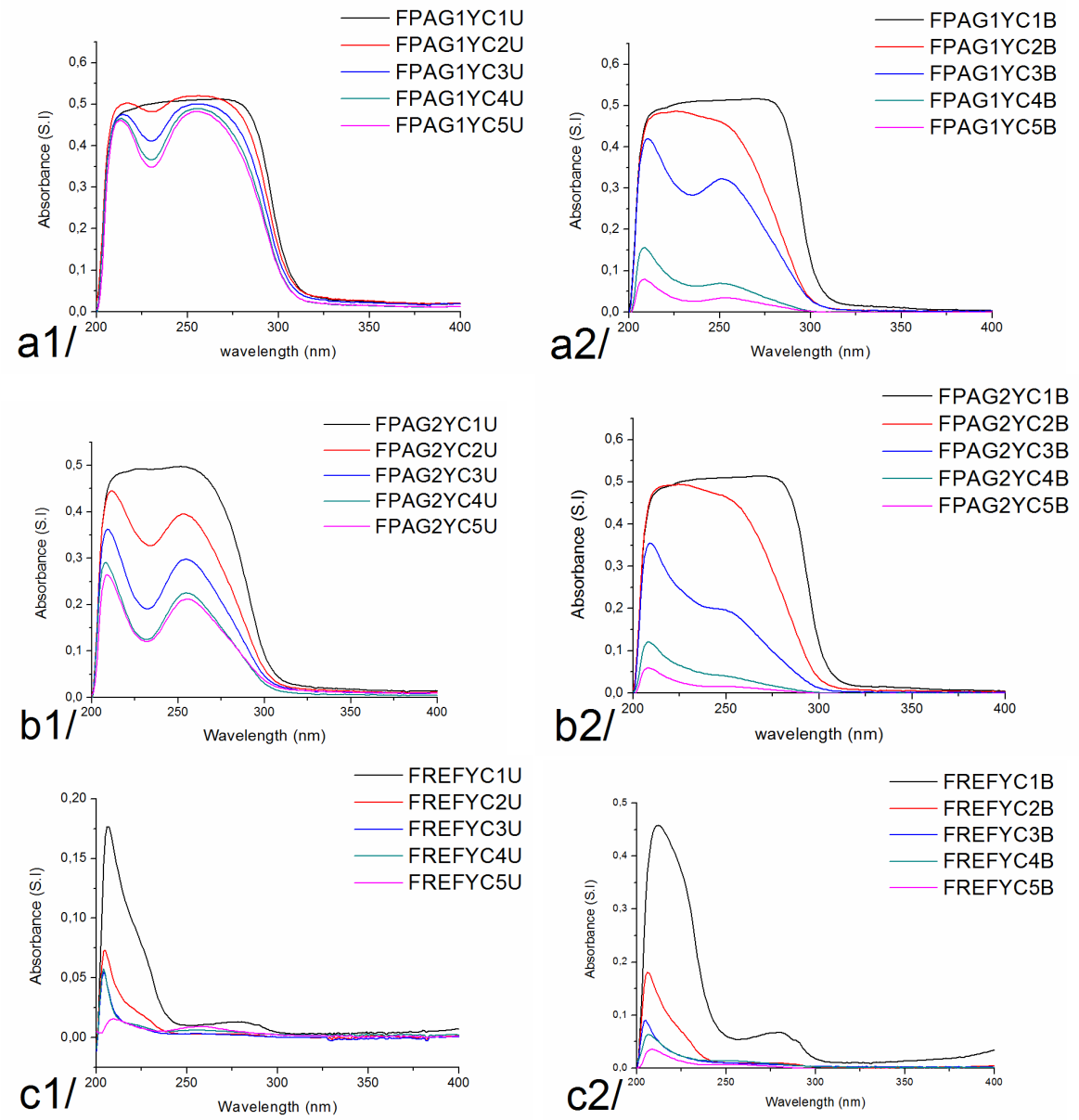


Figure 30: Uv-Vis spectra recorded during centrifugal purification. Spectra corresponding to nanoreactors are labeled (a1) for the nanoreactor fraction and (a2) for the "other compound" fraction. Similarly, non-porous nanoreactors spectra are label (b1) for the nanoreactor fraction and (b2) for the "other compound" fraction. Finally, the reference free LPO solution is also divided into two factions labeled (c1) for the fraction from the upper part of the centrifugal device and (c2) for the spectra from the "other compound" fraction. The sequential centrifugation steps yield the various spectra labeled as described in Materials and methods.

Finally, using UV-Vis spectroscopy we demonstrated that the majority of the polymer stayed in the nanoreactor fraction due to the size of the self-assembly and we demonstrated that, in the free enzyme solution, all free enzymes cross the purification membrane to stay in the "other compound" fraction. However, due to the overlap of the absorption peaks of polymer and LPO, we could not detect the enzyme in the polymer containing solution with the UV-Vis technique. Therefore, we ensured that all the free enzyme in the nanoreactor and non-porous nanoreactor solutions have been eliminated, by monitoring enzyme activity in the "other compound"

fraction at each step of the purification. Results are displayed in Figure 31, in which fluorescence spectroscopy monitoring of the enzyme activity provides direct proof of the presence of enzyme. We can observe in Figure 31 (a) that, before filtration, enzyme concentration is high, leading to saturation in all samples. After Millex-HV filtration of nanoreactors and non-porous nanoreactors the enzyme concentration seems to decrease slightly, since the fluorescence intensity decreased. Some of the enzymes might have been eliminated with the non-dissolved copolymers. Monitoring of the enzyme activity of the nanoreactors confirms that, after three sequential centrifugal separation steps, no activity of free enzyme is detectable. A similar assertion can be made with the reference sample of the free enzyme and in agreement with UV-Vis spectroscopy. Finally, the graph corresponding to non-porous nanoreactors (Figure 31(b)) displays 'oscillating' activity. This activity was monitored prior to the fourth centrifugal separation step. The shape of this 'oscillating' curve does not correspond to classical enzymatic activity. Such a curve has been observed in solutions in which enzymes are present (as free enzyme, for example) but they are not able to process substrate normally for reasons that are not clear. Nevertheless, we can again assert that, after the third purification step, no activity can be detectable in the "other compound" fraction. These observations clearly demonstrate the elimination of free enzyme from the nanoreactor fraction. In the first three separation steps free enzyme can be detected in the other compound fraction, while after the fourth separation, no more activity can be monitored in this fraction, and this is true for all three samples: reference free enzyme, nanoreactors, and non-porous nanoreactors.

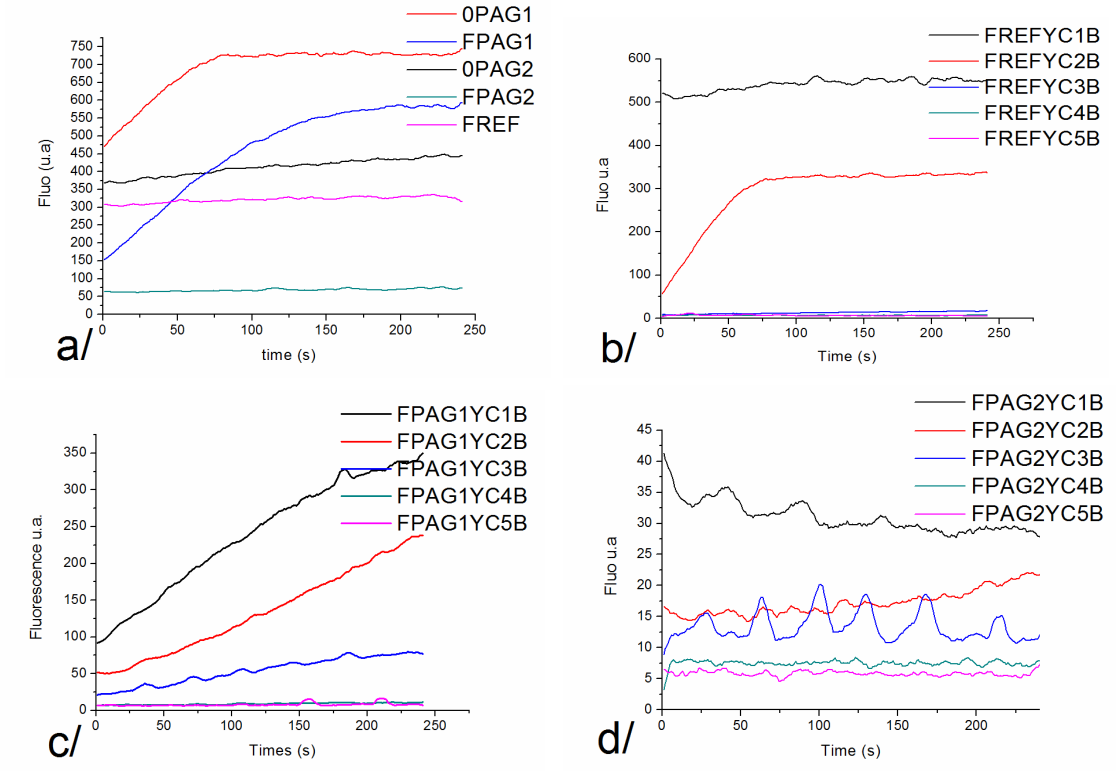


Figure 31: Graph (a) displays of enzymatic activity of the different solutions before and after Millex-HV filtration. (b, c, d) represent the enzymatic activity of the "other compound" fraction at each purification step for, respectively, reference free enzyme, nanoreactors and non-porous nanoreactors.

In conclusion, we can assert that the purification procedure allows the production of nanoreactors suspensions cleared of active free enzyme. Finally, the nanoreactor concentration can be determined by simply using polymer concentration measurements.

2.1.b. Nanoreactor activity, Michaelis-Menten kinetics and encapsulation efficiency.

Nanoreactor activity was first analyzed by a qualitative comparison between nanoreactor activity measurements and free enzyme solutions. For this purpose, we measured the enzyme activity for different enzyme concentrations (0.5, 1 and 5 µM) but a constant concentration of the tyrosine substrate. Activity of the purified nanoreactor solution (FPAG1YC5U) was measured under the same conditions as the activity of the purified, non-porous nanoreactors (FPAG2YC5U). Fluorescence intensity measurements resulting from enzymatic activity of LPO on the tyrosine substrate are presented in Figure 32. As expected, in the case of the free enzyme in Figure 32(a), reaction speed (start slope) and steady state (conversion limit) values depend on the enzyme concentration at a constant substrate value, illustrating that the enzyme activity increases as a function of enzyme concentration.

Similar experiments performed with the two nanoreactor solutions provided evidence (Figure 32(b)) of enzymatic activity for purified porous nanoreactors while the curve slope was equivalent to background noise (obtained without enzyme, see Figure 31) for the non-porous nanoreactor solution. These results demonstrated that LPO is encapsulated inside the nanoreactors. Secondly, this result demonstrated the necessity and the efficiency of using OmpF to confer porosity to the vesicular shell. Finally, the comparison of FPAG1YC5U to free enzyme activity curves (see Figure 32 a and b) allowed evaluating the activity of the nanoreactor solution. In this way, we can at first roughly estimate an activity equivalent to 0.5 µM of free enzyme. This rough estimation will be cleared by later calculation, with the help of Michealis-Menten kinetics.

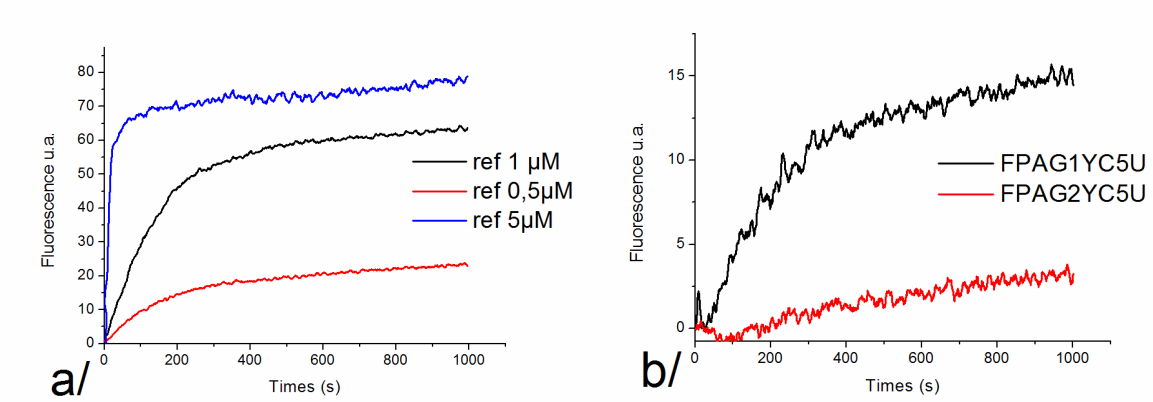


Figure 32: Graph (a) displays enzymatic activity of LPO at enzyme concentrations of 0.5, 1 and 5 µM. Graph (b) displays enzymatic activity of purified nanoreactors (FPAG1YC5U) and non-porous purified nanoreactors (FPAG2YC5U).

The Michaelis-Menten kinetics is described in Materials and methods. It allow determining the kinetic constants K_M, K_{cat} and enzyme concentration from activity measurements obtained with different substrate concentrations (from 0.014 to 0.049 mg/mL). The obtained results are shown in Table 6. A small difference between K_M constants of the free LPO (0.5µM) solution and the nanoreactor solution is observed. However, the order of magnitude is conserved, confirming the non-denaturation of LPO in nanoreactors, since the substrate affinity for LPO is conserved. Slight variations in the hydrogen peroxide co-substrate concentrations may explain the weak variation observed in K_M values, due to the pseudo first order of the reaction. Comparing the K_{cat} value we can notice a reduction by a factor 8.16 in the case of nanoreactor solution compared to the 0.5µM free LPO solution. Kcat is the catalytic constant i.e. the turn-over rate of the enzyme. The reduction of Kcat, for encapsulated enzyme (nanoreactor), corresponds to a reduction of enzyme processing activity. This reduction can be attributed to the enzyme encapsulation. The encapsulation leads to steric constraint, interactions with the charged shell (PIB_{31}-G_7A_5 is highly negatively charged due to oligonucleotide phosphate backbone) and interaction with oligonucleotide functional groups (capable of forming hydrogen bonds). All of these hindrances probably reduce the enzyme turnover by adding a new energetic barrier to the enzymatic conversion of tyrosine into dityrosine.

Diffusion of the substrate and product through the OmpF channel may also reduce enzyme turnover by displacing the reaction equilibrium due to substrate deficiency and the product richness of the reactor inner pool, but diffusion limitation, using OmpF as channel, was never demonstrated for nanoreactor activity in the literature [45]. Finally, K_{cat} variation is an additional indication of LPO encapsulation in PIB_{31}-G_7A_5 nanoreactors. Results also demonstrated that encapsulation did not result in denaturation of the enzyme and that affinity of the substrate for the enzyme was conserved, but with a significant reduction in K_{cat}.

	Free LPO	**Nanoreactors**
Km	253 µM	344 µM
Kcat	10.94 s^{-1}	1.34 s^{-1}
[E]0	0.5 µM	0.35 µM(calculated)

Table 6: Michaelis-Menten kinetic parameters for free LPO and for purified nanoreactors. K_m, K_{cat} and enzyme concentration were calculated with the Lineweaver-Burk [155] calculation.

Finally, coupled with UV-VIS spectroscopy measurements, kinetic measurements and analysis permitted to demonstrate the encapsulation of LPO in the nanoreactors. Knowing the polymer concentration at each step of the preparation and purification as well as the enzyme concentration from the Michelis-Menten equation, the efficiency of encapsulation can be calculated. First, we calculated (with the Lineweaver-Burk [147] calculation) that, for 0.3 $mg.mL^{-1}$ of bulk polymer, we have encapsulated an equivalent activity of 0.35 µM of LPO. Since the nanoreactor solution volume was adjusted to 500 µL, the total enzyme quantity contained in all nanoreactors

present in the solution was evaluated at 0.175 nmole. Therefore, knowing that the initial enzyme solution used for the encapsulation procedure contained 5µM in 1 mL (i.e. 5 nmole of enzyme), the encapsulation efficiency can be assessed to 3.5% for 0.3 $mg.mL^{-1}$ of polymer. Considering a linear equivalence (but knowing that fluctuations may be due to solubility issues), we can estimate encapsulation efficiency of 11.7% for 1 $mg.mL^{-1}$ of polymer. Nevertheless, we proved during the purification of the polymer that only a part of the dissolved polymer formed nanoreactors, while the other part formed micelles or remained as non-dissolved polymer. Corresponding nanoreactor concentration was measured by the UV-Vis absorption of the polymer oligonucleotide. This evaluation led to a final purified solution of 0.016 mg/mL while the initial concentration was 0.3 mg/mL of bulk polymer, i.e. an efficiency of polymer conversion into nanoreactors of 5.3%. Finally we can conclude that, for the use of 1 mg of PIB_{31}-G_7A_5 bulk polymer dissolved in 1 mL of 5 µM LPO solution, encapsulation efficiency is 11.7% leading to the formation of 0.053 mg/mL of nanoreactors containing 0.175 nmoles of LPO.

2.1.c. Proteinase K experiment.

Proteinase K is widely used in molecular biology for its ability to inactivate any other enzymes. In our case, we aimed at demonstrating the efficiency of encapsulation to protect the enzyme. For this purpose, we incubated purified nanoreactors (FPAG1YC5U), the free enzyme (FREFYC5U), and purified non porous nanoreactors (FPAG2YC5U), with Proteinase K, and we determined the enzymatic activity by using tyrosine as the LPO substrate. Fluorescence intensity resulting from LPO-related tyrosine conversion is presented in Figure 33. In this measurement we can observe activity due to nanoreactors but no activity from non-porous nanoreactors and no activity for the free enzyme reference solution. The free enzyme reference solution does not display activity due to the Proteinase K presence. In the absence of protection of the enzyme by the nanoreactors, LPO was inactivated, preventing oxidation of tyrosine and the corresponding emission of fluorescence signal.

This result about incubation with proteinase K allows the assertion that nanoreactors are able to protect the encapsulated enzyme. Moreover, the detected activity of nanoreactors proves that LPO is encapsulated inside vesicles and not merely adsorbed to the external shell of nanoreactors. Accordingly and as expected considering the barrier property of the nanoreactor shell in the absence of pores, non-porous nanoreactors solution did not display any activity. This result demonstrated the ability of the nanoreactors to retain their vesicular shape in medium containing proteinase K, by protecting encapsulated enzyme of porous vesicles from inactivation.

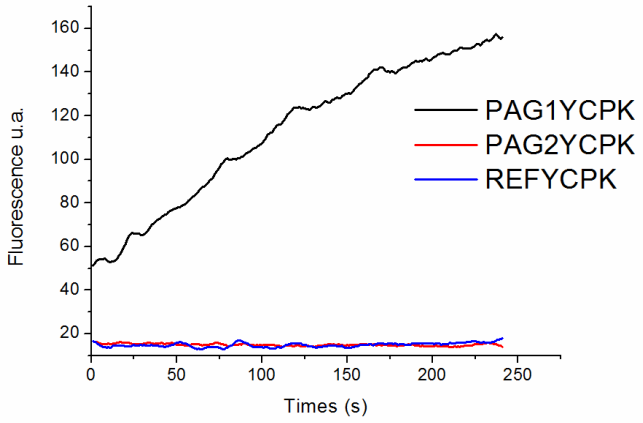


Figure 33: Enzymatic activity of LPO on tyrosine measured after incubation of nanoreactor solution (PAG1) and control solutions (REF & PAG2) in the presence of proteinase K.

2.2. Conclusion

In this chapter, we demonstrated and characterized the efficiency of LPO encapsulation in PIB_{31}-G_7A_5 nanoreactors with OmpF proteins as membrane channels. In this work we proved that it is possible to obtain a pure solution of nanoreactors with encapsulation of enzyme in the aqueous pool of the vesicles.

More than merely proving the possibility of purifying nanoreactors, we determined kinetic constants K_M and K_{cat} of the encapsulated LPO. Comparing those constants with value obtained for free enzymes, we conclude that the enzyme was not denatured, despite a reduction of the turnover rate. This turnover rate decrease was hypothesized as due to crowding and to surrounding effect provided by the nanoreactor shell, which results in an increase in the tyrosine conversion energetic barrier. We also determined bulk polymer-to-nanoreactor conversion and encapsulation efficiency. The literature on encapsulation is not precise regarding efficiency and polymer-to-nanoreactor conversion. This is mainly due to the issue of exactly quantifying the polymer concentration in solution. In our work, we were able to precisely quantify the bulk polymer to nanoreactor conversion as well as the encapsulation efficiency. The value obtained for encapsulation efficiency is comparable to the few published values for polymeric nanoreactors i.e. around 10% [59].

Finally, we can conclude that the investigated polymer allows the production of functional nanoreactors that can ensure enzymatic activity even in an environment unfavorable to the enzyme.

Chapter 3. Surfaces based on vesicles deposition

In the two previous chapters we demonstrated the possibility to design a block copolymer composed of an oligonucleotide capable of self-assembly in nanoreactors and of incorporation of OmpF as channels in the polymeric shell as shown by the encapsulation of LPO. To achieve the goal of the study we aimed at producing surfaces resulting from the immobilization of the nanoreactors. The deposition of nanoreactors can appear trivial at first. Nevertheless, obtaining a controllable and stable coating is a challenge. In the state of the art we described the different techniques to immobilize nanoreactors or vesicles to surfaces and we emphasized the possibility of using oligonucleotides to anchor them to surfaces. Recognition of complementary oligonucleotides has been exploited to produce a surface coated with vesicles or nanoreactors. Several previous steps are needed for that purposes and are described in following.

We have first investigated surface coating with single stranded oligonucleotides self-assembled monolayer. These smooth surfaces were characterized by various techniques (XPS, QCM-D, fluorescence microscopy, ellipsometry) that demonstrated grafting. More than merely be a support for vesicles, those surfaces were useful for fundamental consideration about bacterial adhesion as presented in Part II. Due to this consideration, a protocol was ad apted to provide surfaces with two densities of oligonucleotides, so-called “low density” and a “high density” surfaces, which were characterized in terms of their physico-chemical properties (contact angle, XPS) and their topography (AFM, microscopy).

In a second stage, we deposited vesicles on oligonucleotide modified surfaces. The first type of vesicle deposition described herein is not driven by hybridization. The PB_{65}-A_5G_7 block copolymer vesicles were deposited on a “smooth” surface coated with the oligonucleotide A_5G_7. Driven by nonspecific interactions, such as non-Crick-Watson base pairing and electrostatic interactions due to the presence of counter-ions, we ended up with a surface homogeneously bearing one type of oligonucleotide but with a “rough” topography due to the presence of vesicles. The deposited structures were then crosslinked by UV, to provide similar mechanical properties to both “smooth” and “rough” oligonucleotide coated surfaces. The surfaces were characterized by AFM and contact angle measurement.

Finally, we used the hybridization properties of the complementary oligonucleotides to prepare the second type of surfaces bearing a stable dense packing of immobilized vesicles. For this purpose we used PIB_{31}-G_7A_5 and deposited it on to complementary oligonucleotide coated surfaces (C_7T_5). The entire process was followed by fluorescence microscopy and QCM-D, demonstrating the spontaneity of the process and the stability of the coating. Mechanical properties were discussed on the basis of QCM-D experiments, while fluorescence experiments under flow conditions proved stability and illustrated the mechanical properties of the obtained layer. Finally AFM, contact angle, and XPS were performed, ensuring surface properties and topography compared to the other types of surfaces (“smooth” and “rough” oligonucleotide modified surfaces).

3.1. Results and discussion

3.1.a. Oligonucleotide self-assembled monolayers (SAM) modified surfaces.

3.1.a.i. "Low density" oligonucleotide modified surfaces.

Since amino groups are susceptible to undergo many reactions, silanization by APTES is the most common and an effective method for the modification of silicon surfaces. The reaction between a silicon surface and APTES is a condensation reaction occurring in toluene and releasing ethanol. Similarly, glutaraldehyde is widely used as a cross-linking reagent due to its reactivity with the side-chain amino groups of biomolecules to form a Schiff base. This part of the grafting procedure was modified from the one previously published by Y. Jiang et al. [129] according to L. Longo et al. [130]. The grafting of glutaraldehyde was performed at acidic pH in order to ensure the reaction of glutaraldehyde with the APTES amine groups while preventing the polymerization of glutaraldehyde. Surfaces were eventually modified with a stable oligonucleotide layer according to the ideal stepwise procedure of grafting presented in Figure 34, in which oligonucleotide double strands (step 3) and single strands (step 5) were assumed to be perpendicular to the surface.

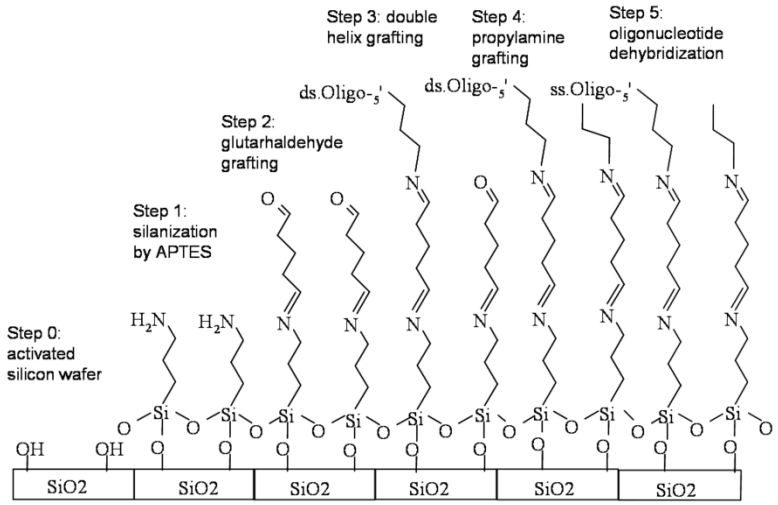


Figure 34: Theoretical description of each step of the grafting procedure.

The oligonucleotide detection and surface chemical characterisation were performed by X-ray photoelectron spectroscopy. Performing a two-angle XPS survey spectrum allows detection and evaluation of the thickness of the layer. The survey spectrum (Figure 35) first allows the detection of all atoms which composed the grafted layer and secondly allows an interpretation of the grafting molecule position on the surface by comparing atomic proportion at take of angles of 90° and 45° (Table 7). We could then interpret these survey spectrums on the basis of the description provided in Figure 34.

First, the spectrum shows the presence on the surface of C, O, N and Si elements. We also notice that the P2p (Phosphorous from oligonucleotide backbone) transition (135 eV) was not detected due to overlapping with the plasmon peak of the Si2p transition. Nevertheless, the N1s transition is characteristic of the reaction process.

The height of this peak after oligonucleotide grafting proves that the reaction between oligonucleotide sequences and the surface was effective. The survey spectrum in Figure 35 tends to confirm the presence of oligonucleotides at the surface of the sample after achieving all steps of the grafting procedure as well, but high resolution spectra and chemical environment analysis were needed to confirm that point.

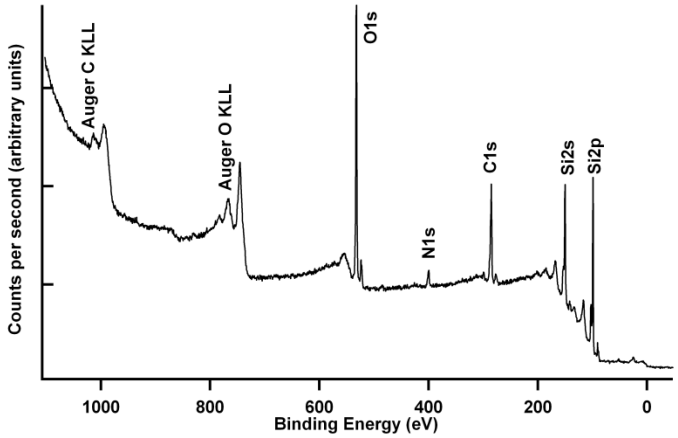


Figure 35: Survey spectrum at take-off angle at 90°. Unlabelled peaks around Si2p and Si2s are due to the vibration of the silicon plasmon.

Moreover, data obtained at a take-off angle at 90° showed a very high Si2p peak compared to that resulting from the presence of the other components. In addition, we observed an increase in the intensity in all peaks and a small decrease in the intensity corresponding to the silicon characteristic peak when the take-off angle was moved to 45°. At a take-off angle of 90° (collecting photoelectrons emitted normal to the surface), and assuming that the coating was homogenous, we can hypothesize a probing depth of approximately 8 − 9 nm with this technique. At 45°, the probing depth fall to 5 - 6 nm, but we still had a strong Si2p peak on the survey spectrum (Table 7). Since the theoretical size of the layer (around 10 nm) for a highly packed oligonucleotide layer should be sufficient to eliminate the silicon peak, these data shows that either the surface coverage was partial or the depth of the coating was lower than 5 nm i.e. that oligonucleotides were collapsed over the surface under vacuum conditions. Both assumptions are linked, since non-dense oligonucleotide packing should provide space to allow the collapse onto the surface.

	C1s	O1s	N1s	Si2p
TOA 90°	28.8	28.7	3.4	39.1
TOA 45°	32.7	28.4	4.4	34.4

Table 7: Average elemental composition (Atoms %) at take-off-angles (TOA) of 90 and 45°.

XPS high resolution spectra show the different chemical environment for each detected atom and allow to assess the grafting efficiency. Moreover, the N1s high resolution spectra are characteristic of the grafted layer.

These high resolution spectra studies, in terms of the proportion of each chemical environment, enable assurance of conservation of oligonucleotide bases.

As usual, C1s high resolution spectra were used to determine the components that reflect the different chemical environments found in the carbon peak, since a carbon involved in a given chemical environment is defined by a specific binding energy. In the case of this specific study, a carbon peak could originate from desoxyribose rings (CHx and C-O) and nitrogen bases (-C-N, C=N, and -N-C(=O)). C-C, C-H were located at 285.0 eV, C-O, C-N at 286.5 eV, -N-C=N-, -O-C-N- and O=C-N at 288.2 eV. This assignment was confirmed by O1s and N1s high resolution spectra. The peak fitting analysis showed three components in the O1s region: 530.8 eV (SiO_2), 532.4 eV (-C=O) and 534.0 eV (-C-O), which allows differentiation of oxygen atoms linked to silicon and oxygen atoms from organic molecules. Three chemical environments were distinguishable in the N1s high resolution spectrum (Figure 36). Accordingly, nitrogen atoms are present under various forms in the nitrogen base of the oligonucleotide: 399.1 eV –N= (nitrogen with unsaturated bonds in nitrogen base rings and monolayer), 400.3 eV –NH- and N with three single bonds (amide and nitrogen base rings), 401.9 eV $-NH_2$ from adenine and guanine residues. Binding energies and intensity percentages of N1s core level peak, summarized in Table 8, show very good agreement with the theoretical percentages calculated on the basis of the following data: the spacer (between the surface and the nucleotide sequence) is composed of two nitrogen atoms in the –N= form; guanine and adenine residues both contain 5 nitrogen atoms but under different forms (3 –N=, 1 –NH- and 1 $–NH_2$) for adenine residues and (2 –N=, 2 –NH- and 1 $–NH_2$) for guanine residues. The oligonucleotide used in the study contains 14 guanine and 10 adenine residues.

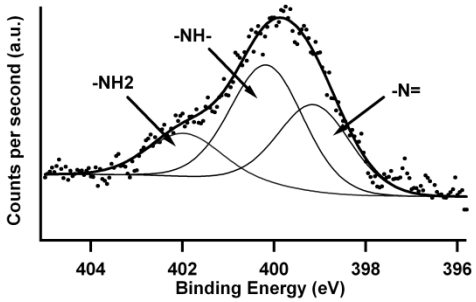


Figure 36: N1s high resolution peak and peak fitting.

Binding Energy (eV)	Assignment	At % (theoretical)	At % (experimental)
399.1	-N=	50.0	47.8
400.3	-NH-	30.3	34.8
401.9	$–NH_2$	19.7	17.4

Table 8: Peak fitting for N1s high resolution spectra.

Since we are able to correlate the expected nitrogen atom forms and the experimental data, we can conclude that the oligonucleotide is effectively grafted and not denatured by the grafting process, which means that the binding, as expected, occurs at the 5'-amino modification and not at the amine of the bases along the oligonucleotide backbone.

A water static contact angle measurement was performed after each step of the grafting process to follow the evolution of the wetting properties of the surface. For interpretation, we have focused on the variation between contact angles at each step of the process. This allows an interpretation in term of variation of the wetting properties of the surface.

After UV/ozone cleaning (step 0), the contact angle value was close to 0° (in fact, not measurable by the technique we used) in accordance with a high density of the hydroxyl groups on the surface, which led us to expect high grafting efficiency. After silanization (step 1) an increase in the contact angle was observed. This increase is due to the grafting of an amine moiety, which leads to a lower wettability of the surface. The measured value (71 ± 4)° is in extremely good agreement with the reported values by A. Krishnan et al. [148] (70° after APTES grafting). The contact angle measured (59 ± 3)° after the glutaraldehyde grafting (step 2) is also in agreement with previously published data by Nugaeva et al. [149] and corresponds to the addition of the aldehyde moiety to the surface, which has wetting properties intermediate between hydroxyl and amine species. Finally, the three other steps were aimed at obtaining dangling hydroxyl groups at the end of the carbon-phosphate chain of the oligonucleotides. This chain should lead to a wettable surface. The contact angle of steps 3, 4 and 5, ((49 ± 1) °, (76 ± 7)° and (53 ± 2)° respectively) are in agreement with published data by C. Zhao et al. [150]. The average increase between steps 3 and 4 agreed with the grafting of propylamine (hydrophobic molecule) on non-reacted glutaraldehyde, despite its smaller size in comparison to the oligonucleotide strain.

Thus, the variation in the static water contact angle at each step of the process demonstrated at each step the success and efficiency of the grafting.

Ellipsometry measurements were done step by step in air and in aqueous solution. To enable further analysis of these results, we calculated the theoretical length of each grafted molecule. For this purpose, we have considered the molecules in steps 0, 1 and 2 as rigid chains with fixed angles between the bonds, and the oligonucleotides after steps 3, 4 and 5 as helices with 10.5 bases in one full rotation (i.e. 36° rotation between two sugars) and a vertical size of 3.4 Å per full rotation. According to the description given in Figure 34, for theoretical thickness we assumed a perfect layer, i.e. perpendicular to the surface and highly packed. The comparison between each step and between theoretical and experimental results provides the data in Table 9.

In step 0, the slight thickness corresponds to the oxide layer, which is due to the cleaning procedure. As expected, the environmental conditions for measurement had no impact on the thickness of the oxide layer, which was identical in water and in air. In steps one and two, after the grafting of APTES and glutaraldehyde, a short

deviation between the results obtained in air and in liquid was observed. This is in accordance with the properties of these two molecules, known for their ability to form dense, self-assembled monolayers on surfaces. Moreover, the deviations between experimental and theoretical data were probably due to the ability of APTES and glutaraldehyde to form small, multilayer patches during the grafting process. In step 3, 4 and 5, experimental thicknesses in solution were close to the expected theoretical value, which indicates that the oligonucleotides were in a brush-like conformation. Nevertheless some deviations exist, due to the calculation of the oligonucleotide length, which was done assuming a dense mono-layer of oligonucleotides. Since, in liquid, the refractive indices of oligonucleotide and water are close (i.e. 1.35 and 1.33 respectively), any deviation between the theoretical and experimental thicknesses can be due to experimental errors. Moreover, the oligonucleotide double-stranded helices grafted in step 3 were large, charged molecules, with likely repulsive interactions. Accordingly, they could not be grafted in a perfectly dense mono-layer, leading to an average thickness of "coated" and non-occupied areas on the surface. Additionally, the theoretical size of the layer grafted in the three last steps was calculated for a double helix, without taking into account the following aspects: in step 4, the size increased due to the graft of propylamine on glutaraldehyde occupying the space left free, whereas in step 5 the length increased due to the dehybridization of the nucleotide sequences, which lose their compact helical conformation and stretch in aqueous solution, due to charge repulsion along the oligonucleotide backbone.

The lengths observed in air in the three last steps were identical and significantly smaller than those expected for a brush-like conformation. In addition, no variations were observed between each step. These results confirm our hypothesis that the oligonucleotides collapse onto the surface. Those results further confirm the conclusion drawn after XPS measurements. The oligonucleotides were grafted at the 5'-amino terminus. However, the density of grafting was low enough to allow the oligonucleotides to adopt their free conformation in aqueous solution and to collapse in air. According to C. Y. Lee et al. [151], who showed that the effect of too high grafting density of oligonucleotides results in lower efficiency of hybridization, this result suggests good accessibility of the oligonucleotide bases for specific recognition or binding, especially in the case of biological adhesion.

step		**0**	**1**	**2**	**3**	**4**	**5**
Theoretical thickness (Å)		0	7.79	14.32	101.02	101.02	**101.02**
Experimental thickness (Å)	**air**	17	20	20	33	30	**30**
	water	**17**	**17**	**27**	**86**	**147**	**173**

Table 9: Comparison between theoretical and experimental thickness of the layer after each step; step 0: clean silicon; step 1: APTES grafting; step 2: glutaraldehyde grafting; step 3: double stranded helix; step 4: propylamine grafting and; step 5: dehybridization of the double stranded helix.

AFM was performed on dried samples. Mean roughness (Ra, Rms) and maximal height difference were measured at each step of the procedure. Experiments were also conducted in aqueous solution at step 5 to compare

the roughness coefficient in dry and wet environmental conditions. Table 10 presents the results. Since the grafting coverage is supposed to be homogeneous, mean roughness should be conserved in the course of the grafting procedure. As expected, a comparison between step 5 in dry condition and step 5 in aqueous solution showed that all coefficients were comparable. In dry conditions, the mean roughness (Ra and Rms) was conserved between each step, and was the same as the roughness coefficient of the clean silicon wafer. This result indicates homogeneous coverage of the surface. Considering the topography of the surface, AFM pictures (data not shown) and maximal height show conservation of this topography, as well as a small decrease in maximal height between clean silicon and the subsequent layers grafted at each step. This decrease can be attributed to the ability of the oligonucleotide to collapse onto the surface and to flatten the surface in a dry environment.

Surface	SiO_2	Step 1	Step 2	Step 3	Step 4	Step 5	Step 5 aqueous medium
Ra (nm)	0.4 ± 0.3	0.2 ± 0.1	0.4 ± 0.1	0.2 ± 0.06	0.1 ± 0.02	0.3 ± 0.1	**0.3 ± 0.2**
Rms (nm)	0.6 ± 0.3	0.6 ± 0.5	0.6 ± 0.2	0.5 ± 0.2	0.6 ± 0.7	0.9 ± 0.2	**1.1 ± 1.1**
Maximal height (nm)	**4.8 ± 0.3**	**2.7 ± 0.4**	**2.9 ± 0.1**	**2.4 ± 0.2**	**2.8 ± 0.6**	**3.5 ± 0.1**	**2.2 ± 0.9**

Table 10: Ra, Rms and maximal height at each step of the procedure; step 0: clean silicon; step 1: APTES grafting; step 2: glutaraldehyde grafting; step 3: double stranded helix and reduction of the Schiff base; step 4: propylamine grafting and; step 5: dehybridization of the double stranded helix.

Nevertheless, since no main variation of the roughness coefficient was observed, surfaces can be assumed to be smooth at the nanoscale.

3.1.a.ii. "High density" oligonucleotide modified surfaces.

The second protocol, used for SAMs elaboration displays a slight variation in the experimental procedure, compared to the one used for "low density" SAMs, aiming at reducing the Schiff-base obtained by the reaction of oligonucleotide amino termination with the glutaraldehyde aldehyde moiety. This allows to enhance grafting stability, protecting oligonucleotides from detachment during the dehybridization step (step 5), leading to a higher density of grafted oligonucleotides.

Surfaces were modified with two different oligonucleotides. We modified surfaces with the oligonucleotide complementary to that involved in the self-assembly, i.e. C_7T_5 (5'-TCTCTCTCTCCC-3') surface tethered at the 5' end, and surfaces bearing the same oligonucleotide as the one involved in the self-assembly, i.e. A_5G_7 (5'-AGAGAGAGAGGG-3'). Monitoring of the oligonucleotide grafting at each step of the process allowed an assessment of the proper anchoring of the oligonucleotide on silicon oxide modified quartz crystals and quantification of the oligonucleotide grafted mass as presented in Figure 37. The QCM frequency shift displayed

in graph (a) decreases, indicating a mass deposition onto a glutaraldehyde covered crystal. Upon rinsing steps after the deposition process (visible by the frequency jump), the frequency remained stable. The dissipation shift curve indicates the deposition of a layer with very little dissipative behavior (dissipation shift less than $0.5.10^{-6}$ u.a.). Both results illustrate the deposition and grafting of the double stranded DNA as a monolayer covalently linked to the surface. Since the double stranded DNA molecule investigated in this study are small and rigid, the monolayer is not dissipative. Therefore, the quantification of the deposited mass does not depend on the dissipative contribution and can be calculated with the help of the Sauerbrey equation, as shown in graph (b). Following this grafting, quenching with glycine in presence of sodium cyanoborohydrate in the medium is performed, ensuring the stability of the layer. This quenching step is followed by the dehybridization, providing the single-stranded coated surface.

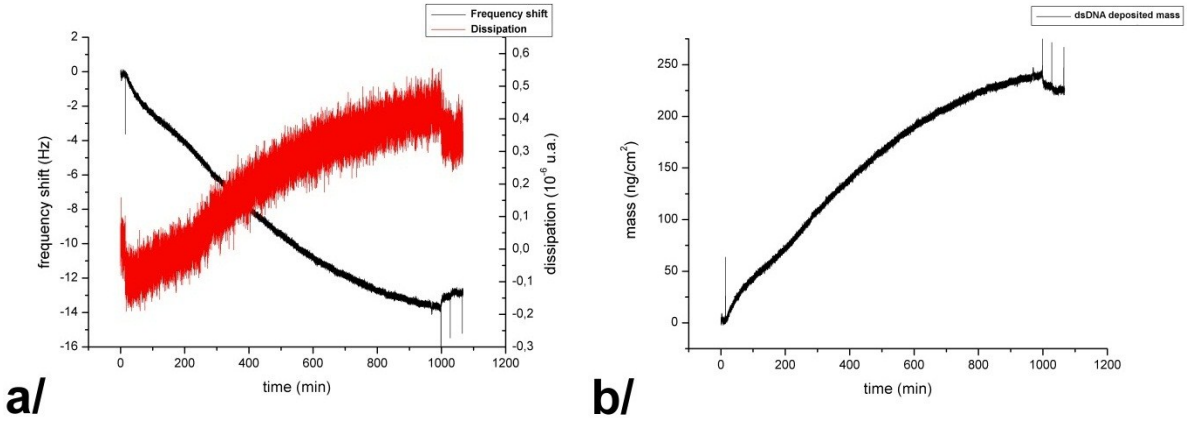


Figure 37 : (a) Frequency shift of QCM crystal and dissipation monitored after injection of double stranded DNA (NH_2- C7T5 hybridizes with A_5G_7) (b) calculation of mass deposited according to the frequency shift from the Sauerbrey equation.

To ensure that the obtained surface displayed, as expected, a higher oligonucleotide surface density compared to the "low density" surface, we measured XPS survey- and high resolution spectra as presented in Figure 38. These spectra demonstrate, as discussed for a "low density" surface, the grafting of the desired oligonucleotide. Moreover, with survey spectra normalized from to silicon peaks of the background, we determined an increase of 10% of the oligonucleotide surface density in the case of "high density" surfaces. This increase was evaluated from the comparative measurement of the intensity of the nitrogen (N1s) peak between both surfaces.

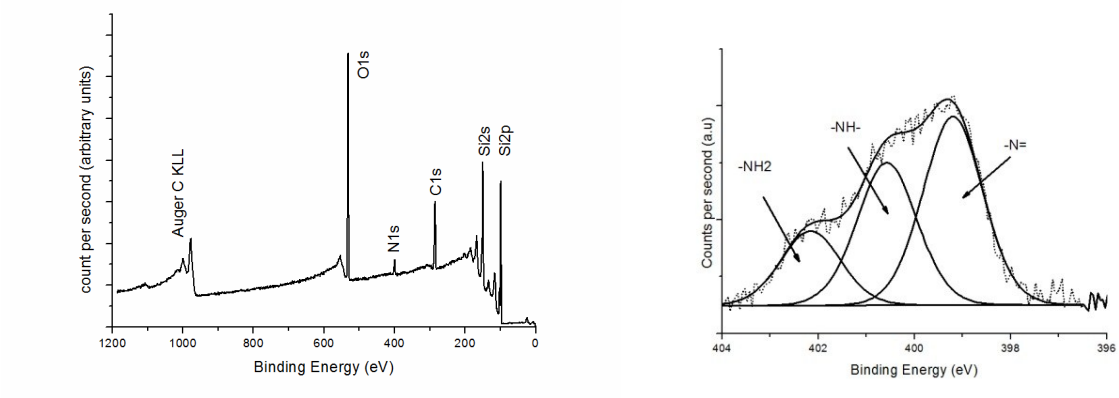


Figure 38 : (a) survey and (b) high resolution spectrum of a surface coated with (C_7T_5)

Finally contact angle measurements value was quantified as 53±2° for "low density" surfaces modified with A_5G_7. "High density" A_5G_7 surfaces yielded values of 48±2°, whereas a value of 45±2° was measured on "high density" C_7T_5 surfaces. These results lead to similar contact angle for the different smooth oligonucleotide-modified surfaces of "high density", which proves comparable physico-chemical properties of the different surfaces in term of hydrophobicity. The slight difference between "high density" and "low density" oligonucleotide surfaces can be attributed to the variation in the hydrophobic character of the molecule used at the quenching step (step 4): the "low density" surface was quenched with propylamine (hydrophobic), while "high density" surfaces are quenched with glycine (hydrophilic).

3.1.b. Surface based on immobilization of vesicles through nonspecific interaction.

Through preparing surfaces based on immobilization by nonspecific base pairing of vesicles, the aim was not to design a surface bearing nanoreactors, but to produce a model surface to ensure variation of surface topography, keeping other parameters constant (physico-chemical properties, chemistry and mechanical properties) in comparison to the "smooth" oligonucleotide modified surfaces. For this purpose we used an oligonucleotide surface bearing A_5G_7 oligonucleotide, to deposit PB_{65}-A_5G_7 vesicles. This polymer, composed of poly(butadiene), allows to crosslink the vesicular shell after deposition. This process allowed enhancement of surface stability and provided stiff mechanical properties to the surface.

We characterized this surface to assess topography and chemical properties subsequent to vesicles deposition. AFM was performed under the same conditions as on the oligonucleotide-modified surfaces; the mean roughness (Ra, Rms) and maximal height difference were measured. Results compared to data obtained for the oligonucleotide SAM modified surfaces (step 5) showed, as expected, a significant increase in the Ra values (5.9 ± 0.2 nm) and Rms (12.9 ± 0.2 nm). Nevertheless, the significant mean roughness at the submicron scale was low compared to the size of the deposited vesicles. However, this is consistent with the configuration observed by AFM imaging (Figure 39) and with the maximal height difference (130 nm) i.e.: a highly flat surface (nanoscale) modified with high dots (130 nm high, 200 nm large) dispersed on the surface. The size of these dots is in

accordance with the deposition of 180 nm diameter reticulated vesicles. The number of vesicles on the oligonucleotide SAM, measured by AFM (Figure 39) and optical microscopy (data not shown), was low (1.4 ± 0.2 10^8 vesicles.cm^{-2}), which corresponds to 5.6 ± 0.7% of the total area (vesicles of 0.2 µm diameter). This surface coverage provides a topographical feature of high objects dispersed on a flat surface, which leads to a submicron roughness. Since the nanostructured surfaces consist of vesicles deposited on the oligonucleotide-modified surface, we expected similar wetting properties for both oligonucleotide surface and non-hybridized vesicle surface. The measured value (60 ± 4°) on the nanostructured surface confirmed our hypothesis (53 ± 2° for "low density" oligonucleotide-modified surfaces).

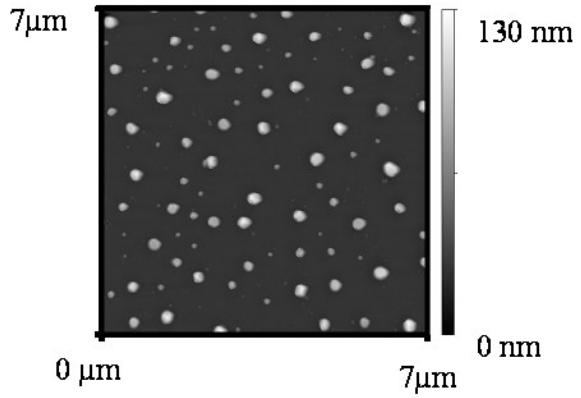


Figure 39: AFM picture of the oligonucleotide nanostructure surface

Since several rinsing steps and incubation times in culture medium have shown the stability of the topographical feature, the adhesion of those reticulated oligomersomes on the surface was assumed to be driven by physical forces as schematically described in Figure 40.

Moreover, stabilization of the vesicular structures by UV-irradiation should prevent vesicles to collapse. The stability of the morphology has indeed been ensured in an AFM preliminary study (I. Moldan, unpublished results) to be enhanced by cross-linking polymerization of the poly(butadiene) constituting the hydrophobic part of the oligomersome shell [121].

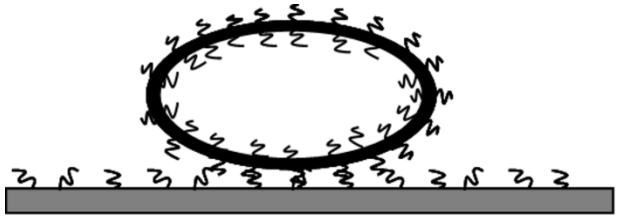


Figure 40 : schematic description of the cross-linked vesicular shape adhering to the surface by physical interaction. The deformation of the shape, that is expected due to deposition and adhesion is illustrated.

3.1.c. Surface resulting from hybridization of vesicles on oligonucleotide modified surfaces.

To prepare this type of surfaces, we hybridized vesicles with their complementary oligonucleotide tethered on the surface. Vesicle hybridization with the oligonucleotide–modified surfaces was monitored with the QCM-D. Oligonucleotide sequence C_7T_5 grafting was followed by QCM-D prior to injection of an aqueous solution of self-assembled PIB_{31}-G_7A_5. We monitored the frequency and dissipation shifts due to the vesicle immobilization (Figure 41). Interestingly, we observed a large and rapid deposition of mass: 80% of the mass was deposited within the first hour. The frequency shift decrease correlates with a dissipation shift increase, due to the vesicular structure dissipative properties. According to R. Richter et al. [92,152], the association of both shifts is characteristic of the immobilization of vesicles that retain their morphology over time. The deposition was stable to rinsing, demonstrating the strength of the immobilization of the vesicles held by hybridization.

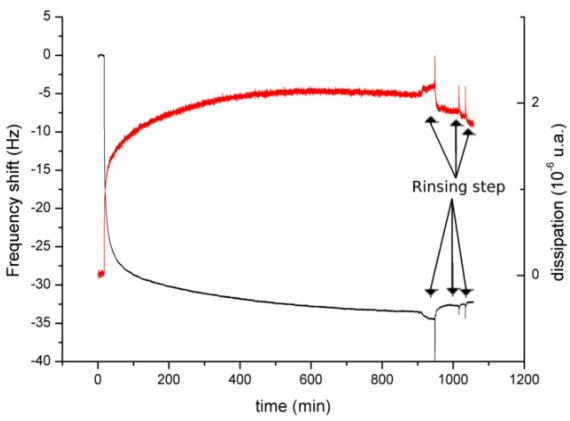


Figure 41: QCM-D monitoring of oligonucleotide-based vesicle immobilization on surfaces modified with the complementary sequence. The black curve corresponds to the time course of the frequency, whereas the red curve represents the dissipation shift induced by vesicles immobilization on the surface.

To quantify the deposited mass, a model of the deposited layer is needed. We selected the Voigt model [117], since it takes into account the dissipative contribution of the dissipative layer of a visco-elastic solid layer. We quantified an experimental, deposited mass of 630 ± 40 ng.cm^{-2}, larger than the theoretical value (deposited mass of 470 ng/cm^2) estimated for a monolayer of vesicles (60 nm in diameter and 2.12 10^{-7} ng expected for PIB_{31}-G_7A_5 self-assembled copolymer). However, the heterogeneity in the size of the vesicles (observed previously in Chapter 1) combined with the ability of the block copolymer to form aggregates of vesicles, probably explain the difference between the experimental and theoretical values.

From the Voigt model, the mechanical properties of the vesicle layer can also be determined. The shear force modulus and layer viscosity quantified with the Voigt model of the layer of vesicles deposited were estimated to respectively 6.10^5 Pa and 0.0038 kg/m^2, which, compared to published values [117], correspond a low viscosity and a high shear modulus, demonstrating a highly hydrated visco-elastic layer.

In order to assess the strength of hybridization between the vesicles and the surface tethered nucleotide sequences, we compared the frequency and dissipation shifts after rinsing with pure water and after rinsing with a urea solution (4M), which is known for its ability to de-hybridize double stranded oligonucleotides. Results are shown in Figure 42. A positive frequency shift was observed after injection of the solution of urea, showing that a part of the total mass was washed away from the surface, which did not occur upon rinsing with water. This proves that the vesicles were hybridized and not only adsorbed to the surface, since urea enables the dehybridization of vesicles. The desorbed mass, calculated according to the Voigt model, was about 130 ± 10 ng.cm^{-2}, leading to evidence of partial dehybridization of the vesicles. This amount of de-hybridized vesicles (about 20%) is smaller than expected, which is probably due to the low accessibility of hybridized oligonucleotide to urea compared to the total number of oligonucleotide strands involved in hybridization, hidden by steric hindrance.

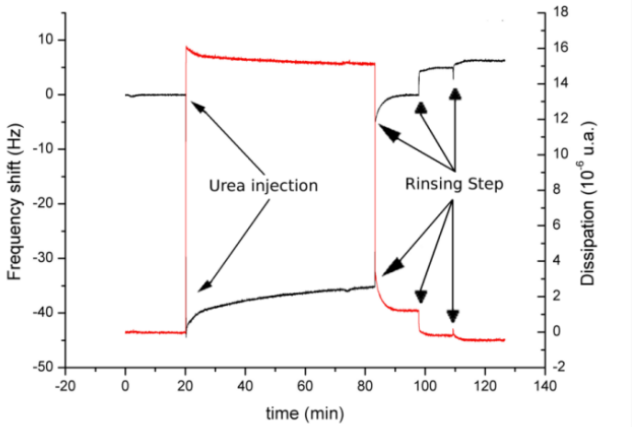


Figure 42: QCM-D monitoring of the effect of urea (4M solution) on oligonucleotide-based vesicles immobilization on surfaces modified with the complementary oligonucleotide. The black curve corresponds to the time course of the frequency, whereas the red curve represents the dissipation shift upon elimination of the vesicles from the surface due to dehybridization.

The dynamic process of the immobilization of the vesicles on the surface was followed by confocal laser scanning microscopy (using an upright Zeiss CLSM LSM700) enabling both reflection and fluorescence detection modes. Typical images are presented in Figure 43. As previously revealed by the QCM-D analysis (Figure 41), the main increase in the mass deposition was observed within the two first hours of vesicle hybridization. Interestingly, the vesicles did not cover the surface as a monolayer before building up multilayered structures, but they were instead immobilized as vesicles aggregates observable under the confocal microscope, which appear as large labeled aggregates with sizes ranging from 1 to 5 µm in diameter. This hybridization of aggregates, probably of large, compound micelles or higher order vesicular structures, is probably at the origin of the large mass deposition measured with the QCM-D (larger than monolayer).

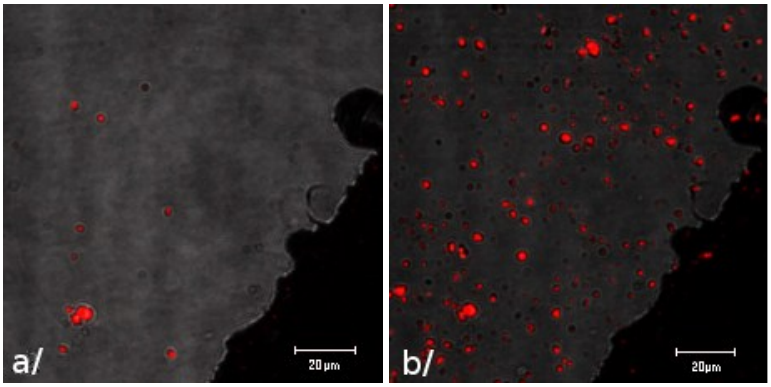


Figure 43: CLSM micrographs of PIB_{31}-G_7A_5 vesicle aggregates immobilized on surfaces modified with the complementary strands (a) after 5 min (b) and after 2 h of incubation.

In order to illustrate the fast spontaneous deposition process, previously observed with the QCM-D, the surface was scanned every 2 min over 2 hours in a liquid static mode (movie, data not shown). Despite some shifts in the intensity of the reflected light due to medium evaporation, leading to brightness variation, we were able to follow the fast, spontaneous deposition of vesicles on an oligonucleotide-coated surface over time, demonstrating the high affinity of the vesicles for the surface. Moreover, we observed that the aggregates retain their shape and were not destroyed or modified by the hybridization process.

In a second step, we performed the hybridization of the vesicles to surface in the flow-cell setup presented in Part II Materials and methods. The deposition was performed without any flow over 12 hours as illustrated in Figure 44. A peristaltic pump flow of 18 $mL.h^{-1}$ was initiated and the hybridized vesicles were observed every 2 min in order to evaluate the stability of the deposited layer (movie, not shown). Only few aggregates were eliminated by the flux, demonstrating the strength of linkage through hybridization. The most interesting observation is the wave-like movement induced by the peristaltic pump flow. When the pump drives the liquid in the cell, the aggregates of vesicles bend due to the flow while, when the pump is down, vesicle aggregates return to their original position and their shape is restored.

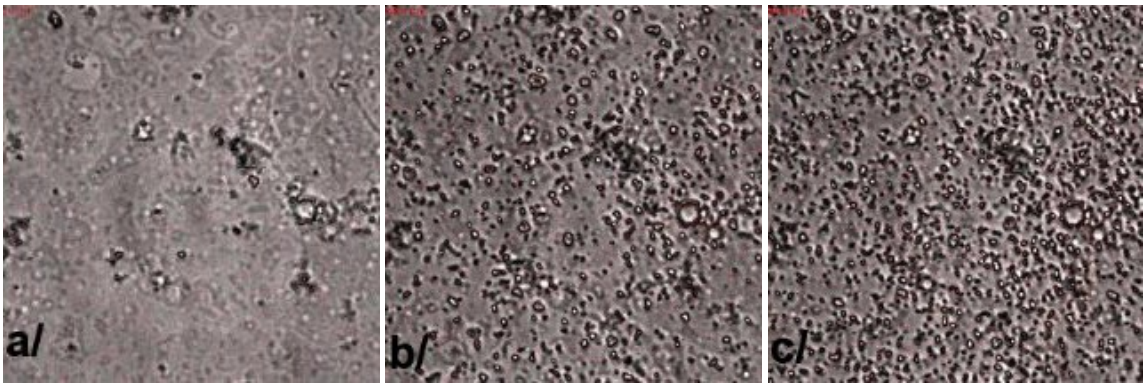


Figure 44: Reflection CLSM micrographs showing vesicle attachment on surfaces modified with a complementary sequence to that involved in the self-assembly in the flow cell under static condition, at (a) 0 min, (b) 120 min and (c) 200 min.

The surface coverage and deposition homogeneity were evaluated by AFM in the tapping mode in dry conditions. Results are shown in Figure 45. AFM pictures clearly show a vesicle layer on which some aggregates of vesicles can be observed, probably formed in solution owing to oligonucleotide interactions through electrostatic interactions and unspecific guanosine non- Crick-Watson base-pairing. This result, in accordance with the results of QCM-D analysis, clearly confirms full coverage of the surface. The dense packing of the vesicular structures is enabled by the ability of the amphiphilic block copolymer to overcome electrostatic repulsion in the presence of counter-ions, enhanced by oligonucleotide interactions, as in the case of aggregates formation. This compact arrangement leads to small average roughness values (Ra) of 0.6 ± 0.2 nm. Since AFM was performed in dry conditions, it is important to notice that the vesicular structures were stable upon short term drying, but long term drying results in the destruction of the self-assembled structures (data not shown).

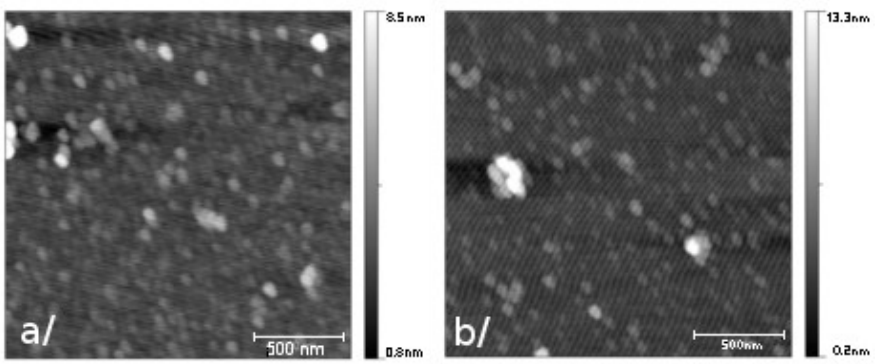


Figure 45: AFM micrographs of PIB_{31}-G_7A_5 vesicles hybridized on surfaces modified with the complementary strands. Full coverage of the surface by vesicles (a), and presence of aggregates of vesicles dispersed on the surface (b) are observed.

Finally the entire process of vesicle hybridization to the oligonucleotide-modified surface can be represented as shown in the scheme in Figure 46. It is clear according to this study that incubating a PIB_{31}-G_7A_5 vesicle solution with a surface coated with the complementary sequences leads to a spontaneous deposition of vesicles and aggregates on the surface (Figure 46(a)). This adsorption is a fast, spontaneous and strongly-interacting process, but the size, shape and stability of the vesicular structure prevents collapsing of the self-assembly. The hybridization interaction strength allows the vesicles to remain at the surface under flow conditions (Figure 46(b)) while polymer softness and fluidity allow the vesicular aggregate super-structures to bend, as observed with the vesicular wave-like movement under peristaltic flow (Figure 46(c)).

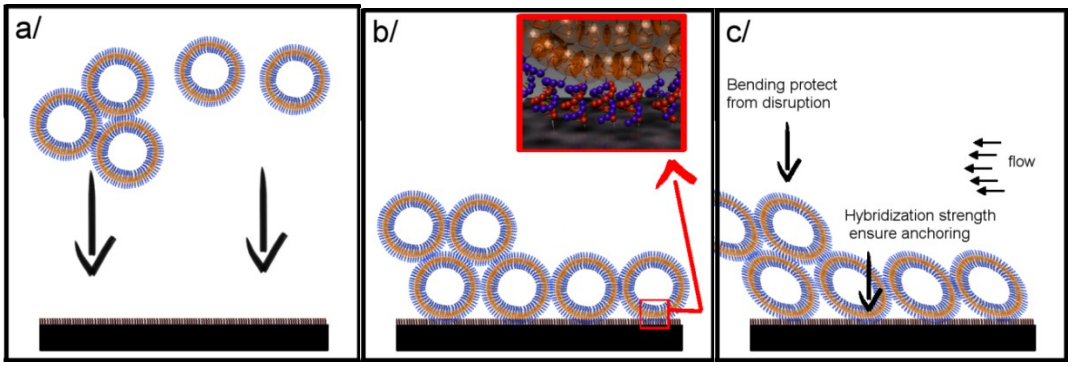


Figure 46: The oligonucleotide-coated surface is immersed in a vesicle solution (a), hybridization occurs rapidly (b), leading to full surface coverage with a layer of vesicles and aggregates thereof. Vesicle bending is due to the peristaltic flow, while hybridized oligonucleotides ensure anchoring (c). Block copolymer softness and membrane fluidity allow vesicles to bend and come back to their initial position, preventing the disruption of the vesicular membrane.

3.2. Conclusion

In this chapter, we first described the preparation of "smooth" surfaces resulting from the coating with an oligonucleotide self-assembled monolayer. These surfaces were prepared with two different densities of oligonucleotides and fully characterized over the preparation steps to assess their properties (physico-chemical properties and topography). We then prepared surfaces resulting from the adsorption of vesicles through nonspecific interaction. This surface was stabilized by intravesicular crosslinking, ensuring surface rigidity, and then characterized by similar methods than used with "smooth" oligonucleotide-coated surfaces.

Finally we hybridized polymeric vesicles self-assembled from PIB_{31}-G_7A_5 block copolymers to surfaces coated with the complementary oligonucleotide strand. This fast process led to a strongly-bound layer of vesicles to the surface. Their stability upon hybridization was demonstrated by the retention of their morphologies, either as singulate or as aggregates. This layer of vesicles was demonstrated to be resistant to flow stress. The hybridization strength ensured anchoring of the vesicles, while block-copolymer membrane softness and fluidity allowed bending of those vesicles, which is preventing them from disruption.

All of the surfaces were characterized, considering physico-chemical properties, topography and mechanical properties, ensuring the possibility of performing comparative studies on the basis of surface property variations.

Conclusion to part I

In the first part of this work, in three chapters, we demonstrated the possibility of producing surfaces based on the attachment of nanoreactors resulting from the self-assembly of an amphiphilic "chimera". In the first chapter we described the synthesis of oligonucleotide- based block copolymers, coupling a short single stranded oligonucleotide to a highly hydrophobic block such as poly(butadiene) or poly(isobutylene), and subsequent chemical characterization. We performed a study of the self-assembly process for this amphiphilic "chimera," leading to evidence of the formation of mixture of micelles and vesicles. Based on the hybridization of this hybrid, we prepared nanoreactors combining lactoperoxidase encapsulation and OmpF embedded in the polymeric shell. We demonstrated the preparation of a pure solution of nanoreactors and precisely quantified the encapsulation and activity efficiency (encapsulation and nanoreactor production) of the nanoreactors. We furthermore discussed enzyme activity and kinetic constants, demonstrating a decreased turnover rate, probably due to encapsulation (steric hindrance, shell charge effect). Finally, we proved the protective action of encapsulation against enzymatic degradation. To conclude this first part, we showed the preparation of surfaces from the immobilization of vesicles. For this purpose we prepared "smooth" surfaces based on self-assembled monolayer of an oligonucleotide, with two different densities. We prepared surfaces resulting from the immobilization of vesicles either interacting through nonspecific or Crick-Watson base pairing. All surfaces were characterized over the course of the entire preparation process, and were characterized to determine their physico-chemical properties, topography and mechanical properties.

Part I was inspired by the preparation of potentially bioactive surfaces. We explored fundamental questions pertaining to polymer self-assembly processes, enzyme kinetics, encapsulation influences, and finally vesicle-surface interaction upon deposition driven by a hybridization process. These topics were of direct interest for our purposes, but several additional questions arise from this work and these were not answered herein. Considering polymer synthesis and self-assembly, some questions regarding buffer counter ion content, pH, and hybridization in solution and their influence on the self-assembly process are of interest for further investigation of this block copolymer self-assembly. Nanoreactor preparation and enzyme activity studies raised some questions regarding the process involved in this encapsulation, since turnover of the enzyme is reduced. Investigating the influence of the polymer and enzyme type on the kinetic parameters would be of interest. Moreover, the use of an enzyme capable of producing a drug to prove the concept of the design of an antimicrobial nanoreactor and studies with different drug- producing nanoreactors is currrently under investigation in Prof. Dr. W. Meier's group. Finally, vesicle deposition on surfaces proved to be a great challenge; some questions about vesicle stability and interactions with surfaces were explored during this work. Additional questions about the thermodynamic processes involved by the deposition is of interest, as well as investigations of vesicle packing and aggregation as a function of th properties of the aqeous environment (pH, counterions…).

References

[1] J. Mark, Polymer data handbook, Oxford University Press, New York, 1999.

[2] H.K. Cho, I.W. Cheong, J.M. Lee, J.H. Kim, Polymeric nanoparticles, micelles and polymersomes from amphiphilic block copolymer, Korean J. Chem. Eng. 27 (2010) 731-740.

[3] A.B. Lowe, N.C. Billingham, S.P. Armes, Synthesis and Characterization of Zwitterionic Block Copolymers, Macromolecules. 31 (1998) 5991-5998.

[4] F.S. Bates, G.H. Fredrickson, Block Copolymer Thermodynamics: Theory and Experiment, Annu. Rev. Phys. Chem. 41 (1990) 525-557.

[5] L. Leibler, Theory of Microphase Separation in Block Copolymers, Macromolecules. 13 (1980) 1602-1617.

[6] Z. Tuzar, P. Kratochvil, Surface and Colloid Science, Matijevic, Plenum Press: New York, 1993.

[7] H. Schlaad, M. Antonietti, Block copolymers with amino acid sequences: Molecular chimeras of polypeptides and synthetic polymers, The European Physical Journal E - Soft Matter. 10 (2003) 17-23.

[8] O.A. Gus'kova, P.G. Khalatur, A.R. Khokhlov, Molecular chimeras: New strategies in the design of functional materials, Nanotechnol Russia. 3 (2008) 481-493.

[9] H.G. Börner, H. Schlaad, Bioinspired functional block copolymers, Soft Matter. 3 (2007) 394.

[10] K. Velonia, Protein-polymer amphiphilic chimeras: recent advances and future challenges, Polym. Chem. (2010).

[11] F.E. Alemdaroglu, A. Herrmann, DNA meets synthetic polymers, highly versatile hybrid materials, Org. Biomol. Chem. 5 (2007) 1311.

[12] M. Bednarek, T. Biedroń, P. Kubisa, Synthesis of block copolymers by atom transfer radical polymerization of tert-butyl acrylate with poly(oxyethylene) macroinitiators, Macromolecular Rapid Communications. 20 (1999) 59-65.

[13] D.A. Shipp, J. Wang, K. Matyjaszewski, Synthesis of Acrylate and Methacrylate Block Copolymers Using Atom Transfer Radical Polymerization, Macromolecules. 31 (1998) 8005-8008.

[14] G. Fleury, F.S. Bates, Hierarchically structured bicontinuous polymeric microemulsions, Soft Matter. 6 (2010) 2751.

[15] B. Keoshkerian, P.J. MacLeod, M.K. Georges, Block Copolymer Synthesis by a Miniemulsion Stable Free Radical Polymerization Process, Macromolecules. 34 (2001) 3594-3599.

[16] L. Hartmann, E. Krause, M. Antonietti, H.G. Börner, Solid-Phase Supported Polymer Synthesis of Sequence-Defined, Multifunctional Poly(amidoamines), Biomacromolecules. 7 (2006) 1239-1244.

[17] R.B. Merrifield, Solid Phase Peptide Synthesis. I. The Synthesis of a Tetrapeptide, J. Am. Chem. Soc. 85 (1963) 2149-2154.

[18] D.J. Gravert, K.D. Janda, Organic Synthesis on Soluble Polymer Supports: Liquid-Phase Methodologies, Chem. Rev. 97 (1997) 489-510.

[19] K.J. Watson, S. Park, J. Im, C.A. Mirkin, DNA−Block Copolymer Conjugates, J. Am. Chem. Soc. 123 (2001) 5592-5593.

[20] J.H. Jeong, T.G. Park, Novel Polymer−DNA Hybrid Polymeric Micelles Composed of Hydrophobic Poly(d,l-lactic-co-glycolic Acid) and Hydrophilic Oligonucleotides, Bioconjugate Chem. 12 (2001) 917-923.

[21] B. de Lambert, C. Chaix, M. Charreyrex, A. Laurent, A. Aigoui, A. Perrin-Rubens, Polymer−Oligonucleotide Conjugate Synthesis from an Amphiphilic Block Copolymer. Applications to DNA Detection on Microarray, Bioconjugate Chem. 16 (2005) 265-274.

[22] C. Minard-Basquin, C. Chaix, C. Pichot, B. Mandrand, Oligonucleotide−Polymer Conjugates: Effect of the Method of Synthesis on Their Structure and Performance in Diagnostic Assays, Bioconjugate Chem. 11 (2000) 795-804.

[23] K. Osada, R.J. Christie, K. Kataoka, Polymeric micelles from poly(ethylene glycol)-poly(amino acid) block copolymer for drug and gene delivery, Journal of The Royal Society Interface. 6 (2009) S325-S339.

[24] F. Alemdaroglu, J. Wang, M. Börsch, R. Berger, A. Herrmann, Enzymatic Control of the Size of DNA Block Copolymer Nanoparticles, Angew. Chem. Int. Ed. 47 (2008) 974-976.

[25] M. Kwak, A.J. Musser, J. Lee, A. Herrmann, DNA-functionalised blend micelles: mix and fix polymeric hybrid nanostructures, Chem. Commun. 46 (2010) 4935.

[26] J. Wang, F.E. Alemdaroglu, D.K. Prusty, A. Herrmann, R. Berger, In-Situ Visualization of the Enzymatic Growth of Surface-Immobilized DNA Block Copolymer Micelles by Scanning Force Microscopy, Macromolecules. 41 (2008) 2914-2919.

[27] K. Ding, F. Alemdaroglu, M. Börsch, R. Berger, A. Herrmann, Engineering the Structural Properties of DNA Block Copolymer Micelles by Molecular Recognition, Angew. Chem. Int. Ed. 46 (2007) 1172-1175.

[28] A. Gissot, M. Camplo, M.W. Grinstaff, P. Barthélémy, Nucleoside, nucleotide and oligonucleotide based amphiphiles: a successful marriage of nucleic acids with lipids, Org. Biomol. Chem. 6 (2008) 1324.

[29] F.J. Teixeira, P. Rigler, C. Vebert-Nardin, Nucleo-copolymers: oligonucleotide-based amphiphilic diblock copolymers, ChemComm. (2007) 1130-1132.

[30] M. Oishi, T. Hayama, Y. Akiyama, S. Takae, A. Harada, Y. Yamasaki, Supramolecular Assemblies for the Cytoplasmic Delivery of Antisense Oligodeoxynucleotide: Polyion Complex (PIC) Micelles Based on Poly(ethylene glycol)-SS-Oligodeoxynucleotide Conjugate, Biomacromolecules. 6 (2005) 2449-2454.

[31] A.(.J. Dirks, S.S. van Berkel, H.I.V. Amatdjais-Groenen, F.P.J.T. Rutjes, J.J.L.M. Cornelissen, R.J.M. Nolte, Synthesis and aggregation behavior of biohybrid amphiphiles composed of a tripeptidic head group and a polystyrene tail, Soft Matter. 5 (2009) 1692.

[32] H.R. Marsden, J. Handgraaf, F. Nudelman, N.A.J.M. Sommerdijk, A. Kros, Uniting Polypeptides with Sequence-Designed Peptides: Synthesis and Assembly of Poly(γ-benzyl L -glutamate)-b-Coiled-Coil Peptide Copolymers, J. Am. Chem. Soc. 132 (2010) 2370-2377.

[33] F.E. Alemdaroglu, N.C. Alemdaroglu, P. Langguth, A. Herrmann, Cellular Uptake of DNA Block Copolymer Micelles with Different Shapes, Macromol. Rapid Commun. 29 (2008) 326-329.

[34] H. Liu, Z. Zhu, H. Kang, Y. Wu, K. Sefan, W. Tan, DNA-Based Micelles: Synthesis, Micellar Properties and Size-Dependent Cell Permeability, Chemistry - A European Journal. 16 (2010) 3791-3797.

[35] A. Baccaro, A. Marx, Enzymatic Synthesis of Organic-Polymer-Grafted DNA, Chem. Eur. J. 16 (2010) 218-226.

[36] Y. Wu, K. Sefah, H. Liu, R. Wang, W. Tan, DNA aptamer-micelle as an efficient detection/delivery vehicle toward cancer cells, Proceedings of the National Academy of Sciences. 107 (2009) 5-10.

[37] P. He, L. He, Synthesis of Surface-Anchored DNA−Polymer Bioconjugates Using Reversible Addition−Fragmentation Chain Transfer Polymerization, Biomacromolecules. 10 (2009) 1804-1809.

[38] F. Cavalieri, A. Postma, L. Lee, F. Caruso, Assembly and Functionalization of DNA−Polymer Microcapsules, ACS Nano. 3 (2009) 234-240.

[39] L. Caseli, C. Pascholati, F. Teixeira Jr., S. Nosov, C. Vebert, A. Müeller, Interaction of oligonucleotide-based amphiphilic block copolymers with cell membrane models, Journal of Colloid and Interface Science. 347 (2010) 56-61.

[40] N. Nasongkla, X. Shuai, H. Ai, B.D. Weinberg, J. Pink, D.A. Boothman, cRGD-Functionalized Polymer Micelles for Targeted Doxorubicin Delivery, Angew. Chem. Int. Ed. 43 (2004) 6323-6327.

[41] W. Meier, Polymer nanocapsules, Chem. Soc. Rev. 29 (2000) 295-303.

[42] C. Nardin, T. Hirt, J. Leukel, W. Meier, Polymerized ABA Triblock Copolymer Vesicles, Langmuir. 16 (2000) 1035-1041.

[43] S.F.M. van Dongen, H.M. de Hoog, R.J.R.W. Peters, M. Nallani, R.J.M. Nolte, J.C.M. van Hest, Biohybrid Polymer Capsules, Chem. Rev. 109 (2009) 6212-6274.

[44] N. Galvez, B. Fernandez, E. Valero, P. Sanchez, R. Cuesta, J. Dominguezvera, Apoferritin as a nanoreactor for preparing metallic nanoparticles, Comptes Rendus Chimie. 11 (2008) 1207-1212.

[45] K. Kitatokarczyk, J. Grumelard, T. Haefele, W. Meier, Block copolymer vesicles using concepts from polymer chemistry to mimic biomembranes, Polymer. 46 (2005) 3540-3563.

[46] C. Nardin, J. Widmer, M. Winterhalter, W. Meier, Amphiphilic block copolymer nanocontainers as bioreactors, The European Physical Journal E. 4 (2001) 403-410.

[47] C. Nardin, J. Widmer, M. Winterhalter, W. Meier, Amphiphilic block copolymer nanocontainers as bioreactors, The European Physical Journal E. 4 (2001) 403-410.

[48] C. Nardin, S. Thoeni, J. Widmer, M. Winterhalter, W. Meier, Nanoreactors based on (polymerized) ABA-triblock copolymer vesicles, Chem. Commun. (2000) 1433-1434.

[49] M. Grzelakowski, O. Onaca, P. Rigler, M. Kumar, W. Meier, Immobilized Protein-Polymer Nanoreactors, Small. 5 (2009) 2545-2548.

[50] A. Graff, M. Winterhalter, W. Meier, Nanoreactors from Polymer-Stabilized Liposomes, Langmuir. 17 (2001) 919-923.

[51] S. van Dongen, M. Nallani, J. Cornelissen, R. Nolte, J. van Hest, A Three-Enzyme Cascade Reaction through Positional Assembly of Enzymes in a Polymersome Nanoreactor, Chemistry - A European Journal. 15 (2009) 1107-1114.

[52] D.M. Vriezema, M. Comellas Aragonès, J.A.A.W. Elemans, J.J.L.M. Cornelissen, A.E. Rowan, R.J.M. Nolte, Self-Assembled Nanoreactors, Chem. Rev. 105 (2005) 1445-1490.

[53] D. Vriezema, P. Garcia, N. Sancho Oltra, N. Hatzakis, S. Kuiper, R. Nolte, Positional Assembly of Enzymes in Polymersome Nanoreactors for Cascade Reactions, Angew. Chem. Int. Ed. 46 (2007) 7378-7382.

[54] K.T. Kim, J.J.L.M. Cornelissen, R.J.M. Nolte, J.C.M.V. Hest, A Polymersome Nanoreactor with Controllable Permeability Induced by Stimuli-Responsive Block Copolymers, Advanced Materials. 21 (2009) 2787-2791.

[55] K.T. Kim, S.A. Meeuwissen, R.J.M. Nolte, J.C.M. van Hest, Smart nanocontainers and nanoreactors, Nanoscale. 2 (2010) 844.

[56] A. Blanazs, S.P. Armes, A.J. Ryan, Self-Assembled Block Copolymer Aggregates: From Micelles to Vesicles and their Biological Applications, Macromolecular Rapid Communications. 30 (2009) 267-277.

[57] V. Balasubramanian, O. Onaca, R. Enea, D.W. Hughes, C.G. Palivan, Protein delivery: from conventional drug delivery carriers to polymeric nanoreactors, Expert Opin. Drug Deliv. 7 (2010) 63-78.

[58] O. Onaca, D.W. Hughes, V. Balasubramanian, M. Grzelakowski, W. Meier, C.G. Palivan, SOD antioxidant nanoreactors: influence of block copolymer composition on the nanoreactor efficiency, Macromol Biosci. 10 (2010) 531-538.

[59] P. Broz, S. Driamov, J. Ziegler, N. Ben-Haim, S. Marsch, W. Meier, Toward Intelligent Nanosize Bioreactors: A pH-Switchable, Channel-Equipped, Functional Polymer Nanocontainer, Nano Lett. 6 (2006) 2349-2353.

[60] G. Xu, H.L. McLeod, Strategies for Enzyme/Prodrug Cancer Therapy, Clinical Cancer Research. 7 (2001) 3314-3324.

[61] K.D. Bagshawe, C.J. Springer, F. Searle, P. Antoniw, S.K. Sharma, R.G. Melton, A cytotoxic agent can be generated selectively at cancer sites, Br. J. Cancer. 58 (1988) 700-703.

[62] Q. Chen, M.G. Espey, M.C. Krishna, J.B. Mitchell, C.P. Corpe, G.R. Buettner, Pharmacologic ascorbic acid concentrations selectively kill cancer cells: Action as a pro-drug to deliver hydrogen peroxide to tissues, Proceedings of the National Academy of Sciences of the United States of America. 102 (2005) 13604-13609.

[63] K. Wu, A New Classification of Prodrugs: Regulatory Perspectives, Pharmaceuticals. 2 (2009) 77-81.

[64] M. Grima, C. Welsch, B. Michel, M. Barthelmebs, J.L. Imbs, In vitro tissue potencies of converting enzyme inhibitors. Prodrug activation by kidney esterase, Hypertension. 17 (1991) 492-496.

[65] H. Han, G.L. Amidon, Targeted prodrug design to optimize drug delivery, AAPS PharmSci. 2 (2002) 48-58.

[66] T.P. Smyth, M.E. O'Donnell, M.J. O'Connor, J.O. St Ledger, [beta]-Lactamase-Dependent Prodrugs--Recent Developments, Tetrahedron. 56 (2000) 5699-5707.

[67] M.L. Rodrigues, P. Carter, C. Wirth, S. Mullins, A. Lee, B.K. Blackburn, Synthesis and [beta]-lactamase-mediated activation of a cephalosporin-taxol prodrug, Chemistry & Biology. 2 (1995) 223-227.

[68] C.C. Fuglsang, C. Johansen, S. Christgau, J. Adler-Nissen, Antimicrobial enzymes: Applications and future potential in the food industry, Trends in Food Science & Technology. 6 (1995) 390-396.

[69] M. Morrison, W.F. Steele, Lactoperoxidase, the peroxidase in the salivary gland, Biology of the Mouth. (1968).

[70] B. Reiter, G. Harnulv, Lactoperoxidase antibacterial system: natural occurrence, biological functions and practical applications, J Food Prot. 47 (1984) 724 - 732.

[71] E.L. Thomas, Lactoperoxidase-catalyzed oxidation of thiocyanate: equilibria between oxidized forms of thiocyanate, Biochemistry. 20 (1981) 3273 - 3280.

[72] E.L. Thomas, T.W. Milligan, R.E. Joyner, M.M. Jefferson, Antibacterial activity of hydrogen peroxide and the lactoperoxidase-hydrogen peroxide-thiocyanate system against oral streptococci, Infect Immun. 62 (1994) 529 - 535.

[73] P.A. Samant, M.M. Jefferson, E.L. Thomas, Lactoperoxidase antimicrobial activity against Candida albicans, J Dent Res. 78 (1999) 1208.

[74] A. Welk, C. Meller, R. Schubert, C. Schwahn, A. Kramer, H. Below, Effect of lactoperoxidase on the antimicrobial effectiveness of the thiocyanate hydrogen peroxide combination in a quantitative suspension test, BMC Microbiology. 9 (2009) 134.

[75] L.W.T. Fweja, M.J. Lewis, A.S. Grandison, Challenge Testing the Lactoperoxidase System Against a Range of Bacteria Using Different Activation Agents, J. Dairy Sci. 91 (2008) 2566-2574.

[76] J. Tenovuo, K.M. Pruitt, B. Mansson-Rahemtulla, P. Harrington, D.C. Baldone, Products of thiocyanate peroxidation: properties and reaction mechanisms, Biochim Biophys Acta. 870 (1986) 377 - 384.

[77] E. Seifu, E.M. Buys, E.F. Donkin, I.-. Petzer, Antibacterial activity of the lactoperoxidase system against food-borne pathogens in Saanen and South African Indigenous goat milk, Food Control. 15 (2004) 447-452.

[78] M. Theraud, Y. Bedouin, C. Guiguen, J.P. Gangneux, Efficacy of antiseptics and disinfectants on clinical and environmental yeast isolates in planktonic and biofilm conditions, J Med Microbiol. 53 (2004) 1013 - 1018.

[79] A.J. Ratner, A. Prince, Lactoperoxidase . New Recognition of an "Old" Enzyme in Airway Defenses, Am. J. Respir. Cell Mol. Biol. 22 (2000) 642-644.

[80] A.K. Singh, N. Singh, S. Sharma, S.B. Singh, P. Kaur, A. Bhushan, Crystal Structure of Lactoperoxidase at 2.4 Å Resolution, Journal of Molecular Biology. 376 (2008) 1060-1075.

[81] K.D. Kussendrager, A.C.M. van Hooijdonk, Lactoperoxidase: physico-chemical properties, occurrence, mechanism of action and applications, Bjn. 84 (2007).

[82] L. Pasquardini, L. Lunelli, L. Vanzetti, M. Anderle, C. Pederzolli, Immobilization of cationic rifampicin-loaded liposomes on polystyrene for drug-delivery applications, Colloids and Surfaces B: Biointerfaces. 62 (2008) 265-272.

[83] E. Forssen, M. Willis, Ligand-targeted liposomes, Advanced Drug Delivery Reviews. 29 (1998) 249-271.

[84] C. Yoshina-Ishii, S.G. Boxer, Arrays of Mobile Tethered Vesicles on Supported Lipid Bilayers, Journal of the American Chemical Society. 125 (2003) 3696-3697.

[85] N. Huang, G. Csucs, K. Emoto, Y. Nagasaki, K. Kataoka, M. Textor, Covalent Attachment of Novel Poly(ethylene glycol)−Poly(lactic acid) Copolymeric Micelles to TiO2 Surfaces, Langmuir. 18 (2002) 252-258.

[86] I. Stanish, J.P. Santos, A. Singh, One-Step, Chemisorbed Immobilization of Highly Stable, Polydiacetylenic Phospholipid Vesicles onto Gold Films, J. Am. Chem. Soc. 123 (2001) 1008-1009.

[87] C. Guo, P. Boullanger, L. Jiang, T. Liu, One-step immobilization of alkanethiol/glycolipid vesicles onto gold electrode: Amperometric detection of Concanavalin A, Colloids and Surfaces B: Biointerfaces. 62 (2008) 146-150.

[88] S. Chemburu, E. Ji, Y. Casana, Y. Wu, T. Buranda, K.S. Schanze, Conjugated Polyelectrolyte Supported Bead Based Assays for Phospholipase A2 Activity†, J. Phys. Chem. B. 112 (2008) 14492-14499.

[89] Y. Li, N. Gu, Thermodynamics of Charged Nanoparticle Adsorption on Charge-Neutral Membranes: A Simulation Study, J. Phys. Chem. B. 114 (2010) 2749-2754.

[90] V.P. Zhdanov, B. Kasemo, Comments on Rupture of Adsorbed Vesicles, Langmuir. 17 (2001) 3518-3521.

[91] P. Vermette, L. Meagher, E. Gagnon, H.J. Griesser, C.J. Doillon, Immobilized liposome layers for drug delivery applications: inhibition of angiogenesis, Journal of Controlled Release. 80 (2002) 179-195.

[92] R.P. Richter, R. Bérat, A.R. Brisson, Formation of Solid-Supported Lipid Bilayers: An Integrated View, Langmuir. 22 (2006) 3497-3505.

[93] T.M. Allen, E. Brandeis, C.B. Hansen, G.Y. Kao, S. Zalipsky, A new strategy for attachment of antibodies to sterically stabilized liposomes resulting in efficient targeting to cancer cells, Biochimica Et Biophysica Acta (BBA) - Biomembranes. 1237 (1995) 99-108.

[94] E. Nice, B. Catimel, Instrumental biosensors: new perspectives for the analysis of biomolecular interactions, BioEssays. 21 (1999) 339-352.

[95] H. Urakawa, S. El Fantroussi, H. Smidt, J.C. Smoot, E.H. Tribou, J.J. Kelly, Optimization of Single-Base-Pair Mismatch Discrimination in Oligonucleotide Microarrays, Applied and Environmental Microbiology. 69 (2003) 2848-2856.

[96] J. SantaLucia, A unified view of polymer, dumbbell, and oligonucleotide DNA nearest-neighbor thermodynamics, Proceedings of the National Academy of Sciences of the United States of America. 95 (1998) 1460-1465.

[97] J.R. Williamson, G-Quartet Structures in Telomeric DNA, Annu. Rev. Biophys. Biomol. Struct. 23 (1994) 703-730.

[98] S. Sivakova, S.J. Rowan, Nucleobases as supramolecular motifs., Chemical Society Reviews. 34 (2005) 9-21.

[99] B.A. Armitage, The impact of nucleic acid secondary structure on PNA hybridization, Drug Discovery Today. 8 (2003) 222-228.

[100] S.J. Miller, DNA as a template for reaction discovery, Nat Biotechnol. 22 (2004) 1378-1379.

[101] A.A. Zinchenko, K. Yoshikawa, D. Baigl, DNA-Templated Silver Nanorings, Advanced Materials. 17 (2005) 2820-2823.

[102] J. Wang, Survey and summary: From DNA biosensors to gene chips, Nucl. Acids Res. 28 (2000) 3011-3016.

[103] F.C. Simmel, W.U. Dittmer, DNA Nanodevices, Small. 1 (2005) 284-299.

[104] N. Cottenye, F.T. Jr, A. Ponche, G. Reiter, K. Anselme, W. Meier, Oligonucleotide Nanostructured Surfaces: Effect on Escherichia coli Curli Expression, Macromolecular Bioscience. 8 (2008) 1161-1172.

[105] N.A. Horn, J.A. Meek, G. Budahazi, M. Marquet, Cancer Gene Therapy Using Plasmid DNA: Purification of DNA for Human Clinical Trials, Human Gene Therapy. 6 (1995) 565-573.

[106] H.L. McLeod, W.E. Evans, Pharmacogenomics: Unlocking the Human Genome for Better Drug Therapy, Annual Review of Pharmacology and Toxicology. 41 (2001) 101-121.

[107] Y.K. Cheng, B.M. Pettitt, Hoogsteen versus reversed-Hoogsteen base pairing: DNA triple helixes, J. Am. Chem. Soc. 114 (1992) 4465-4474.

[108] R. Lipowsky, The conformation of membranes, Nature. 349 (1991) 475-481.

[109] T.S. Davies, A.M. Ketner, S.R. Raghavan, Self-Assembly of Surfactant Vesicles that Transform into Viscoelastic Wormlike Micelles upon Heating, J. Am. Chem. Soc. 128 (2006) 6669-6675.

[110] B.M. Discher, Y. Won, D.S. Ege, J.C. Lee, F.S. Bates, D.E. Discher, Polymersomes: Tough Vesicles Made from Diblock Copolymers, Science. 284 (1999) 1143-1146.

[111] J. Smeulders, C. Blom, J. Mellema, Linear viscoelastic study of lipid vesicle dispersions: Hard-sphere behavior and bilayer surface dynamics, Phys. Rev. A. 42 (1990) 3483-3498.

[112] K. Seki, S. Komura, Viscoelasticity of vesicle dispersions, Physica A: Statistical and Theoretical Physics. 219 (1995) 253-289.

[113] S. Mishra, B.K. Mishra, D.K. Chokappa, D.O. Shah, C. Manohar, Some concepts on design of surfactant gels and vesicles, Bull. Mater. Sci. 17 (1994) 1103-1108.

[114] Z. Tu, L. Ge, J. Li, Z. Ou-Yang, Elasticity of polymer vesicles by osmotic pressure: An intermediate theory between fluid membranes and solid shells, Phys. Rev. E. 72 (2005).

[115] V. Heinrich, B. Bozic, S. Svetina, B. Zeks, Vesicle deformation by an axial load: from elongated shapes to tethered vesicles, Biophys. J. 76 (1999) 2056-2071.

[116] P. Ziherl, S. Svetina, Flat and sigmoidally curved contact zones in vesicle-vesicle adhesion, Proceedings of the National Academy of Sciences. 104 (2007) 761-765.

[117] M.V. Voinova, M. Rodahl, M. Jonson, B. Kasemo, Viscoelastic Acoustic Response of Layered Polymer Films at Fluid-Solid Interfaces: Continuum Mechanics Approach, Phys. Scr. 59 (1999) 391-396.

[118] A. Graneli, M. Edvardsson, F. Hook, DNA-Based Formation of a Supported, Three-Dimensional Lipid Vesicle Matrix Probed by QCM-D and SPR13, ChemPhysChem. 5 (2004) 729-733.

[119] I. Reviakine, F.F. Rossetti, A.N. Morozov, M. Textor, Investigating the properties of supported vesicular layers on titanium dioxide by quartz crystal microbalance with dissipation measurements, J. Chem. Phys. 122 (2005) 204711.

[120] I. Reviakine, Effects of finite crystal size in the quartz crystal microbalance with dissipation measurement system: Implications for data analysis, J. Appl. Phys. 95 (2004) 7712.

[121] S. Nosov, H. Schmalz, A.H. Müller, One-pot synthesis of primary amino end-functionalized polymers by reaction of living anionic polybutadienes with nitriles, Polymer. 47 (2006) 4245-4250.

[122] A.V. Tataurov, Y. You, R. Owczarzy, Predicting ultraviolet spectrum of single stranded and double stranded deoxyribonucleic acids, Biophysical Chemistry. 133 (2008) 66-70.

[123] A. Prilipov, P.S. Phale, P. Gelder, J.P. Rosenbusch, R. Koebnik, Coupling site-directed mutagenesis with high-level expression: large scale production of mutant porins from E. coli, FEMS Microbiology Letters. 163 (1998) 65-72.

[124] A. Graff, Insertion of membrane proteins in artificial polymer membranes, University of Basel, 2006.

[125] S.F. Mahmoud, S.E. Bialkowski, Laser-Excited Fluorescence of Dityrosine, Appl Spectrosc. 49 (1995) 1669-1676.

[126] J.E. Dowd, D.S. Riggs, A Comparison of Estimates of Michaelis-Menten Kinetic Constants from Various Linear Transformations, Journal of Biological Chemistry. 240 (1965) 863-869.

[127] B.K. Hamilton, C.R. Gardner, C.K. Colton, Effect of diffusional limitations on lineweaver-burk plots for immobilized enzymes, AIChE Journal. 20 (1974) 503-510.

[128] P. Müller-Buschbaum, Influence of surface cleaning on dewetting of thin polystyrene films, The European Physical Journal E - Soft Matter. 12 (2003) 443-448.

[129] Y. Jiang, C. Zhu, L. Ling, L. Wan, X. Fang, C. Bai, Specific Aptamer−Protein Interaction Studied by Atomic Force Microscopy, Anal. Chem. 75 (2003) 2112-2116.

[130] L. Longo, G. Vasapollo, M.R. Guascito, C. Malitesta, New insights from X-ray photoelectron spectroscopy into the chemistry of covalent enzyme immobilization, with glutamate dehydrogenase (GDH) on silicon dioxide as an example, Anal Bioanal Chem. 385 (2006) 146-152.

[131] S. Onclin, B.J. Ravoo, D.N. Reinhoudt, Engineering Silicon Oxide Surfaces Using Self-Assembled Monolayers, Angewandte Chemie International Edition. 44 (2005) 6282-6304.

[132] W. Mueller, K. Koynov, K. Fischer, S. Hartmann, S. Pierrat, T. Basché, Hydrophobic Shell Loading of PB-b-PEO Vesicles, Macromolecules. 42 (2009) 357-361.

[133] J. Razumovitch, K. de França, F. Kehl, M. Wiki, W. Meier, C. Vebert, Optimal Hybridization Efficiency Upon Immobilization of Oligonucleotide Double Helices, The Journal of Physical Chemistry B. 113 (2009) 8383-8390.

[134] J. Mark, Polymer data handbook, 2 éd., Oxford University Press, Oxford ;;New York, 2009.

[135] J.F. O'Keefe, Identification of polymers by IR spectroscopy. - Free Online Library, Rubber World. (2004).

[136] M. Banyay, M. Sarkar, A. Gröslund, A library of IR bands of nucleic acids in solution, Biophysical Chemistry. 104 (2003) 477-488.

[137] A. Seuvre, M. Mathlouthi, F.T.-I.R. spectra of oligo- and poly-nucleotides, Carbohydrate Research. 169 (1987) 83-103.

[138] Z. Li, Y. Zhang, P. Fullhart, C.A. Mirkin, Reversible and Chemically Programmable Micelle Assembly with DNA Block-Copolymer Amphiphiles, Nano Letters. 4 (2004) 1055-1058.

[139] D.E. Discher, A. Eisenberg, Polymer Vesicles, Science. 297 (2002) 967-973.

[140] J. Weil, Biochimie générale, 10 éd., Dunod, imprimerie CHIRAT, Saint-Just-la-pendue (France), 2006.

[141] M. Antonietti, S. Förster, Vesicles and Liposomes: A Self-Assembly Principle Beyond Lipids, Advanced Materials. 15 (2003) 1323-1333.

[142] H. Kukula, H. Schlaad, M. Antonietti, S. Forster, The Formation of Polymer Vesicles or "Peptosomes" by Polybutadiene-block-poly(l-glutamate)s in Dilute Aqueous Solution, Journal of the American Chemical Society. 124 (2002) 1658-1663.

[143] Jaroslav Kypr, Iva Kejnovská, Daniel Renčiuk, Michaela Vorlíčková, Circular dichroism and conformational polymorphism of DNA, Nucleic Acids Research. 37 (2009) 1713-1725.

[144] D.M. Hatters, L. Wilson, B.W. Atcliffe, T.D. Mulhhern, N. Guzzo-Pernell, G.J. Howlett, Sedimentation analysis of novel DNA structures formed by homo-oligonucleotides., Biophys J. 81 (2001) 371-381.

[145] Paul C Hiemenz, Thimothy P Lodge, Polymer Chemistry, second, CRC Press:, Boca Raton, 2007.

[146] C. Nardin, M. Winterhalter, W. Meier, Giant Free-Standing ABA Triblock Copolymer Membranes, Langmuir. 16 (2000) 7708-7712.

[147] H. Lee, I. Wilson, Enzymic parameters: Measurement of V and Km, Biochimica Et Biophysica Acta (BBA) - Enzymology. 242 (1971) 519-522.

[148] A. Krishnan, Y. Liu, P. Cha, R. Woodward, D. Allara, E. Vogler, An evaluation of methods for contact angle measurement, Colloids and Surfaces B: Biointerfaces. 43 (2005) 95-98.

[149] N. Nugaeva, K.Y. Gfeller, N. Backmann, M. Düggelin, H.P. Lang, H. Güntherodt, An antibody-sensitized microfabricated cantilever for the growth detection of Aspergillus niger spores, Microsc. Microanal. 13 (2007) 13-17.

[150] C. Zhao, X. Liu, M. Nomizu, N. Nishi, Blood compatible aspects of DNA-modified polysulfone membrane--protein adsorption and platelet adhesion, Biomaterials. 24 (2003) 3747-3755.

[151] C. Lee, G.M. Harbers, D.W. Grainger, L.J. Gamble, D.G. Castner, Fluorescence, XPS, and TOF-SIMS surface chemical state image analysis of DNA microarrays, J. Am. Chem. Soc. 129 (2007) 9429-9438.

[152] R. Richter, A. Mukhopadhyay, A. Brisson, Pathways of Lipid Vesicle Deposition on Solid Surfaces: A Combined QCM-D and AFM Study, Biophysical Journal. 85 (2003) 3035-3047.

Part II: Bacterial adhesion to nanoreactor-based surfaces: influence of chemistry, topography and mechanical properties on bacteria-surface interactions.

A. *Introduction.*

In the development of antimicrobial surfaces, knowledge of surface-bacteria interactions is essential to properly understand surface action and efficiency. Therefore, bacterial behavior when in contact with nanoreactor-based coatings must be thoroughly characterized. Moreover, we believe that our oligonucleotide-based vesicle surfaces, aside from merely providing tools for the development of new coatings, will improve knowledge concerning diverse aspects of surface-bacteria interactions during the adhesion process. This part of the manuscript is devoted to studies conducted to this end.

As we will review in state of art, different surface properties can influence bacteria-surface interactions. Two properties are commonly accepted to strongly influence the bacterial adhesion onto surface and biofilm formation: the surface topography and the surface chemistry (including surface physical-chemical properties). A third surface property, the mechanical properties, is generally neglected during bacterial adhesion and biofilm formation. Due to the unusual visco-elastic properties of the surfaces produced in the present study, expected from QCM-D analysis results presented in Part I, Chapter 3, the consideration of the influence of surface mechanical properties onto bacterial adhesion seems relevant.

In this Part II we will focus on the influence of these three properties onto bacterial adhesion. We studied the bacterial response to the different properties, quantitatively (number of adherent bacteria) in static culture conditions and under flow culture conditions by real time or differed observation. Those different culture conditions allowed to investigate the quantitative surface colonization but also the dynamic of bacterial attachment and detachment involved during bacterial adhesion and biofilm growth, in relation with surface properties variation. Furthermore, the use of several mutants of *E.coli* allowed us to investigate the influence of curli, which is an organelle frequently highlighted for its role in bacterial adhesion (one organelle among the wide variety of organelles potentially involved in bacterial adhesion), onto bacterial adhesion in relation with the variation of the surface properties.

This part II will start with the state of the art in which we will briefly describe the biofilm formation. Then we will review the influence of surface chemistry and topography, followed by the influence of mechanical properties onto bacterial adhesion. We will also present curli and their biological function and finally we will review the bacterial motility at interfaces. Following the literature review, we will describe materials and methods used in this second part of our work. We will briefly remember the surfaces used for the different bacterial studies, reviewing their properties, before describing the static and dynamic cultures conditions.

All results will be displayed and described in the results part, while discussion will be separate and will center around four topics of consideration as surface influences on bacteria. First, we will discuss surface toxicity, demonstrating the non-toxicity of surfaced produced in this study. Secondly, we will discuss the influence of the surfaces chemistry and charge on bacterial adhesion and bacterial curli expression. Then, we will discuss the

influence of surface topography onto the bacterial adhesion. In the last part of the discussion, the surface visco-elastic properties on bacterial attachment and detachment in static and dynamic culture mode will be studied and linked to bacterial motility as observable for agar hydrogels of various rigidities.

Finally, we will draw conclusions, which will provide new consideration for outlook and future work.

B. *State of the art.*

B.1 Biofilm formation.

The major discoveries about biofilm formation arose in the early 80's, during which dentistry focused research on the environment of dental plaque [1] and microbial ecologist on spring water microbial environment [2]. Due to these intensive studies, increasing evidences of the structure and process of biofilm formation were assessed.

Classical biofilm formation, shown in Figure 47, starts with surface conditioning by the medium (protein, ions, etc). This process can strongly modify surface properties and therefore influence biofilm formation. Following surface conditioning and prior to the first step of bacterial adhesion, the transport of bacteria from the medium to the surface is occurring and followed by the first step of adhesion: the reversible adhesion. Several studies considered this step as a purely physical-chemical process [3-6], following the rules described by the extended DLVO theory [7]. In this theory, bacteria were described as colloids. This assumption allows to model and predict bacterial adhesion on the basis of physical-chemical parameter measurements (surface tension or charge to cite few), but needs important simplification concerning bacterial morphology and cell wall properties. Moreover, bacterial metabolism is completely ignored in such approach. Recently, some studies [8-12] have led to the evidence of a more complex process involving surface sensing by the bacteria that can detect microenvironments at the substrate interface, such as local pH variation [8], osmolarity variation [11], with sensing procedure such as flagellum surface wetness sensing [12] or detection of contact with the surface [10]. The second step is the irreversible adhesion during which bacteria start to express adhesion protein such as curli or fimbriae to adhere to the surface. In step 3 the bacteria start to produce intercellular connections (intercellular curli for example) and a polymeric matrix, usually called extracellular polymeric substances (EPS). This matrix is a complex hydrogel embedding the bacteria community and building up in three dimensions. The backbone of this gel is mainly composed of polysaccharides produced by bacteria (such as colanic acid, chitosan, alginate, dextran to cite a few), other components such as enzymes, DNA, RNA, nutrients, proteins, surfactants [13]. The exact role of the matrix is not yet completely elucidated but it has been demonstrated that the matrix acts as a protective layer [14] and is microenvironment-conservative [15]. In the last step of biofilm formation, the biofilm is considered mature, many processes already having taken place, such as quorum sensing [16], gene transfer [17], persister development [18] etc. All of these processes contribute to the community life of the biofilm and play an

important role in biofilm survival and biofilm spreading, since they allow also detachment of biofilm parts and release of free bacteria, which is the most common way for biofilm to spread [19].

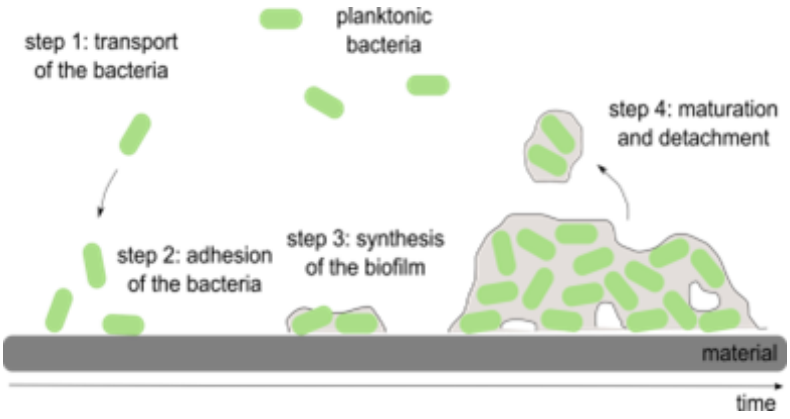


Figure 47: Classical biofilm formation process (Illustration from L. Ploux et al. [20]).

In this work, we focused our efforts on the bacterial adhesion step and the control of the surface to avoid adhesion.

B.2 Influence of surface chemical and biochemical function.

During bacterial adhesion, which includes reversible and irreversible adhesion processes, surfaces properties and chemical composition have a strong influence and are commonly pointed as influencing factors for bacterial adhesion. Despite this influence, no general rules exist to describe and predict bacterial adhesion, due especially to bacterial diversity and their wide variety of properties but also due to the diversity of the environmental conditions. Nevertheless some trends have been identified, which are briefly presented below.

Effects of surface hydrophobicity and surface charges have been widely studied in the context of the extended DLVO theory [7,3], demonstrating their influence as components of the free energy [21,22]. However, the limitation of extended DLVO in describing the early adhesion process has been shown [23]; The limitations are due to the absence of consideration of both bacterial organelles and the ability of bacteria to sense and metabolically respond to the surface. Experimentally, some studies have suggested that hydrophobicity of adherent bacteria correlates with that of the surface [24]. This rule, oftently accepted, is not universal and contradictory results were published, as recently reviewed [20]. In the case of surface charges, bacteria are thought to be attracted by oppositely charged surfaces [25]. Indeed, except for few species, bacteria are negatively charged at physiological pH (pH~7) (values can vary from a few to several tenths of mV [26,27]), attractive interactions are expected to occur between bacterial cells and positively charged surfaces. Roberts [28] and Terada et al. [29] showed that electrostatic interaction is the most decisive factor for bacterial adhesion when it works as an attractive force, i.e. on positively charged surfaces. Nevertheless, some studies have highlighted

that bacterial adhesion onto charged surfaces is not only related to surface but also involve the influence of incubation time and obviously the influence of surrounding ionic strength [30,31]. Thus, bacterial behaviour on charged surfaces is not obvious. Gottenbos et al. [32] reported a higher bacterial attachment on positively charged surfaces for the four species tested (*E.coli*, *Pseudomonas aeruginosa*, *Staphylococcus epidermidis* and *Saphylococcus aureus*). However, after attachment, bacteria grew faster on negatively charged than on positively charged surfaces. These behaviours were attributed to the probable decrease of cell viability, due to strong binding between surface and bacteria. Recently, surprising results were obtained by Komarony et al. [33] stating that *E.coli* and *S.aureus* attached better on surfaces (unmodified silicon wafers and 11-mercapto-1-undecanol grafted surfaces) with similar zeta-potential to cell surface zeta-potential. In this study, neither hydrophilic character nor roughness alone could be related to bacterial retention differences. urface charge, roughness and medium ionic strength might have combined influence, leading to this surprising result.

The presence of biochemical functions on the surface is also able to influence bacterial adhesion (probably the irreversible stage more strongly) by providing binding sites for bacterial organelles such as flagellae, pili and other fimbriae. A typical example is given by mannose-fimH interactions [34], as illustrated by studies demonstrating that mannose patterns are favorable for bacterial attachment [35,36]. Other biomolecules are known to undergo specific interactions with bacteria, such as fibronectin [37], or to non-specifically prevent bacterial adhesion, such as albumin [38,39]. However, the influence of many biomolecules remains unknown. This is the case for oligonucleotides and oligonucleotide-based surfaces, as used in this study.

B.3 Influence of surface topographical properties.

Recent reviews exploring the influence of surface topography onto bacterial adhesion were published [40,41] and described the recent knowledge on this topic. We can notice that exact correlation between topography and bacterial adhesion is not clear, although it is usually accepted that topographical features with dimensions similar to bacterial size favor bacterial adhesion, probably by providing a protective effect. For instance, they adhere preferentially to the bottom of crevices [42], rather than to the top. However, the bacterial response to microscale surface features is not extensively studied. In the few studies, the surface topography is frequently described only by the mean roughness parameter and the topographical feature shapes and organization is often neglected. The effects at the nanoscale level are even less well understood and few papers addressed the question of the effect of nanotopography on bacterial response. Bruinsma et al. [43] showed that initial deposition rates of bacteria were statistically different on a material with a R_a of 4 nm (unworn contact lenses) compared with a material with a R_a of 10 nm (overworn lenses). Bakker et al. [44], using multiple linear regression analysis, showed a relationship between roughness and adherent bacteria number on polyurethane-coated glass plates preconditioned in sea water. Surface properties in these studies were complex, due to the commercial origin of the

materials used, and the multiple other chemical changes occurring during wear or preconditioning processing of the material, rendered difficult to contend that the effect observed was solely due to the surface topography. Recently, Mitik-Dineva et al. [45] addressed the influence of small topographical changes (1, 8 and 10 nm for R_a (and R_q), R_{max} and R_z respectively) of glass surfaces, etched by hydrofluoric acid, on bacterial adhesion characteristics. Oppositely to the trend observed in previously cited publications, they demonstrated an increase in the number of attached bacteria resulting from a decrease in the topographical feature size due to etching. The question of the influence of the size and the morphology of surface features onto bacterial adhesion has been addressed by few authors [46-48], using model surfaces structured at the limit of nanoscale and microscale level. They confirmed the trend reported by Bakker et al., showing a general increase in adherent bacteria number with surface roughness (Ra). However, the impact of the topographical feature (i.e. retaining properties, alignment and orientation) remains contradictory and no conclusion about the ability of bacteria to react to topographical features should be drawn.

Commonly proposed explanations of results showing enhanced adhesion and retention of bacteria with surface roughness are the higher surface area available for attachment, protection from shear forces and the increase in convection mass transport due to the topographical features [42,49-52]. Therefore, the attachment of bacteria in and on surface features may enhance the cell–surface contact area, thereby allowing an increase in binding energy. However, the cost to the microbial cell in terms of elastic energy when distorting, as well as the thermal energy in the environment, may lead to an energetic barrier to bacterial adhesion. This may be the reason why roughness and surface topographical features do not always result in bacterial localization or alignment on the surface [52]. The optimal size for bacterial interaction with the surface may, therefore, be at the microscale level. Shape, profile and orientation of these features should also play an important role in the quality of the binding, as Edwards and Rutenberg [52] have already proposed and theoretically demonstrated at the microscale level.

The bacterial organelles (flagella, pili and other fimbriae) may play a role in bacterial attachment. On the nanoscale it may be possible for these structures to improve binding energy with topographical and even chemical features, due to their small size. Scheuerman et al. [49] and Medilanski et al. [53] showed that non-motile mutant bacteria colonized microstructured surfaces less than the wild strains, suggesting that flagellae help bacteria to move into grooves or crevices and/or to recognize topographical features. However, the involvement of bacterial membrane structures in attachment to nanotopographical surfaces has not been addressed in the literature, although some authors have proposed that bacterial responses to nanometre scale roughness is mediated by structures such as fimbriae [44].

The amount, localization and orientation of bacteria, as well as the intracellular mechanisms involved in surface topographical feature sensing, remain largely unknown. An optimal feature size may exist at the microscale due to the limited capability of bacteria to deform, and extracellular structures of the cell membrane

like flagellae and fimbriae may be involved in bacterial responses to smaller topographical features. Bacterial responses to topographical features are highly species- and strain-dependent.

B.4 Influence of surface mechanical properties on bacterial adhesion.

Mechanical properties are not commonly assumed to influence bacterial adhesion. In recent years, they were however, considered as a critical factor in modulating eukaryotic cell adhesion, as well as the functioning and differentiation of stem cells [54-56]. Eukaryotic cells are able to respond to substrate mechanical compliance and substrate stiffness independent of physical-chemical parameters [54]. It has been demonstrated that this response is mediated by sensing of the micromechanical properties of the surface [57].

In the case of bacteria, few publications have reported the influence of the mechanical properties of the surface on bacterial adhesion [58-60]. Van der Mei and coworkers [58] have studied the influence of fluorinated surface with various elasticity modulus (prepared by deposition of fluorinated polyurethane onto substrate) on bacterial adhesion. They showed a positive correlation between the surface elastic modulus increase and bacterial adhesion rate increase during mass transport toward a collector surface in the stagnation point flow chamber, while no correlation for convective mass transport, like in the parallel plate flow chamber, could be drawn. To explain the trend observed, they hypothesize a rebound effect due to surface elasticity, inducing a reduction of the number of bacteria adhering onto elastic surfaces, while the mass transport (convective or not) will influence collision energy between bacteria and surface disturbing the rebound effect for convective mass transport. The hypothesized rebound effect is assumed to be induced by the collision between bacteria and surface. This hypothesis is not fully satisfying since the bacteria are simply considered as an inert particle, which is far from being an accurate way to consider bacteria. More recently, Lichter et al. [59], working on polyelectrolyte hydrogels, asserted that material softness can allow the control of bacterial adhesion and even that soft layer can induce bacterial adhesion avoidance [59,60]. They worked with polyelectrolyte multilayers with variable hydration states. The elastic modulus E of the surface was varied by changing the pH over the course of the layers that assembled during surface preparation. The resulting surfaces were shown to modulate bacterial adhesion as a function of stiffness [59]. In particular, it was showed that the number of adherent cells decreases with decreasing stiffness.

Although hydrogels [59] or polymeric coating [58] can be formulated to provide surfaces with desired elastic modulus, mechanical properties of hydrogels or polymeric coatings remain complex and can not only be described by stiffness or elastic modulus. Surface properties anisotropy due to the surface-medium interface, the coating viscous modulus and interfacial fluidity should probably be also considered, which has not been the case in the literature. Moreover, to describe these interfacial interactions, the knowledge of the specific mechanical properties characterization of the surface is needed but the bacteria properties should also be considered.

The mechanical properties of the bacterial membrane have been studied in order to better understand bacterial adhesion and virulence of various strains [61], but rarely considered for their role in bacterial adhesion

[52] and never linked with bacterial response to material mechanical properties. However, some authors [62,63], focusing on bacterial sensing of the surface, highlight several mechanosensitive pathways for surface detection. The signaling CpX/NIpE pathway was studied in literature and was demonstrated to be involved in bacteria to sense outer membrane stresses [64]. These stresses can be detected by different sensors: osmotic variation due to contact with surfaces can be detected by a mechanosensitive channel [11,65,66], or mechanical stimuli can be detected by NIpE, a membrane lipoprotein of gram negative bacteria [67]. Other signaling pathways for surface sensing were highlighted in literature, such as for example flagella blocking by contact with surfaces, inducing either biofilm formation or community mobility [68] (swarming bacteria community like *Vibrio*), or the surface wetness detection by flagella through up- or down-regulation upon flagella polymerization at non wet interfaces leading to either motility or adhesion on surfaces of *E.coli and Salmonella typhimurium* [12].

B.5 Oligonucleotides as a support for bacterial adhesion.

In general, single stranded oligonucleotides are likely to interact specifically with bacteria. Indeed, oligonucleotide/bacteria binding is at the heart of DNA uptake by bacteria, which is an important process for the interaction of bacteria with their environment [69]. For example, DNA uptake is used by bacteria to exchange genes [70] for biological resistance, in planktonic cultures, as well as in biofilms. It has also been shown to be involved in nutrient incorporation, due to DNA phosphorous and nitrogen richness [70,71], and in DNA repair and genetic diversification [72]. On this basis, it has already been proposed that oligonucleotides could be specifically designed in order to induce a specific bacterial response, aiming, for example, at preventing biofilm formation [73] (oligonucleotide used as a drug in solution). In our case, since oligonucleotides are grafted to the surface, their uptake by bacteria is not expected. Nevertheless, binding protein [74], quorum sensing pathways [69] and cellular receptor detection [75] involved in DNA uptake may be activated by bacteria binding with grafted oligonucleotides.

In general, pili type IV and II are known for their role [75,76] in DNA binding that occurs during microbial growth. For some of these pili-type organelles, ability to interact with DNA was shown to be specific. However, Van Schaik et al. observed that pili type IV of *Pseudomonas aeruginosa* [77] were able to bind DNA (specifically compared to other polyelectrolytes) but without sequence specificity (except a preference for pyrimidine bases). In our study, the bacterial strain used does not express pili type IV organelles [78] but possesses so-called curli, which are known for their wide variety of bindings [79]. Curli are not known for their ability to bind specifically DNA and oligonucloetide. However, some interactions may occur due to physical-chemical events.

Oligonucleotides, at physiological pH, are negatively charged polyelectrolytes [80]. In the case of our oligonucleotide-based block copolymer, independently of the sequence and independently of the hydrophobic block, the charge consists of twelve negative charges located on the phosphate backbone. Despite the lack of studies on physical-chemical influence of oligonucleotide onto bacterial adhesion, we can expect an impact of the oligonucleotide coating on bacterial adhesion due to electrostatic interactions between oligonucleotides and the

bacterial membrane, since charges are known to influence bacterial adhesion as presented above in Part II – B.2. The negative bacterial charge should then result in a repellent effect of the oligonucleotide coating on bacterial adhesion.

B.6 Curli: description and biological function.

Curli were defined by Barnhart and **Chapman** [81] as the major proteinaceous fiber at the curli expressive cell surface and as the major component of a complex extracellular matrix produced by many *Enterobacteriaceae*, as illustrated in Figure 48. Curli were first discovered in the late 1980s on *E.coli* strains that cause bovine mastitis, and have since been implicated in many physiological and pathogenic processes of *E.coli* and *Salmonella* spp. [82]. Curli fibers are involved in adhesion to surfaces [79], cell aggregation [83], and biofilm formation [84]. They also mediate host cell adhesion and invasion [85], and they are potential inducers of the host inflammatory response [86]. Concerning structure and biochemistry, curli belong to a class of fibers known as amyloids [87]. Their biogenesis is not fully elucidated, but some key steps have already been explained: curli growth displays a unique pathway different from the other well-known fimbriae (pili type IV pathway for example) even if there are some analogies [88]. Curli growth is an external process that is called the nucleator pathway. The assembly of curli organelles involves a nucleator component (CsgB), proteins with apparent chaperone functions (CsgE), or a nucleator center (CsgG), and the CsgA and CsgB fimbrial subunits secreted from the bacteria and self-polymerized. Obtained fimbriae are characterized by an 'aggregative' and chemically robust character and do not appear straight but rather as twisted, curly structures [88].

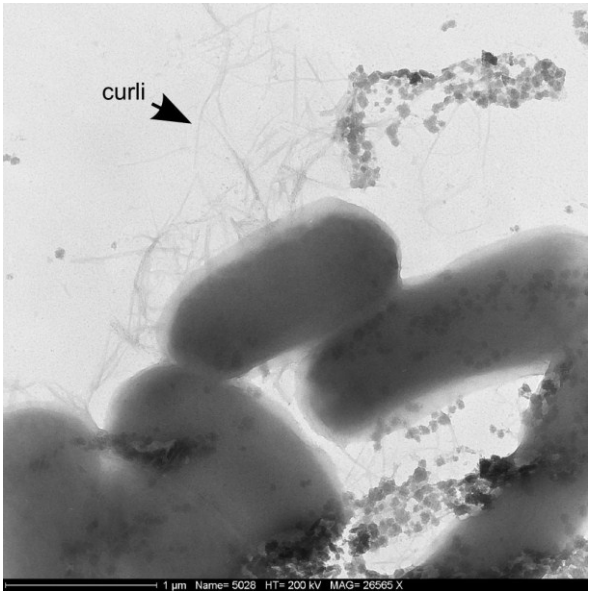


Figure 48: *E.coli* K12 curli observed by Transmission Electron Microscopy (From Ploux et al. [20]).

Curli were demonstrated to be involved in bacteria-substrate interactions [89,90]. Their key role for adhesion and biofilm formation was demonstrated but any definitive action has not yet been elucidated. We

actually know that curli are involved in non-specific bacteria-surface interactions [89], specific bacteria-surface interactions [85] and biofilm structure [84] through cell-cell interactions [85]. Indeed, curli are known to have a wide range of receptor targets, allowing enhanced binding [83,85,91]. In particular, one receptor region of the curli fiber was reported to mediate binding to mouse small intestine epithelial cells [83], in addition to binding various plasma and cell extracellular matrix proteins [85].

Finally, on our oligonucleotide-based surfaces, both specific and unspecific interaction types may occurs see section B.5. Therefore, in the study of oligonucleotide-based surfaces on bacterial adhesion and biofilm formation, the investigation of the curli expression involved in this process may be helpful to enhanced understanding of surface-bacteria interactions during the entire adhesion process. For this purpose, specific *E.coli* strains have been selected for this study as discussed in Material and methods of this Part II.

B.7 Bacterial motility at interfaces.

Bacterial colonization of surfaces generally starts with bacteria mobility and motility, which drives their contact and colonization of the surface. Classically, the mobility of bacteria in a fluid to achieve surface adhesion is called swimming and is followed by the adhesion process, i. e. the first step of biofilm development [92]. Motility processes have been rather identified at the interfaces (air/surface and liquid/surface) and are involved in bacterial colonization and spreading [93]. At least four motility types were identified: swarming, twitching, gliding and sliding motility. These motilities are still under investigation [94] and the processes involved are not clearly elucidated. All bacteria do not possess all types of motility. Swarming and twitching have been reported to be related to certain types of organelles (respectively flagella and pili type IV) [94] while the gliding mechanism has not been elucidated, and sliding has been identified as a passive translocation [94].

The swarming process involves a community moving as groups of bacteria through a synergetic use of flagella [88]. Swarming was observed for flagellated bacteria species such as *Escherichia, Bacillus, Pseudomonas* and *Salmonella*. This motility is involved in surface colonization through fast displacement (2-10µm/s). Swarming was intensively studied and was demonstrated to be dependent on substrate moisture. Substrate wettability may therefore play a key role in this motility type [87-89], but the complete influence of the substrate on swarming is not yet elucidated.

A second type of motility that has already been highly studied is twitching, involving pili type IV. Bacteria able to twitch produce pili type IV such as *Streptococcus, Legionella, Neisseria, Pseudomonas* and *Vibrio*. In this case bacteria pull on the pili to move [90]. Twitching motility is slower compared to swarming ($0.06 - 0.3$ µm/s). Twitching motility was demonstrated to be involved in a wide variety of bacterial colonization processes such as surface colonization, biofilm formation, biofilm structure formation, bacterial transformation and conjugation [87]. This motion was studied by Holz et al. [91], who demonstrated the influence of substrate fluidity on the twitching motion by the use of a solid-supported lipid bilayer with or without fluidic membrane behavior. They showed that *Neisseria gonorrhoae* are not able to twitch on lipid membranes that have fluid behavior. Moreover,

on patterned fluid and non-fluid lipid membranes, bacteria preferentially locate on parts favorable to twitching, i.e. non-fluidic membranes.

Gliding motion is another type of motion but is less understood. It is involved in surface colonization and leads to slightly faster motion (0.025 to 10 µm/s) displayed on purely solid supports. It is known that moisture eradicates this motion type [92]. However, the exact process, pathway or organelles involved in this motility have not been elucidated yet.

Finally sliding is another motion type, known as passive spreading, i.e. this motility may not involve active motion and organelles. Sliding is linked to external forces such as the colony expansion forces and Brownian movement at interfaces, involved in surface colonization at a speed of 0.03 to 6 µm/s. This motility was shown to be favored by high surface fluidity and by the bacterial production of bacterial surface active compounds such as peptidolipids, glycolipids and LPS [87,93].

Finally, several of these works demonstrate the impact of surface mechanical properties on bacterial motility [86,92,93]. In particular, surface wetness or fluid-like behavior are factors at the air-surface interface which were demonstrated to either induce motility (swarming, swimming, sliding) [87] or to limit motility (gliding, twitching) [87,90]. Nevertheless, studies on motility were only performed at the air-substrate interface, as commonly done in Petri dishes, and there was no consideration of surface elasticity.

C. *Materials and methods.*

C.1 Surfaces and their sterilization.

In this study we used glass and wafer references as internal control, and oligonucleotide-modified surfaces and vesicle-coated surfaces, for which the preparations are described in Part I - Material and methods. We also used complementary surfaces based on agar hydrogel, as described below. Surfaces properties are summarized in Table 11. Briefly, oligonucleotide-modified surfaces were obtained as described for oligonucleotide modification of a silicon wafer with different sequences. We grafted either the sequence A_5G_7 (5'-AGAGAGAGAGGG-3') or its complementary oligonucleotide sequence i.e. the C_7T_5 (5'-CCCTCTCTCTCT-3'). The hybridized vesicle coated surface consisted in hybridizing PIB_{31}-G_7A_5 vesicles onto a surface coated with the complementary single-stranded nucleotide sequence to that used in vesicle self-assembly. The non-hybridized vesicle coating was based on PB_{65}-A_5G_7 vesicles deposited on the same oligonucleotide layer as that used in vesicle self-assembly (A_5G_7).

Finally, agar coated surfaces were obtained by dissolving the desired quantity of agar in a bottle containing NaCl buffer (150 mM). Bottles were then autoclaved (120 °C, 10 min) for sterilization and cooled to 50 °C. At this temperature, a cleaned silicon wafer, obtained with the cleaning procedure for internal control described in Materials and methods of Part I, is dipped in this solution and stored until the hydrogel fully solidifies (overnight, room temperature under sterile condition). Four different concentrations of agar in NaCl buffer have been used: 5, 15, 30 and 80 g/L. Mechanical properties of these surfaces were qualitatively notice in the present study. The quantification of the agar surfaces elastic modulus by Atomic Force Microscopy indentation is actually under progress.

Surfaces name	Surface chemical properties		Surface topographical properties		Surface mechanical properties		
	Coating type	**Contact angle**	**Ra**	**Observation**	**Shear modulus**	**Viscosity**	**Qualitative observation**
A5G7 LD	"low density" A_5G_7 oligonucleotide coated silicon wafer	53 ± 2°	0.3 ± 0.2 nm	smooth	/	/	STIFF
A5G7 HD	"high density" A_5G_7 oligonucleotide coated silicon wafer	48±2°	0.3 ± 0.2 nm	smooth	/	/	STIFF
C7T5 HD	"high density" C_5T_7 oligonucleotide coated silicon wafer	45±2°	0.3 ± 0.2 nm	smooth	/	/	STIFF
Non-hybridized vesicles	PB_{65}-A_5G_7 vesicles deposited, and crosslinked, on "low density" A_5G_7 oligonucleotide coated silicon wafer	60 ± 4°	5.9 ± 0.2 nm	Topographical features of 100nm high spaced every micrometers.	/	/	STIFF
Vesicles "smooth"	PIB_{31}-G_7A_5 vesicles filtered and hybridized onto "high density" C_5T_7 oligonucleotide coated silicon wafer	54± 4°	3 ± 2 nm	Densely packed topographical features (close to monolayer).	6.10^5 Pa	0.0038 $kg.m^{-2}$	VISCOELASTIC
Vesicles "rough"	PIB_{31}-G_7A_5 vesicles not-filtered and hybridized onto "high density" C_5T_7 oligonucleotide coated silicon wafer	54± 4°	20 ± 3 nm	Densely packed topographical features (close to monolayer) with aggregates on top of the layer, forming micrometer scale features (observable with light microscopy)	6.10^5Pa	0.0038 $kg.m^{-2}$	VISCOELASTIC
Internal control	Clean silicon wafer reference	15°± 2°	0.4 ± 0.3 nm	smooth	/	/	STIFF
	Clean glass coverslip reference	15°± 2°	/	/	/	/	STIFF
Agar 5g/L	5 g/L agar hydrogel dipcoated onto clean silicon wafer	/	/	smooth	/	/	FLUID-JELLY
Agar 15g/L	15 g/L agar hydrogel dipcoated onto clean silicon wafer	/	/	smooth	/	/	JELLY
Agar 30g/L	30 g/L agar hydrogel dipcoated onto clean silicon wafer	/	/	smooth	/	/	STIFF-JELLY
Agar 80g/L	80 g/L agar hydrogel dipcoated onto clean silicon wafer	/	/	smooth	/	/	STIFF

Table 11: summary of surfaces name and properties

C.2 Bacterial strains, culture condition and observation under static culture condition.

C.2.a Bacterial strains.

Experiments were conducted with an *E.coli* MG1655 strain [95]: PHL818 (*E.coli* PHL818) known to be able to produce curli (curli +) and exo-cellular polymeric substances (EPS +) [96], or its analogous green fluorescent strain SCC1 which expresses also curli and EPS but have a green fluorescent protein genetic insert [97].

To study the relation between adhesion, curli expression and the modification of the surface with either oligonucleotides or vesicles, two additional *E.coli* PHL818 mutant strains were selected: PHL847 (*E.coli* PHL847) which keeps the ability to produce EPS (EPS +) but does not produce curli (curli -) and PHL1273 (*E.coli* PHL1273) known to express the green fluorescent protein (*gfp*) upon production of curli (GFP curli +) and known to produce EPS (EPS +) [98]. All these mutant strains were provided by P. Lejeune (Unité de Microbiologie et Génétique Composante INSA, UMR CNRS 5122, Université Claude Bernard Lyon I, 10 rue Dubois, 69622 Villeurbanne cedex, France) except the SCC1 strain provided by C. Chau Sze (School of Biological Sciences, Nanyang Technological University, 60 Nanyang Drive, Singapore 637551) [97]. They were obtained from the same strain known for its ability to produce biofilms onto abiotic surfaces [79], All those strains and their relevant genotype are reported in Table 12.

Strain	Relevant genotype	Comment	Source or reference
SCC1	MG1655 with chromosomal insertion of PA1/04/03-gfpmut3	Constitutive promoter driving the expression of green fluorescent protein gene	[97]
PHL 818	MG1655 malT54::Tn10 ompR234	Wild strain	[99]
PHL 847	PHL818(MG1655 ompR234 malT::Tn10) csgA::uidA-kan	Curli deficient strain	Not published
PHL 1273	PHL818/p127 (pPROBE-gfp_LVA carrying the gfp_LVA coding sequence under the control of the csgBA promoter; Kanr)	Curli gfp fusion: fluorescent during curli expression	[98]

Table 12: *E.coli* strains used in this study, and their relevant genotype and origin.

C.2.b Culture medium and inoculum.

Bacteria were cultivated in a selective M63G medium (pH 6.8) at 30°C. Prior to each experiment, bacteria were grown for 14 h in fresh medium. This culture was used to inoculate a second pre-culture (10 v/v% of the first pre-culture) which was grown for 4 h before inoculating the final culture (10 v/v% of second pre-culture) for an OD_{600} = 0.01 (i.e. 10^6 bacteria/ml).

C.2.c Static culture condition.

The substrates were placed in six-well plates and 4 mL of fresh bacterial culture was added to each well. Bacteria were grown on the substrates at 30°C. Up to six incubation times were explored: 1 h, 2 h, 4 h, 24 h, 48 h and 168 hours, depending on the experiment. One series consists of two substrates of each type (i.e. oligonucleotide SAM, oligonucleotide nanostructured surfaces and control substrates) for each incubation time.

After incubation, the samples were rinsed twice to eliminate non-adherent bacteria. For this purpose, 3 mL of supernatant, i.e. bacterial suspension for the first rinsing and NaCl solution for the second rinsing, were removed and replaced with fresh NaCl solution (9 g/L in water). The rising step is performed without direct flushing, by softly removing supernatant with the help of 1 mL micropipettes and gently replacing it with the NaCl solution.

C.2.d Cytotoxicity of the surface.

In order to test the potential toxicity of the coating releasing from surface on bacteria, cells growth in planktonic state was measured. For that purpose, the absorbance at 600 nm (A_{600nm}) of each culture (supernatant from each well) was measured.

C.2.e Biofilm observation and fluorescence staining.

In order to visualize all cells, fluorescent staining of bacteria was done prior to biofilm observation of *E.coli* PHL818 and *E.coli* PHL847 strains using Syto9® (Molecular Probes). After rinsing the samples as described above, 1µL/mL of a 5mM Syto9® stock solution was added to the last NaCl solution.

After 15 min of incubation at room temperature for these two strains, or immediately after rinsing without staining for *E.coli* PHL 1273 and SCC1 which express *gfp*, microscopy images were taken. The main part of the experiments was conducted with an upright confocal microscope (Zeiss, LSM700) with a 9.1 mm working distance focal objective (Zeiss LD EC "epiplan neofluar" 50X/055 DIC M27). Fluorescence of *gfp* from SCC1 and PHL1273 bacteria, and Syto9® labeling of PHL847 and PHL818 were exploited for imaging in fluorescence with laser wave length of 488 nm for excitation, while the collection of emission fluorescence was done in the range 420 - 550nm. In addition, excitation at 405 nm was used for imaging the surface in reflection mode. Few experiments (A5G7 LD and non-hybridized vesicles tested for PHL818, PHL847 and PHL1273) were not conducted with the confocal microscope, since the confocal microscope was acquired in September 2009. These experiments were conducted with an epifluorescent microscope (Olympus BX51) and biofilms were observed directly after the last rinsing step using a 15 mm working distance focal objective (Olympus SLMPL50X/0.45). The observation was conducted in fluorescence mode. Irradiation of the sample was performed with mercury lamp and fluorescence emission was collected in the range 420 - 550nm (FITC filter).

(i) Differed observation.

Two surfaces of each type were used for each experiment and each surface was imaged after incubation time at 10 different locations chosen randomly. Pinhole size (for confocal microscopy) and exposure time (for both confocal and epifluorescence microscopy) was kept constant during each experiment.

(ii) Time series differed observation.

To highlight bacterial motility on agar surfaces, for bacteria cultivated in static culture condition, surfaces were scanned with the upright confocal microscope (Zeiss, LSM700) after incubation time during 1 to 5min and picture were taken every 2 seconds.

C.3 Setup, culture and observation under flow culture condition.

C.3.a Flow cell design and setup configuration.

A specific flow cell was designed, during this work, for experiments conducted under a Zeiss LSM700 confocal microscope (Figure 49). The flow cell was made with the technical help of The Technical University of Denmark (Lyngby, Denmark) [100].

The flow cell was designed with various constraints: The flow cell was produced in polycarbonate to be autoclavable. Surfaces of 1 cm^2 for a thickness of 1 to 3mm can be placed inside. Observation of biofilm formed on the sample surface is possible using 9.1 mm working distance focal objective (Zeiss LD EC “epiplan neofluar” 50X/055 DIC M27). The flow cell design allows peristaltic laminar flow at the surface of the sample (tested for 1 mm thick silicon wafer, unpublished result). The chamber has a volume large enough to avoid any border effect in the flow at the surface (reduced flow speed or non-laminar flow). Finally, the entire setup consists of a flow cell connected with Tygon® tubing (⌀1.21mm) to a peristaltic pump (Ismatech IP multichannel peristaltic pump) with an intermediate bubble trap (provided by The Technical University of Denmark, Lyngby, Denmark [100]). Medium and trash bottles are closed with autoclavable caps equipped with filters (0.2µm, Millipore) and a three-way connector is used to allow injection. This setup is illustrated in the annotated picture in Figure 50.

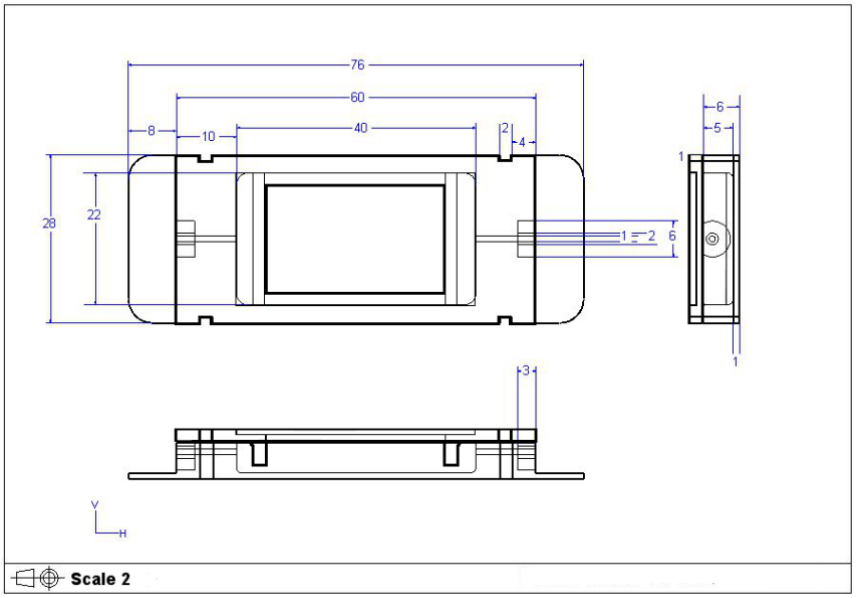


Figure 49: Home-made flow cell plan.



Figure 50: Picture of the complete experimental setup: (1) bottle with the bacteria nutritive medium, (2) peristaltic pump, (3) bubble trap, (4) injection system (syringe and adequate connector), (5) home-made flow cell, (6) trash bottle (bacteria nutritive medium after culture) and (7) Zeiss LSM700 confocal microscope.

C.3.b Bacterial culture and real-time observation under flow condition.

The experiment consists on a real-time observation of bacterial adhesion and biofilm growth onto surface under flow culture condition. The experimental procedure starts with the setup mounting. The two parts of the

flow cell are glued together with silicone rubber (Soudal aquarium^{TM}). After sterilization of all parts of the setup (flow-cell, tubing, connectors and bottles were autoclaved at 105°, 21min) the complete setup is mounted under sterile condition (under a laminar hood). The sterile surface is placed in the center of the flow cell, which is then closed by sealing a sterile glass cover slip with an external bead of silicon rubber (Soudal aquarium^{TM}).

Following the mounting procedure, the entire setup is installed under an LSM700 confocal microscope. The peristaltic pump is turned on and the culture medium (M63G) flows at a flow rate of 18 mL/h for 2 h. The pump is turned off. 5 mL of 0.1 A_{600} bacterial culture (10^7 bacteria/ml, obtained by a dilution of overnight culture) is injected into the cell and incubated 20 min without flow at room temperature (stability controlled by thermometer). During that time, confocal microscope is adjusted to image the surface. The medium is then flown at 18 mL/h and pictures are taken every 2 min for 10 h.

Both fluorescence and reflection modes are used as described above for fluorescence microscopy with LSM700. Images are taken in reflection and fluorescence modes (488/420-550 nm and 532/560-700nm). Image files were then processed using Zeiss ZEN2009 software in order to extract videos and pictures from the dynamic culture experiments. Quantification of the number of bacteria, determination of bacterial attachment an detachment, and determination of bacterial motility followed the analysis describe in Part II - C.2.f (CellC software and ImageJ with particle tracking plugin).

The experiment with *in situ* visualization of vesicles required an additional step before inoculation of bacteria. A surface bearing a C_7T_5 oligonucleotide sequence was inserted in the flow cell chamber and 5 ml of a fluorescently labeled vesicle solution (Nile Red labeling described in Part I) was injected into the flow cell without running the flow. The surface is incubated without flow for 12 h. Images were taken every 2 min in reflection and fluorescence modes (488/420-550 nm and 532/560-700nm). Medium flow was then turned on for 2 h before injection of bacteria and imaging was performed as described above.

C.4 Analysis of biofilm micrographs.

In order to determine the quantity of adherent bacteria, micrographs obtained with standard epifluorescence microscopy were analyzed using a method based on a cell-density scale, which consisted of 10 typical micrographs originating from several previous experiments. Practically, analysis was done by comparing new micrographs to the 10 micrographs of the scale. A preliminary technical study (data not published) demonstrated the relevance of this analysis in comparison with computer analysis. In the case of confocal micrographs, image processing was performed by using ImageJ V.1.44d software with LSMtoolbox V4.0g plugins [101], allowing separation of fluorescence and reflection images from Zeiss LSM raw data. Extracted images were then processed with CellC [102] software to determine adherent bacteria numbers. Finally, we reported the number of bacteria per square centimeters. To allow comparison between the different results obtained during different experiments and with the two different techniques, results are usually presented after normalization to internal control.

The determination of bacterial motility was performed with the help of ImageJ V.1.44d software with particle tracking plugin [103], which provides bacterial position on each pictures and their trajectory. These positions were then converted into displacement vectors between each picture and referred to originate position of the bacteria. The sum vector translating the full displacement of one bacterium at the end of the image series is called sum vector. Finally, the bacterial motility speed is calculated from the norm obtained for each displacement vector.

The determination of bacterial attachment and detachment was performed with the help of ImageJ V.1.44d with particle tracking plugin to determine the number of bacteria detaching between two pictures. The attachment-detachment balance corresponds to the balance of the number of bacteria attaching to the surfaces minus the number of bacteria leaving the surface. This balance was averaged, over the experiment course, with the help of a rolling average. The rolling average consists in averaging the balance value of each picture with the last 15 attachment-detachment balance values corresponding to the 15 pictures of the series. This aims at representing the trend of the variation over the course of the experiment rather than unitary picture to picture variations.

C.5 Quality control.

The results are expressed in terms of mean values and standard deviations for two samples (10 images per sample) of each substrate type, including control. Significant differences between sample sets were determined using the classical parametric test for mean comparison, the so-called Student test (n-1 degree of freedom).

To test reproducibility, attachment and toxicity experiments were repeated and the graphs presented in following results section display the average of the experiment repetitions. The number of reproduction, for each incubation time and each type of surfaces was as following: A5G7 HD, C7T5 HD, and internal control were reproduced 4 times for PHL818 and SCC1 and twice for PHL847 and PHL1273. A5G7 LD and non-hybridized vesicles were reproduced twice for PHL818, PHL847 and PHL1273. Finally, vesicles “smooth”, vesicles “rough” and agar surfaces were tested once for SCC1 (repetition under progress).

D. *Results.*

D.1 Surface supernatant toxicity test.

The toxicity of the surface for bacterial growth was tested by measuring the absorbance of the supernatant of each well at 600 nm (A_{600}). The growth profiles that we obtained did not show any inhibition of bacterial growth in the presence of either oligonucleotide coated surfaces or a nanostructured surface, as illustrated in Figure 51(a) for non-hybridized vesicles and A5G7 LD and in Figure 51(b) for hybridized vesicles, A5G7 HD and C7T5 HD.

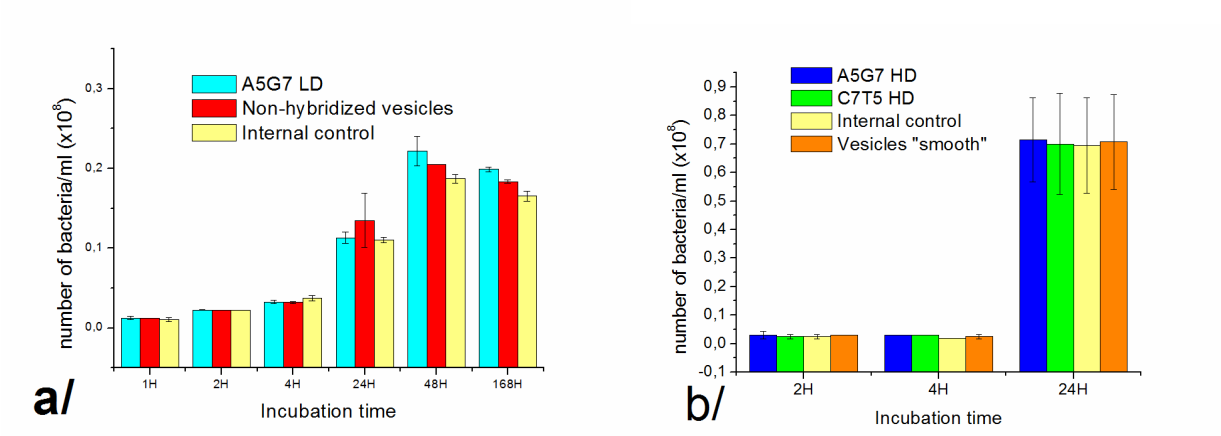


Figure 51: Growth profile of bacteria in the supernatant of different surfaces, measured by UV-Vis absorption at 600 nm (a) for internal control, A5G7 LD and non-hybridized vesicles. (b) for vesicles "smooth", A5G7 HD, C7T5 HD and Internal control.

D.2 Bacterial adhesion study.

In this study we quantified the bacteria that adhered to the different surfaces, for strains with and without curli, in order to examine the bacterial adhesion and biofilm growth on the oligonucleotide surfaces, either smooth or with vesicles structures.

A preliminary study allowed to observe the general colonization behavior of bacteria on oligonucleotide surfaces. Then 3 surface properties were considered, in particular chemistry, topography and mechanical properties. First, the influence of oligonucleotide strand type and density was studied by comparing bacterial adhesion onto A5G7 LD, the two types of "high density" oligonucleotide surfaces: A5G7 HD and C7T5 HD, and internal control (glass cover slip and silicon wafer). Secondly, the topography influence on the bacterial adhesion was investigated, comparing A5G7 LD with non-hybridized vesicles and comparing vesicles "smooth" with vesicles "rough". Finally, the influence of the mechanical properties of the surfaces onto bacterial adhesion was investigated comparing non-hybridized vesicles, A5G7 HD, C7T5 HD, A5G7 LD and internal control (mechanically stiff), "vesicles "smooth" and vesicles "rough" (viscoelastic properties).

D.2.a Bacterial adhesion, proliferation and biofilm formation on oligonucleotide modified surfaces.

In this first step, we studied the influence of oligonucleotide modified surfaces on the adhesion, proliferation and biofilm formation of curli+ (PHL818) and curli- (PHL847) bacteria.

For this purpose, we compared adherent cells numbers on the "low density" oligonucleotide-coated surface A5G7 LD, on non-hybridized vesicles (providing a coating with the same chemistry and mechanical properties but different topography) and on internal control. Numbers of adherent bacteria on surfaces were measured during the entire biofilm growth process (from initial adhesion at 1 h to mature biofilm at 168 h). Results are presented in Figure 52.

At first, we can notice in Figure 52(a), that the number of bacteria possessing curli is similar at 1 h and 2 h of incubation on surfaces and then strongly increases at 4 h to reach a 'plateau' until the end of the experiment, illustrating the classic surface colonization followed by 3D growth of the biofilm structure. Since the study was conducted by epifluorescence experiments, the increase of bacterial number growing in the 3D structure was not quantifiable, leading therefore to the observable leveling-off. We can also notice that the comparison between the three different surfaces does not show any difference in bacterial numbers, which implies that chemistry and topography properties of the surface did not influence bacterial adhesion in term of cell amount, for bacteria possessing curli.

The same was observed for bacteria unable to express curli, since no significant difference in number of adherent cells could be observed between the different types of surfaces. Nevertheless, we observed in Figure 52(b) that the number of bacteria was the same at 1 and 2 h, and increased at 4 h but decreased back at 24 and 48 h before increasing again at 168 h. This behavior corresponds to normal surface colonization and biofilm structure growth followed by biofilm detachment (24-48 h) and new 3D growth again (168 h), occurring faster than in the case of curli expressing *E.coli*.

Finally, comparing Figure 52(a) and Figure 52(b), we notice a number of adherent bacteria at the same order of magnitude (10^4-10^5 bacteria per surface (1cm^2)) during the first hours of adhesion, implying similar adhesion and spreading properties for both strains.

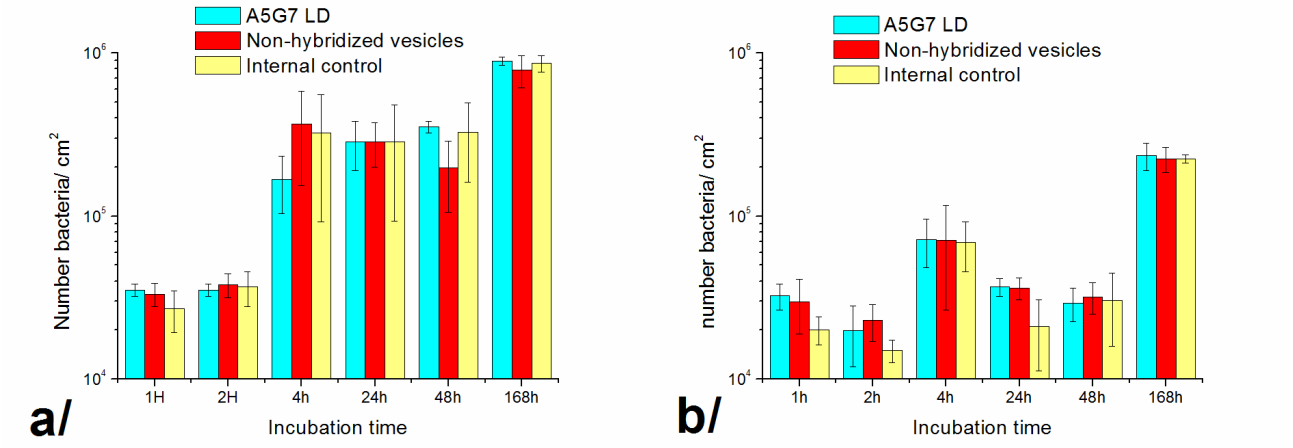


Figure 52: (a) Quantity of bacteria for *E.coli* PHL 818 and (b) *E.coli* PHL847 for six incubation times on A5G7 LD (blue), on non-hybridized vesicles (red) and internal control (yellow).

D.2.b Influence of oligonucleotide strand type and density.

The influence of different density of oligonucleotides and the influence of two different strands on bacterial adhesion (at 2 h of incubation) were studied by incubating surfaces coated with a "high density" protocol: A5G7 HD and C7T5 HD, surface coated with "low density" oligonucleotide: A_5G_7 LD and internal controls (wafer

and/or glass), with curli + and curli- strains (SCC1 and PHL847, respectively). Since adhesion should not go beyond the two first hours, we decided to apply the static growth protocol for incubation during 2 h.

Example of pictures obtained in this study, combining micrographs obtained at each sample location, in both confocal reflection and fluorescence modes, are presented in Figure 53. First, the difference in the image quality must be noticed, as well as the consequence for the quantification of bacteria number by image analysis: Figure 53(a), (b) and (d) display good quality for quantification, while quality of Figure 53(c) was affected by the substrate nature (glass) and its reflection properties. Quantification of bacteria number was therefore more difficult, leading to an increased standard deviation. Secondly, those images provide a first qualitative observation of the bacterial adhesion to these oligonucleotide "high density" surfaces. We notice a lower number of bacteria on oligonucleotide surfaces (Figure 53(a) and (b)) compared to the number of bacteria on the internal controls (Figure 53(c) and (d)). Moreover, the number of bacteria was similar among the different oligonucleotide surfaces (Figure 53(a) and (b)) and similar between both internal controls (Figure 53(c) and (d)). The last qualitative observation from these images is on bacterial spreading. We did not observe any patterns and bacteria seemed randomly dispersed on the surface for both oligonucleotide and reference internal controls as expected for homogeneous surfaces.

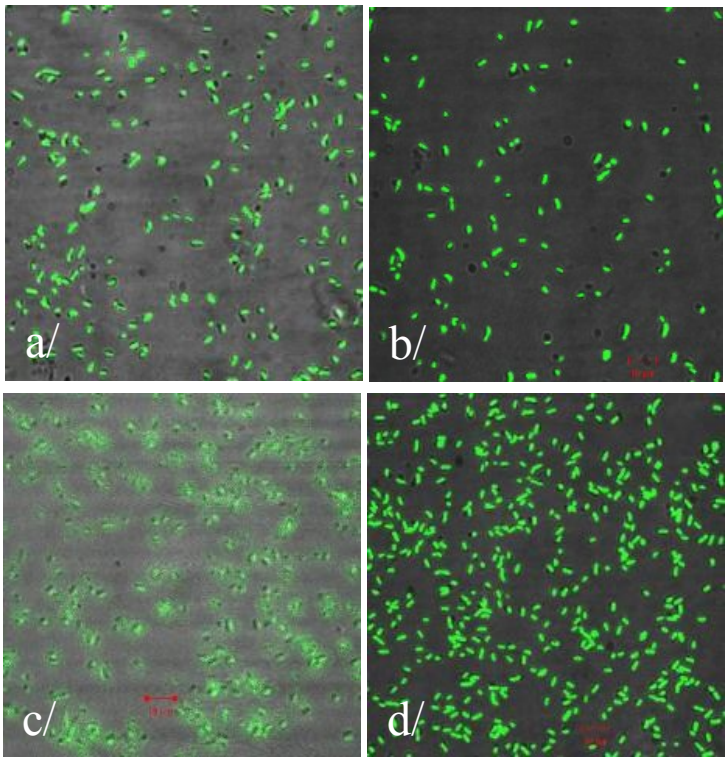


Figure 53: Confocal microscopy pictures, obtained by combining fluorescence and reflection images. These pictures show SCC1 bacteria adhered to (a) "A5G7 HD (b) C7T5 HD (c) glass internal control (d) silicon wafer internal control.

We quantified the number of bacteria on the A5G7 HD and C7T5 HD, and compared them to the number of bacteria on A5G7 LD. Figure 54 presents the normalized results (normalized to results obtained on internal control, set to 100% as specified in Materials and methods) of the bacterial adhesion on these surfaces, under static conditions after 2 h of incubation for all strains used in this study. We observe a number of cells adhering to "low density" oligonucleotide surface (A5G7 LD) close to 100% (i.e. similar to internal control), as already described in Figure 52(a). This shows that the "low density" oligonucleotide surface does not influence the intensity of bacterial adhesion. At the opposite, Figure 54 shows a lower number of cells adhered to A5G7 HD and C7T5 HD "high density" oligonucleotide surfaces compared to the internal control. This effect is observable for both the curli+ (PHL818, SCC1 and PHL1273) and the curli- (PHL847) strains and is therefore not due to an action of curli. This results lead to the conclusion that "high density" oligonucleotide coated surfaces does reduce bacterial adhesion compared to internal control and "low density" oligonucleotide surfaces. We also notice the similar quantity of bacteria adhering to both A_5G_7 and C_7T_5 oligonucleotide strands, which was observable for both the curli+ and the curli- strains. Since no significant difference in the number of adherent cells can be observed between surfaces coated with both strands, we can conclude that surfaces coated with "high density" oligonucleotide reduces the number of adherent bacteria compared to internal control independently of the oligonucleotide strand used herein (A_5G_7 or either C_7T_5).

Finally, we notice that the relative bacterial adhesion was similar between all strains: SCC1 (*gfp* chromosomal insertion), PHL1273 (plasmid curli *gfp* fusion), PHL847 (curli deficient) and PHL818 (wild type) strains. "High density" oligonucleotide coating reduced the number of adherent bacteria for all strains. This result was expected, since those strains are mutants of the same *E.coli* K12 MG1655, but proves that the bacterial adhesion results are not influenced by the mutations (*gfp,* curli *gfp* fusion and curli-).

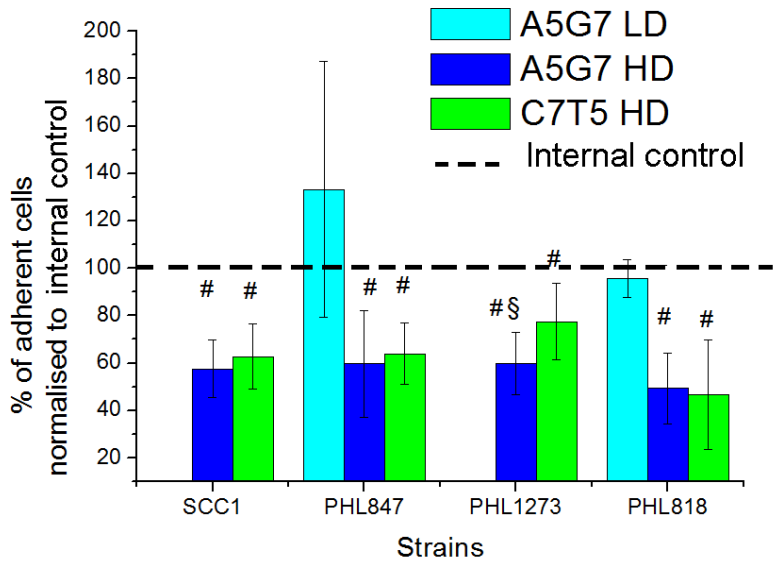


Figure 54: Relative number of adherent bacteria attached to "low density" A_5G_7 oligonucleotide surfaces (A5G7 LD, light blue), "high density" A_5G_7 oligonucleotide surfaces (A5G7 HD, dark blue) and "high density" C_7T_5 oligonucleotide surfaces (C7T5 HD, green), compared to internal control (dash line) for the four strains of *E.coli*: SCC1, PHL 818 normal strain, PHL 847 curli deficient strain and PHL 1273 (curli-*gfp*). Black hatch-marks highlight significant differences according to the Student t test. "#" stands for significance > 99.995 compared to internal control and "§" stands for significance > 99.5 compared to C7T5 HD surface.

D.2.c Influence of topography.

To determine the influence of the topography independently of other factors we need to compare surfaces with similar mechanical properties and similar oligonucleotide strand type and density. For this purpose, we first compared vesicles "smooth" surfaces and vesicles "rough" surfaces, which have similar properties except the topography scale as illustrated in Figure 55. In this figure, we can clearly see that vesicles "rough" surfaces displayed microtopography associated with nanotopography, while vesicles "smooth" surfaces did not. They only displayed nanotopography as described in Part I-Chapter3. Similarly, we compared non-hybridized vesicles surfaces with A5G7 LD surfaces, which were both mechanically stiff and based on the "low density" oligonucleotide coating protocol. Both surfaces differed in the presence of nanotopographical features on the non-hybridized vesicles surfaces, while A5G7 LD surfaces were perfectly smooth at the nanoscale, as presented in Part I-Chapter3.

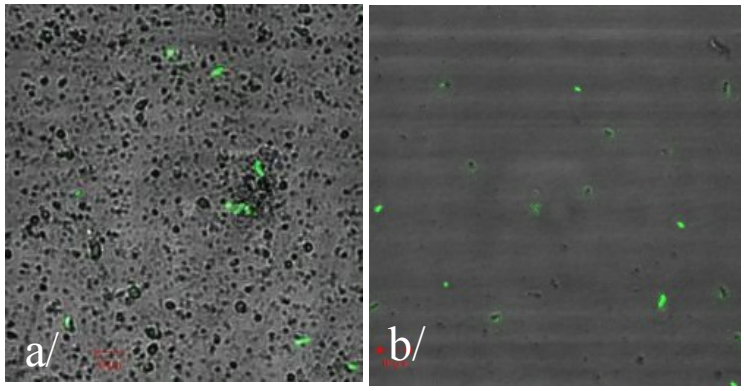


Figure 55: Confocal fluorescence pictures, combining reflection and fluorescence mode, of bacteria adhered on a (a) vesicles "rough" surfaces (b) vesicles "smooth" surfaces

Quantification of the influence of topography onto bacterial adhesion is performed by comparing results obtained in static culture conditions at 2 and 4 h, normalized to internal control at 2 h. We notice, in Figure 56(a), that no significant difference in the number of adherent bacteria, between non-hybridized vesicles surfaces and A5G7 LD surfaces can be observed. We can conclude that on mechanically stiff surfaces, the nanotopography displayed in the present study does not influence bacterial adhesion. Looking now at Figure 56(b), we do not observe significant differences between numbers of adherent bacteria on vesicles "rough" and vesicles "smooth" surfaces. Both surfaces reduce similarly the number of adherent bacteria compared to internal control. The microtopography, observable in Figure 55 and obtained by varying the protocol for vesicle hybridization, seems not to further influence bacterial adhesion in the present case.

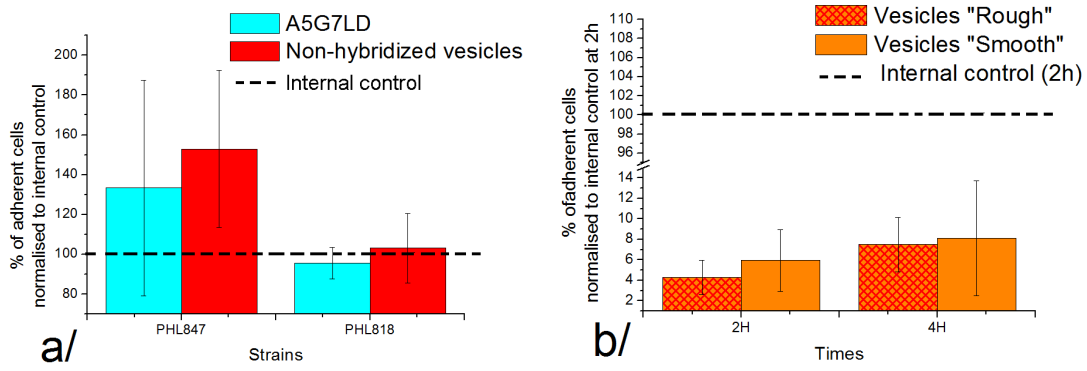


Figure 56: (a) number of adherent cells (PHL818 and PHL847) on non-hybridized vesicle surface and A5G7 LD, at 2 h of incubation (b) comparison between vesicles "rough" (orange with red pattern) and vesicles "smooth" (orange) surfaces at 2 and 4 h incubation with SCC1, normalized to glass at 2 h set as 100% colonization.

D.2.d Influence of vesicles mechanical properties.

The influence of the mechanical properties of surfaces coated with vesicles on bacterial adhesion was observed by comparing the number of adherent cells on vesicles "smooth" surfaces, which are expected to display

a visco-elastic behavior due to the vesicle layer (see Part I- chapter3), on oligonucleotide "high density" surfaces (same strand as on the vesicular shell. i.e. A_5G_7) and on internal control, which are both mechanically stiff surfaces. We incubated the surfaces in static condition during 2 and 4 h with curli+ (SCC1) *E.coli* strain and observed them with confocal microscopy CLSM700 as described in Material and methods. In addition, a similar experiment was conducted with PHL818 (which is equivalent to SCC1) and epifluorescence microscopy on the non-hybridized vesicles surfaces compared to A5G7 LD surfaces and internal control, which are all mechanically stiff. All the quantitative results are presented in the same graph after normalisation to internal control as specified in Materials and methods.

To illustrate this experiment, pictures of Figure 57 are presented adherent bacteria on vesicles "smooth" surfaces, on A_5G_7 HD surfaces and on internal control. In this figure we can qualitatively notice the low number of bacteria adhered to vesicles "smooth" surfaces of Figure 57 (a), compared to A5G7 HD surfaces of Figure 57 (b) and compared to internal reference of Figure 57(c). This observation allows to qualitatively highlighting of the high impact of hybridized vesicles on bacterial adhesion, leading to this visibly smaller amount of adhered bacteria.

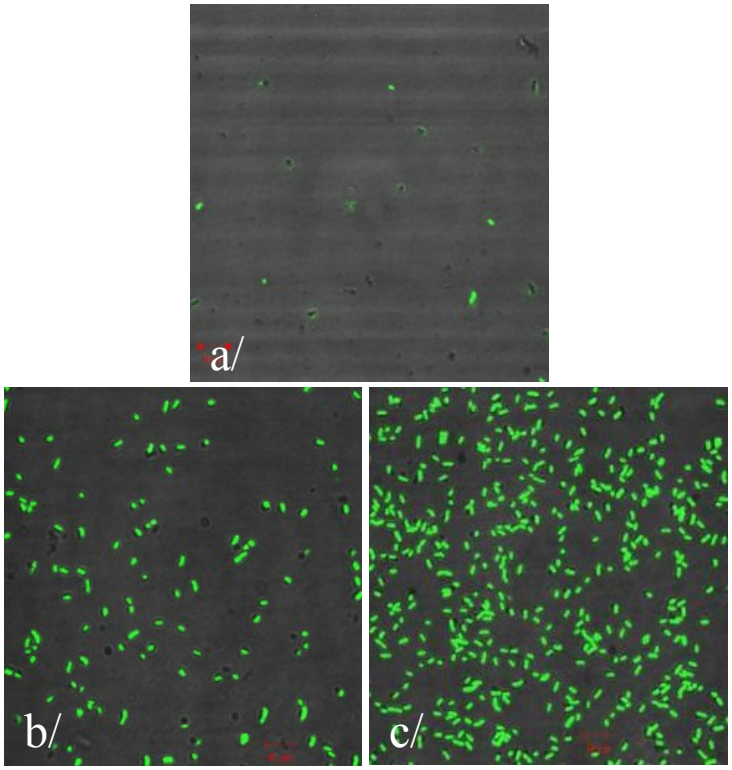


Figure 57: Confocal fluorescence imaging, as a combined reflection and fluorescence picture, of bacteria adhered to the different surfaces (a) vesicles "smooth" vesicles (b) A5G7 HD surfaces (c) internal control (wafer).

Quantification of the number of adhered bacteria per micrograph was performed. Results are presented in Figure 58. In this figure we first notice the greatly reduced number of bacteria adhered to hybridized vesicles

surfaces compared internal control and "high density" oligonucleotide surfaces. We can further notice that the reduction is greater than that observable on A5G7 HD surfaces compared to internal control. From this observation, we suggest a different origin for both effects, which will be discuss in the discussion section. Briefly, the "high density" oligonucleotide surface may influence bacterial adhesion due to the oligonucleotide chemical properties, while vesicle coating may influence adhesion due to the vesicular layer soft mechanical properties. This hypothesis is consistent with the similar number of bacteria adhered on internal control and on non-hybridized vesicles, which are both mechanically stiff. This means that the nanotopography due to such vesicles layer is not able to influence bacterial adhesion. We can further notice in Figure 58(a) that a similar effect, comparing internal control and non-hybridized vesicles, is observable for curli deficient strain, demonstration the independence of the number of adherent cells with the curli expression. Finally, we notice on Figure 58(b), that the effect is significant and persistent 2 and 4 h of incubation.

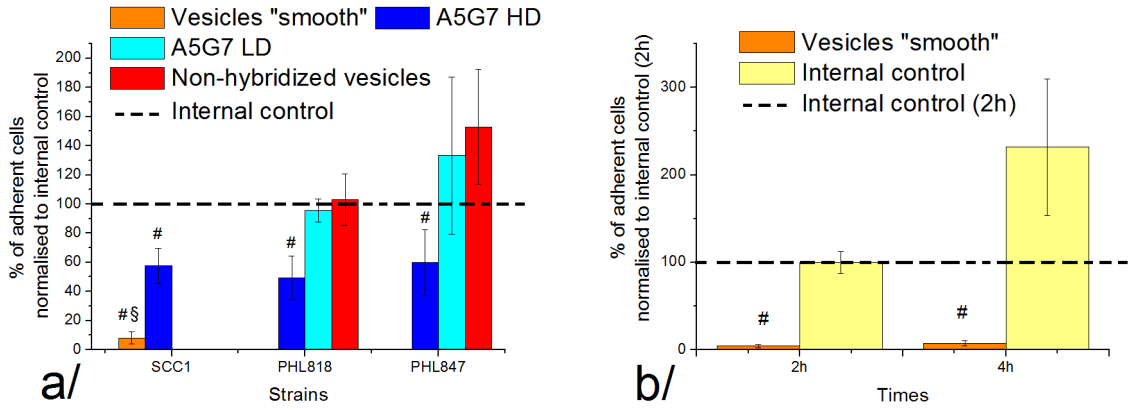


Figure 58: (a) number of adherent cells (SCC1, PHL818 and PHL847) on Vesicles "smooth" surfaces, Non-hybridized vesicle surface, A5G7 HD surface and internal control, at 2 h of incubation (b) comparison between vesicles "smooth" (orange) surfaces and internal control at 2 and 4 h incubation. Black hatch-marks highlight significant variation according to the Student t test. "#" stands for significance > 99.995 compared to internal control and "§" stand for significance >99.995 compared to A5G7 HD surface

D.3 Adhesion and detachment experiment under flow.

Observations of bacterial growth on wafer internal control, on C7T5 HD surfaces and on vesicles "smooth" surfaces were performed under dynamic conditions. With these experiments, we aimed at observing bacterial growth on the surface and at better understanding observed results in static conditions in terms of adherent bacteria numbers. We also aimed at determining the attachment and detachment of bacteria during the adhesion step, and during biofilm growth. In addition, vesicles "rough" surfaces were prepared *in situ* by the hybridization of labeled vesicles and allowed the co-localization of vesicles and bacteria. We should notice that dynamic experiments provide video that cannot be presented here. Therefore, results are shown in graphs obtained after analysis of the pictures, and some of these pictures are shown for qualitative observation.

The Figure 59 displayed micrographs obtained for the bacterial growth of the SCC1 strain on a silicon wafer internal control at different incubation times under flow conditions. Similar pictures were obtained on C7T5

HD surfaces. In this experiment, as described in Material and methods, the flow was started after 20 min of incubation in static conditions, and the image labeled at T=0 min corresponds to the first picture after the start of flow. We see, in the picture labeled 0 min that colonization already occured. We should notice that bacteria are present in the flow during the first 60 min, due to the distance between injection connectors and the flow cell in our protocols. In the following pictures, we see classical bacterial growth, in which surface colonization occured in the three dimensions. We notice, in comparison with the observed biofilm growth in static culture, that the main observable difference is the slightly lower 2D colonization of the surface, replaced by faster 3D structure-building. Nevertheless, the growth corresponds, as expected, to a complete colonization of the surface with the building of three dimensional biofilm structures.

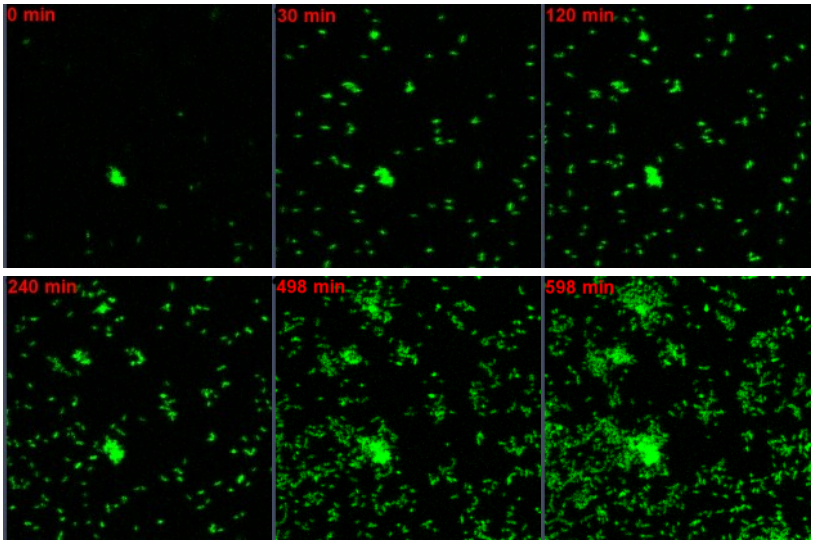


Figure 59: SCC1 bacterial growth on control wafer under flow. Images illustrate growth at 0, 30, 120, 240, 480 and 600 min.

The results presented in Figure 60 show pictures of the growth of SCC1 on vesicles "smooth" surfaces, combining reflection and fluorescence modes, in order to visualize simultaneously bacteria and surface topographical features. In this series of pictures, we notice a starting number of bacteria similar to internal control and C7T5 HD surfaces. However, only a small increase in the number of bacteria was observed over time. This result qualitatively correlates with results from static culture conditions, in which bacteria were in small amount on the surface after 2 and 4 h. Adhered bacteria seem to be as strongly bound to the surface as observed on internal control surfaces, and seem to divide normally. Nevertheless, we observed that, in the most cases, one of the daughter bacteria did not adhere and was released in the flow. In addition, the daughter bacterium was always highly motile before leaving the surface. All these aspects, attachment, detachment and motility, were quantified. Results are presented in the following paragraphs.

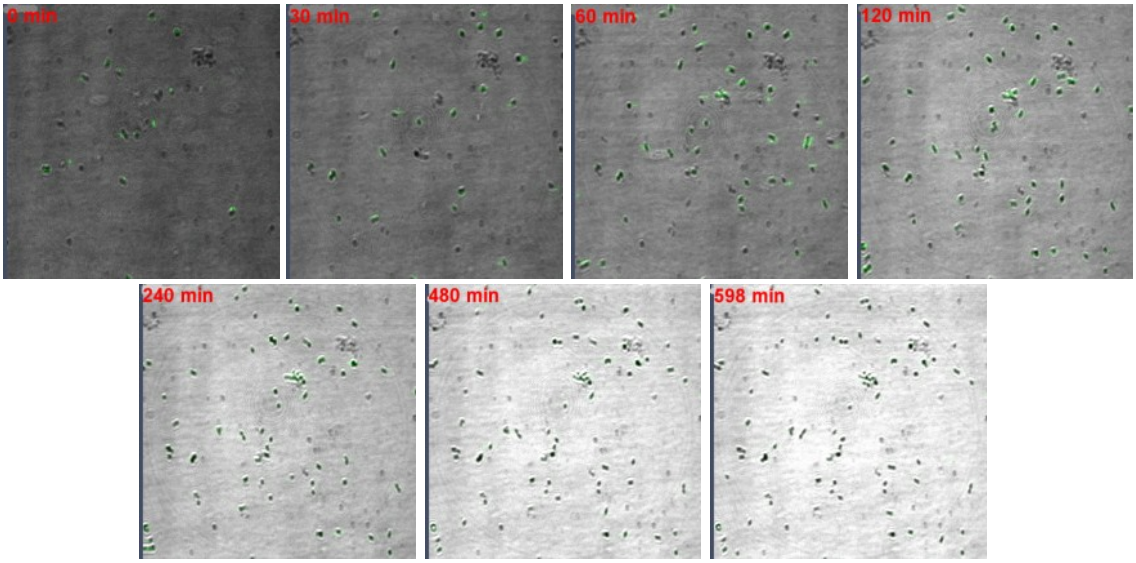


Figure 60: Bacterial growth on vesicles "smooth" surface under flow. Images illustrate growth at 0, 30, 60, 120, 240, 480 and 600 min.

The number of bacteria adhered on the surfaces under the flow conditions are presented in Figure 61(a). These results show the evolution of the number of bacteria over time. Before describing this figure, we have to specify that the bacterial count is biased in the case of three dimensional biofilm structures on a wafer and "high density" oligonucleotide surface. This biased count is due to the difficulty of counting a single bacterium from a 3D structure. To improve the extraction of such single bacterium, we performed the evaluation of the number of bacteria with the help of a dividing algorithm, known as Watershed algorithm, that divided bacterial cluster into single cells. One parameter, the "division factor" needs to be chosen according to fluorescence intensity. In our case, the division factor was set to 0.4. Its relevance was controlled by comparing obtained values with manual counting. As usual for dividing algorithm, this one does not be accurate to precisely count bacteria but rather properly provides growth trend.

In Figure 61(a), we observe the rapid increase in bacterial number on a wafer internal control, vesicles "smooth" surfaces and C7T5 HD surfaces in the part A of the graph. The first rapid increase in the number of bacteria is linked to bacterial deposition and bacterial growth on surfaces in the first 60 min. After this first phase on the internal control and A5G7 HD surface, a slope break followed by smaller slope indicates the increase in bacteria number due to bacterial growth on the surface corresponding to the start of 3D growth and biofilm development (part B and C of the graph). On vesicles "smooth" surfaces, we can see a similar number of adherent bacteria at the start of the experiment. The number of bacteria does not increase over the course of the experiment showing that no biofilm is built up. This can be related to detachment of bacteria from the vesicles "smooth" surface (part B) since number of bacteria is decreasing, followed by the conservation of a constant number of bacteria on the surface due to the conservation of adherent bacteria and the constant release of one of the daughter

bacteria during growth division (part C). This initially increasing number of bacteria is attributed to the incoming bacteria from the flow, while after this first period, and since no more bacteria are brought from the flow, the detachment may become higher than the attachment, leading to a decrease in the number of bacteria adhered on the surface. This interesting observation suggests that the vesicles "smooth" surfaces influence the bacterial detachment more than the bacterial attachment.

To be able to further discuss attachment and detachment on the vesicles "smooth" surfaces, we quantified the number of bacteria attaching and detaching on each picture. We calculated the balance between attachment and detachment for each of these pictures and calculated a rolling average (based on the 15 last successive images) as described in Materials and methods. We compared this value to the rolling average obtained on internal control, as presented in Figure 61(b). In this graph we notice that the balance alternates between a positive and negative value, showing an increase in the number of bacteria, alternating with a decrease of the number of bacteria on the surface. Considering the rolling average calculated for vesicles "smooth" surface, we observe that the number of bacteria increases slightly during the first 60 min (part A) during which bacterial growth is combined with attachment of bacteria coming from the medium. Then, right after this first phase, the rolling average is negative during a short period (20 min, part B) and then stabilizes around zero for the last part of the experiment (part C). The short negative period for average balance is due to detachment of adhered bacteria, while no more bacteria are coming from the medium to reverse the balance. The bacteria appearing should only come from bacterial growth on the surface. Then the number of bacteria appearing becomes similar to the number of bacteria detaching. This neutral balance should correspond to the following scenario: upon division, one daughter cell stays on the anchoring point while the other is not able to stay and releases in the medium (i.e. disappearing in following pictures) as highlighted by the alternating balance (growth followed by detachment on the following picture). On internal control, the rolling average started also with a high value before decreasing over time in the part A of the graph, due to diminution of the number of bacteria coming from the medium. In part B and C the rolling average stabilizes to a constant value (around 1 bacteria per micrograph), which correlates well with the constant positive slope observable in Figure 61(a).

Finally, in the case of vesicles "rough" surfaces, we observed a low number of adhering cells compared to vesicles "smooth" surfaces. This low number does not allow a reasonable discussion of any increase or decrease in the number of bacteria, but looking at the pictures of Figure 63, suggests that there is a similar compensation phenomenon between bacteria proliferation and daughter cell detachment, leading to a similar stabilization of the attached bacteria number, however, at a weaker value.

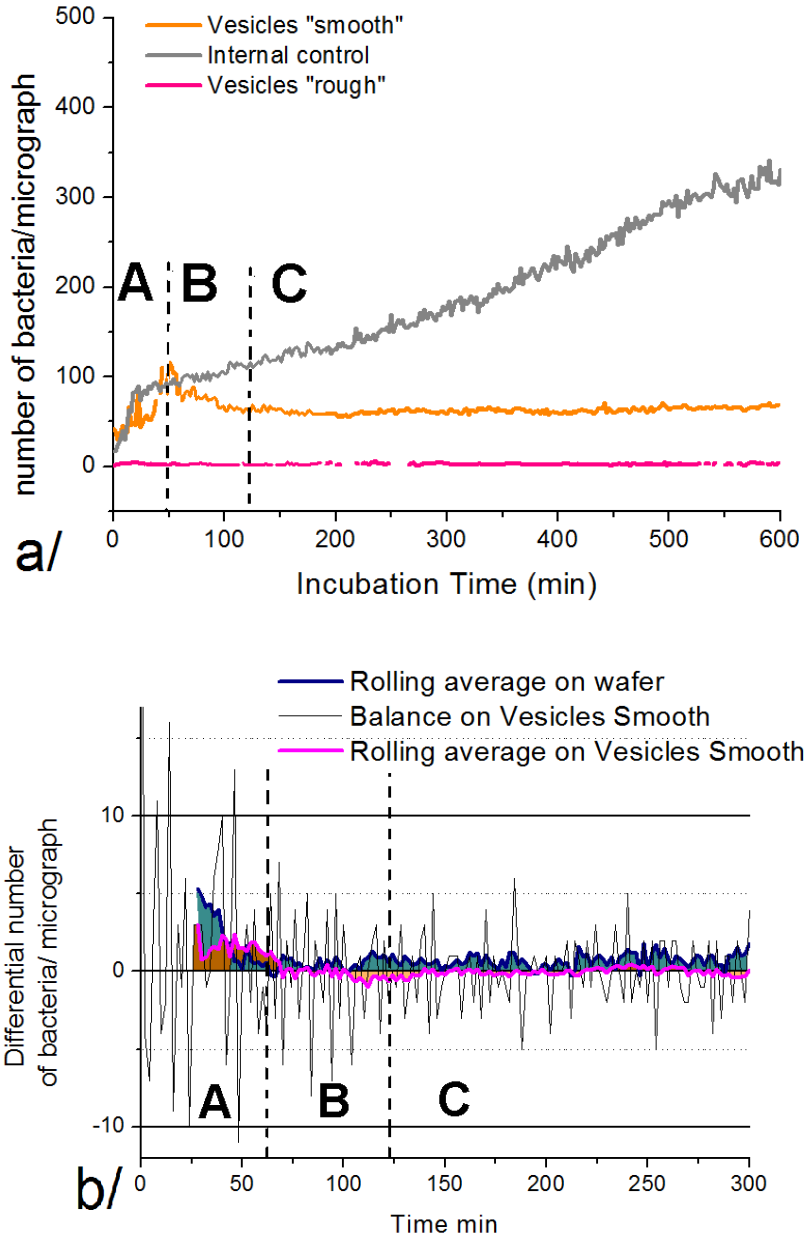


Figure 61: (a) number of bacteria on internal control (wafer, gray), vesicles "smooth" surface (orange) and vesicles "rough" surface (pink), under dynamic experimental condition. (b) Balance of the attachment and detachment event occurring on vesicles "smooth" surface (gray line) and mobile average on fifteen last balance values for vesicles "smooth" surface (pink line) and for internal control (blue line).

To quantify the bacterial motility on the surface, we followed bacterial movement on surfaces over the experiment course. We represented this movement between two measurements by black vectors in Figure 62(a) and the global displacement of the bacteria (sum of all unitary displacement vectors) in red. With the Figure 62(b) we can identify the two populations cited above: an adhered population, presenting global displacement smaller or equal to unitary displacement (marked with blue dashed line of Figure 62(b)), and a detaching

population, presenting a global displacement bigger than unitary displacement. These populations correspond to non-motile bacteria and bacteria motile before detachment respectively. The reason why one of these daughter bacteria can stay adhered while the second one is released in the flow cannot be explained by this experiment, since the vesicles "smooth" surface does not allow discussing local position of vesicles compared to local position of bacteria. Therefore, *in situ* preparation of surfaces by the hybridization of labeled vesicles was performed in order to allow the simultaneous co-localization of vesicles and bacteria.

For this purpose, fluorescently labeled vesicles were used and were hybridized *in situ* during the experiment. Vesicles were spread on the surface as aggregates of vesicles, leading to the formation of a "visibly rough" topography, which allowed locating vesicles simultaneous to the topography determination and localization of bacteria. In the series presented in Figure 63, we see few bacteria adhering onto this surface. This result correlates with the observation from static experiments and from experiments on vesicles "smooth" surface. The adhered bacteria did not display motility, while daughter cells displayed high motility, attaching for a few minutes at various positions before being released in the flow. Finally, we notice that the bacteria adhering on the surface seem to have preferentially adhered in a pack of vesicles but no quantification could be performed because of the very low number of bacteria present on the surface.

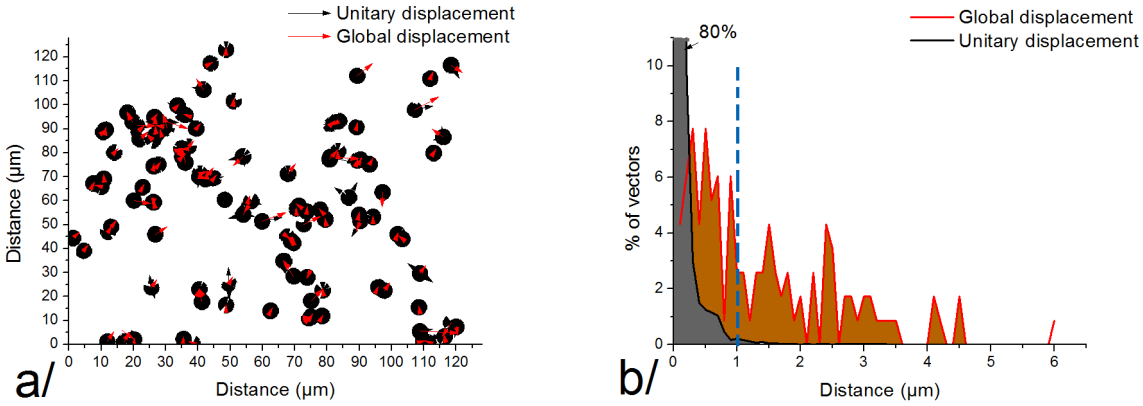


Figure 62: (a) Vectorial representation of SCC1 bacterial displacement on vesicles "smooth" surface from dynamic experiment. Black arrows represent vectors normalized to the original bacterial position, representing bacterial displacement every two minutes. Red arrows represent sum vectors corresponding to the global displacement of the bacteria measured until bacteria detached or until the end of the experiment. (b) Quantification of the vectors dispersion, in per cent of the total numbers of vectors, as a function of vectors size (distance in µm) incremented every 0.1µm.

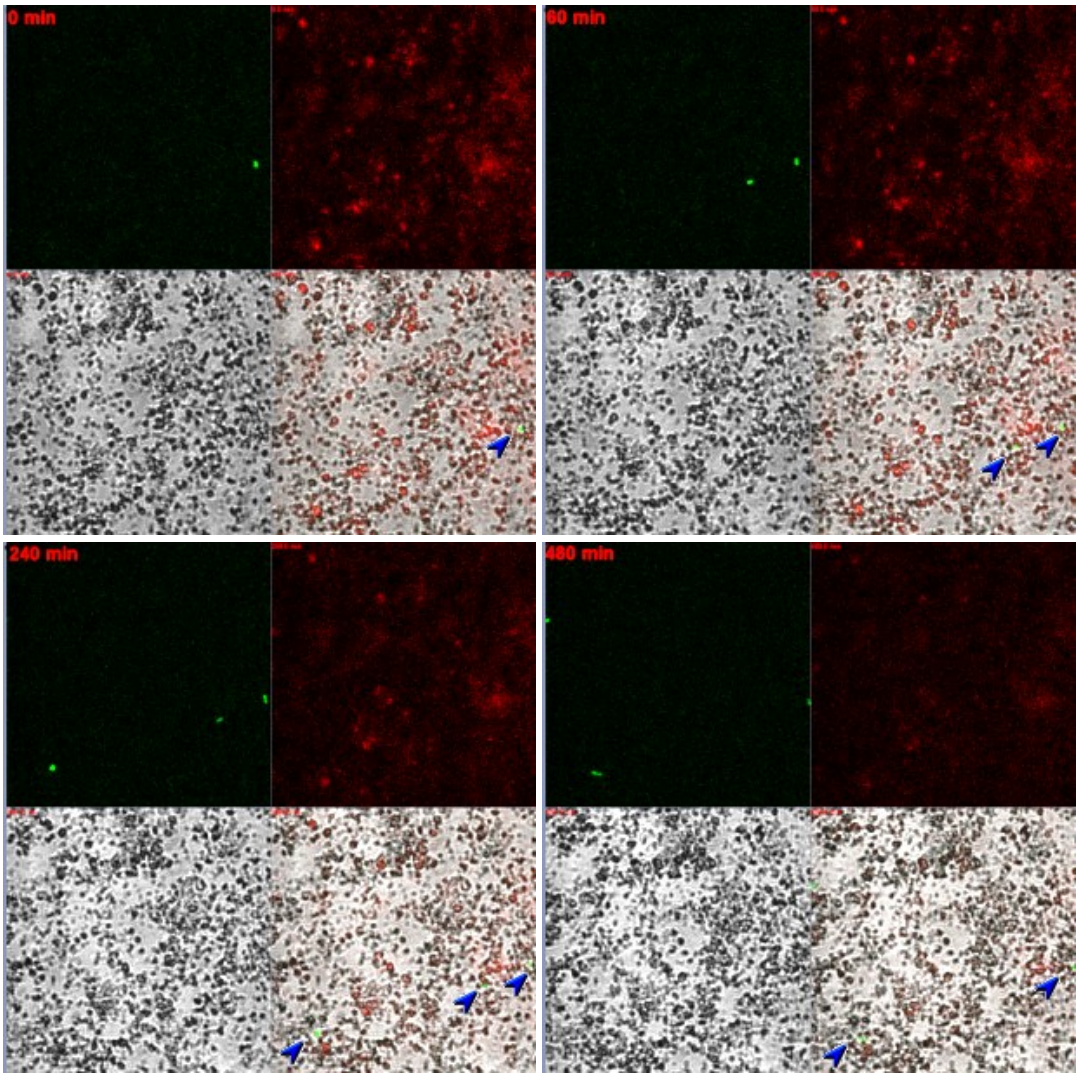


Figure 63: SCC1 bacterial growth monitoring on *in situ* prepared vesicles "rough" surfaces. Selected images of the surface at 0, 60, 240 and 480 min are presented. The pictures at each incubation time display four parts: the green channel is displayed in the left upper corner (detection of *gfp* bacteria), the red channel is shown on the right upper corner (detection of Nile Red labeled vesicles), reflection light micrograph is displayed at the bottom left corner, and finally the merged pictures of those three channels are shown at the bottom right corner and contain blue arrows to locates bacterial position.

D.4 Complementary experiment with an agar coating: link between mechanical properties, bacterial adhesion and bacterial motility.

We saw above the strong influence of vesicles surfaces on the number of bacteria on the surface, leading to a low number of bacteria on the surface. We propose that this antiadhesive effect is due to a higher detachment of bacteria on surfaces with visco-elastic properties compared to stiff surfaces.

To confirm the link between visco-elastic properties and the increase of detachment leading to a potential increased bacterial detachment, we made complementary experiments on hydrogel surfaces with different stiffnesses. The agar surface preparation, at 5g/L, 15g/L, 30g/L and 80g/L, are described in Material and methods. The qualitative observation of the surface stiffness was assessed in bulk hydrogels, where 5g/L agar is fluid-jelly,

15 g/L jelly, 30 g/L stiff-jelly and 80g/L stiff. Quantitative characterization of elastic modulus, by AFM indentation, is under progress. We observed the bacterial adhesion on these surfaces in static conditions as performed with oligonucleotide modified surfaces.

The first observation concerns the number of visible adherent SCC1 bacteria after 2 h incubation compared to adhesion on a silicon wafer. Results are presented in Figure 64. In this figure we can observe the strong influence of jelly agar coated surfaces (5, 15 and 30 g/L) on the number of adherent bacteria compared to silicon wafer. A really low number of bacteria were able to adhere to these hydrogels compared to the stiff solid silicon wafer, since no variation in the supernatant growth was visible (i.e. similar quantity of bacteria per ml on all surfaces: at 0.02 10^8 bacteria/mL at 2 h and 0.03 10^8 bacteria/mL at 4 h). On the contrary, stiff 80g/L agar surface induced a similar bacterial response as a silicon wafer, with a rather high number of bacteria adhered on the surface compared to other agar coated surfaces. No difference between numbers of bacteria on the "jelly" agar surfaces was observable. This is probably due to low reproducibility and difficulties in ensuring the stability of the agar coating on wafers. Nevertheless, the significant difference between "jelly" and "stiff" agar surfaces provides new evidence of the influence of surface mechanical properties on the number of adherent bacteria.

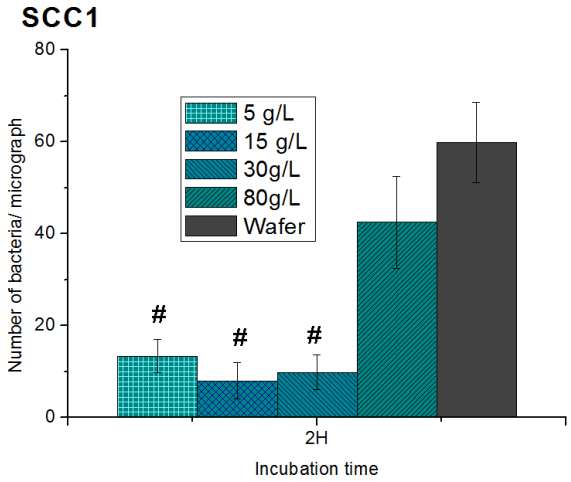


Figure 64: Number of adherent SCC1 bacteria on agar prepared with different concentrations and on silicon wafer. Hatch-mark highlights significant variation according to the Student t test. "#" stands for significance > 99.995 compared to silicon wafer.

We quantified also the influence of the surface mechanical properties on motility. For this purpose we scanned one location of each surface over time, using confocal microscopy. Some selected pictures are displayed bellow: Figure 65 presents the results obtained with 5g/L agar, whereas Figure 66 displays the results for 80g/L, and Figure 67 for the silicon wafer.

In Figure 65 we observed that all bacteria displayed motility over time. This motility is not collective but inherent to each single cell, not limited to certain areas, and it seems to be random. In Figure 66 we do not observe motility of bacteria, but they are moving around an anchoring point without any directional displacement. Finally, in Figure 67, we do not observe any motility and, if some of the bacteria move, they are moving around

their anchoring point, as observed in Figure 66. From those results we can qualitatively observe the influence of the surface visco-elastic properties on bacterial motility: bacteria on jelly surfaces display motility, whereas bacteria on stiff surfaces do not display directional motility but movement around an anchoring point.

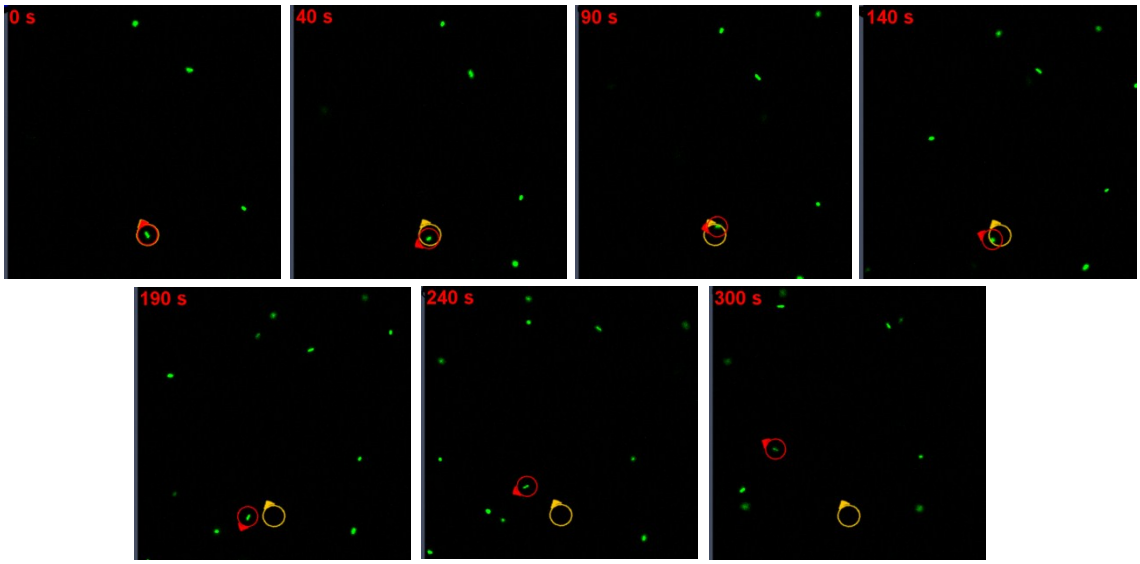


Figure 65: Bacterial adhesion on a 5 g/l agar-coated surface. The red ellipsoid locates a bacterium (position and orientation) followed over time, to address its motility and the yellow ellipsoid locate the originated bacterium position and orientation. Pictures were recorded at 0, 40, 90, 140, 190, 240, 300 seconds.

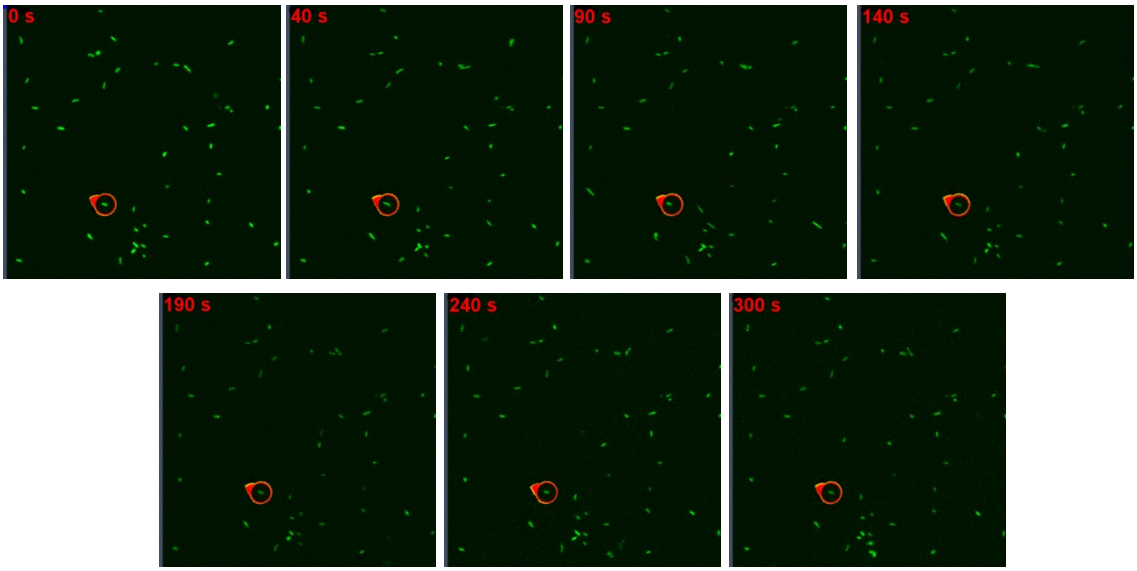


Figure 66: Bacteria adhered to 80g/l an agar-coated surface. The red ellipsoid locates a bacterium (position and orientation) followed over time, to address its motility and the yellow ellipsoid locate the originated bacterium position and orientation. Pictures were recorded at 0, 40, 90, 140, 190, 240 and 300 seconds.

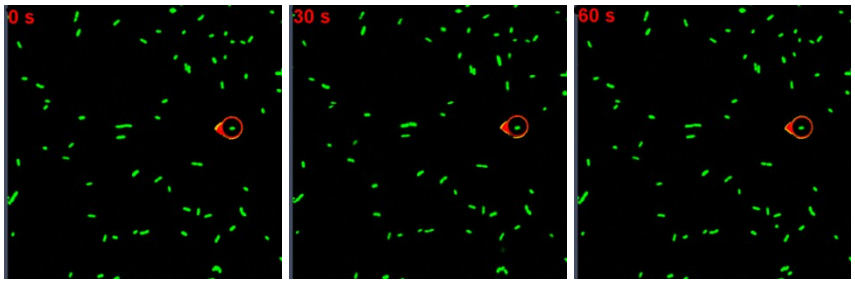


Figure 67: bacteria adhered to wafer surface. The red ellipsoid locates a bacterium (position and orientation) followed over time, to address its motility and the yellow ellipsoid locate the originated bacterium position and orientation. Pictures were recorded at 0, 30 and 60 seconds

We quantified bacterial displacement by using vectorial representation as presented in section D-3. We did this analysis for each bacterium on 5, 15 and 80 g/L agar and on silicon wafer surfaces (respectively Figure 68 (a), (b) (c) and (d)). We also presented in Figure 69(a) and (b) two typical trajectories of individual bacterium, respectively on silicon wafer and on 5 g/L agar surface. These vectorial representations provide information on bacterial displacement directionality, size and orientation. Based on Figure 68, we first notice that each global bacterial displacement is independent of the displacement of other bacteria in directionality, size and orientation. Moreover, each bacterial displacement on "jelly" agar (5 and 15 g/L) is directional (there is a displacement in one direction), while each bacterial displacement is limited (small vector size) on a stiff surface (silicon wafer and 80 g/L agar) and not directional for silicon wafer. In Figure 69 we notice that the sum vector size on "jelly" agar corresponds to a displacement of several micrometers (10 to 20 µm), which is ten-fold the value of an instant displacement. This displacement reveals the high motility of the bacteria on this surface type. Oppositely, the sum vector for displacement on wafer corresponds to a few hundreds of nanometers of displacement (200-500nm), similar to an instant displacement. This displacement is smaller than the bacterial size (1µm) and certainly corresponds to bacterial movement around the anchoring point, but not to motility.

Despite this directionality of global displacement on "jelly" agar surfaces, we notice from Figure 69(a) and (b) that, in both cases, bacteria move in every direction with narrow variation in vectors norms (displacement length).

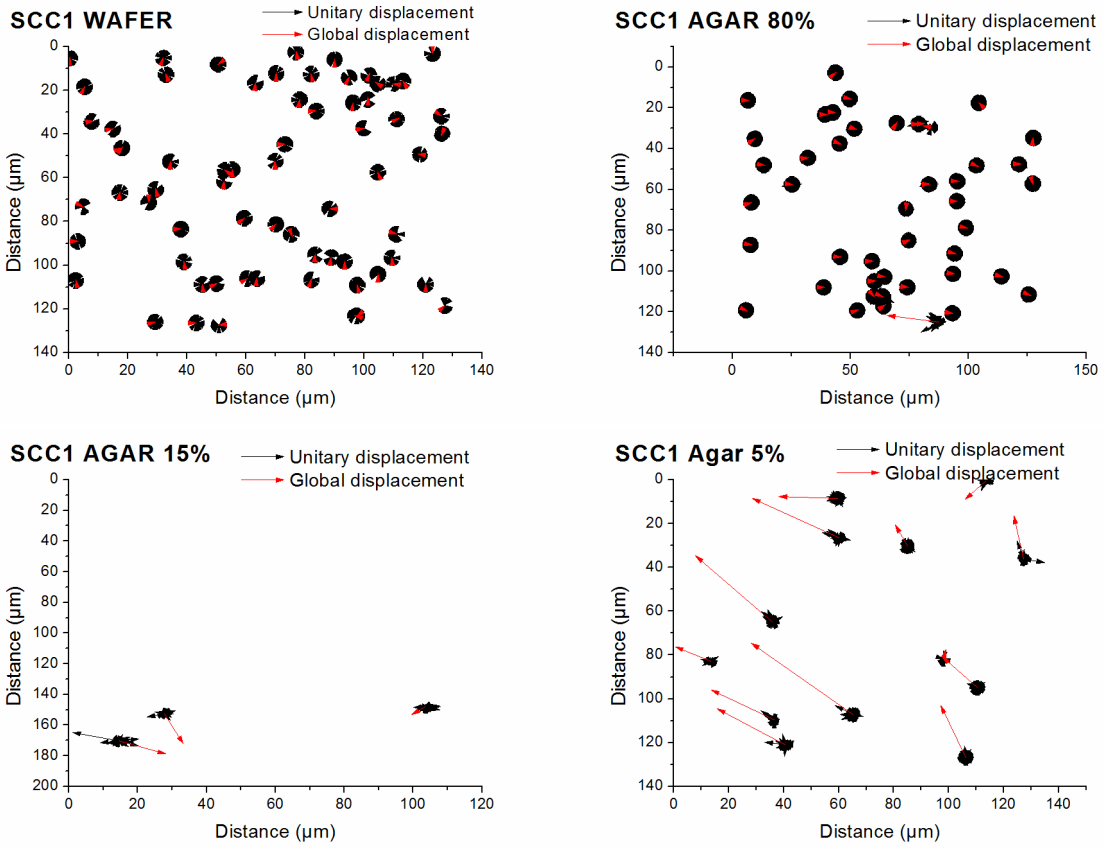


Figure 68 : Vectorial representation of SCC1 bacterial displacement on (a) silicon wafer, (b) agar 80 g/L (c) agar 15 g/L and (d) agar 5 g/l. Black arrows represent unitary displacement vectors normalized to the original bacterial position, representing bacterial displacement every two seconds. Red arrows represent global displacement vectors corresponding to the global displacement of the bacteria measured at the end of the experiment.

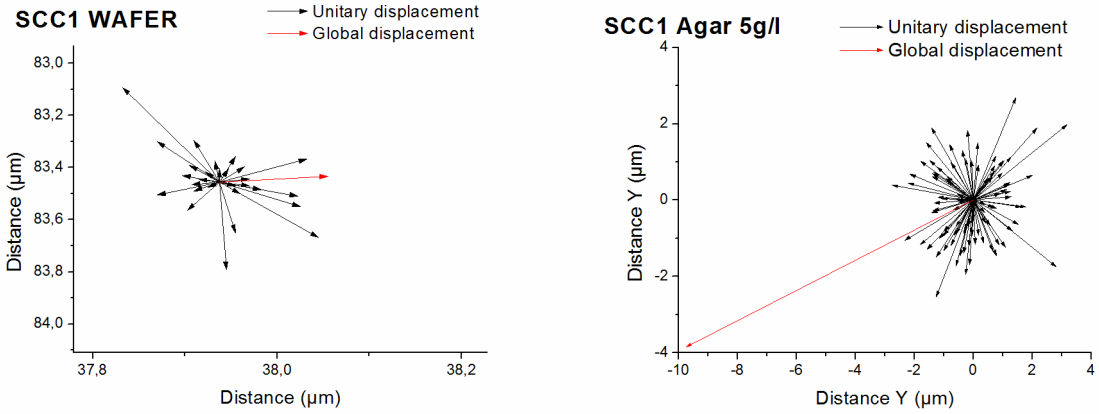


Figure 69: Vectorial representation of one SCC1 bacterium displacement representative for each bacterial displacement on (a) silicon wafer, (b) agar 5 g/l. Black arrows represent vectors normalized to the original bacterial position, representing bacterial displacement every two seconds. Red arrows represent sum vectors corresponding to the global displacement of the bacterium measured at the end of the experiment.

We quantified bacterial displacement speed on 5, 15, 80g/L agar and on silicon wafer. Results are presented in Figure 70(a), in which we included the value similarly measured for bacteria adhered on a vesicles “smooth”

surface but determined in flow condition. In this figure, we clearly observe decreasing bacterial motility while agar concentration increases. We can assume a decrease in bacterial motility linked with a surface stiffness increase, which however seems not to be quantitative. Moreover, the comparison of motility speed on vesicles "smooth" hybridized vesicles surface with motility speed on agar and silicon wafer place this surface between 80g/L agar and silicon wafer but with a high standard deviation. As we explained above the deviation is due to the presence of two populations: The sessile population with a behavior close to behavior on wafer (low motility) and the motile population with a motility level in between observable one for agar 15 g/L and agar 80 g/L as we can observed in Figure 70(b).

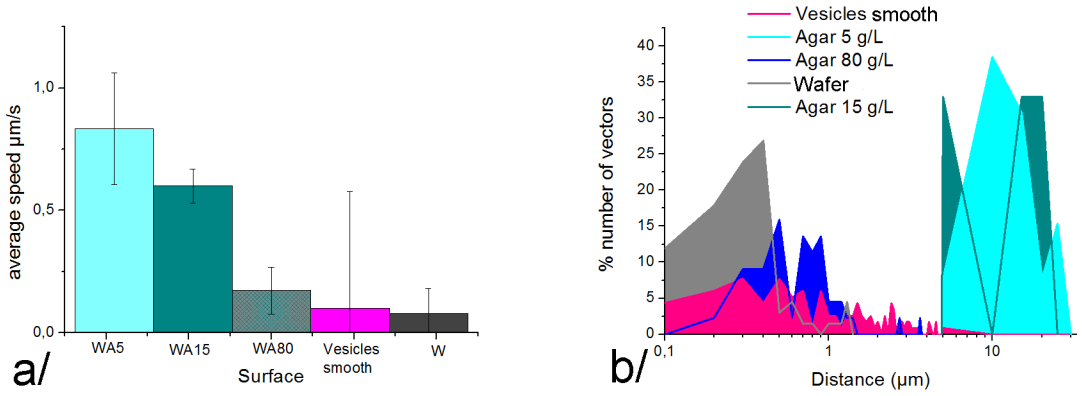


Figure 70: (a) displacement speed of SCC1 bacteria onto surfaces prepared with different concentrations of agar, on the vesicles "smooth" surface from experiment under flow and on silicon wafer. (b) Comparison of vectors norms dispersion (distance in µm) in per cent to total number of vectors for each surfaces: surfaces prepared with different concentrations of agar, the vesicles "smooth" surface from experiment under flow and silicon wafer.

D.5 Curli expression study

We quantified the number of bacteria expressing curli during the adhesion process. For this purpose, we used the curli *gfp* fusion bacterial strain (PHL1273) which fluoresces upon bacterial curli expression. The total number of bacteria expressing curli gene was evaluated, during the entire adhesion and biofilm formation, per square centimeter on A5G7 LD surfaces, non-hybridized vesicles and internal control. Results are presented in Figure 71(a). The relative numbers of expressive cells in percent per micrograph (relative to total number of adherent cells normalized to internal control) were also compared (see Figure 71(b)) for A5G7 LD surfaces, non-hybridized vesicles surfaces, A5G7 HD and C7T5 HD surfaces, and internal control. These evaluations could not be performed for hybridized vesicle surfaces, due to the low number of adherent bacteria.

Comparing the absolute value of curli expressing bacteria as in the Figure 71(a), to the corresponding total number of adherent bacteria of Figure 52(a), we notice that at the adhesion step (1 h, 2 h and 4 h) only a few bacteria are expressing their curli, while at 24 h and higher incubation time, all of the adherent bacteria expressed their curli. This shows that, as expected, curli were produced mainly at late stages of biofilm formation, probably for strengthening biofilm structures as already reported in the literature [104].

In Figure 71(a), we also notice the difference in curli expression between A5G7 LD surfaces and non-hybridized vesicles surfaces compared to internal control, on which a lower number of bacteria expressed curli gene at 1 h, 2 h and 4 h incubation. The strongest significant difference in curli gene expression compared to internal control was observed at 2 h and 4 h, while incubation at 1 h did not display any significant variation in curli expression. Interestingly, this effect was not observable at 24 h and higher incubation time, for which curli expression is similar between all of the three surfaces. Focusing on 2 h of incubation , the relative number of expressing bacteria (relative to total number) for all oligonucleotide surfaces, expressed in percent of expressive cells and normalized to internal control, were compared for all of the oligonucleotide surfaces, as presented in Figure 71(b). This figure shows the result of the curli expression of bacteria adhered on the A5G7 HD surface, C7T5 HD surface, A5G7 LD surface and non-hybridized vesicles surface compared to internal control, at 2 h of incubation with the curli *gfp* fusion bacterial strain (PHL1273). We first observe significant ($p > 99.95\%$) over-expression of curli on "low density" oligonucleotides surfaces (A5G7 LD and non-hybridized vesicles) compared to internal control. A similar curli over-expression exists when comparing both "high density" oligonucleotide surfaces, i.e. A5G7 HD and C7T5 HD, with internal control, but the significance of the difference is reduced to 99.5%. This observation demonstrates that the observed over-expression of curli gene on oligonucleotide surfaces is not strictly strand specific since it does not vary if we use either one oligonucleotide strand or its complementary strand (opposite nucleo-base).

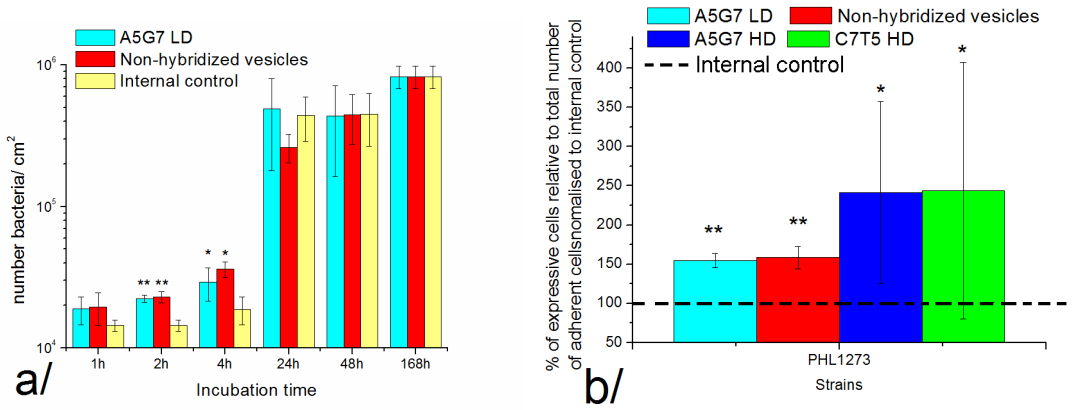


Figure 71: (a) number of bacteria expressing curli per square centimeter onto A5G7 LD (light blue) and non-hybridized vesicles (red) compared to internal control (yellow) at different incubation time from 1 to 168 h. Stars-marks highlight significant variation according to the Student t test. "**" stands for significance > 99.995 and "*" stand for significance >99.5, both compared to internal control. (b): Relative number of expressive cells (relative to total number of adherent cells), normalized to internal control, at 2 h of incubation on A5G7 LD, non-hybridized vesicles, A5G7 HD and C7T5 HD compared to internal control (set to 100%). All bars display standard deviations. Stars-marks highlight significant variation according to the Student t test. "*" stand for significance >99.5 compared to internal control.

E. *Discussion.*

In the Part I, we described the production and the characterization of antimicrobial surfaces made by nanoreactors self-assembled from oligonucleotide amphiphiles. The choice of oligonucleotide polymer was based on interest it has received as a polymer that is able to form vesicles as well as specific interactions such as hybridization. Considering that the polymer will be used as a support for bacterial adhesion, the influence of oligonucleotides immobilized on surfaces on bacterial adhesion and growth needs to be studied. In particular, oligonucleotide-based surfaces are expected to offer potential specific binding sites for bacteria, through fimbriae and other membrane receptors. They may also offer favorable or unfavorable physical-chemical properties for non-specific bacterial adhesion.

Furthermore, extracting the separate contribution of topographical, chemical and mechanical properties of surfaces on bacterial adhesion is difficult even on model surfaces. Most of the publications in this field display surfaces with more than one factor varying at the same time, such as, for example, charge and roughness [39,105,106], or chemistry and topography [107]. Authors generally attempt to separate the different effects by applying multiple linear regression analysis [108]. Ideal strategy should be to independently vary the surface properties corresponding to these factors. In our work, the versatility of the surface preparation allows such an approach. Aside from creating drug delivery system, our surfaces were originally designed for studying topography effect independently to other factors. Nevertheless, surface chemistry, mechanical properties and even, in some extend, surface charge could be varied independently. However, systematic independent variation could not be performed and would require further modifications of surface preparation for this purpose. In particular, the complete elucidation of the independent influence of these factors needs further works that will be discussed in the outlook section.

According to the results obtained, we will here discuss the surface toxicity in the supernatant, the influence of surface chemistry and surface charge on bacterial adhesion and curli expression, before discussing the influence of surface topography. Finally, we will focus on the influence of the mechanical properties, which is the most significant result of the biological part of this work.

E.1 Surface toxicity.

The experiment performed in Part II section D.1 is not a classical toxicity experiment, since a classical toxicity experiment would have been conducted by comparing the growth of the supernatant on the surface of interest with the growth of the supernatant on a control surface and with a toxic surface/agent (with different toxicity levels) [109]. Our experiment consisted in simply comparing the surface of interest (oligonucleotide, vesicles) and internal control (wafer or glass), allowing to highlight presence or absence of toxicity. From the results, it is clear that the type of surface used in this study did not influence the growth in the supernatant. This

observation leads to the conclusion that all effects further observed at the substrate surface cannot be attributed to growth variation and are due to surface properties.

E.2 Influence of surface chemistry and surface charge.

As evoked above, oligonucleotides are likely to influence bacterial adhesion due to their physical-chemical properties (charge and hydrophilicity) and due to their biomolecular nature. In this part, we will therefore discuss the role of oligonucleotide strand type and density on bacterial adhesion. Furthermore, *E.coli* bacteria possess fimbriae that are likely to interact with the surface. Among them, curli are known to be involved in biofilm formation on both abiotic and biotic surfaces [79] and were already shown to specifically interact with several proteins [85]. Therefore, curli are membrane structures likely to be involved in both specific and non-specific adhesion to surfaces presenting biomolecule-based polymers. For that reason, we have chosen to focus on curli for addressing the potential role of fimbriae in the bacterial response to our surface. We will here therefore discuss the curli production on the oligonucleotide-modified surfaces.

E.2.a Chemistry and charge effect on bacterial adhesion.

The study of the influence of surface chemistry and charge effect on bacterial adhesion was performed by studying influence of two different densities of oligonucleotides and studying influence of two different strands on bacterial adhesion. We compared a "low density" A_5G_7 oligonucleotide surface, two types of "high density" oligonucleotide surfaces (A_5G_7 and C_7T_5) with internal control. The results presented in Part II - D.2.b display an interesting effect: "Low density" of oligonucleotides does not influence bacterial adhesion while "high density" of oligonucleotides reduces the number of adherent bacteria compared to internal control.

In this experiment, we have the potential combination of two factors: The surface chemistry, (i.e. oligonucleotides) and the surface physical-chemical properties (i.e. mainly charges). These two factors are linked, since oligonucleotides display their biomolecular properties and chemical functions but also display surface physical properties, such as charges and hydrophilicity. Despite the weakness of the knowledge concerning the effect of immobilised oligonucleotides on bacterial adhesion, we expected that the chemical functionalities are favourable for adhesion of the bacterial strain used in this study, since oligonucleotides are known to be at least a source of nitrogen [70]. On the contrary, negative charges of the oligonucleotide molecules were expected to be unfavourable [20]. Based on these opposite effects, we propose that our results are due to a balanced effect between the favourable influence of surface chemical functionalities and the unfavourable influence of charge on bacterial adhesion. Then, in the case of "low density" oligonucleotide surfaces, the similar number of adherent bacteria on the oligonucleotide surfaces and on the internal control should be explained by the balance between the two effects, which should have led to a neutral influence of the oligonucleotide surface compared to internal control. In contrast, in the case of "high density" oligonucleotides, the influence of charge should have been

greater compared to the influence of chemistry, leading to a globally unfavourable influence of the surface for bacterial adhesion, and then to a decrease in the number of adherent cells compared to internal control.

In the experiment herein we could not vary charge density and surface chemical function independently, but we varied the oligonucleotide strand while conserving similar surface charge, by considering complementary oligonucleotides (A_5G_7 and C_7T_5). Comparing influences of A_5G_7 and C_7T_5 on adherent bacteria number, the results show clearly that both sequences display similar effects. This result demonstrates that the effect previously observed for A_5G_7 on curli expression cannot be specifically attributed to this sequence. Since a change in the oligonucleotide strand composition does not change the balance, this supports the idea that the predominant effect is due to the charge compared to chemistry.

We saw also (see Part II - D.2.c) that this balanced effect is not influenced by a variation of surface topography. In addition, the capability of bacteria to produce curli was shown not to influence this balance, since similar influences of oligonucleotide surfaces ("high density" and "low density") were reported for curli expressive and curli deficient strains (see Part II-D.2.a).

E.2.b Chemistry and charge effect on curli expression.

Before considering the influence of surface chemistry and charge on curli expression, two general observations concerning the role of curli in adhesion and biofilm growth on the surfaces used in this study should be noticed. In the results presented in Part II - D.5. we observed, on all three surfaces ("low density" oligonucleotide, non-hybridized vesicles and internal control) that the number of adherent curli deficient bacteria reached a maximum after 4 hours incubation time and decreased to a minimum value at 48 h, before regrowing. On the contrary curli expressive bacteria grew until 168 h, without decreasing after 4 h incubation as in the case above. The alternation of increasing and decreasing phases of curli deficient *E.coli* biofilm is likely due to growth and detachment events which cyclically should occur in relation to the structural cohesion of the biofilm. In the case of curli expressive bacteria, structural cohesion was secured by curli, whose importance for biofilm structure was already made clear [110]. Another role of curli in the biofilm formation, which is often emphasized, is that curli usually enhance the primary colonisation on abiotic surfaces [79]. Our observation did not confirm this assertion, since the number of adhering bacteria at 1 h incubation time was identical for both strains. However, the ability of bacteria to express curli seems to allow a more intense development of the biofilm (adherent bacteria number at 168 h is higher for curli expressive than for curli deficient strain) through consolidation of the biofilm structure (as discussed above). This is supported by the results obtained with bacteria strains fluorescing upon curli expression. Indeed we showed that only a few of the adherent cells were shown to express their curli gene at short incubation times (1, 2 and 4 h), while all cells expressed it at long incubation time. This confirms the

important role of curli in the structure formation within the biofilm, and also suggests that curli are not predominantly involved in the primary phase of bacterial attachment to surfaces.

Curli are known to be involved in some interactions between bacteria and biomolecules [111]. In addition, as their expression is regulated by external factors such as osmolarity for example [112], bacterial curli expression is likely to be affected by oligonucleotide surfaces. The results of Part II - D.5. addressed the question of possible modification of bacterial curli gene expression on immobilized "low density" oligonucleotides. We observed significant differences between the number of curli-expressing cells on oligonucleotide-modified surfaces (smooth and nanostructured) and on internal control at short incubation times. This result shows that oligonucleotides grafted surfaces induce an over-expression of curli compared to internal control. This over-expression, according to the results obtained upon cell counting, cannot be related to higher attachment, but rather to a favorable recognition of the surface by the cell, since the surface chemistry and charge balance were shown to have a neutral influence on the number of adherent bacteria in the case of the "low density" oligonucleotide (A_5G_7). In the case of "high density" oligonucleotide surfaces, this slight over-expression of curli seems to be disturbed by the influence of the surface charge leading to a high deviation and a decrease of significance for the variation (99.995 to 99.5% of significance). We hypothesize that the oligonucleotide influence on curli over-expression can be screened by the influence of charges. This hypothesis correlates with a balanced influenced between surface chemistry and charges. Then, in the case of "low density" oligonucleotide, the negative charge influences balanced by positive influence of oligonucleotide chemical functionalities may not influence the adhesion but may induce curli over-expression. In the case of "high density" oligonucleotide and high charge influences, oligonucleotide chemical functionalities influences on curli expression may be disturbed and screened by the stronger repulsive influence of charges on the number of adherent bacteria, leading to a visibly weaker effect of oligonucleotide chemical functionalities on curli gene over-expression.

The discussion above is based on the hypothesis that curli are able to interact with the immobilized oligonucleotides, allowing bacteria to attach to the surface despite the negative charges which should, to the contrary, prevent their adhesion as shown and reported by other authors [113]. This is supported by the evidence that curli are able to specifically bind several biomolecules, proteins in particular [114], and that other pili-type organelles present specific ability to interact with DNA, sometimes without sequence specificity (except a preference for pyrimidine bases) [77]. A similar mechanism may be involved in our case: Bacterial cells may over-express their curli for increasing the binding to the oligonucleotides present on this type of surfaces. However, the domain of oligonucleotides that may be recognized by curli is not clear. Two main sites could have binding properties for the curli: The oligonucleotide bases and the sugar backbone. Analogy with pili type IV [77] which recognizes oligonucleotide bases, or with pili type I of *E.coli*, which can bind D-mannose [115], suggests

that, at this stage, both moieties can be considered as binding sites for *E.coli* curli on oligonucleotides. Comparing the influences of A_5G_7 and C_7T_5 on curli gene expression, both sequences display a similar effect. This demonstrates that the effect previously discussed for A_5G_7 on curli expression cannot be specifically attributed to this sequence and excludes the oligonucleotide bases as a specific binding site for curli.

No definitive conclusion can be drawn, on a general point of view, about the specific or non-specific nature of the bacterial response, due to the small number of oligonucleotide sequences tested. However, the tested oligonucleotide sequences were made of particular orders of only two bases, which probably do not correspond to natural sequences. This supports again the idea that the bacterial response by over-expressing the gene for curli production is the result of non-specific bacteria/surface interactions in the present study.

E.3 Influence of surface topography.

The influence of the surface topography on bacterial adhesion can be split into two different studies, the topography variation on stiff surfaces and the topography variation on surfaces with visco-elastic properties. In both cases we observed a variation in the roughness at the nanoscale level (around 10 nm) and a variation of the topographical features.

In the case of the topography variation on stiff oligonucleotide surfaces, the variation of roughness (5nm) is associated with the variation of topographical features (topographical features of 100nm high spaced out from around 1 µm). The number of bacterial cells adhered to each surface was evaluated for three different strains, all able to produce exopolysaccharides but differing in the production of curli. In the results Part II - D.2.c, no significant difference in the number of adhering cells on the surface was observed for the three strains. This indicates that, with or without curli, the bacterial adhesion was not affected by the topography and the roughness of the surfaces in term of the number of adherent bacteria, this suggests also that curli are not involved in the recognition of the topographical features on the surface. Obviously, the mean roughness may have been too low to affect bacterial adhesion. The low coverage of the surface by vesicles can also be suspected. Indeed, considering a bacterial area of 0.5 μm^2, the topographical feature of the nanostructured surface led to an average of one vesicle for two bacteria. However, we believe that, through the use of fimbriae like curli, bacteria should be able to respond to topographical feature at the nanoscale, but that the topographical features and the mean roughness factor have been too low to affect the adhesion of *E.coli*.

In the case of the oligonucleotide surfaces with mechanical visco-elastic properties, the variation of topography is performed by changing the deposition of vesicles. The roughness was different at the nanoscale, (Ra= 3 ± 2 nm for vesicles “smooth” surface and 20nm ± 2 nm for vesicles “rough” surfaces, and difference in topography could be observed upon micrometer observation (light microscopy), leading to “visibly rough” and “visibly smooth” structures on vesicles “rough” surface and vesicles “smooth” surface respectively, as we

illustrated in Part I - Chapter 3. The bacterial adhesion to these two different surfaces was studied in Part II - D.5. The results presented in Figure 58(b) clearly show that the anti-adhesive effect observed on the vesicles-based surfaces is independent of the topography used, since both topographies present the same anti-adhesive effect without significant differences. This result is not surprising, since we showed that similar roughness on stiff surfaces did not influence bacterial adhesion and curli expression in similar static culture conditions.

Interestingly, the observation of bacterial adhesion on the two types of hybridized vesicle coated surfaces in the dynamic conditions (Part II - D3) highlighted a lower number of adherent cells on vesicles "rough" surfaces compared to vesicles "smooth" surfaces at early stage of adhesion. The origin of this difference is not clear. We hypothesize an influence of the surface preparation process. Vesicles "smooth" surfaces were prepared outside the chamber and rinsed thoroughly after deposition, leading to a surface coated with vesicles as a "monolayer". This layer of vesicles is not a perfect monolayer, as discussed in Part I - Chapter3, and certainly presents some defects (collapsed vesicles or detached vesicles) as illustrated in Figure 72. These defects should act as stiff places to which bacteria may be able to adhere. In the other hand, vesicles "rough" surfaces were prepared *in situ*, rinsed by peristaltic flow (milder rinsing compared to vesicles "smooth" surface rinsing process), and consisted in vesicle multilayers, decreasing the chance of providing a stiff place on the surface by the formation of a layer defect. Considering the effect, discussed in the next section, of the mechanical properties of the surface on bacterial adhesion, defects providing stiff position may enhance bacteria adhesion on soft surfaces.

Despite this difference in the initial number of adherent cells, no influence of the topography on further adhesion or on the detachment rate could be seen. Nevertheless, observing the video of the dynamic experiments, we could see a non-quantifiable (due to low number of bacteria observable) influence of the roughness on "visibly rough" hybridized vesicles surfaces, which seems to prevent release into the flow, as fast as in the case of vesicles "smooth" surfaces. This is probably due to the micrometer scale aggregates which may have offered protection against flow for the bacteria.

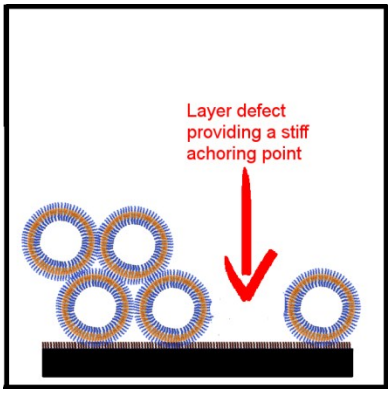


Figure 72: scheme of vesicle layer possessing a defect, which provides a mechanically stiff position, which may enhanced bacterial adhesion compared to surfaces perfectly coated with vesicles.

Finally, we demonstrated in this study that the nanoscale topography used herein does not influence bacterial adhesion, curli expression or biofilm growth. In addition, the other effects highlighted in this study (oligonucleotide influence on curli expression and anti-adhesive effect of hybridized vesicular surfaces) were independent to the topography used. However, we believe that nanoscale topography may influence bacterial adhesion, especially in the case of bacterial expression of fimbriae-like curli. In that case, nanotopography could act as anchorage point for fimbriae adhesion. However we demonstrated herein that this effect does not exist for the adhesion to our vesicle-coated surfaces. A systematic variation of topography on mechanically stiff surfaces should permit the elucidation of this effect and would be of interest for future work.

E.4 Influence of surface mechanical properties on bacterial adhesion and motility.

In Part II - D.2.d, we observed a strong influence of vesicle coated surfaces on the number of adherent bacteria, which was reduced by a factor 20-fold compared to the number of cells counted on internal control and a factor of 10-fold compared to "high density" oligonucleotide modified surfaces. This strong antibacterial effect of vesicle-modified surfaces was not due to the surface chemistry, which was similar for both oligonucleotide- and vesicle-modified surfaces. As discussed above, this effect was also not due to the topography. Finally, planktonic bacteria were shown to grow normally, proving that the antibacterial effect of the vesicle-modified surfaces was not due to a toxic effect but rather an anti-adhesive effect.

We attribute this anti-adhesive effect of vesicle based surfaces to visco-elastic properties of the vesicles. This is supported by the bacterial adhesion results on cross-linked vesicles (i.e. stiff) which were similar to the adhesion on glass and oligonucleotides, as presented in Part II - D.2.d. In addition, the visco-elastic properties of hybridized vesicles surfaces were discussed in Part I - Chapter 3, in which we showed from QCM-D that the deposited layer possessed a high shear modulus and low viscosity (respectively 6.10^5 Pa and 0.0038 kg/m^2). This behavior was consistent with the literature, since vesicles based on diblock polymers with hydrophobic blocks that possess low glass transition are known to have a membrane with fluid properties [116]. In the other hand, we emphasized in the State of the art the weakness of the literature regarding the influence of surface mechanical properties on bacterial adhesion. In this literature a few authors, such as Bakker [117] and Lichter [59], discussed the mechanical influence of the surface that they linked to the elastic modulus of the surface. However, they always neglected the viscous component of the layer. We thought that surfaces mechanical properties should not only be described with a simple elastic modulus. Surfaces mechanical properties should be described at least by the two elastic and viscous moduli. This last one is crucial since the viscosity of the layer is related to interfacial properties as discussed in the State of the art. Neglecting either the viscous part or the elastic part of the visco-elastic properties of the coated surface should lead to a misunderstanding of the process involved.

To understand the process involved in the anti-adhesive effect, we followed bacterial adhesion and detachment during early adhesion and biofilm formation under flow on silicon wafers and vesicle-modified surfaces. We showed that the number of adherent cells is similar between vesicles-based surfaces, “high density” oligonucleotide surfaces and silicon wafer, but a higher number of cells detached from the surface in the case of vesicles based surfaces. This effect was visible during the entire experiment. Bacteria were not repelled by the surface (they still came to adhere on the surface) and they were not killed (no toxic effect) but their binding to the surface seemed to be weak and reversible for the majority of them. Therefore, we hypothesize that bacteria arrived normally on the surface due to their swimming in the medium and physical-chemical interactions, then started the adhesion process, but that the visco-elastic behavior of the vesicles coated surfaces did not offer the necessary anchoring properties to allow bacteria to adhere “irreversibly”. Then the majority of the bacteria left the surface. The few bacteria staying on it may have found a defect on the vesicle coating or other possible anchoring points. This hypothesis would explain the difference in the initial adhesion between vesicles “smooth” and vesicles “rough” surfaces under flow, since efficient defects (i.e. location without any vesicles) are expected to be in higher number on vesicles “smooth” surfaces than on vesicles “rough” surfaces ones. This hypothesis is reinforced by the two populations observable on the vesicles “smooth” surfaces under flow conditions, as illustrated in Figure 62: The sessile population may have found anchoring point to adhere, while the motile population did not.

In order to test this hypothesis on different type of surfaces with various visco-elastic properties, we conducted the preliminary study presented in Part II – D.4. In this study, we used a model surface often used as a fluid-like surface in microbiology, i.e. agar hydrogels. The mechanical properties depend on the agar concentration [118,119], allowing us to obtain different levels of visco-elasticity. Those surfaces were already used in motility studies of bacteria on surfaces. For example, some investigations demonstrated that the agar concentration is likely to influence various type of motility (swarming, sliding, gliding) [93,94,120]. On the contrary to those studies, which were conducted at the air-agar interface with nutrient in the agar layer, experiments at the liquid-agar interface without nutrient in the agar layer, like in our case, were never performed to study bacteria adhesion and motility. Moreover, analysis of bacterial motility by quantitative vectorial representation was never performed.

After cultivation of bacteria on coatings of different agar concentrations in liquid medium containing nutrient, followed by differed time series observation under confocal microscopy, results demonstrated that agar “jelly” surfaces were anti-adhesive, while agar “stiff” surfaces displayed normal adhesion compared to silicon wafer surfaces. This confirmed the anti-adhesive influence of visco-elastic properties. However, no trend of increasing number of bacteria with increasing surface stiffness was observed. This can be attributed to the difficulties in reproducing the agar surfaces with the protocol that we used, but also to a potential level effect:

below a certain value of visco-elastic properties, bacterial adhesion may be prevented, while above this value, bacteria may adhere normally.

High motility of bacteria was shown on "jelly" surfaces while low motility was observed on "stiff" surfaces (Figure 68). The motility was not a collective effect but inherent to each single cell. It was not limited to certain areas, and it seemed to be random. This motility was quantified (Figure 70(a)), and we observed that increased motility speed correlated with the decrease of qualitative surface stiffness. The faster motility was shown on 5g/L agar surface at 0.83±0.22µm/s. This value, in combination with the nature of the surface (non-stiff surfaces), is consistent with a sliding motion and supports the idea of an important role of the mechanical properties on the motility we observed. The hypothesis is thus that the low stiffness of agar surfaces induced a sliding motion, i.e. passive translocation, of *E.coli K12* SCC1.

Although, some obvious differences exist between the vesicles and agar surfaces types, these experiments provide therefore a new evidence of the role of surface visco-elastic properties on adherent bacteria behavior. Even if the exact process is not elucidated yet, surface with visco-elastic behavior seems not to offer anchoring points for bacterial "irreversible" adhesion, inducing a bacterial sliding motility for *E.coli*. This further motility should be at the origin of the high detachment rate observed in dynamic culture condition on vesicles based surfaces.

How bacteria should be able to sense the visco-elastic properties of the surfaces was not explored in this work. However, some hypothesis can be risked, in particular on the basis of the work of C.Dorel [63] or K.Otto [64] on surface sensing by bacteria. In the lecture "Perception des surfaces" at the Ecole Thématique du CNRS "Microbiologie et physico-chimie des biofilms" (Vittel, Octobre 2009), C. Dorel highlighted the influence of the substrate to induce biofilm formation by activation of the CpX/NIpE signaling pathway of bacteria. This pathway was demonstrated to be involved in the bacterial capacity to sense stresses with the outer membrane [64]. These stresses can be detected by different sensors. An example is given by osmotic variation which can be detected by a mechanosensitive channel [11,65,66]. An another example is mechanical stimuli that can be detected by NIpE, a membrane lipoprotein of gram negative, responding to membrane stress [67]. Even if no studies directly highlighted the role of surface visco-elastic properties on inducing the CpX signaling pathway, both the sensing of the osmotic variation by the mechano-sensitive channel or by the sensing of mechanical stimulus by NIpE, involve the surface visco-elastic properties. A stiff surface induces a high change in local osmolarity due to surface charges present on the surfaces and therefore a high stress on bacterial membranes during the adhesion process can be created. In the other hand, fluid-like surface (visco-elastic with highly viscous behavior) displays a smaller influence on bacterial membrane stress and weak influence on local osmolarity due to the possible diffusion of charges at the interfaces during the adhesion process. As a consequence, a stiff surface may stimulate sensors of CpX signaling, inducing biofilm formation, while a fluid-like surface may not activate CpX signaling

leading to the prevention of biofilm formation by bacteria. Other signaling pathways for surface sensing, that were highlighted in literature, may also be involved in the case of both agar and vesicles surfaces. For example flagella rotation will be blocked by contact of the bacteria with surfaces, inducing either biofilm formation or community mobility (swarming bacteria community like *Vibrio*) [68]. A second example is the surface wetness detected by flagella through up/down-regulation upon flagella polymerization at wet/non wet interfaces [12] (*E.coli and Salmonella typhimurium*) leading to either motility or adhesion on surfaces.

Finally, we demonstrated that surface visco-elastic properties can strongly influence the behavior of bacteria on surfaces. We believe that providing stiff properties to the surface will allow bacteria to sense a surface suitable for biofilm formation. On the other hand, providing fluid-like properties to the surface (visco-elastic properties) should not allow bacteria to sense the surface as favorable for adhesion, preventing "irreversible" adhesion. Due to the avoiding of "irreversible" adhesion, bacteria should remain highly motile at the interface, finally detaching from the surface, leading to the antiadhesive properties of the vesicles layer. Obviously, to further understand this effect, a study with systematic variation of surface elasticity and viscosity is now necessary and will be of interest for future work. Moreover, in the hypothesis of bacterial surface sensing ability of mechanical properties, the investigation of the stimuli and signaling pathways involved by variation of surface visco-elasticity to induce or not biofilm formation would be obviously of high interest. Particular attention to CpX signaling and flagella blocking by surfaces would be a pertinent way to follow.

F. *Conclusion.*

In this part II, we aimed at understanding the influence of surfaces based on vesicle coating on bacterial adhesion and biofilm formation. For this purpose we used the different surfaces designed in Part I to vary the surface properties of the independently from each other, in order to elucidate each factor's influences on bacterial adhesion.

We studied the influence of the oligonucleotide moiety on bacterial adhesion independently of other factors. Nevertheless, the oligonucleotide grafting density could not be discorrelated from the charge density. We showed that high density of grafted oligonucleotides decreases the number of observable adherent cells, whereas a low density of surface tethered oligonucleotide does not induce any observable effect. We hypothesize a balanced effect between electrostatic repulsion of the negatively charged cell membrane by the negative charges along the oligonucleotide backbone, and a bacterial recognition of the biological/chemical cues present on the surface favoring bacterial adhesion. Surface tethered nucleotide sequences were also shown to influence curli expression independently to other factors. But the weakness of the effect could be influenced by grafting density of nucleotide sequences.

Oligonucleotide vesicles based surfaces possess sub-micrometer scale topography which was likely to influence bacterial adhesion. However, no significant effect was detected in this study, neither on adherent bacteria amount nor on curli expression. Nevertheless, our study suggests that, if sub-micrometer topography is able to influence bacterial adhesion, this effect is weaker than the influence of oligonucleotide charge, chemistry, and fluid visco-elastic properties of vesicles based surfaces. To further discuss the influence of topography onto bacterial adhesion, a study with systematic variation of topography amplitude and organization on more biologically inert surfaces would be necessary.

Finally we demonstrated a strong influence of vesicles-based surfaces and we attributed this effect to the visco-elastic properties of the coating. We hypothesize that the observable decrease in the number of adherent bacteria on a surface coated with non-crosslinked vesicles is due to the reduced number of anchoring points on the surface leading to higher motility of some of the bacteria, then allowing a higher detachment rate from the surface for finally reducing the number of irreversibly attached bacteria. We similarly highlighted an influence of coating mechanical properties to induce motility and to reduce number of adherent bacteria with a preliminary study on agar coated surfaces. However, the process involved remains unclear and investigation on that purpose would lead to important findings for application in antiadhesive and anti-biofouling coating.

With this study, we highlighted the independent influence of oligonucleotides, topography and mechanical properties of vesicle-based surfaces on bacterial adhesion, curli expression and biofilm growth. We hypothesized a mechanism to explain each influencing factor and we demonstrated their combination as either enhancing or counteracting each other, leading to the global properties of the surface. The present study provides therefore the needed bases for further investigations of bacterial adhesion and biofilm growth on either oligonucleotide modified-surfaces or surfaces with various visco-elastic properties. New studies varying the nucleotide sequences, the size of the vesicles and the surface coverage is needed for deeper elucidation bacteria-surface interactions. In the same way, investigations of the effect of surface visco-elastic properties on bacterial adhesion and biofilm formation with a special focus on CpX signalling and flagella blocking are of interest to elucidate bacterial internal response to surface mechanical properties.

G. *References.*

[1] W.J. Loesche, Role of Streptococcus mutans in human dental decay., Microbiol. Mol. Biol. Rev. 50 (1986) 353-380.

[2] E. van der Wende, W. Characklis, D. Smith, Biofilms and bacterial drinking water quality, Water Research. 23 (1989) 1313-1322.

[3] H. Rijnaarts, DLVO and steric contributions to bacterial deposition in media of different ionic strengths, Colloids and Surfaces B: Biointerfaces. 14 (1999) 179-195.

[4] S. Bayoudh, A. Othmane, L. Mora, H. Ben Ouada, Assessing bacterial adhesion using DLVO and XDLVO theories and the jet impingement technique, Colloids and Surfaces B: Biointerfaces. 73 (2009) 1-9.

[5] X. Liu, G. Sheng, H. Yu, DLVO Approach to the Flocculability of a Photosynthetic H2 -Producing Bacterium, Rhodopseudomonas acidophila, Environ. Sci. Technol. 41 (2007) 4620-4625.

[6] N.P. Boks, W. Norde, H.C. van der Mei, H.J. Busscher, Forces involved in bacterial adhesion to hydrophilic and hydrophobic surfaces, Microbiology. 154 (2008) 3122-3133.

[7] M. Hermansson, The DLVO theory in microbial adhesion, Colloids and Surfaces B: Biointerfaces. 14 (1999) 105-119.

[8] L. Ponsonnet, M. Boureanu, N. Jaffrezic, A. Othmane, C. Dorel, P. Lejeune, Local pH variation as an initial step in bacterial surface-sensing and biofilm formation, Materials Science and Engineering: C. 28 (2008) 896-900.

[9] C. Dorel, P. Lejeune, A. Rodrigue, The Cpx system of Escherichia coli, a strategic signaling pathway for confronting adverse conditions and for settling biofilm communities?, Research in Microbiology. 157 (2006) 306-314.

[10] K. Otto, T.J. Silhavy, Surface sensing and adhesion of Escherichia coli controlled by the Cpx-signaling pathway, Proceedings of the National Academy of Sciences of the United States of America. 99 (2002) 2287-2292.

[11] I.R. Booth, M.D. Edwards, S. Black, U. Schumann, S. Miller, Mechanosensitive channels in bacteria: signs of closure?, Nat Rev Micro. 5 (2007) 431-440.

[12] Q. Wang, A. Suzuki, S. Mariconda, S. Porwollik, R.M. Harshey, Sensing wetness: a new role for the bacterial flagellum, Embo J. 24 (2005) 2034-2042.

[13] H. Flemming, T.R. Neu, D.J. Wozniak, The EPS Matrix: The "House of Biofilm Cells", Journal of Bacteriology. 189 (2007) 7945-7947.

[14] C. Fux, J. Costerton, P. Stewart, P. Stoodley, Survival strategies of infectious biofilms, Trends in Microbiology. 13 (2005) 34-40.

[15] I. Beech, Biocorrosion: towards understanding interactions between biofilms and metals, Current Opinion in Biotechnology. 15 (2004) 181-186.

[16] C.D. Nadell, J.B. Xavier, S.A. Levin, K.R. Foster, The Evolution of Quorum Sensing in Bacterial Biofilms, Plos Biol. 6 (2008) e14.

[17] S. Molin, Gene transfer occurs with enhanced efficiency in biofilms and induces enhanced stabilisation of the biofilm structure, Current Opinion in Biotechnology. 14 (2003) 255-261.

[18] K. Lewis, Persister cells and the riddle of biofilm survival, Biochemistry Mosc. 70 (2005) 267-274.

[19] J.B. Kaplan, M.F. Meyenhofer, D.H. Fine, Biofilm Growth and Detachment of Actinobacillus actinomycetemcomitans, J. Bacteriol. 185 (2003) 1399-1404.

[20] L. Ploux, K. Anselme, A. Ponche, Bacteria/material interfaces: role of the material and cell wall properties, J Adhes Sci Technol. in press (2010).

[21] R. Bos, Physico-chemistry of initial microbial adhesive interactions – its mechanisms and methods for study, FEMS Microbiology Reviews. 23 (1999) 179-229.

[22] D.R. Absolom, F.V. Lamberti, Z. Policova, W. Zingg, C.J. van Oss, A.W. Neumann, Surface thermodynamics of bacterial adhesion, Appl. Environ. Microbiol. 46 (1983) 90-97.

[23] Y. Ong, A. Razatos, G. Georgiou, M.M. Sharma, Adhesion Forces between E. coli Bacteria and Biomaterial Surfaces, Langmuir. 15 (1999) 2719-2725.

[24] G. Bruinsma, Bacterial adhesion to surface hydrophilic and hydrophobic contact lenses, Biomaterials. 22 (2001) 3217-3224.

[25] A. Poortinga, Electric double layer interactions in bacterial adhesion to surfaces, Surface Science Reports. 47 (2002) 1-32.

[26] P. Lens, Biofilms in medicine, industry and environmental biotechnology : characteristics, analysis and control, IWA Pub.,

London, 2003.

[27] J. Li, L.A. McLandsborough, The effects of the surface charge and hydrophobicity of Escherichia coli on its adhesion to beef muscle, Int. J. Food Microbiol. 53 (1999) 185-193.

[28] J. Roberts, Inhibition and enhancement of microbial surface colonization: the role of silicate composition, Chemical Geology. 212 (2004) 313-327.

[29] A. Terada, A. Yuasa, T. Kushimoto, S. Tsuneda, A. Katakai, M. Tamada, Bacterial adhesion to and viability on positively charged polymer surfaces, Microbiology. 152 (2006) 3575-3583.

[30] X. Sheng, Y.P. Ting, S.O. Pehkonen, The influence of ionic strength, nutrients and pH on bacterial adhesion to metals, Journal of Colloid and Interface Science. 321 (2008) 256-264.

[31] B. Li, B.E. Logan, Bacterial adhesion to glass and metal-oxide surfaces, Colloids and Surfaces B: Biointerfaces. 36 (2004) 81-90.

[32] B. Gottenbos, D.W. Grijpma, H.C. van der Mei, J. Feijen, H.J. Busscher, Antimicrobial effects of positively charged surfaces on adhering Gram-positive and Gram-negative bacteria, J. Antimicrob. Chemother. 48 (2001) 7-13.

[33] A. Komaromy, R.I. Boysen, H. Zhang, I. McKinnon, F. Fulga, M.T. Hearn, Micro-structures modulate bacterial cell viability and attachment, Microelectronic Engineering. 86 1431-1434.

[34] C. Blumer, Regulation of type 1 fimbriae synthesis and biofilm formation by the transcriptional regulator LrhA of Escherichia coli, Microbiology. 151 (2005) 3287-3298.

[35] I.C. Scaletsky, M.L. Silva, L.R. Trabulsi, Distinctive patterns of adherence of enteropathogenic Escherichia coli to HeLa cells., Infect. Immun. 45 (1984) 534-536.

[36] K.A. Barth, G. Coullerez, L.M. Nilsson, R. Castelli, P.H. Seeberger, V. Vogel, An Engineered Mannoside Presenting Platform:Escherichia coli Adhesion under Static and Dynamic Conditions, Adv. Funct. Mater. 18 (2008) 1459-1469.

[37] A. Olsen, Identification of Two Protein-binding and Functional Regions of Curli, a Surface Organelle and Virulence Determinant of Escherichia coli, Journal of Biological Chemistry. 277 (2002) 34568-34572.

[38] Y. Liu, J. Strauss, T.A. Camesano, Adhesion forces between Staphylococcus epidermidis and surfaces bearing self-assembled monolayers in the presence of model proteins, Biomaterials. 29 (2008) 4374-4382.

[39] J. Strauss, Y. Liu, T.A. Camesano, Bacterial adhesion to protein-coated surfaces: An AFM and QCM-D study, Jom. 61 (2009) 71-74.

[40] L. Ploux, A. Ponche, K. Anselme, Bacteria/Material Interfaces: Role of the Material and Cell Wall Properties, J Adhes Sci Technol. 24 (2010) 2165-2201.

[41] K. Anselme, P. Davidson, A. Popa, M. Giazzon, M. Liley, L. Ploux, The interaction of cells and bacteria with surfaces structured at the nanometre scale, Acta Biomaterialia. 6 (2010) 3824-3846.

[42] W.G. Characklis, Bioengineering report: Fouling biofilm development: A process analysis, Biotechnol. Bioeng. 23 (1981) 1923-1960.

[43] G.M. Bruinsma, M. Rustema-Abbing, J. de Vries, B. Stegenga, H.C. van der Mei, M.L. van der Linden, Influence of Wear and Overwear on Surface Properties of Etafilcon A Contact Lenses and Adhesion of Pseudomonas aeruginosa, Investigative Ophthalmology & Visual Science. 43 (2002) 3646-3653.

[44] D.P. Bakker, H.J. Busscher, J. van Zanten, J. de Vries, J.W. Klijnstra, H.C. van der Mei, Multiple linear regression analysis of bacterial deposition to polyurethane coatings after conditioning film formation in the marine environment, Microbiology. 150 (2004) 1779-1784.

[45] N. Mitik-Dineva, J. Wang, V.K. Truong, P.R. Stoddart, F. Malherbe, R.J. Crawford, Differences in colonisation of five marine bacteria on two types of glass surfaces, Biofouling: The Journal of Bioadhesion and Biofilm Research. 25 (2009) 621 - 631.

[46] K.A. Whitehead, J. Colligon, J. Verran, Retention of microbial cells in substratum surface features of micrometer and sub-micrometer dimensions, Colloids and Surfaces B: Biointerfaces. 41 (2005) 129-138.

[47] D. Campoccia, L. Montanaro, H. Agheli, D.S. Sutherland, V. Pirini, M.E. Donati, Study of Staphylococcus aureus adhesion on a novel nanostructured surface by chemiluminometry., Int J Artif Organs. (2006) 622-629.

[48] C. Díaz, P.L. Schilardi, R.C. Salvarezza, M. Fernández Lorenzo de Mele, Nano/Microscale Order Affects the Early Stages of Biofilm Formation on Metal Surfaces, Langmuir. 23 (2007) 11206-11210.

[49] T.R. Scheuerman, A.K. Camper, M.A. Hamilton, Effects of Substratum Topography on Bacterial Adhesion, Journal of Colloid and Interface Science. 208 (1998) 23-33.

[50] K. Whitehead, J. Verran, The Effect of Surface Topography on the Retention of Microorganisms, Food and Bioproducts

Processing. 84 (2006) 253-259.

[51] S.H. Flint, J.D. Brooks, P.J. Bremer, Properties of the stainless steel substrate, influencing the adhesion of thermo-resistant streptococci, Journal of Food Engineering. 43 (2000) 235-242.

[52] K.J. Edwards, A.D. Rutenberg, Microbial response to surface microtopography: the role of metabolism in localized mineral dissolution, Chemical Geology. 180 (2001) 19-32.

[53] E. Medilanski, K. Kaufmann, L.Y. Wick, O. Wanner, H. Harms, Influence of the Surface Topography of Stainless Steel on Bacterial Adhesion, Biofouling: The Journal of Bioadhesion and Biofilm Research. 18 (2002) 193 - 203.

[54] L. Richert, A.J. Engler, D.E. Discher, C. Picart, Elasticity of Native and Cross-Linked Polyelectrolyte Multilayer Films, Biomacromolecules. 5 (2004) 1908-1916.

[55] M.T. Thompson, M.C. Berg, I.S. Tobias, M.F. Rubner, K.J. Van Vliet, Tuning compliance of nanoscale polyelectrolyte multilayers to modulate cell adhesion, Biomaterials. 26 (2005) 6836-6845.

[56] D.E. Discher, Tissue Cells Feel and Respond to the Stiffness of Their Substrate, Science. 310 (2005) 1139-1143.

[57] F. Rehfeldt, A. Engler, A. Eckhardt, F. Ahmed, D. Discher, Cell responses to the mechanochemical microenvironment—Implications for regenerative medicine and drug delivery, Advanced Drug Delivery Reviews. 59 (2007) 1329-1339.

[58] D.P. Bakker, F.M. Huijs, J. de Vries, J.W. Klijnstra, H.J. Busscher, H.C. van der Mei, Bacterial deposition to fluoridated and non-fluoridated polyurethane coatings with different elastic modulus and surface tension in a parallel plate and a stagnation point flow chamber, Colloids and Surfaces B: Biointerfaces. 32 (2003) 179-190.

[59] J.A. Lichter, M.T. Thompson, M. Delgadillo, T. Nishikawa, M.F. Rubner, K.J. Van Vliet, Substrata Mechanical Stiffness Can Regulate Adhesion of Viable Bacteria, Biomacromolecules. 9 (2008) 1571-1578.

[60] J.A. Lichter, M.F. Rubner, Polyelectrolyte Multilayers with Intrinsic Antimicrobial Functionality: The Importance of Mobile Polycations, Langmuir. 25 (2009) 7686-7694.

[61] P. Schaer-Zammaretti, Imaging of lactic acid bacteria with AFM—elasticity and adhesion maps and their relationship to biological and structural data, Ultramicroscopy. 97 (2003) 199-208.

[62] K. Otto, J. Norbeck, T. Larsson, K. Karlsson, M. Hermansson, Adhesion of Type 1-Fimbriated Escherichia coli to Abiotic Surfaces Leads to Altered Composition of Outer Membrane Proteins, J. Bacteriol. 183 (2001) 2445-2453.

[63] C. Prigent-Combaret, O. Vidal, C. Dorel, P. Lejeune, Abiotic surface sensing and biofilm-dependent regulation of gene expression in Escherichia coli, J. Bacteriol. 181 (1999) 5993-6002.

[64] K. Otto, Surface sensing and adhesion of Escherichia coli controlled by the Cpx-signaling pathway, Proceedings of the National Academy of Sciences. 99 (2002) 2287-2292.

[65] C.A. Kumamoto, Molecular mechanisms of mechanosensing and their roles in fungal contact sensing, Nat Rev Micro. 6 (2008) 667-673.

[66] L. Bianchi, Mechanotransduction: Touch and Feel at the Molecular Level as Modeled in Caenorhabditis elegans, Mol Neurobiol. 36 (2007) 254-271.

[67] G. Rowley, M. Spector, J. Kormanec, M. Roberts, Pushing the envelope: extracytoplasmic stress responses in bacterial pathogens, Nat Rev Micro. 4 (2006) 383-394.

[68] M. Alavi, R. Belas, [3] Surface sensing, swarmer cell differentiation, and biofilm development, dans: Microbial Growth in Biofilms - Part A: Developmental and Molecular Biological Aspects, Academic Press, 2001: p. 29-40.

[69] A. Spoering, M. Gilmore, Quorum sensing and DNA release in bacterial biofilms, Current Opinion in Microbiology. 9 (2006) 133-137.

[70] R.J. Redfield, Genes for Breakfast: The Have-Your-Cake and-Eat-It-Too of Bacterial Transformation, J Hered. 84 (1993) 400-404.

[71] R.J. Redfield, Opinion: Do bacteria have sex?, Nat Rev Genet. 2 (2001) 634-639.

[72] D. Dubnau, DNA uptake in bacteria, Annu. Rev. Microbiol. 53 (1999) 217-244.

[73] C.B. Whitchurch, Extracellular DNA Required for Bacterial Biofilm Formation, Science. 295 (2002) 1487-1487.

[74] I. Chen, D. Dubnau, DNA uptake during bacterial transformation, Nat Rev Micro. 2 (2004) 241-249.

[75] M. Bakkali, Genome Dynamics of Short Oligonucleotides: The Example of Bacterial DNA Uptake Enhancing Sequences, PLoS ONE. 2 (2007) e741.

[76] F.E. Aas, M. Wolfgang, S. Frye, S. Dunham, C. Lövold, M. Koomey, Competence for natural transformation in Neisseria

gonorrhoeae: components of DNA binding and uptake linked to type IV pilus expression, Molecular Microbiology. 46 (2002) 749-760.

[77] E.J. van Schaik, C.L. Giltner, G.F. Audette, D.W. Keizer, D.L. Bautista, C.M. Slupsky, DNA binding: a novel function of Pseudomonas aeruginosa type IV pili, J. Bacteriol. 187 (2005) 1455-1464.

[78] F.R. Blattner, The Complete Genome Sequence of Escherichia coli K-12, Science. 277 (1997) 1453-1462.

[79] O. Vidal, R. Longin, C. Prigent-Combaret, C. Dorel, M. Hooreman, P. Lejeune, Isolation of an Escherichia coli K-12 mutant strain able to form biofilms on inert surfaces: involvement of a new ompR allele that increases curli expression, J. Bacteriol. 180 (1998) 2442-2449.

[80] J. Weil, Biochimie générale, 10 éd., Dunod, imprimerie CHIRAT, Saint-Just-la-pendue (France), 2006.

[81] M.M. Barnhart, M.R. Chapman, Curli Biogenesis and Function, Annu. Rev. Microbiol. 60 (2006) 131-147.

[82] J.G. Dyer, N. Sriranganathan, S.C. Nickerson, F. Elvinger, Curli Production and Genetic Relationships Among Escherichia coli from Cases of Bovine Mastitis, J. Dairy Sci. 90 (2007) 193-201.

[83] S. Sukupolvi, R.G. Lorenz, J.I. Gordon, Z. Bian, J.D. Pfeifer, S.J. Normark, Expression of thin aggregative fimbriae promotes interaction of Salmonella typhimurium SR-11 with mouse small intestinal epithelial cells, Infect. Immun. 65 (1997) 5320-5325.

[84] C. Prigent-Combaret, G. Prensier, T.T.L. Thi, O. Vidal, P. Lejeune, C. Dorel, Developmental pathway for biofilm formation in curli-producing Escherichia coli strains: role of flagella, curli and colanic acid, Environmental Microbiology. 2 (2000) 450-464.

[85] A. Olsen, M.J. Wick, M. Morgelin, L. Bjorck, Curli, Fibrous Surface Proteins of Escherichia coli, Interact with Major Histocompatibility Complex Class I Molecules, Infect. Immun. 66 (1998) 944-949.

[86] Ç. Tükel, J.H. Nishimori, R.P. Wilson, M.G. Winter, A.M. Keestra, J.P.M. Van Putten, Toll-like receptors 1 and 2 cooperatively mediate immune responses to curli, a common amyloid from enterobacterial biofilms, Cellular Microbiology. (2010) 1495-1505.

[87] N.D. Hammer, J.C. Schmidt, M.R. Chapman, The curli nucleator protein, CsgB, contains an amyloidogenic domain that directs CsgA polymerization, Proceedings of the National Academy of Sciences. 104 (2007) 12494-12499.

[88] A. Jonson, S. Normark, M. Rhen, Fimbriae, pili, flagella and bacterial virulence, Contrib Microbiol. 12 (2005) 67-89.

[89] O. Vidal, R. Longin, C. Prigent-Combaret, C. Dorel, M. Hooreman, P. Lejeune, Isolation of an Escherichia coli K-12 Mutant Strain Able To Form Biofilms on Inert Surfaces: Involvement of a New ompR Allele That Increases Curli Expression, J. Bacteriol. 180 (1998) 2442-2449.

[90] A. Cookson, The role of type 1 and curli fimbriae of Shiga toxin-producing in adherence to abiotic surfaces, International Journal of Medical Microbiology. 292 (2002) 195-205.

[91] A. Olsén, H. Herwald, M. Wikström, K. Persson, E. Mattsson, L. Björck, Identification of Two Protein-binding and Functional Regions of Curli, a Surface Organelle and Virulence Determinant ofEscherichia coli, Journal of Biological Chemistry. 277 (2002) 34568 -34572.

[92] A.J.D. Kerchove, M. Elimelech, Bacterial Swimming Motility Enhances Cell Deposition and Surface Coverage, Environ. Sci. Technol. 42 (2008) 4371-4377.

[93] J.G. Shoesmith, The Measurement of Bacterial Motility, Microbiology. 22 (1960) 528-535.

[94] R.M. Harshey, Bacterial motility on a surface: Many Ways to a Common Goal, Annu. Rev. Microbiol. 57 (2003) 249-273.

[95] F.R. Blattner, The Complete Genome Sequence of Escherichia coli K-12, Science. 277 (1997) 1453-1462.

[96] C. Prigent-Combaret, E. Brombacher, O. Vidal, A. Ambert, P. Lejeune, P. Landini, et al., Complex regulatory network controls initial adhesion and biofilm formation in Escherichia coli via regulation of the csgD gene, J. Bacteriol. 183 (2001) 7213-7223.

[97] H. Miao, S. Ratnasingam, C.S. Pu, M.M. Desai, C.C. Sze, Dual fluorescence system for flow cytometric analysis of Escherichia coli transcriptional response in multi-species context, Journal of Microbiological Methods. 76 (2009) 109-119.

[98] C. Perrin, R. Briandet, G. Jubelin, P. Lejeune, M. Mandrand-Berthelot, A. Rodrigue, et al., Nickel promotes biofilm formation by Escherichia coli K-12 strains that produce curli, Appl. Environ. Microbiol. 75 (2009) 1723-1733.

[99] C. Prigent-Combaret, E. Brombacher, O. Vidal, A. Ambert, P. Lejeune, P. Landini, et al., Complex regulatory network controls initial adhesion and biofilm formation in Escherichia coli via regulation of the csgD gene, J. Bacteriol. 183 (2001) 7213-7223.

[100] R. Coico, T. Kowalik, J. Quarles, B. Stevenson, R. Taylor, éd., Current Protocols in Microbiology, John Wiley & Sons, Inc., Hoboken, NJ, USA, 2005.

[101] W. Rasband, ImageJ, U. S. National Institutes of Health, Bethesda, Maryland, USA, 1997.

[102] J. Selinummi, J. Seppälä, O. Yli-Harja, J. Puhakka, Software for quantification of labeled bacteria from digital microscope images by automated image analysis, Biotech. 39 (2005) 859-863.

[103] I.F. Sbalzarini, P. Koumoutsakos, Feature point tracking and trajectory analysis for video imaging in cell biology, J. Struct. Biol. 151 (2005) 182-195.

[104] C. Prigent-Combaret, G. Prensier, T.T.L. Thi, O. Vidal, P. Lejeune, C. Dorel, Developmental pathway for biofilm formation in curli-producing Escherichia coli strains: role of flagella, curli and colanic acid, Environmental Microbiology. 2 (2000) 450-464.

[105] M. Chin, A. Sandham, J. Devries, H. Vandermei, H. Busscher, Biofilm formation on surface characterized micro-implants for skeletal anchorage in orthodontics, Biomaterials. 28 (2007) 2032-2040.

[106] W. Teughels, N.V. Assche, I. Sliepen, M. Quirynen, Effect of material characteristics and/or surface topography on biofilm development, Clinical Oral Implants Research. 17 (2006) 68-81.

[107] D.P. Bakker, B.R. Postmus, H.J. Busscher, H.C. van der Mei, Bacterial Strains Isolated from Different Niches Can Exhibit Different Patterns of Adhesion to Substrata, Applied and Environmental Microbiology. 70 (2004) 3758-3760.

[108] D.P. Bakker, H.J. Busscher, J. van Zanten, J. de Vries, J.W. Klijnstra, H.C. van der Mei, Multiple linear regression analysis of bacterial deposition to polyurethane coatings after conditioning film formation in the marine environment, Microbiology. 150 (2004) 1779-1784.

[109] W. Jiang, H. Mashayekhi, B. Xing, Bacterial toxicity comparison between nano- and micro-scaled oxide particles, Environmental Pollution. 157 (2009) 1619-1625.

[110] J. Costerton, The biofilm primer, Springer, Berlin; New York, 2007.

[111] E. Brombacher, A. Baratto, C. Dorel, P. Landini, Gene expression regulation by the Curli activator CsgD protein: modulation of cellulose biosynthesis and control of negative determinants for microbial adhesion, J. Bacteriol. 188 (2006) 2027-2037.

[112] G. Jubelin, A. Vianney, C. Beloin, J. Ghigo, J. Lazzaroni, P. Lejeune, CpxR/OmpR interplay regulates curli gene expression in response to osmolarity in Escherichia coli, J. Bacteriol. 187 (2005) 2038-2049.

[113] E. Dague, J. Duval, F. Jorand, F. Thomas, F. Gaboriaud, Probing Surface Structures of Shewanella spp. by Microelectrophoresis, Biophysical Journal. 90 (2006) 2612-2621.

[114] M.M. Barnhart, M.R. Chapman, Curli biogenesis and function, Annu. Rev. Microbiol. 60 (2006) 131-147.

[115] W.R. Schwan, M.T. Beck, S.J. Hultgren, J. Pinkner, N.L. Woolever, T. Larson, Down-regulation of the kps region 1 capsular assembly operon following attachment of Escherichia coli type 1 fimbriae to D-mannose receptors, Infect. Immun. 73 (2005) 1226-1231.

[116] Z. Tu, L. Ge, J. Li, Z. Ou-Yang, Elasticity of polymer vesicles by osmotic pressure: An intermediate theory between fluid membranes and solid shells, Phys. Rev. E. 72 (2005) 1539-3755.

[117] D. Bakker, Bacterial deposition to fluoridated and non-fluoridated polyurethane coatings with different elastic modulus and surface tension in a parallel plate and a stagnation point flow chamber, Colloids and Surfaces B: Biointerfaces. 32 (2003) 179-190.

[118] A. Mitchell, J. Wimpenny, The effects of agar concentration on the growth and morphology of submerged colonies of motile and non-motile bacteria, Journal of Applied Microbiology. 83 (1997) 76-84.

[119] U. Hamhaber, F. Grieshaber, J. Nagel, U. Klose, Comparison of quantitative shear wave MR-elastography with mechanical compression tests, Magn. Reson. Med. 49 (2003) 71-77.

[120] L.L. McCarter, Bacterial Acrobatics on a Surface: Swirling Packs, Collisions, and Reversals during Swarming, J. Bacteriol. 192 (2010) 3246-3248.

General Conclusion.

This work has demonstrated proof of concept in the preparation of bioactive surfaces based on surface-tethering polymeric nanoreactors in order to prevent biofilm formation. Additionally, several fundamental aspects of polymer physical chemistry and biological interfaces have been explored.

The first part of this work was dedicated to basic investigations of the synthesis, self-assembly, and surface immobilization of nucleotide-based amphiphilic block copolymers, leading to the successful preparation of surfaces modified with self-assembled nanoreactors. The second part of this work was dedicated to the investigation of bacterial response to vesicle-modified surfaces and to the influence of surface properties on bacterial adhesion, leading to a comprehensive understanding of the mechanisms involved in global interactions between bacteria and surfaces.

The first part of this thesis has been divided into three chapters, each providing individual contribution to a comprehensive understanding of the surface-nanoreactor system.

In the first chapter we demonstrate the possibility of designing a hybrid amphiphilic copolymer by functionally grafting a nucleotide sequence to a hydrophobic polymer segment. Due to the versatile chemistry of self-assembling copolymers, we were able to synthesize a nucleotide-based amphiphilic block copolymer by solid phase synthesis that self-assembled into vesicular structures in dilute aqueous solution. The characterization of the self-assembly process of this copolymer demonstrated the influence of the stifness of the hydrophilic oligonucleotide block, which enabled the formation of vesicles, despite the fact that, given the hydrophilic to hydrophobic volume fraction, self-assembly into core-shell micelles is usually expected in such cases.

The second chapter deals with the ability of this polymer to provide nanoreactors by actively encapsulating an enzyme in the presence of protein channels, which ensured the permeability of the polymeric shell. The system is functional and efficiently prevents enzymatic degradation in a non-favorable environment.

In the third chapter we demonstrate that the nucleotide sequence, subsequent to polymer modification and self-assembly, retains its ability to hybridize with its complementary sequence grafted to a surface. The morphology of the self-assembled structure is preserved. In this chapter we also describe and characterize various types of surfaces produced to better understand bacterial adhesion on vesicles based surfaces.

The second part of this work revolved around four topics. After a brief, initial part concerning surface toxicity, the next part concerns the influence of the composition and physical-chemical properties of surface-tethered oligonucleotides on bacterial adhesion and curli expression. The third part focused on the influence of

topography on bacterial adhesion, while the fourth and final discussion reported on the influence of the mechanical properties of the vesicles coating on bacterial response.

In the part discussion we demonstrated the non-toxicity of differing surfaces produced in this study in comparison to glass and silicon wafer references.

Subsequently, we discussed the balanced influence of charges and chemical cue due to grafting density of nucleotide sequences, which lead to a decreased number of adherent cells at high grafting density and no influence at low grafting density compared to control surfaces. We also substantiated the influence of surface-tethered nucleotide sequences on curli expression. A slight over-expression was observed which seemed to be easily disturbed by other effects such as oligonucleotide grafting density. This over-expression effect was independent of the composition of the nucleotide sequence, leading to the hypothesis that this effect is not specific to the strands used in this study.

In the following section, we discussed the influence of topography and, in particular, the lack of influence by the sub-micrometer topography used in this study on bacterial adhesion and curli expression. We hypothesize that nanoscale topography influence on bacterial adhesion may have been screened by the strong influence of the oligonucleotide and vesicles surfaces mechanical properties observed in this study.

In the fourth section, we considered the influence of the mechanical properties of the layer of vesicles immobilized on surfaces on bacterial adhesion. This part of the study leads to interesting evidence of a decrease in the number of visible, adherent bacteria on surfaces that were based on vesicles with visco-elastic properties. Combined investigations of bacterial adhesion and motility on surfaces coated with either self-assembled vesicles in dynamic conditions or agar in static conditions led us to hypothesize that the decrease in observable, adherent cells is, in fact, induced by a higher detachment rate from the surface during the early adhesion stage linked with greater bacterial motility. The bacterial motility, that we showed to certainly be sliding, is probably induced by the dissipative properties of the substrate, which should not offer anchoring properties for the bacteria, therefore not allowing irreversible adhesion and further biofilm formation to occur.

Finally, we have achieved the various goals as defined: we proved the feasibility of the nanoreactor-based antimicrobial surface design concept and we explored fundamental aspects that underlie this surface concept and the bacterial response to such an atypical surface. Moreover we highlight the unique mechanical properties of such type of surfaces and showed their possible relevance to produce antimicrobial coating due to both their anti-adhesive properties, and the nanoreactor activity, cumulating advantages of passive antimicrobial action with a controllable drug delivery system.

Outlook.

The investigations included in this study pave the way to further investigations in the design of antimicrobial surfaces that will eventually be used in biotechnology and human therapy. Besides proof of concept, these PhD activities have addressed several fundamental aspects that still demand further work, some of them currently in progress.

The self-assembly of nucleotide-based block copolymers exhibits unique properties. A comprehensive understanding of the underlying mechanism will be achieved by studying the influence of electrostatic interactions, pH, and hybridization with the sequence complementary to that involved in the self-assembly, on the properties of this system.

The preparation of efficient nanoreactors resulting from the self-assembly of the polymer modified nucleotide sequences was demonstrated by the functional encapsulation of an enzyme. Extension of this concept to the design of prodrug-drug systems for antimicrobial therapy is actually being successfully developed in our group for various applications.

Hybridization on surfaces of self-assembled nucleotide-based block copolymer vesicles is of interest for the development of novel biosensor technologies based on the unique recognition properties of nucleotide sequences and further investigation will followed in a next future.

The elucidation of the influence of surface-tethered nucleotide sequences on bacterial adhesion and curli expression is of wide interest, since bacteria are sensitive to the physical-chemical properties of the oligonucleotide-modified surface. Identification of the functional grafting density is still under debate. For this purpose, additional studies with a controlled variation of the grafting density of oligonucleotide and including various compositions and sizes are foreseen. The influence of the composition of the nucleotide sequence on curli expression is also of great interest with respect to a fundamental understanding of bacterial sensing and will be investigated using bacteria membrane proteomics and genomic.

Finally, the influence of the mechanical properties of the surface on bacterial adhesion highlighted over the course of these studies is of primary interest. Few studies report the effect of this factor on bacterial adhesion. At least two mechanical parameters, viscosity and elasticity, are shown to affect the adhesion, the motility and the detachment rate of bacteria. Differentiating these two mechanical parameters is critical to a further understanding of biofilm formation and to the design of new strategies for antimicrobial action. Further works to fully quantify those parameters and to determine other relevant visco-elastic parameters influencing bacterial adhesion will be performed on the surfaces presented in the present study. Following this work, model surfaces will be designed to further study the influence of mechanical properties to avoid or enhance bacterial adhesion, but also to study bacterial response by surface sensing, either by CpX signaling pathway or flagella blocking detection.

List of abbreviations.

- A_5G_7: oligonucleotide sequence (5'-AGAGAGAGAGGG-3')
- A_{600}: UV-Vis absorbance at 600nm
- AFM: Atomic force microscopy
- APTES : Aminopropyl triethoxysilane
- C_7T_5: oligonucleotide sequence (5'-CCCTCTCTCTCT-3')
- CD: circular dichroism
- CLSM: confocal laser scanning microscopy
- CP-MAS NMR: charge polarized magic angle spinning nuclear magnetic resonance
- DLVO theory: Derjaguin, Landau, Verwey and Overbeek theory
- DNA: Deoxyribonucleic acid
- *E.coli : Escherichia coli*
- EPS: Exo-polysaccharides
- *gfp*: green fluorescent protein
- LPO: Lactoperoxidase
- PBS: phosphate buffer saline
- QCM-D: quartz crystal microbalance with dissipation
- RNA: Ribonucleic acid
- SAMs: Self-assembled monolayers
- UV-Vis: Ultraviolet to visible wavelength

Impact of the work.

Published work:

Cottenye, N. et al. Oligonucleotide Nanostructured Surfaces: Effect on *Escherichia coli* Curli Expression. *Macromolecular Bioscience* **8**, 1161-1172 (2008).

Publication under preparation:

N. Cottenye et al. " Nanoreactors based on the self-assembly of polymer-modified nucleotide sequences", in preparation

N. Cottenye et al. " Surface tethering through hybridization of oligonucleotide based amphiphilic block copolymers. ", in preparation

Oral contributions in conference:

N. Cottenye et al. "Self-Assembled Nanoreactors Immobilized On Surfaces: characterization and application to bacterial adhesion and biofilm growth" EMRS, Strasbourg (FR), June 2010

L. Ploux et al. "How to fight against biomaterial-related infections: Example of a "smart" antibacterial surface" NanoSMH, Pont-à-Mousson (FR), June 2010

N. Cottenye et al. "Self-Assembled Nanoreactors Immobilized On Surfaces: Characterization and Application to Bacterial Adhesion", APTEN, Poitiers (FR) February 2010

N. Cottenye et al. "Self-assembling nanoreators immobilized on surfaces: characterization and application to bacterial adhesion" Bioadh09, Le Mans November 2009 (Presented by L.Ploux)

N. Cottenye et al. "Nanostructured polymers for bioactive surfaces: development, characterization and application to biological adhesion" Nanotech meeting, Mulhouse (FR) May 2009

N. Cottenye et al. "Nanostructured polymer for bioactive surfaces: effect of Oligonucleotide nanostructured surfaces on Escherichia coli curli expression", GDA, Bordeaux (FR) July 2008

N. Cottenye et al. "Oligonucleotide nanostructured surfaces: effect on *Escherichia coli* curli expression", Biofilm III, Munich (DE) October 2008

Poster in conference:

N. Cottenye et al. "Self-Assembled Nanoreactors Immobilized On Surfaces: Characterization and Application to Bacterial Adhesion" Biofilm IV, Winchester (UK), 2010.

N. Cottenye et al. "Self-Assembled Nanoreactors Immobilized On Surfaces: Characterization and Application to Bacterial Adhesion" Nano SMH, Pont-à-Mousson (FR), 2010.

N. Cottenye et al. "Nanostructured surfaces for bioactives application: characterization and application to bacterial adhesion and biofilm growth" JED2010, Mulhouse, June 2010.

N. Cottenye et al. "Nanostructured surfaces for bioactives application: characterization and application to bacterial adhesion and biofilm growth" école biofilm, Vittel (FR) October 2009

N. Cottenye et al. "Self-assembling nanoreactors from poly(butadiene)-b-oligonucleotide amphiphilic block copolymers" ESB, Lausanne (CH) September 2009

N. Cottenye et al. "Self-assembled nanoreactors for the design of bioactive surfaces" NCCR meeting Basel (CH), June 2009

N. Cottenye et al. "Oligonucleotide nanostructured surfaces: effect on *Escherichia coli* curli expression" PILS, Basel (CH) September 2008

N. Cottenye et al. "Nanostructured DNA-Butadiene surfaces for studying bacterial adhesion and biofilm growth" Biosurf IV, Zurich (CH) September 2007 and ISBRM, Mulhouse September 2007

Seminars and workshops:

Universität Basel group seminar: 8 scientific presentations

IS2M presentation: 1 institute seminar and 3 scientific presentations

Awards:

University of Southampton travel bursary for Biofilm IV international conference, Winchester, September 2010 (UK)

NanoSMH 2010 best poster award (Biomat sponsored), June 2010 (FR)

Independent grant and financial support:

SNF postdoctoral fellowship: "Determination of amphiphilic molecule interactions with biofilm matrices to develop new antimicrobial drug vectors: influence of physico-chemical parameters on diffusion, adhesion and affinity of bacteria". 12 month postdoctoral grant at the Université de Montréal, Canada, starting 1 January 2010

"CRUS stipend for 'cotutelle' thesis, Program 2010" between the University of Basel in Switzerland and the IS2M in France (Funding for laboratory research activities and consumables)

Curriculum Vitae

COTTENYE Nicolas
14 rue de battenheim
68200 Mulhouse
e-mail : nicolas.cottenye@unibas.ch
nicolas_cottenye@hotmail.com
tel : +33389445053

EDUCATION

European Master (Ms. sc.) from the University de Haute Alsace in Mulhouse, France, obtained in June 2007. Major in Polymer materials, Minor in Surfaces and Interfaces. With honors.
European Bachelor (B.S) from the University de Haute Alsace in Mulhouse, France, obtained in 2005. Major in physical chemistry, minor in polymer science.
High school diploma (baccalauréat) in Niort, France, obtained in 2001. With honors

PROFESSIONAL EXPERIENCE

Currently:
PhD student at the "Universität Basel", Department of Chemistry, in Prof. Dr. W. Meier team in collaboration with Dr. K. Anselme at the Institut de Science des Matériaux de Mulhouse (IS2M, CNRS LRC 7228), University de Haute Alsace, Since 1 September 2007
Subject: "Antimicrobial surface based on self-assembled nanoreactors: from bloc copolymer to bacterial adhesion study."

Training:
- Institut de Science des Matériaux de Mulhouse (IS2M, CNRS LRC 7228), University de Haute Alsace, France, in collaboration with the Department of Chemistry of Basel University, Switzerland.

Research on bacterial adhesion onto surfaces modified with self-assembled amphiphilic copolymers.
Acquired skills: Microbiology basics, surface modification, surface analysis, polymer analysis, enzyme encapsulation, separation and activity detection. Master thesis 2007 and 3 months training course 2006.

- Departement de Photochimie Générale (CNRS UMR 7525), University de Haute Alsace in Mulhouse, France.

Training in research on photo-initiated polymerization kinetics.
Acquired skills: Infrared spectroscopy, transitory absorption spectroscopy, formulation of photo-polymerizable solutions. One-year training course in 2005
- Food industry: DSM Nutritional Product in Village neuf, France (summer 2004), Rhodia Food in Melle, France (summer 2001 and 2002). Employee.

Acquired Skills: Operation in food safety conditions. Water analysis: chemical oxygen demand (COD), ions concentration determination.

Other professional experiences:
- ATV, Transport Company in Mulhouse, France: Night driver in a Newspaper Company. Every Weekend from November 2006 to august 2007 plus every day in July 2007
- Mgel logement, student housing in Mulhouse, France: Housekeeper 2 hours per day from April 2005 to January 2007
- System U, national food chain provider in Mulhouse, France. Employee in the ordering section every Saturday and every holyday in year 2003 and 2004

LANGUAGE & HOBBIES

French: native speaker, **English:** Advanced, **German:** Lower intermediate
Computer skills: Windows XP/vista/7 and Linux (Ubuntu based), Office2003/2007, Open Office3.x, Blender2.49, Gimp2.6, Zeiss Zen, Image J, CellC, Qtools, Gwyddions. Plus general basic skills in Web and software use.
Hobbies: Enjoy playing rugby, heroic-fantasy literature and computer hardware tweaking
Chairman of the student association: "association des élèves de L'ENSCMu" in 2004. In charge of the general organization and budgeting for several events like Fresher's week-end, sport and cultural events.

Annex
Résumé Français de la thèse

Introduction.

Les Biofilms et leur contrôle.

Au cours de la dernière décennie, le concept de "biofilm" a considérablement modifié notre perception et compréhension de la microbiologie. En particulier dans le domaine biomédical où ce nouveau concept a permis de changer la perception des interfaces bactérie-substrat, permettant le développement de nouvelles stratégies pour combattre les infections dues aux pathogènes.

La notion de "biofilm" a été introduite il y a 30 ans par W.Costerton[1]. Le biofilm a été défini comme une population bactérienne incluse dans une matrice extracellulaire et adhérée à une surface ou une interface. Cette définition permet d'inclure les agrégats microbiens, les floculats et les populations adhérées dans les interstices de substrats poreux. Le biofilm est aujourd'hui considéré comme un mode de vie majeur des bactéries et non pas comme une simple réponse à un stress environnemental puisque 99% des bactéries présentes sur terre semblent capables de former des biofilms. Ce mode de vie communautaire des bactéries inclut un métabolisme et un développement spécifiques des bactéries. En particulier, il a été montré que l'intensité d'expression des gènes de bactéries vivant en biofilms peut varier de plusieurs 10^{nes} de % en comparaison de bactéries vivant sous forme planctonique. De plus, loin de n'être qu'un simple amoncèlement de bactéries, le biofilm se développe par la prolifération de bactéries pionnières, i.e. fraîchement adhérées, et suit une croissance spécifique aux biofilms, dont une évolution schématique est donnée en Figure 1. Brièvement, cette croissance peut être résumée comme suit : après l'adhésion primaire de la bactérie sur la surface, la bactérie pionnière prolifère et synthétise des exobiopolymères, principalement des exopolysaccharides qui constituent la matrice du biofilm. Finalement, les biofilms sont des systèmes dynamiques, dont la structure en trois dimensions évolue, et dont certaines parties peuvent se détacher, permettant la colonisation de surfaces vierges. Enfin, outre de l'environnement dans lequel il se développe, les propriétés et les évolutions du biofilm dépendent essentiellement du métabolisme des bactéries qui les constituent.

[1] J.W. Costerton, G.G. Geesey, K. Cheng, How Bacteria Stick, Sci Am. 238 (1978) 86-95.

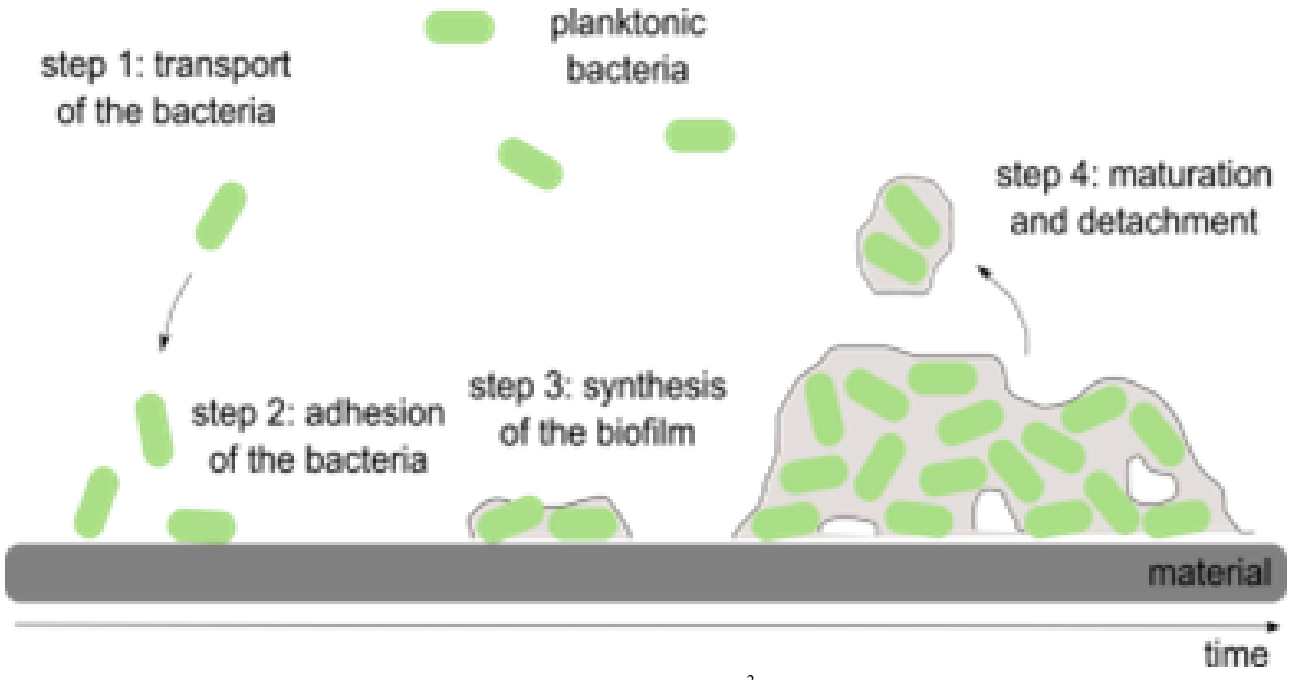


Figure 1: Schéma de croissance d'un biofilm (Illustration issue de L. Ploux et al.[2])

Au sein du biofilm, les bactéries sont protégées des stress environnementaux tels que les températures extrêmes, la déshydratation, l'action d'agents antiseptiques ou antimicrobiens, ou encore l'action d'anticorps ou de phagocytes. Les traitements habituels contre les pathogènes ciblent les bactéries planctoniques, et se révèlent inefficaces pour traiter les biofilms bactériens (quelques exemples d'infections dues à la formation de biofilms bactériens sur une surface sont listés dans la Figure 2a) ; un exemple de biofilm bactérien se développant sur une surface et conduisant au développement d'une infection est également illustré en Figure 2b). Au cours de ces 50 dernières années, l'augmentation du nombre d'actes de chirurgie invasive utilisant l'implantation de biomatériaux, a menée à la prévalence de ces infections. Par conséquent, le développement de nouveaux traitements antimicrobiens spécifiquement dédiés au traitement des infections liées au développement de biofilms sur les surfaces est devenu crucial. La recherche dans ce domaine a d'ailleurs fait de grand progrès au cours des 20 dernières années.

[2] L. Ploux, A. Ponche, K. Anselme, Bacteria/Material Interfaces: Role of the Material and Cell Wall Properties, J Adhes Sci Technol. 24 (2010) 2165-2201.

a/

Infection or disease	Common biofilm bacterial species
Dental caries	Acidogenic Gram-positive cocci (e.g., *Streptococcus*)
Periodontitis	Gram-negative anaerobic oral bacteria
Otitis media	Nontypable strains of *Haemophilus influenzae*
Musculoskeletal infections	Gram-positive cocci (e.g., staphylococci)
Necrotizing fasciitis	Group A streptococci
Biliary tract infection	Enteric bacteria (e.g., *Escherichia coli*)
Osteomyelitis	Various bacterial and fungal species—often mixed
Bacterial prostatitis	*E. coli* and other Gram-negative bacteria
Native valve endocarditis	Viridans group streptococci
Cystic fibrosis pneumonia	*P. aeruginosa* and *Burkholderia cepacia*
Meloidosis	*Pseudomonas pseudomallei*
Nosocomial infections	
ICU pneumonia	Gram-negative rods
Sutures	*Staphylococcus epidermidis* and *S. aureus*
Exit sites	*S. epidermidis* and *S. aureus*
Arteriovenous shunts	*S. epidermidis* and *S. aureus*
Schleral buckles	Gram-positive cocci
Contact lens	*P. aeruginosa* and Gram-positive cocci
Urinary catheter cystitis	*E. coli* and other Gram-negative rods
Peritoneal dialysis (CAPD) peritonitis	A variety of bacteria and fungi
IUDs	*Actinomyces israelii* and many others
Endotracheal tubes	A variety of bacteria and fungi
Hickman catheters	*S. epidermidis* and *C. albicans*
Central venous catheters	*S. epidermidis* and others
Mechanical heart valves	*S. aureus* and *S. epidermidis*
Vascular grafts	Gram-positive cocci
Biliary stent blockage	A variety of enteric bacteria and fungi
Orthopedic devices	*S. aureus* and *S. epidermidis*
Penile prostheses	*S. aureus* and *S. epidermidis*

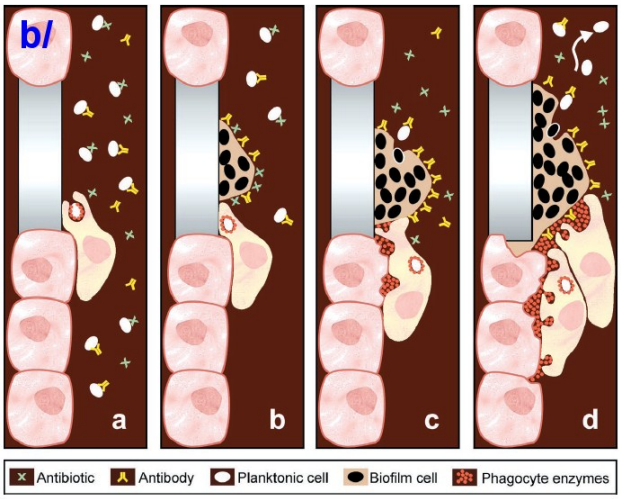


Figure 2: (a) Exemples d'infections cliniques typiques impliquant les biofilms. (b) Schéma de la croissance d'un biofilm clinique. La bactérie planctonique peut être ciblée par les anticorps, phagocytes et est sensibles aux antibiotiques. La bactérie adhérente forme un biofilm sur les surfaces inertes de façon préférentielle. Ces communautés sessiles sont résistantes aux antibiotiques, phagocytes et anticorps. Les phagocytes sont attirés par le biofilm. La phagocytose est impossible mais les enzymes phagocytiques sont relarguées et endommagent les tissus environnants. De plus, des bactéries planctoniques sont relarguées par le biofilm, autorisant la dissémination et l'infection des tissus environnants. Ces deux illustrations sont extraites de Costerton et al.[3]

Deux approches ont principalement été considérées dans le combat contre les biofilms. La première approche consiste à se concentrer sur le biofilm mature par l'optimisation de la diffusion de molécules antibactériennes au sein de la matrice du biofilm. Dans la seconde approche, l'accent est mis sur la modification de la surface sur laquelle se développe le biofilm. Cette seconde approche est celle qui nous a intéressée dans ce travail de thèse.

Dans ce contexte, la possibilité d'agir à différentes étapes du développement du biofilm a été étudiée. Les différentes stratégies se divisent en deux catégories : les stratégies passives et les stratégies actives. Dans une stratégie passive, la surface est modifiée pour empêcher l'adhésion bactérienne par le biais de l'altération des propriétés intrinsèques de la surface. Plusieurs possibilités ont été rapportées : en premier lieu, la modification des facteurs physico-chimiques de la surface s'est montrée efficace pour réduire l'adhésion bactérienne[4]. Ceci inclus, par exemple, l'augmentation de l'hydrophobicité de la surface par le dépôt d'une couche de Téflon, la modification de la charge de la surface, ou encore l'utilisation d'une énergie de surface élevée, ou de l'écrantage entropique généré par le greffage de brosses de polymères sur la surface. La seconde stratégie consiste à greffer des molécules capables de repousser ou tuer les bactéries dès leur adhésion sur la surface. Cette stratégie se traduit généralement par le greffage de molécules antibiotiques, d'enzymes et de polymères aux propriétés antimicrobiennes (chitosan, copolymère de chlorures de methacryloylethyl trialkyl phosphonium /*N*-

[3] J.W. Costerton, Bacterial Biofilms: A Common Cause of Persistent Infections, Science. 284 (1999) 1318-1322.

[4] B.A. Jucker, H. Harms, A.J. Zehnder, Adhesion of the positively charged bacterium Stenotrophomonas (Xanthomonas) maltophilia 70401 to glass and Teflon, J. Bacteriol. 178 (1996) 5472-5479.

isopropylacrylamide, par exemple). Néanmoins, ces techniques possèdent des limitations. La première concerne la difficulté à associer le pouvoir antimicrobien ou préventif de ces surfaces avec une biocompatibilité pour les cellules eucaryotes. Cette première difficulté est rarement considérée dans le contexte du traitement du biofilm. Une autre limitation provient des grandes différences de propriétés physico-chimiques entre les souches bactériennes (différences de charge de la membrane bactérienne, différences d'hydrophobicité et différences de formes, pour ne citer que quelques exemples), ce qui limite le spectre d'action des surfaces antibactériennes réalisées. Finalement, le principal désavantage de ces approches vient de leur durée d'action: de simples rayures sur la surface ou la formation d'un film de conditionnement peuvent suffire à offrir des points d'ancrage pour les bactéries, contrant localement l'action antibiofilm de la surface. La stratégie active de surface antibactérienne focalise maintenant l'attention. Elle est considérée comme plus fiable que la stratégie passive pour empêcher la formation de biofilm, ainsi qu'il a été montré sur des cathéters, par exemple[5]. Cette stratégie consiste à incorporer un agent antimicrobien dans le matériau ou dans un dépôt effectué sur le matériau, et à contrôler le relargage de cet agent dans le milieu environnant. Le contrôle du relargage constitue la principale difficulté puisqu'un relargage trop important risque d'entraîner un effet toxique ou une réponse immunitaire, alors qu'un relargage trop faible serait inefficace et pourrait même induire l'apparition de mécanismes de résistance chez les bactéries. Pour éviter ces problèmes, le contrôle doit concerner à la fois la dose délivrée, mais également le temps de traitement. Pour cela, deux approches sont classiquement envisagées : un relargage continu ou un relargage déclenché par un stimulus. Grâce à sa relative simplicité, le relargage continu est le plus fréquemment envisagé et développé[6]. Cette stratégie consiste à mélanger l'agent antimicrobien tel que des antibiotiques ou des nanoparticules d'argent par exemple, et de les inclure dans une matrice, polymère le plus souvent. Le relargage est alors obtenu par diffusion des agents antimicrobiens au travers de la matrice. Leur diffusion est par conséquent l'aspect critique du contrôle du relargage et est dirigée par les propriétés physico-chimiques de la matrice, telle que le taux de réticulation ou les interactions entre les agents antimicrobiens et les molécules composant la matrice. Des produits basés sur le relargage continu sont déjà commercialisés pour de nombreuses applications médicales. Néanmoins, cette approche est contestable puisque l'agent antibactérien est délivré même lorsqu'il est inutile, ce qui risque d'induire l'apparition de résistances chez les bactéries de l'environnement. Le relargage déclenché par un stimulus est donc préférable. Cette approche consiste à délivrer l'agent bioactif en réponse à un stimulus externe, ce qui limite la quantité d'agent relargué. Le risque d'effets secondaires indésirables sera ainsi limité, ainsi que le risque d'induction d'apparition de résistances chez les bactéries et permettra par la même occasion d'augmenter le temps de vie du system antimicrobien. Un certain nombre de stimuli ont été utilisés pour provoquer ce relargage contrôlé, tels que la réponse au changement de pH ou à la force ionique, la réponse à un

[5] A. Casey, L. Mermel, P. Nightingale, T. Elliott, Antimicrobial central venous catheters in adults: a systematic review and meta-analysis, The Lancet Infectious Diseases. 8 (2008) 763-776.

[6] H. Yu, X. Xu, X. Chen, T. Lu, P. Zhang, X. Jing, Preparation and antibacterial effects of PVA-PVP hydrogels containing silver nanoparticles, Journal of Applied Polymer Science. 103 (2007) 125-133.

stimulus lumineux, la réponse à des stimuli mécaniques, la réponse à des variations de température, ou encore la réponse à un stimulus électrique. Ces approches ont déjà démontré leur aptitude à fournir des dépôts antimicrobiens fonctionnels. Cependant, des questions restent en suspens, telle que la biocompatibilité qui reste un problème majeur pour certains de ces dépôts. Plus encore, malgré l'amélioration apportée par ces dépôts antimicrobiens dits « intelligents », en comparaison des dépôts à relargage continu, ces approches ne permettent pas de régler le problème de la durée de vie limitée du dépôt (lorsque tout l'agent actif est relargué, le dépôt devient complètement inactif). De plus, un soin particulier doit être apporté au dépôt pour s'assurer que chaque stimulus entraînera un relargage suffisant d'agent actif pendant toute la durée de vie du dépôt.

Finalement, malgré de nombreux tentatives pour passer outre les défauts inhérentes à chacune de ces stratégies, en combinant par exemple stratégie passive et active dans le même dépôt, certaines limitations et questions subsistent, notamment dues au contenu limité des dépôts en agent actif, entraînant une durée de vie limitée du système. Pour dépasser ces limitations, de nouvelles approches doivent être imaginées.

Molécules amphiphiles, vésicules, et leurs applications.

Les molécules amphiphiles contiennent une partie polaire et une partie non-polaire, respectivement hydrophile et hydrophobe. Dû à cette incompatibilité chimique, les molécules amphiphiles s'auto-assemblent et s'organisent aux interfaces aqueuses. L'auto-assemblage conduit à la formation de nombreuses structures en fonction de divers facteurs, tels que la température, la composition du solvant, la concentration en amphiphile, la masse moléculaire, le ratio volumique entre la partie hydrophile et hydrophobe et les charges de la chaîne polymère. Quelques exemples de ces structures sont présentés dans la Figure 3, pour un copolymère amphiphile à blocs, constitué d'un bloc hydrophile attaché de manière covalente à un bloc hydrophobe. Toutes ces structures sont le résultat du processus d'auto-assemblage, qui peut être dirigé soit par l'équilibre thermodynamique, soit par l'équilibre cinétique d'auto-assemblage des molécules. La morphologie des structures auto-assemblées répond à la nécessité de minimiser l'énergie libre du système en diminuant la tension de surface. Par conséquence, en prenant en compte les interactions potentielles entre molécules, telles que les interactions électrostatiques ou la propension aux liaisons hydrogènes, ainsi que la masse moléculaire et le ratio volumique entre la partie hydrophile et hydrophobe, une molécule amphiphile peut être optimisée pour contrôler les caractéristiques et la morphologie de son auto-assemblage.

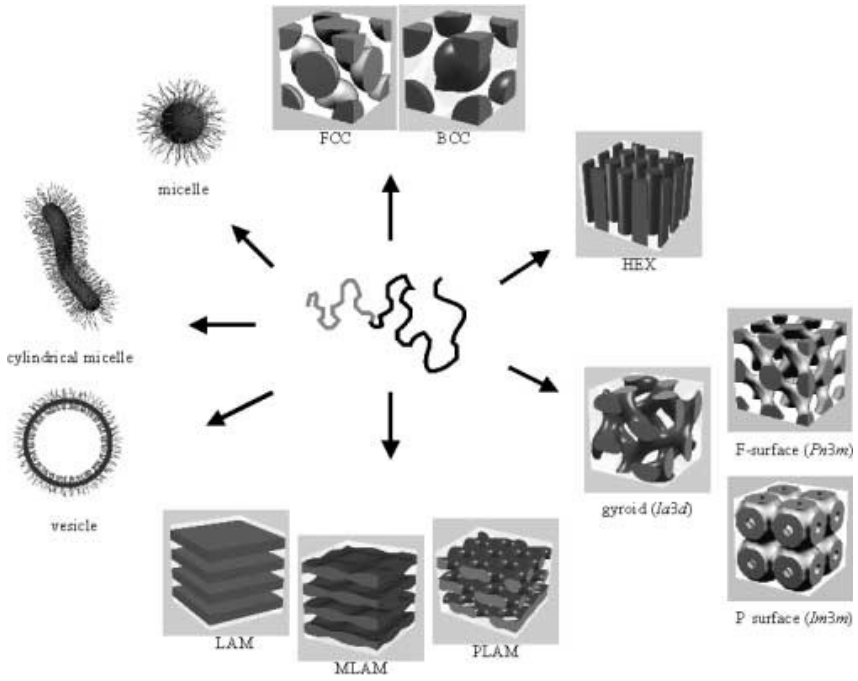


Figure 3: Exemples de structure auto-assemblées obtenues avec des copolymères amphiphiles à blocs: micelles sphériques, micelles cylindriques, vésicules, assemblages cubiques face centrée (fcc) et cubique centré (bcc), sphères compactes, cylindre sous forme compacte hexagonale (HEX), plusieurs types de surfaces d'énergie minimum tel que pour les structures gyroïdes, surface F, surface P), simples couches lamellaires (LAM), ainsi que lamelles modulées et perforées (MLAM, PLAM) peuvent être auto-assemblés (de Förster et al.[7]).

Pour les applications biomédicales, l'utilisation de structures auto-assemblées a été largement étudiée dans le cadre de la vectorisation des médicaments. Pour de telles applications, les amphiphiles présentent l'avantage d'être solubles en milieux aqueux, avec une morphologie prédominante de type micelle, sphérique ou cylindrique, et vésicule. Les polymères amphiphiles sont donc sélectionnés pour leur aptitude à s'auto-assembler en vésicules ou en micelles pour transporter des médicaments, gènes ou ARN interférant, par exemple. Une illustration de la formation de vésicules par l'auto-assemblage de molécules amphiphile sous forme d'une bicouche se refermant sur elle-même est présentée dans la Figure 4. De plus, la modification chimique de la membrane vésiculaire permet de fonctionnaliser la vésicule pour optimiser le ciblage et le transport, comme illustré par la Figure 5. Les lipides, analogues de faible masse moléculaire des copolymères amphiphiles à blocs, sont souvent étudiés dans ce type d'approche pour leur simplicité de mise en œuvre. Néanmoins, à cause de leur masse moléculaire plus faible face aux copolymères à blocs, les lipides ont une stabilité plus faible, ce qui est très problématique notamment pour leur stockage. Dans ce contexte, l'utilisation de polymères amphiphiles est très intéressante puisqu'ils permettent une plus grande stabilité de l'auto-assemblage. De plus, la chimie macromoléculaire offre une infinité de combinaisons pour la conception de polymères fonctionnalisés. Malgré cela, les copolymères à blocs sont

[7] S. Förster, T. Plantenberg, From Self-Organizing Polymers to Nanohybrid and Biomaterials, Angewandte Chemie International Edition. 41 (2002) 688-714.

rarement utilisés en comparaison des lipides, ceci étant dû essentiellement à l'absence d'autorisation de la FDA (Food and Drug Administration).

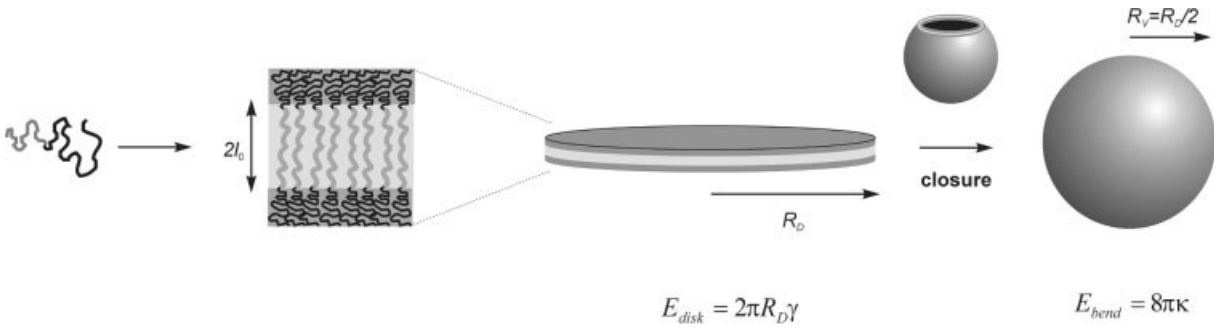


Figure 4: Représentation de la formation et de la fermeture d'une bicouche de polymères auto-assemblée, formant une vésicule afin de diminuer l'énergie libre du système (Antonietti et al.[8]).

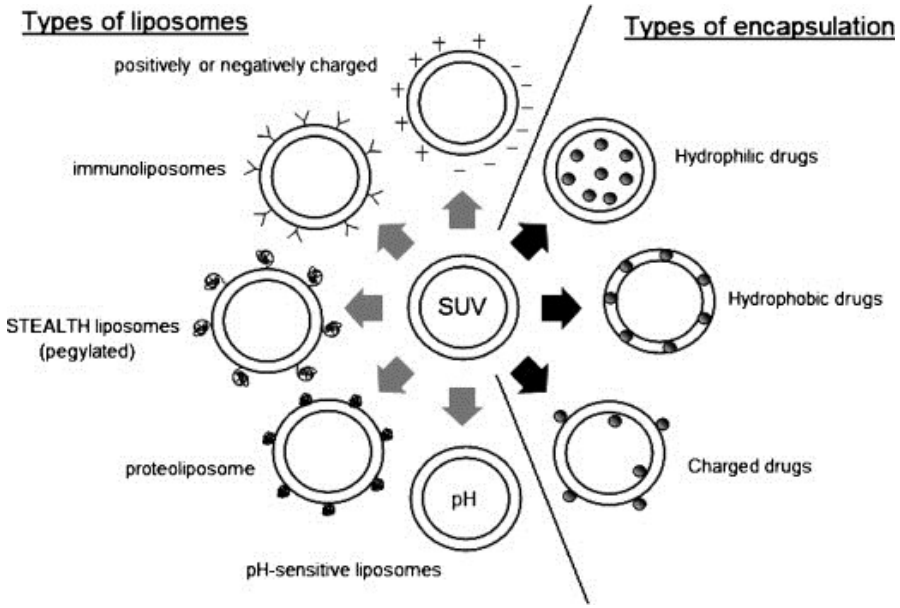


Figure 5: Stratégies typiques pour concevoir un système de vectorisation de médicaments basés sur les liposomes (Drulis-kawa et al.[9]).

Le nombre virtuellement infini de combinaisons possibles pour synthétiser un polymère amphiphile s'auto-assemblant et étant fonctionnalisé pour une application précise, est la clé de leur utilisation dans le domaine biomédical. Le besoin de concevoir des amphiphiles pour des applications spécifiques a poussé à de nombreuses

[8] M. Antonietti, S. Förster, Vesicles and Liposomes: A Self-Assembly Principle Beyond Lipids, Advanced Materials. 15 (2003) 1323-1333.

[9] Z. Drulis-Kawa, A. Dorotkiewicz-Jach, Liposomes as delivery systems for antibiotics, International Journal of Pharmaceutics. 387 (2010) 187-198.

études en chimie macromoléculaire, synthèse et conception de nanocontaineurs basés sur des amphiphiles ou nanoréacteurs pour la vectorisation de médicaments et gènes, ou encore pour des réactions en cascades multienzymatiques.

Champs d'application de la thèse.

Il y a un besoin évident de définir de nouvelles stratégies pour préparer des dépôts antimicrobiens capables de lutter contre la formation et la croissance des biofilms. Pour ce faire, des études tant fondamentales qu'appliquées sont nécessaires, et ce, en particulier, pour développer des revêtements de surface luttant contre la colonisation initiale des bactéries. La préparation de ces surfaces antibactériennes se doit de prendre en comptes les critères de biocompatibilité et de durée de vie des propriétés antibactériennes. Pour atteindre ces objectifs, nous nous proposons de produire des revêtements bioactifs basés sur l'immobilisation de vésicules polymériques sur la surface à traiter, ce dépôt autorisant la combinaison des stratégies antimicrobiennes passive et active. Pour cela, nous allons élaborer, synthétiser et utiliser un copolymère amphiphile à blocs capable d'induire une réponse à la fois bactérienne et cellulaire pour assurer les propriétés antimicrobiennes autant que la biocompatibilité. Ce polymère doit s'auto-assembler en structures qui peuvent être immobilisés sur la surface pour produire un dépôt capable de relarguer une quantité d'agent antibactérien contrôlée au cours du temps.

En parallèle de ce développement et de la caractérisation du revêtement pour ses applications antibactériennes, ce travail nous a permis d'étudier plusieurs questions fondamentales. Tout d'abord, nous avons synthétisé un copolymère à blocs basé sur un oligonucleotide et nous l'avons caractérisé dans le but de définir ses propriétés d'auto-assemblage en solution. Puis nous avons utilisé les propriétés d'auto-assemblage pour préparer des nanoréacteurs dont nous avons étudié l'activité. Finalement, l'immobilisation de ces vésicules sur les surfaces a été étudiée, l'objectif étant notamment de montrer la possibilité de conserver la structure vésiculaire au cours de l'immobilisation. L'influence des propriétés chimiques, topographiques et mécaniques du revêtement sur la colonisation bactérienne a été étudiée par la détermination du nombre de bactéries adhérentes, de leur mobilité et de l'expression de protéines d'adhésion tels que les curli.

Part I: Polymère, nanoréacteurs et hybridation pour la préparation contrôlée d'un dépôt de surface.

La surface antimicrobienne que nous nous proposons de préparer est basée sur l'immobilisation de vésicules sur la surface du matériau. Le choix de cette technique, pour produire un dépôt antimicrobien, se base sur l'aptitude des vésicules à fournir une action antimicrobienne par plusieurs voies, comme schématisé dans la Figure 6. La conception d'un polymère qui peut s'auto-assembler sous une forme vésiculaire et possédant intrinsèquement un effet répulsif pour les bactéries est la première voie pour créer un dépôt antimicrobien basé sur les structures vésiculaires. La seconde voie consiste à concevoir un système antimicrobien actif, résultant de

l'auto-assemblage du polymère (qui ne possède pas nécessairement de propriétés antimicrobiennes intrinsèques) sous la forme de nanocontaineurs contenant un agent antimicrobien pouvant être relargué de façon contrôlée. La troisième voie consiste à préparer des nanoréacteurs, résultant de l'auto-assemblage du polymère (qui ne possède pas nécessairement de propriétés antimicrobiennes intrinsèques) produisant une substance antimicrobienne à partir d'un ou de précurseur(s) inactif(s).

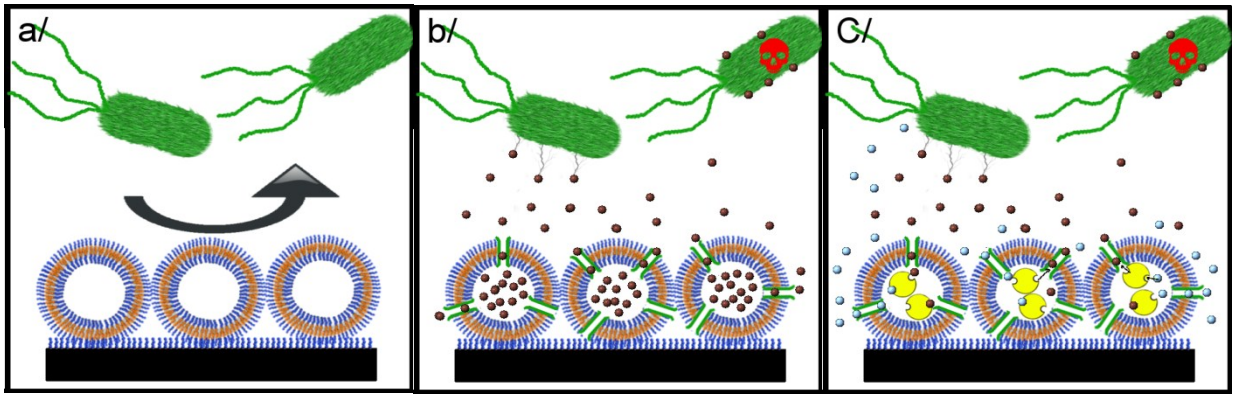


Figure 6: Trois voies possibles aboutissant à des surfaces basées sur l'immobilisation de vésicules possédant des propriétés antimicrobiennes : (a) vésicules possédant des propriétés antimicrobiennes intrinsèques, (b) nanocontaineurs antimicrobiens, (c) nanoréacteurs antimicrobiens.

Ces trois voies ne sont pas équivalentes, que ce soit en termes d'efficacité que dans leurs limitations. La première possibilité, consistant en la sélection d'un amphiphile capable de former des vésicules repoussant les bactéries, est limitée, comme toutes les stratégies passives, par le spectre d'action du dépôt (la diversité des propriétés bactériennes empêche l'existence d'un polymère repoussant pour toutes les souches bactériennes). De plus, comme discuté précédemment, les défauts du dépôt peuvent conduire à la non-protection de certaines parties de la surface (en provoquant l'apparition de zones favorables à l'adhésion ou « point d'ancrages » des bactéries), or, une seule bactérie adhérente est apte à initier la formation d'un biofilm. Dans la seconde stratégie, les vésicules sont utilisées en tant que nanoréacteurs encapsulant un agent antimicrobien. Le relargage de la molécule bioactive nécessite une perméabilité contrôlée de la membrane vésiculaire. Réaliser ce relargage contrôlé est la plus grande difficulté de cette stratégie et conduit à une limitation de la taille des molécules bioactives utilisables. De plus, la durée de vie de tels nanocontainers est limitée par la quantité d'agent actif stocké en leur sein, ainsi que par la vitesse de relargage. Finalement, la troisième voie consiste à utiliser des nanoréacteurs formés par l'encapsulation d'enzymes au sein des vésicules. L'enzyme rend possible la conversion d'une molécule inactive (Figure 6c ─ sphères bleu clair) en une molécule active (Figure 6c ─ sphères brunes). Le principal avantage de cette technique, en comparaison de la technique classique du nanocontaineur, est l'élimination du problème de la durée de vie due à une capacité de stockage limitée de l'agent actif. De même le relargage ne doit plus être contrôlé puisqu'on peut contrôler la production de l'agent actif en ajoutant ou non le précurseur dans l'environnement. Malgré ces

avantages, cette dernière technique possède aussi ses limitations, la principale étant la limitation de l'activité de l'enzyme, due à la diffusion du précurseur et à la conversion par l'enzyme, qui pourraient se révéler trop lentes pour empêcher la colonisation primaire des bactéries.

Afin de lutter contre les limitations de ces diverses stratégies, nous avons choisi de concevoir des surfaces combinant stratégies active et passive. Plus précisément, nous combinons des propriétés antiadhésives des polymères utilisés avec les propriétés antimicrobiennes de nanoréacteurs encapsulant une enzyme (concept schématisé dans la Figure 7). Un tel type de surface devrait permettre de passer outre les différentes limitations : les propriétés antiadhésives contreront les adhésions primaires, permettant à la conversion enzymatique de prendre un rythme de croisière pour une pleine efficacité de l'agent antimicrobien. Les bactéries potentiellement adhérentes seront alors éliminées par l'agent antibactérien produit par les nanoréacteurs. L'utilisation des nanoréacteurs permet l'élaboration d'un matériau dit « intelligent », l'activation du système étant fonction de la concentration en précurseur dans le milieu et ce, par simple ajout du précurseur en fonction des besoins.

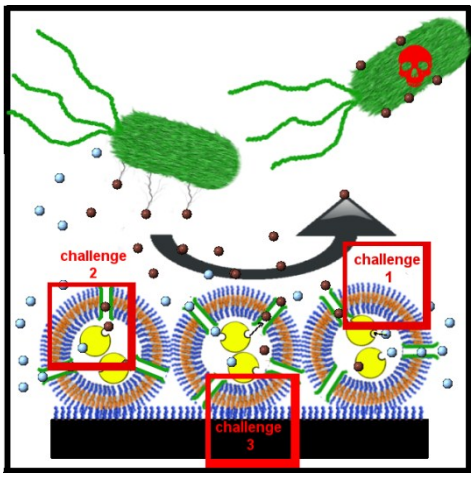


Figure 7: Schéma de la stratégie développée dans cette étude, combinant propriété antibactérienne passive (propriété « repoussante » inhérente au polymère) et propriété antimicrobienne active (nanoréacteurs) pour prévenir l'adhésion bactérienne et la croissance de biofilms. Trois défis mis en évidence sont : la conception de la molécule amphiphile (challenge 1), l'activité enzymatique des nanoréacteurs (challenge 2) et l'immobilisation des vésicules sur les surfaces (challenge 3).

Pour développer cette stratégie antimicrobienne, trois étapes sont nécessaires. Premièrement, le polymère utilisé pour l'auto-assemblage des nanoréacteurs doit être conçu pour respecter trois critères: le polymère amphiphile doit s'auto-assembler sous forme de vésicules, il doit posséder les fonctions chimiques nécessaires au greffage de vésicules sur les surfaces, et finalement, il doit autoriser la formation de structures prévenant l'adhésion des bactéries tout en étant biocompatible. Pour cela, nous avons synthétisé un copolymère amphiphile à blocs, le poly(butadiène)-bloc-oligonucléotide en accord avec nos trois critères. Cette première étape est détaillée dans le premier chapitre « synthèse et caractérisation du polymère » (Chapitre 1). Deuxièmement, des

nanoréacteurs capables de produire de façon contrôlée un agent antimicrobien à partir d'une molécule inactive doivent être conçus à partir des vésicules. La production doit être suffisante pour assurer l'efficacité antibactérienne, stable dans le temps et effective pendant une durée suffisamment longue. Pour ce faire, nous avons produit de nanoréacteurs à partir de vésicules formées par le copolymère à blocs poly(butadiène)-bloc-oligonucléotides, encapsulant l'enzyme lactoperoxidase et intégrant des canaux protéiniques dans sa membrane vésiculaire. Le rôle des canaux protéiniques (OmpF) est d'assurer la perméabilité de la membrane vésiculaire, autorisant la diffusion du précurseur et de l'agent actif. La préparation et démonstration de la fonctionnalité et stabilité des nanoréacteurs est le sujet du second chapitre « préparation et caractérisation des nanoréacteurs » (Chapitre 2). Finalement, le troisième challenge consiste en l'immobilisation des nanoréacteurs sur la surface d'intérêt. Ce greffage doit être contrôlé et doit assurer la rétention de la forme vésiculaire, ainsi que la conservation de l'activité des nanoréacteurs et la stabilité à long terme pour empêcher tout détachement de vésicules. Pour cela, différentes surfaces ont été préparées sur la base du greffage covalent d'oligonucléotides permettant l'immobilisation de vésicules par hybridation spécifique ou non-spécifiques sur la surface. La préparation et la caractérisation de ces surfaces est le sujet du troisième chapitre « préparation et caractérisation des surfaces » (Chapitre 3).

Chapitre 1. Synthèse et caractérisation du copolymère à blocs

Ce premier chapitre se concentre sur la conception et la caractérisation de 4 polymères amphiphiles à blocs, basés sur une courte séquence d'ADN couplée à un bloc hydrophobe variable. Nous avons montré la possibilité de coupler du poly(isobutylène) ou du poly(butadiène) à une séquence oligonucleotide (quelque soit la séquence), permettant l'obtention d'un copolymère à blocs d'une grande pureté avec un rendement proche de 30% en masse, rendement jugé très bon au regard des rendements publiés pour de telles synthèses[10]. Nous avons aussi démontré que ce copolymère à blocs s'auto-assemble spontanément. Sur des bases théoriques et expérimentales, nous avons émis l'hypothèse d'un auto-assemblage dirigé par la configuration de la structure secondaire des oligonucleotides et par les forces intermoléculaires mises en jeux par le greffage du bloc hydrophobe sur le segment d'oligonucleotide, ce qui amène à la formation de structures micellaires et vésiculaires. En vue de la production de surfaces destinées au domaine biomédical, le copolymère basé sur les oligonucléotides présente plusieurs avantages, dont la biocompatibilité potentielle offerte par les biomolécules et la possibilité de diriger la réponse des cellules eucaryotes par une sélection judicieuse de la séquence ADN. De la même façon, une réponse bactérienne spécifiquement choisie peut être envisagée. Plus encore, l'utilisation d'oligonucléotide simple brin

[10] Z. Li, Y. Zhang, P. Fullhart, C.A. Mirkin, Reversible and Chemically Programmable Micelle Assembly with DNA Block-Copolymer Amphiphiles, Nano Letters. 4 (2004) 1055-1058.

nous permet d'utiliser les remarquables propriétés d'appariement de l'ADN pour immobiliser les vésicules sur les surfaces.

Chapitre 2. Préparation et caractérisation des nanoréacteurs

Sur la base du copolymère à blocs basé sur les oligonucléotides, nous avons préparé des nanoréacteurs par l'encapsulation d'enzymes en tant que cœur réactif, et en insérant des canaux protéiniques pour permettre la perméabilité de la membrane vésiculaire. Pour cela, nous avons vu au Chapitre 1 que le polymère PIB_{31}-G_7A_5 est capable de former des vésicules en milieu aqueux, ce qui est nécessaire à l'encapsulation d'enzyme elle-même soluble dans un tel milieu. De plus, nous avons montré que la membrane vésiculaire a une épaisseur de 11 ± 3 nm, ce qui, associé à la faible température de transition vitreuse du polymère, permet l'incorporation de canaux protéiniques OmpF pour assurer la perméabilité de la membrane vésiculaire. Finalement nous avons choisi comme enzyme la lactoperoxidase, connue pour produire des agents antimicrobiens par oxydation du thiocyanate (inactif) qui converti en hypothiocyanate, est antibactérien. L'enzyme est le cœur actif du nanoréacteur. Celui-ci, combinant l'auto-assemblage du PIB_{31}-G_7A_5, l'encapsulation de la lactoperoxidase avec l'incorporation des OmpF dans la membrane vésiculaire, est schématisé dans la Figure 8.

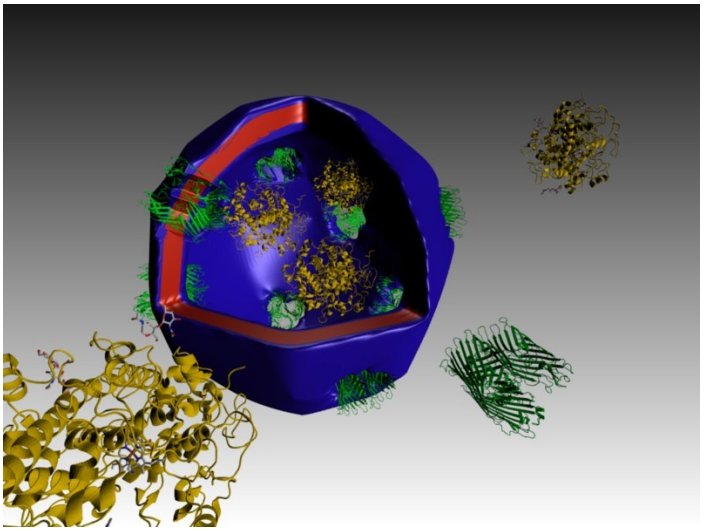


Figure 8: Illustration d'un nanoréacteur auto-assemblé, avec les OmpF insérés dans la membrane vésiculaire (vert) encapsulant des molécules de lactoperoxidase (jaune). Des pores OmpF et des molécules de lactoperoxidase libres sont représentées dans l'environnement du nanoréacteur. Sur cette vésicule schématisée, et ouverte, la zone rouge correspond à la partie hydrophobe de la membrane alors que la partie bleue correspond à sa partie hydrophile.

Dans ce chapitre, nous démontrons et caractérisons l'efficacité des molécules de lactoperoxidase encapsulées au sein des nanoréacteurs formés par le PIB_{31}-G_7A_5 et possédant une perméabilité assurée par les OmpF. Le couple molécule précurseur/molécule active utilisé pour ce travail est le couple dityrosine/tyrosine dont

la forme oxydée présente une fluorescence permettant sa détection. Nous démontrons en particulier la possibilité d'obtenir une solution pure de nanoréacteurs avec des enzymes encapsulées dans la vésicule. De plus, nous avons déterminé les constantes cinétiques K_M et K_{cat} de la lactoperoxidase encapsulée. En comparant ces constantes avec celles obtenues pour les enzymes libres, nous montrons que les enzymes ne sont pas dénaturées malgré une diminution de la vitesse de conversion enzymatique. Pour expliquer cette diminution, nous avons émis l'hypothèse d'une gêne stérique induite par la membrane vésiculaire sur l'enzyme encapsulée, résultant en une augmentation de la barrière énergétique de conversion dans le cas de la tyrosine. Nous avons aussi déterminé le taux de polymère à blocs donnant des nanoréacteurs ainsi que l'efficacité d'encapsulation. Dans le cas du polymère que nous avons utilisé pour l'élaboration des nanoréacteurs, la détermination a pu être effectuée précisément, contrairement aux données rares et imprécises présentes dans la littérature[11]. Finalement, nous avons pu conclure que le polymère conçu dans cette étude autorise la production de nanoréacteurs fonctionnels, c'est-à-dire permettant le maintien de l'activité enzymatique, et ce, même dans un environnement défavorable à l'enzyme (effet « protecteur » de la capsule).

Chapitre 3. Surfaces basées sur l'immobilisation de vésicules.

Pour atteindre notre objectif de produire un revêtement basé sur les nanoréacteurs présentés au chapitre précédent, leur immobilisation sur une surface est un défi crucial. Cette immobilisation, bien pouvant apparaître triviale, est rendue difficile par la nécessité d'obtenir un dépôt stable et contrôlé, même après immersion en milieu aqueux. Pour cela, nous avons opté pour l'utilisation des propriétés d'hybridation de d'un brin d'ADN avec son brin complémentaire. Pour cela, plusieurs étapes de traitement de surface et de caractérisation sont nécessaires, qui sont décrites dans ce chapitre.

Dans un premier temps, nous avons étudié le greffage d'oligonucleotides simples brins sur une couche auto–assemblée de aminopropyltriéthoxysilane (APTES). Ces surfaces ont été caractérisées par XPS, QCM-D, microscopie de fluorescence et ellipsométrie, démontrant l'efficacité du greffage. Outre qu'elles sont le support pour l'immobilisation des vésicules, ces surfaces sont nécessaires pour l'étude des facteurs influençant l'adhésion bactérienne sur les surfaces (étude présentée dans la Partie II). Pour les besoins de cette Partie II, nous avons développé deux protocoles de greffage, permettant d'obtenir deux densités de greffage des oligonucléotides sur les surfaces. Nous appellerons ces surfaces « basse densité » et «haute densité ». Elles ont été caractérisées par leurs propriétés physico-chimiques (angle de contact et XPS) et topographiques (AFM et microscopie).

Des surfaces supportant les vésicules ont été produites. Pour cela, nous avons utilisé l'immobilisation spécifique et non-spécifique des vésicules sur des surfaces recouvertes d'oligonucleotides simples brins. Le

[11] P. Broz, S. Driamov, J. Ziegler, N. Ben-Haim, S. Marsch, W. Meier, Toward Intelligent Nanosize Bioreactors: A pH-Switchable, Channel-Equipped, Functional Polymer Nanocontainer, Nano Lett. 6 (2006) 2349-2353.

premier type de surface met en jeu l'adhésion non-spécifique des vésicules (adhésion non dirigée par l'hybridation de l'ADN). Les vésicules de copolymère à blocs PB_{65}-A_5G_7 ont été déposées sur une couche d'oligonucléotides « basse densité » de la séquence A_5G_7. La non-complémentarité des séquences présentes sur la surface et portées par les vésicules, a amené à l'immobilisation des vésicules par des interactions de type électrostatique. La surface obtenue possède une topographie de type « rugueuse » due à la présence des vésicules, mais complètement homogène d'un point de vue chimique (même séquence oligonucléotide en tout point de la surface). Les structures déposées ont été réticulées par irradiation UV, permettant d'homogénéiser les propriétés mécaniques de la surface, les rendant similaires à celles observables pour les surfaces portant uniquement les oligonucléotides greffés. Ces surfaces portant des vésicules non-hybridées sur la surface ont été caractérisées par AFM et angle de contact. Finalement, nous avons utilisé l'hybridation des vésicules de copolymère PIB_{31}-G_7A_5 sur des surfaces portant le brin complémentaire (C_7T_5) pour préparer les surfaces du second type, portant une forte densité de vésicules immobilisées. Le processus de greffage a pu être suivi en temps réel par microscopie de fluorescence et QCM-D, démontrant la spontanéité du processus de dépôt et sa stabilité. Sur la base des résultats de QCM-D nous avons discuté les propriétés viscoélastiques de ce type de dépôt, alors que les observations en microscopie de fluorescence sous flux nous ont permis de confirmer sa stabilité. De plus, ces deux techniques nous ont permis de démontrer la conservation de la structure vésiculaire durant l'immobilisation. Finalement, par l'utilisation de l'AFM, des mesures d'angle de contact et de l'XPS, nous avons pu extraire les propriétés de surface et de topographie du dépôt. Le procédé de préparation des vésicules avant dépôt nous a permis d'obtenir deux types de topographie, par l'adhésion de vésicules organisées sous forme d'agrégats ou non. Ces deux types de surfaces portant un dépôt de vésicules hybridées seront appelées « vésicules rugueuses » et « vésicules lisses » dans la suite de ce texte, en raison de leur différence de topographie alors que toutes autres propriétés restent identiques.

Conclusions et perspectives de la Partie I

Dans cette première partie du travail, nous avons démontré la possibilité de produire des surfaces basées sur l'immobilisation de nanoréacteurs résultants de l'auto-assemblage d'un copolymère amphiphile. Dans le premier chapitre, nous avons décrit la synthèse et la caractérisation chimique du copolymère amphiphile à blocs basé sur les oligonucléotides, par le couplage d'un court brin d'oligonucléotide à un bloc polymère fortement hydrophobe, tel que le poly(butadiène) ou le poly(isobutylène). Nous avons ensuite étudié le processus d'auto-assemblage de ce polymère amphiphile, mettant en évidence la formation de micelles et de vésicules. Sur la base de cet auto-assemblage sous forme vésiculaire, nous avons ensuite, dans le second chapitre, préparé des nanoréacteurs par encapsulation de lactoperoxidase en tant que cœur actif et par l'incorporation d'OmpF dans la membrane vésiculaire pour assurer la perméabilité membranaire. Nous avons démontré la possibilité d'obtenir une solution pure de nanoréacteurs et nous avons quantifié avec précision l'efficacité d'encapsulation et de conversion des polymères en nanoréacteurs fonctionnels. De plus, sur la base des cinétiques enzymatiques et des constantes

cinétiques au sein des nanoréacteurs, nous avons montré une diminution de la vitesse de conversion du précurseur en produit actif lorsque l'enzyme est encapsulée (probable gêne stérique et influence des charges de la membrane vésiculaire). Finalement, nous avons prouvé l'effet protecteur de l'encapsulation de l'enzyme au sein des vésicules, contre une dégradation enzymatique externe. Dans le troisième chapitre, nous avons préparé des dépôts de vésicules par leur immobilisation sur des surfaces. Pour ce faire, nous avons dans premier temps préparé et caractérisé des surfaces « lisses » par le greffage de différentes densités d'oligonucleotide. Dans un second temps nous avons pu immobiliser les vésicules par deux techniques différentes : l'hybridation spécifique ou non-spécifique. Nous avons aussi caractérisé toutes ces surfaces en termes de propriétés physico-chimiques, de topographie et de propriétés mécaniques.

La Partie I de ce manuscrit a porté sur le développement et la préparation de surfaces antimicrobiennes basées sur un dépôt de nanoréacteurs polymériques. Pour atteindre ce but, nous avons exploré plusieurs aspects fondamentaux sur l'auto-assemblage de polymère amphiphile, la cinétique enzymatique, l'influence de l'encapsulation et finalement les interactions entre vésicules et surfaces durant le processus de dépôt. De nombreuses questions sont également apparues au cours de notre étude, qui mériteraient de plus amples investigations. En particulier, l'influence de l'environnement sur l'auto-assemblage a été brièvement mentionné, mais une étude poussée sur l'influence du pH, des contre-ions, de l'hybridation en solution sur l'auto-assemblage permettrait de mieux connaître ces polymères basés sur l'ADN et leur auto-assemblage. Le mécanisme résultant en la diminution de la vitesse de conversion est un autre exemple de question posée par ce travail. Notamment, étudier les influences croisées du polymère et du type d'enzyme sélectionné sur les cinétiques enzymatiques devrait permettre d'optimiser ce type de système. De plus, l'utilisation d'enzymes capables de produire des antibiotiques au sein des nanoréacteurs est actuellement à l'étude dans le groupe du prof. W. Meier. Finalement, la réalisation du dépôt de vésicules a été l'occasion d'étudier la stabilité des vésicules et des interactions entre la surface et la vésicule, mais les aspects thermodynamiques mis en jeux lors du dépôt, et l'agrégation et organisation des vésicules en fonction des propriétés de l'environnement aqueux (pH, contre-ions…) sont des aspects qu'il reste à étudier.

Part II: Adhésion bactérienne sur les surfaces basées sur les nanoréacteurs: étude de l'influence de la chimie, de la topographie et des propriétés mécaniques sur l'interaction bactérie-surface.

Pour le développement de surfaces antimicrobiennes, la connaissance des interactions bactérie-surface est essentielle pour comprendre l'influence, l'action et l'efficacité de la surface. La réponse bactérienne lors du contact avec le dépôt de nanoréacteurs doit donc être soigneusement caractérisée. De plus, nous pensons que les surfaces créées à partir de dépôt de vésicules basées sur les oligonucleotides sont susceptibles de faciliter

l'investigation de questions fondamentales concernant les interactions entre surface et bactéries pendant le processus d'adhésion. Cette partie est consacrée à ces aspects.

Plusieurs propriétés de surface sont connues comme influençant les interactions bactérie-surface. Deux propriétés sont communément admises comme capables d'un impact important sur l'adhésion bactérienne et la formation du biofilm : la topographie et la chimie de la surface (incluant les propriétés physico-chimiques). Un troisième groupe de propriétés de surface, les propriétés mécaniques, est généralement négligé. Etant donné que notre dépôt de vésicules possède des propriétés mécaniques atypiques, comme nous avons pu le voir en QCM-D dans la Partie I- Chapitre 3, la considération de l'influence des propriétés mécaniques sur l'adhésion bactérienne nous paraît ici pertinente.

Dans cette seconde partie, nous nous sommes attachés à étudier l'influence de ces trois groupes de propriétés sur l'adhésion bactérienne. Pour cela, nous avons étudié la réponse bactérienne aux variations de chaque propriété, d'un point de vue quantitatif (nombre de bactéries adhérentes), en cultures statiques ou dynamiques (sous flux laminaire), par des observations en temps réel ou différées. Ces différentes conditions de culture nous ont permis d'étudier quantitativement la colonisation de la surface mais aussi la dynamique de l'attachement et de détachement bactériens impliqués durant l'adhésion bactérienne et la croissance du biofilm, en lien avec les variations des propriétés de la surface. Nous avons de plus utilisé différents mutants d'*E.coli*, ce qui nous a permis d'étudier l'influence des curli (une organelle bactérienne fréquemment impliquée dans les processus d'adhésion) sur l'adhésion bactérienne, en relation ici aussi avec les variations des propriétés de la surface.

Dans cette seconde partie, nous avons utilisé différentes surfaces conçues dans la Partie I et permettant de faire varier, indépendamment les unes des autres, les propriétés de la surface. Nous avons donc en premier lieu étudié l'influence des oligonucleotides sur l'adhésion bactérienne, indépendamment des autres facteurs, la densité de greffage ne pouvant néanmoins pas être decorrélée de la densité de charge. Nous avons montré que de hautes densités de greffage d'oligonucleotide réduisaient le nombre de bactéries adhérentes observables sur la surface, alors que sur de basses densités d'oligonucleotide sur la surface, aucun effet significatif n'a pu être mis en évidence. Nous avons émis l'hypothèse d'une balance entre l'influence répulsive des charges négatives de la surface face aux charges négatives de la membrane bactérienne, avec l'influence favorable de la fonctionnalité chimique/biologique de l'oligonucléotide pour la bactérie. Ces surfaces d'oligonucleotides greffés ont aussi montré leur influence, indépendamment des autres facteurs, sur l'expression des curli en induisant une surexpression des curli. Néanmoins, la faiblesse de cet effet fait qu'il peut être facilement perturbé par d'autres facteurs capables d'influencer l'adhésion bactérienne.

Les surfaces basées sur les dépôts de vésicules possèdent une topographie sub-micrométrique, ce qui est à même d'influencer l'adhésion bactérienne. Néanmoins, aucun effet significatif n'a pu être détecté dans cette étude, ni sur les bactéries adhérentes, ni sur l'expression des curli. Ce résultat suggère que si la topographie sub-

micrométrique est capable d'influencer l'adhésion bactérienne, cet effet est moins important que l'effet des charges, de la chimie et des propriétés mécaniques des dépôts de vésicules. Pour étudier plus en détails l'influence de la topographie, une étude avec des variations systématiques de l'amplitude et de l'organisation de la topographie sur des surfaces biologiquement inertes serait nécessaire.

Finalement, nous avons montré une forte influence du dépôt de vésicules, associée aux propriétés viscoélastiques des vésicules. Nous avons émis l'hypothèse que le faible nombre de bactéries adhérentes sur les dépôts de vésicules non-réticulées est dû à la faible quantité de points d'ancrage sur la surface. Ceci induit probablement une grande mobilité des bactéries sur la surface, autorisant un fort taux de détachement depuis la surface et réduisant donc le nombre de bactéries adhérées de façon irréversible. Nous avons de la même façon mis en évidence une influence similaire des propriétés mécaniques induisant une mobilité à l'interface, sur des hydrogels d'agar. Néanmoins, le processus mis en jeu n'est pas élucidé. De futures investigations sur ce sujet permettront d'ouvrir de nouvelles voies pour l'utilisation des propriétés mécaniques de surface dans les applications antiadhésives et anti-fouling.

Dans cette étude nous avons mis en avant l'influence indépendante des oligonucleotides, de la topographie et des propriétés mécaniques des surfaces basées sur les vésicules, sur l'adhésion bactérienne, l'expression des curli et la croissance du biofilm. Nous avons proposé un mécanisme pour expliquer l'influence de chaque facteur et avons démontré que l'effet global observable résulte de la combinaison de ces contributions, que ce soit par des actions complémentaires ou des effets antagonistes. Cette étude fournit les bases nécessaires pour d'autres investigations sur l'adhésion bactérienne et la croissance du biofilm sur les surfaces recouvertes d'ADN ou des surfaces aux propriétés viscoélastiques variées. De nouvelles études avec différentes séquences oligonucléotides, faisant varier la taille des vésicules ou encore le recouvrement de la surface par les vésicules, sont programmées. De même, l'étude de l'influence des propriétés viscoélastiques sur l'adhésion bactérienne et la formation du biofilm avec une attention particulière portée sur les voies de signalisation CpX ou le blocage du flagelle sera menée pour élucider la réponse bactérienne face à ces différentes propriétés viscoélastiques.

Conclusion générale.

Ce travail a démontré la faisabilité de la préparation de surfaces bioactives basées sur des dépôts de vésicules polymères pour prévenir la formation du biofilm. Plus encore, de nombreux aspects fondamentaux de la physico-chimie du polymère et des interfaces biologiques ont été explorés.

La première partie de ce travail a été dédiée aux investigations sur la synthèse, sur l'auto-assemblage et sur l'immobilisation sur la surface de vésicules produites par les copolymères amphiphiles à base de nucléotides. Ces premières investigations nous ont permis de préparer et étudier des nanoréacteurs à partir de ces vésicules. Finalement, nous avons élaboré des surfaces supportant des dépôts de vésicules, par hybridation de l'ADN.

La seconde partie de ce travail était consacrée à l'investigation de la réponse bactérienne aux surfaces basées sur les vésicules et à l'influence des différentes propriétés de ces surfaces sur l'adhésion bactérienne.

La première partie de ce travail était divisée en trois chapitres, permettant d'explorer chaque aspect du système surface-nanoréacteur. Dans le premier chapitre, nous avons montré la possibilité de concevoir un amphiphile hybride par le greffage d'une séquence oligonucléotide sur un segment hydrophobe. Grâce à la versatilité de la chimie de ce polymère amphiphiles, nous avons pu synthétiser une série d'amphiphiles par synthèse sur phase solide, variant tant au niveau du bloc hydrophobe que de la séquence nucléotide et capables de s'auto-assembler en solution. La caractérisation du processus d'auto-assemblage de ce copolymère a montré l'importance des propriétés du bloc hydrophile permettant la formation de vésicules, malgré une balance amphiphile favorable à la formation de micelles.

Le deuxième chapitre est axé sur l'étude de la capacité de ces polymères à former des nanoréacteurs par l'encapsulation d'une enzyme active et en présence de canaux protéiniques, assurant la perméabilité de la membrane vésiculaire. Le système s'est montré fonctionnel et efficace pour prévenir la dégradation de l'enzyme encapsulée dans un milieu défavorable.

Dans le troisième chapitre, nous avons montré que la séquence nucléotidique, présente au sein du copolymère, conserve ses propriétés d'hybridation avec sa séquence complémentaire greffée sur une surface. La morphologie de l'auto-assemblage est de plus conservée au cours de l'immobilisation. Dans ce chapitre, nous avons décrit et caractérisé différents types de surfaces qui doivent permettre de mieux comprendre les interactions entre des bactéries et les surfaces basées sur les vésicules.

La seconde partie de ce travail est organisée autour de 4 sujets. Après une brève étude concernant la toxicité des surfaces, nous avons démontré dans un premier temps l'influence de la composition et des propriétés physico-chimiques des oligonucléotides sur l'adhésion bactérienne et l'expression des curli. Le troisième aspect étudié concerne l'influence de la topographie. Enfin, nous nous sommes intéressés à l'influence des propriétés mécaniques particulières des dépôts de vésicules sur l'adhésion bactérienne.

Dans la discussion de cette seconde partie, nous avons mis en avant la non-toxicité des surfaces produites en comparaison des références que sont les surfaces de verre ou des wafers de silicium. Nous avons ensuite étudié la balance entre l'influence défavorable des charges face à l'influence favorable de la fonctionnalité chimique de la surface due au greffage des oligonucleotides. Ceci nous a permis de mettre en évidence une diminution du nombre de bactéries adhérentes sur les surfaces couvertes par une forte densité d'oligonucléotides alors que les surfaces couvertes par de faibles densités n'ont pas révélé d'influence sur ce nombre de bactéries adhérentes. Nous avons aussi montré l'influence de ces surfaces supportant des oligonucléotides pour induire une surexpression du gène des curli. Cette faible surexpression semble être facilement perturbée par d'autres

influences telles que la densité de greffage. Cette surexpression s'est révélée indépendante de la séquence sélectionnée, montrant une non-spécificité de cet effet par rapport à la séquence utilisée.

Nous avons ensuite discuté l'influence de la topographie sur l'adhésion bactérienne et l'expression des curli, et plus particulièrement l'absence d'effet visible de la topographie sub-micrométrique utilisée dans cette étude. Nous avons émis l'hypothèse que l'influence de la topographie est suffisamment faible pour être écrantée par l'influence beaucoup plus forte des oligonucléotides et des propriétés mécaniques des dépôts de vésicules de cette étude.

Dans la quatrième partie de cette discussion, nous avons considéré l'influence des propriétés mécaniques du dépôt de vésicules, immobilisées sur la surface, sur l'adhésion bactérienne. Cette partie de l'étude a mené à des résultats originaux concernant la capacité des propriétés viscoélastiques à induire une diminution du nombre de bactéries adhérentes. L'étude combinée de l'adhésion et de la mobilité des bactéries sur les surfaces couvertes soit par des vésicules soit par des hydrogels d'agar nous permet d'émettre l'hypothèse que la réduction du nombre de bactéries adhérentes sur ces surfaces est due à un plus grand détachement des bactéries au cours de l'adhésion primaire, lui-même induit par une plus grande mobilité. Cette mobilité bactérienne, de type « sliding », est probablement induite par les propriétés dissipatives du substrat, qui n'offre pas de points d'ancrage pour les bactéries, limitant les possibilités d'adhésion irréversible et donc la formation du biofilm.

Finalement, nous avons montré la possibilité de produire des surfaces basées sur les nanoréacteurs polymériques et nous avons exploré les concepts fondamentaux sous-jacents. Nous avons étudié la réponse bactérienne sur ces surfaces atypiques. En particulier, nous avons mis en évidence l'influence des propriétés mécaniques uniques de ce type de surface et montré leur pertinence pour produire des dépôts antimicrobiens grâce à leurs propriétés antiadhésives et grâce à l'activité du nanoréacteur, cumulant ainsi les avantages des stratégies antimicrobiennes active et passive avec un relargage contrôlé d'agent antimicrobien.